

# bradscholars

## Vibrational spectroscopic techniques (Raman, FT-IR and FT-NIR spectroscopy) as a means for the solid-state structural analysis of pharmaceuticals

Item Type	Thesis
Authors	Ali, H.R.H.
Rights	<p><a href="http://creativecommons.org/licenses/by-nc-nd/3.0/">&lt;a rel="license" href="http://creativecommons.org/licenses/by-nc-nd/3.0/"&gt;&lt;img alt="Creative Commons License" style="border-width:0" src="http://i.creativecommons.org/l/by-nc-nd/3.0/88x31.png" /&gt;&lt;/a&gt;&lt;br /&gt;The University of Bradford theses are licenced under a &lt;a rel="license" href="http://creativecommons.org/licenses/by-nc-nd/3.0/"&gt;Creative Commons Licence&lt;/a&gt;.</a></p>
Download date	2026-03-12 01:31:02
Link to Item	<a href="http://hdl.handle.net/10454/3343">http://hdl.handle.net/10454/3343</a>



## **University of Bradford eThesis**

This thesis is hosted in [Bradford Scholars](#) – The University of Bradford Open Access repository. Visit the repository for full metadata or to contact the repository team



© University of Bradford. This work is licenced for reuse under a [Creative Commons Licence](#).

## Abstract

The aim of this work was to assess the suitability of vibrational spectroscopic techniques (Raman, FT-IR and FT-NIR spectroscopy) as a means for the solid-state structural analysis of pharmaceuticals. Budesonide, fluticasone propionate, salbutamol hemisulfate, terbutaline hemisulfate, ipratropium bromide, polymorphic forms of salmeterol xinafoate and two polymorphic forms of sulfathiazole were selected since they are used in the management of certain respiratory disorders and from different chemical and pharmacological entities along with some pharmaceutical excipients. Conventional visual examination is not sufficient to identify and differentiate spectra between different pharmaceuticals. To confirm the assignment of key molecular vibrational band signatures, quantum chemical calculations of the vibrational spectra were employed for better understanding of the first five selected drugs. The non-destructive nature of the vibrational spectroscopic techniques and the success of quantum chemical calculations demonstrated in this work have indeed offered a new dimension for the rapid identification and characterisation of pharmaceuticals and essentially warrant further research.

The application of simultaneous *in situ* Raman spectroscopy and differential scanning calorimetry for the preliminary investigation of the polymorphic transformation of salmeterol xinafoate polymorphs and two polymorphic forms of sulfathiazole has also been explored in this work leading to the development of a new method for the solid-state estimation of the transition temperature of enantiotropically related pharmaceutical polymorphs which represents the first analytical record of the use of this approach for pharmaceutical polymorphs.

**Keywords:** Raman; IR; NIR; DSC; *in situ*; quantum chemical calculations; pharmaceuticals; excipients; polymorphs; solid-state.

## List of sections of this work previously published or reported

### *Papers:*

“Insight to thermally induced solid state polymorphic transformation of sulfathiazole using simultaneous *in situ* Raman spectroscopy and differential scanning calorimetry” H.R.H. Ali, H.G.M. Edwards, I. Scowen, *Journal of Raman spectroscopy*, (accepted and in press).

“Computational and Vibrational Spectroscopic Studies of Ipratropium Bromide” H.R.H. Ali, H.G.M. Edwards, J.Kendrick, I. Scowen, *Drug Testing and Analysis*, 1 (2009) 73 - 80.

“Vibrational spectroscopic study of terbutaline hemisulfate” H.R.H. Ali, H.G.M. Edwards, J.Kendrick, I. Scowen, *Spectrochimica Acta Part A*, 72 (2009) 715 - 719.

“Non invasive *in situ* identification and band assignments of some pharmaceutical excipients inside USP vials with FT near-infrared spectroscopy” H.R.H. Ali, H.G.M. Edwards, I. Scowen, *Spectrochimica Acta Part A*, 72 (2009) 890 - 896.

“Vibrational spectroscopic study of fluticasone propionate” H.R.H. Ali, H.G.M. Edwards, J.Kendrick, I. Scowen, *Spectrochimica Acta Part A*, 72 (2009) 244 - 247

“Vibrational spectroscopic study of salbutamol hemisulfate” H.R.H. Ali, H.G.M. Edwards, J.Kendrick, I. Scowen, *Drug Testing and Analysis*, 1 (2009) 51-56.

“Vibrational spectroscopic characterisation of salmeterol xinafoate polymorphs and a preliminary investigation of their transformation using simultaneous *in situ* portable Raman spectroscopy and differential scanning calorimetry” Hassan Refat H. Ali, Howell G.M. Edwards, Micheal D. Hargreaves, Tasnim Munshi, Ian J. Scowen, Richrad J. Telford, *Analytica Chimica Acta*, 620 (2008) 103-112.

“Vibrational spectroscopic study of budesonide” H.R.H. Ali, H.G.M. Edwards, J. Kendrick, T. Munshi, I.J. Scowen, *Journal of Raman Spectroscopy* 38 (2007) 903-908.

***Published abstracts and posters:***

**1) Proceedings of the Assiut University 5<sup>th</sup> Pharmaceutical Sciences Conference. 7-8 March 2006, Assiut, Egypt.**

“Near infrared screening of some pharmaceutical excipients and drugs” H.R.H. Ali, H.G.M. Edwards, A.J.O’Neil (abstract and poster)

“Raman spectroscopic analysis of salmeterol polymorphs” H.R.H. Ali, H.G.M. Edwards (abstract and poster)

“Raman spectroscopic analysis of ipratropium bromide” H.R.H. Ali, H.G.M. Edwards (abstract and poster)

**2) Proceedings of the International Conference on Raman Spectroscopy (ICORS XX). 20-25 August 2006, Yokohama, Japan.**

“Vibrational spectroscopic study of budesonide” H.R.H. Ali, H.G.M. Edwards, J. Kendrick, T.Munshi, I.J.Scowen (abstract: 123 and invited talk)

“Raman spectroscopic analysis of ipratropium bromide” H.R.H. Ali, H.G.M. Edwards, J. Kendrick, I.J.Scowen (abstract: 303 and poster)

“Near infrared Raman and infrared spectroscopic analysis of salmeterol polymorphs” H.R.H. Ali, H.G.M. Edwards, J. Kendrick, T.Munshi, I.J.Scowen (abstract: 402 and poster)

“Raman spectroscopy of some drugs used in the treatment of certain respiratory disorders” H.R.H. Ali, H.G.M. Edwards (abstract: 403 and poster)

**3) Proceedings of the EUROanalysis XIV, 9-14 September 2007, Antwerp, Belgium.**

“Vibrational spectroscopic study of fluticasone propionate” H.R.H. Ali, H.G.M. Edwards, J.Kendrick, I. Scowen (abstract and poster).

“Vibrational spectroscopic study of terbutaline hemisulfate” H.R.H. Ali, H.G.M. Edwards, J.Kendrick, I. Scowen (abstract and poster).

**4) Proceedings of the International Conference on Raman Spectroscopy (ICORS XXI). 17-22 August 2008, Uxbridge, West London, UK.**

Vibrational spectroscopic characterisation of salmeterol xinafoate polymorphs and a preliminary investigation of their transformation using simultaneous *in situ* portable Raman spectroscopy and differential scanning calorimetry” Hassan Refat H. Ali, Howell G.M.Edwards, Micheal D. Hargreaves, Tasnim Munshi, Ian J. Scowen, Richrad J. Telford (abstract: 1018 and poster).

### **List of sections of this work to be submitted for publication**

“Raman spectroscopy as a primary tool for drug analysis” H.R.H. Ali, H.G.M. Edwards, I. Scowen (in preparation for submission)

“A new method for the solid state estimation of the transition temperature of enantiotropic polymorphic pharmaceutical systems using simultaneous in situ Raman spectroscopy and differential scanning calorimetry” H.R.H. Ali, H.G.M. Edwards, I. Scowen (in preparation for submission)

Sections of this work will be included in a chapter on “Solid state characterisation of pharmaceuticals”, H.R.H. Ali, H.G.M. Edwards, A.J.O’Neil, Eds. R. Storey and P. Royall, Blackwells.

## Acknowledgements

Completion of this work has been possible because of the support and assistance received from many people.

Foremost, I would like to thank my supervisor Professor Howell Edwards for all his valuable support and guidance over the last four years. I am greatly honoured to have had the opportunity to work under his tutelage.

I would like to express my sincere gratitude to the Egyptian government and Assiut University for providing me the scholarship. I am also grateful to all members in the cultural office, Egyptian embassy in London for all their patience and continuous support.

I offer my sincere appreciation and gratitude to Dr Ian Scowen for his continuous help and guidance throughout.

I am deeply grateful and indebted to Dr John Kendrick who has kindly collaborated closely in the quantum chemical calculations part of this work.

I would like to thank Professor Peter York who has kindly supplied samples for my research.

I would like to thank Dennis Farwell for assistance and technical support. I extend my appreciation to Michael Hargreaves and Richard Telford for all their help.

I would like to extend my special thanks to my beloved mother, wife, brother, sister, nieces, family and friends. Their constant support has been the source of my motivation.

## Table of Contents

	<b>Page numbers</b>	
Abstract	ii	
List of sections of this work previously published or reported	iii	
Acknowledgements	vi	
Table of Contents	vii	
List of Figures	xi	
List of Tables	xvi	
<b>Chapter 1</b>	<b>Introduction</b>	
1.1	Introduction	1
1.2	Aims	2
1.3	Thesis structure	3
<b>Chapter 2</b>	<b>Vibrational spectroscopy, spectral pre-processing and computational chemistry</b>	
2.1	Vibrational spectroscopy	4
2.2	Molecular vibrations	4
2.3	The Raman effect	5
2.3.1	Quantum theory	7
2.3.2	Raman intensity	9
2.4	Infrared spectroscopy	9
2.4.1	Infrared selection rules	10
2.4.2	Quantitative infrared measurements	11
2.5	Raman versus IR spectroscopy	12
2.6	X-ray powder diffraction	13
2.7	Differential scanning calorimetry (DSC)	14
2.8	Instrumentation	15
2.8.1	Raman spectrometers	15
2.8.1.1	Fourier-Transform (FT) Raman spectrometer	16
2.8.1.1.1	Standard operation	18
2.8.1.2	Dispersive Raman spectrometers	19
2.8.1.2.1	Renishaw <i>In Via</i> confocal Raman microscope	19
2.8.1.2.2	Charge-coupled device (CCD) detection	20
2.8.1.2.3	Standard operation	20
2.8.1.2.4	Portable Raman analyser	21
2.8.1.3	Dispersive versus non-dispersive Raman spectrometers	22
2.8.2	Infrared spectroscopy	24
2.8.2.1	Scimitar series Digilab UMA-400 FT-IR spectrometer	25
2.8.2.2	Bruker Optics MPA™ FT-NIR spectrometer	26
2.8.3	X-ray powder diffractometer	27
2.8.4	Differential scanning calorimeter	28
2.8.5	The simultaneous <i>in situ</i> Raman –DSC set up	28
2.9	Spectral conversion and manipulation	29
2.9.1	Baseline correction	30

2.9.2	Smoothing	30
2.9.3	Deconvolution	31
2.9.4	Integration of peak areas	31
2.10	Computational chemistry	31
<b>Chapter 3</b>	<b>Raman spectroscopy as a primary tool in drug analysis</b>	
3.1	Introduction	35
3.2	Characterization and detection of pharmaceuticals	35
3.3	Solid-state properties	37
3.4	Quantitative applications of Raman spectroscopy in various pharmaceutical systems	40
3.5	Process pharmaceutical applications	41
3.6	Interactions	43
3.7	Chemical imaging and mapping	46
3.8	Hyphenated techniques	48
3.9	Future pharmaceutical uses of Raman spectroscopy	49
<b>Part I</b>	<b>The evaluation of vibrational spectroscopy/quantum chemical calculations for the characterisation of drugs used in the management of respiratory disorders</b>	
<b>Chapter 4</b>	<b>Vibrational spectroscopic studies of drugs used in the management of respiratory disorders</b>	
4.1	Introduction	64
4.1.1	Budesonide	65
4.1.2	Fluticasone propionate	66
4.1.3	Salbutamol hemisulfate	67
4.1.4	Terbutaline hemisulfate	68
4.1.5	Ipratropium bromide	69
4.2	Experimental	70
4.2.1	Materials	70
4.2.2	Raman spectroscopy	70
4.2.3	Infrared spectroscopy	70
4.2.4	X-ray powder diffractometry	70
4.2.5	Calculation details	71
4.3	Results and discussion	71
4.3.1	Budesonide	72
4.3.1.1	X ray powder Diffractometry)	72
4.3.1.2	Infrared and Raman Spectroscopy	74
4.3.1.2.1	4000– 2600 cm <sup>-1</sup> region	74
4.3.1.2.2	1780 – 1580 cm <sup>-1</sup> region	76
4.3.1.2.3	1800 – 100 cm <sup>-1</sup> region	79
4.3.2	Fluticasone propionate	83
4.3.2.1	3700 – 2600 cm <sup>-1</sup> region	84
4.3.2.2	1800 – 1550 cm <sup>-1</sup> region	85
4.3.2.3	1800 – 100 cm <sup>-1</sup> region	86

4.3.3	Salbutamol hemisulfate	90
4.3.3.1	3800 – 2200 cm <sup>-1</sup> region	91
4.3.3.2	1800 – 1100 cm <sup>-1</sup> region	92
4.3.3.3	1100 – 50 cm <sup>-1</sup> region	94
4.3.4	Terbutaline hemisulfate	100
4.3.4.1	3800 – 2100 cm <sup>-1</sup> region	101
4.3.4.2	1800 – 1100 cm <sup>-1</sup> region	102
4.3.4.3	1100 – 100 cm <sup>-1</sup> region	105
4.3.5	Ipratropium bromide	109
4.3.5.1	Computational studies	109
4.3.5.2	Vibrational spectroscopic analysis	112
4.3.5.2.1	3800 – 2600 cm <sup>-1</sup> region	112
4.3.5.2.2	1750 – 1550 cm <sup>-1</sup> region	113
4.3.5.2.3	1800 – 100 cm <sup>-1</sup> region	114
4.4	Conclusions	117
<b>Chapter 5</b>	<b>Dependence of the Raman spectra of salmeterol xinafoate polymorphs upon laser excitation wavelength</b>	
5.1	Introduction	124
5.2	Experimental	125
5.2.1	Materials	125
5.2.2	Raman spectroscopy	125
5.3	Results and discussion	125
5.3.1	Characterisation of SX polymorphs	125
5.3.2	Dependence of the Raman spectra upon laser excitation wavelength	128
5.4	Conclusions	130
<b>Chapter 6</b>	<b>Non-invasive <i>in situ</i> identification and band assignments of some pharmaceutical excipients inside USP vials with FT- near-infrared spectroscopy</b>	
6.1	Introduction	135
6.2	Experimental	137
6.2.1	Materials	137
6.2.2	FT-NIR spectroscopy	137
6.3	Results and discussion	138
6.3.1	Non-invasive <i>in situ</i> identification of potassium sorbate, sodium starch glycollate, calcium ascorbate, calcium carbonate, candelilla wax and maltodextrin	138
6.3.2.	Non-invasive <i>in situ</i> identification of lactose anhydrous and monohydrate	146
6.4	Conclusions	150

**Part II      A preliminary investigation of the polymorphic transformation of salmeterol xinafoate and sulfathiazole using simultaneous *in situ* Raman spectroscopy and differential scanning calorimetry**

**Chapter 7**

7.1	Introduction	151
7.1.1	Salmeterol xinafoate (SX)	153
7.1.2	Sulfathiazole (SZ)	154
7.2	Experimental	154
7.2.1	Materials	154
7.2.2	X- Ray powder diffractometry	155
7.2.3	Differential scanning calorimetry (DSC)	155
7.2.4	Raman Spectroscopy	156
7.2.5	Near-infrared Spectroscopy	156
7.2.6	The simultaneous <i>in situ</i> Raman –DSC method	156
7.3	Results and discussion	157
7.3.1	Salmeterol xinafoate	157
7.3.1.1	X- Ray powder diffractometry	157
7.3.1.2	Differential scanning calorimetry	157
7.3.1.3	Raman spectroscopy	158
7.3.1.4	Near infrared Spectroscopy	158
7.3.1.5	The simultaneous <i>in situ</i> Raman –DSC method	160
7.3.2	Sulfathiazole	164
7.3.2.1	X- Ray powder diffractometry	164
7.3.2.2	Differential scanning calorimetry	165
7.3.2.3	Raman spectroscopy	166
7.3.2.4	Near infrared Spectroscopy	170
7.3.2.5	The simultaneous <i>in situ</i> Raman –DSC method	172
7.4	Conclusions	176

**Chapter 8      Conclusions and Further Work**

8.1	Conclusions	178
8.2	Further work	179

<b>References</b>	<b>181</b>
-------------------	------------

## List of Figures

		Page numbers
<b>Figure 2.1</b>	An energy level diagram showing transitions equivalent to Raman and Rayleigh scattering and IR absorption	8
<b>Figure 2.2</b>	Electromagnetic spectrum	10
<b>Figure 2.3</b>	Diagram of Bragg theory of X-ray diffraction showing the Bragg angle $\theta$	14
<b>Figure 2.4a</b>	Optical diagram of the Bruker IFS66 spectrometer optical bench with FRA 106 Raman module accessory	17
<b>Figure 2.4b</b>	Diagram of the fore-optics-section A-B on Figure 2.4a	17
<b>Figure 2.5</b>	A schematic diagram of Renishaw <i>In Via</i> confocal Raman microscope	21
<b>Figure 2.6</b>	A schematic diagram of Renishaw portable Raman analyser (RX210)	22
<b>Figure 2.7</b>	A simplified optical layout of a typical ATR-FTIR spectroscopy	26
<b>Figure 2.8</b>	Bruker optics MPA <sup>TM</sup> FT-NIR spectrometer	27
<b>Figure 2.9</b>	Schematic diagram of a typical X-ray powder diffractometer	28
<b>Figure 2.10</b>	An assembly of the fibre-optic coupled portable Raman and DSC	29
<b>Figure 4.1</b>	The chemical structure of epimer 22R of BUD	66
<b>Figure 4.2</b>	The chemical structure of FP	66
<b>Figure 4.3</b>	The chemical structure of SB	67
<b>Figure 4.4</b>	The chemical structure of TBS	68
<b>Figure 4.5</b>	The chemical structure of IPRA	69
<b>Figure 4.6</b>	PXRD pattern of BUD epimers	73
<b>Figure 4.7</b>	The BUD conformation	74
<b>Figure 4.8</b>	The IR spectrum of BUD, 2600 – 4000 cm <sup>-1</sup> region	75

<b>Figure 4.9</b>	The Raman spectrum of BUD, 2600 – 3200 cm <sup>-1</sup> region	<b>76</b>
<b>Figure 4.10</b>	Expanded wavenumber region of the IR spectrum of BUD (1580 – 1780 cm <sup>-1</sup> )	<b>78</b>
<b>Figure 4.11</b>	Expanded wavenumber region of the Raman spectrum of BUD (1580 – 1780 cm <sup>-1</sup> )	<b>79</b>
<b>Figure 4.12</b>	Expanded wavenumber region of the IR spectrum of BUD (100 – 1800 cm <sup>-1</sup> )	<b>80</b>
<b>Figure 4.13</b>	Expanded wavenumber region of the Raman spectrum of BUD (100 – 1800 cm <sup>-1</sup> )	<b>81</b>
<b>Figure 4.14</b>	The crystal structure of FP (code DAXYUX)	<b>83</b>
<b>Figure 4.15</b>	FT-Raman and IR spectral stackplot of FP in the 2600 – 3700 cm <sup>-1</sup> region	<b>85</b>
<b>Figure 4.16</b>	FT-Raman and IR spectral stackplot of FP in the 1550 – 1800 cm <sup>-1</sup> region	<b>86</b>
<b>Figure 4.17</b>	FT-Raman and IR spectral stackplot of FP in the 100 – 1800 cm <sup>-1</sup> region	<b>87</b>
<b>Figure 4.18</b>	The SB conformation	<b>90</b>
<b>Figure 4.19</b>	The crystal structure of SB (code SALBUT)	<b>90</b>
<b>Figure 4.20</b>	FT-Raman and IR spectral stack plot of SB in the 2200 – 3800 cm <sup>-1</sup> region	<b>92</b>
<b>Figure 4.21</b>	FT-Raman and IR spectral stack plot of SB in the 1100 – 1800 cm <sup>-1</sup> region	<b>94</b>
<b>Figure 4.22</b>	FT-Raman and IR spectral stack plot of SB in the 50 – 1100 cm <sup>-1</sup> region	<b>95</b>
<b>Figure 4.23</b>	The PXRD pattern of TBS	<b>100</b>
<b>Figure 4.24</b>	The crystal structure of terbutaline hemisulfate sesquihydrate (code BECVIO).	<b>100</b>
<b>Figure 4.25</b>	FT-Raman and IR spectral stackplot of TBS in the 2100 – 3800 cm <sup>-1</sup> region	<b>102</b>
<b>Figure 4.26</b>	FT-Raman and IR spectral stackplot of TBS in the 1100 – 1800 cm <sup>-1</sup> region	<b>103</b>
<b>Figure 4.27</b>	A comparison between the calculated and experimental	

	Raman spectra of TBS 1100 – 1800 $\text{cm}^{-1}$ region	104
<b>Figure 4.28</b>	A comparison between the calculated and experimental IR spectra of TBS 1100 – 1800 $\text{cm}^{-1}$ region	104
<b>Figure 4.29</b>	FT-Raman and IR spectral stackplot of TBS in the 100 – 1100 $\text{cm}^{-1}$ region	105
<b>Figure 4.30</b>	The calculated Conformations of the ipratropium cation; IPRA1 has no intramolecular hydrogen bond and IPRA2 with an intramolecular hydrogen bond	109
<b>Figure 4.31</b>	The calculated IPRA cation IR conformational shifts in the region 0-2000 $\text{cm}^{-1}$	110
<b>Figure 4.32</b>	The calculated IPRA cation Raman conformational shifts in the region 0-2000 $\text{cm}^{-1}$	111
<b>Figure 4.33</b>	FT-Raman and IR spectral stackplot of IPRA in the 2600 – 3800 $\text{cm}^{-1}$ region	113
<b>Figure 4.34</b>	FT-Raman and IR spectral stackplot of IPRA in the 1550 – 1750 $\text{cm}^{-1}$ region	114
<b>Figure 4.35</b>	FT-Raman and IR spectral stackplot of IPRA in the 100 – 1800 $\text{cm}^{-1}$ region	116
<b>Figure 5.1</b>	Raman spectra of SX (forms I and II) at 1064 and 785 nm	126
<b>Figure 5.2</b>	Raman spectra of SX (forms I and II) at 633 and 514 nm	127
<b>Figure 5.3</b>	Raman spectra of SX (forms I and II) at 488 nm	129
<b>Figure 6.1</b>	NIR spectra of potassium sorbate obtained inside a USP vial and as an open powder	138
<b>Figure 6.2</b>	NIR spectra of sodium starch glycollate obtained inside a USP vial and as an open powder	139
<b>Figure 6.3</b>	NIR spectra of calcium ascorbate obtained inside a USP vial and as an open powder	139
<b>Figure 6.4</b>	NIR spectra of calcium carbonate obtained inside a USP vial and as an open powder	140
<b>Figure 6.5</b>	NIR spectra of candelilla wax obtained inside a USP vial and as an open powder	140
<b>Figure 6.6</b>	NIR spectra of maltodextrin obtained inside a USP vial	

	and as an open powder	141
<b>Figure 6.7</b>	NIR spectra of lactose anhydrous obtained inside a USP vial and as an open powder	146
<b>Figure 6.8</b>	NIR spectra of lactose monohydrate obtained inside a USP vial and as an open powder	147
<b>Figure 6.9</b>	NIR spectra of lactose monohydrate, anhydrous and unknown obtained inside a USP vial.	148
<b>Figure 7.1</b>	The chemical structure of SX.	153
<b>Figure 7.2</b>	The chemical structure of SZ	154
<b>Figure 7.3</b>	DSC head before optical access by the probe	156
<b>Figure 7.4</b>	The PXRD patterns of SX polymorphs I&II	157
<b>Figure 7.5</b>	DSC melting curves of SX	158
<b>Figure 7.6</b>	NIR spectra of SX (forms I and II)	159
<b>Figure 7.7</b>	Typical Raman spectra collected during conversion of SX polymorph I into polymorph II on heating at 115°C then from 118 to 130 °C at 1 degree interval, (500 cm <sup>-1</sup> – 1650 cm <sup>-1</sup> )	161
<b>Figure 7.8</b>	Figure 7.8. Typical Raman spectra collected during conversion of SX polymorph I into polymorph II on heating at 118, 119, 124 and 128°C.	162
<b>Figure 7.9</b>	Temperature dependence of the peak areas of SX polymorphs	163
<b>Figure 7.10</b>	The PXRD pattern of SZ polymorph III	165
<b>Figure 7.11</b>	DSC melting curve of SZ, shows the onset melting points of 168°C for polymorph III and 202°C for polymorph I	166
<b>Figure 7.12</b>	Raman spectra of SZ polymorphs III and I at 785nm	167
<b>Figure 7.13</b>	NIR spectra of SZ polymorphs III and I	170
<b>Figure 7.14</b>	Typical Raman spectra collected during conversion of SZ polymorph III into polymorph I on heating at 150, 155°C then from 160 to 176 °C at 1 degree interval, (250cm <sup>-1</sup> – 1700 cm <sup>-1</sup> )	173
<b>Figure 7.15</b>	Typical Raman spectra collected during conversion of SZ	

polymorph III into polymorph I on heating at 150, 168  
and 170°C. **173**

**Figure 7.16** Temperature dependence of the peak areas of SZ  
polymorphs III and I. **175**

## List of Tables

		<b>Page numbers</b>
<b>Table 3.1</b>	Listing of different pharmaceutical compounds characterised by Raman spectroscopy and computational methods	<b>51</b>
<b>Table 3.2</b>	Listing of different pharmaceutical polymorphic systems studied by Raman spectroscopy	<b>55</b>
<b>Table 3.3</b>	Listing of different pharmaceutical compounds studied by quantitative Raman spectroscopy	<b>58</b>
<b>Table 3.4</b>	Listing of different process pharmaceutical applications of Raman spectroscopy	<b>61</b>
<b>Table 4.1</b>	Vibrational wavenumbers/cm <sup>-1</sup> of BUD	<b>82</b>
<b>Table 4.2</b>	The observed and calculated vibrational wavenumbers/cm <sup>-1</sup> of FP	<b>88</b>
<b>Table 4.3</b>	The observed and calculated vibrational wavenumbers/cm <sup>-1</sup> of SB	<b>97</b>
<b>Table 4.4</b>	The observed and calculated vibrational wavenumbers/cm <sup>-1</sup> of TBS	<b>107</b>
<b>Table 4.5</b>	The key calculated IR spectral features of IPRA1 and IPRA2 in comparison with the observed bands of ipratropium bromide in the range of 600 – 1800 cm <sup>-1</sup>	<b>112</b>
<b>Table 4.6</b>	The observed vibrational frequencies of IPRA and those calculated for IPRA cation	<b>119</b>
<b>Table 5.1</b>	Raman spectral wavenumbers and proposed assignments for SX polymorphs I&II at the selected wavelengths (514, 633, 785 and 1064 nm)	<b>131</b>
<b>Table 6.1</b>	NIR spectral wavelengths, nm and proposed assignments for potassium sorbate, sodium starch glycollate, calcium ascorbate, calcium carbonate, candelilla wax and maltodextrin	<b>143</b>
<b>Table 6.2</b>	NIR spectral wavelengths, nm and proposed assignments for lactose anhydrous and monohydrate	<b>149</b>
<b>Table 7.1</b>	NIR spectral wavelengths/nm and proposed assignments for SX polymorphs I&II	<b>160</b>

<b>Table 7.2</b>	Raman spectral wavenumbers and proposed assignments for SZ polymorphs III&I	<b>168</b>
<b>Table 7.3</b>	NIR spectral wavelengths/nm and proposed assignments for SZ polymorphs III&I	<b>170</b>

## **1.1. Introduction**

Vibrational Raman and IR spectroscopic techniques have been rapidly revolutionised and widely applied in various disciplines, encompassing the chemical, physical, pharmaceutical, medical and natural sciences. The unique chemical fingerprinting capability of these techniques has led to extensive opportunity for fundamental applications in the pharmaceutical sciences. Both techniques are complementary, and play a significant role in providing specific information on the identification and characterisation of materials, as well as providing fundamental molecular spectroscopic information in the structural elucidation of unknown compounds.

The vibrational spectra of pharmaceutical materials are often complex and assignment of the multiple vibrational modes to definitive spectral features has hitherto been difficult to achieve with any confidence. However, with the emergence of quantum chemical calculations, Raman and infrared spectroscopy have been explored further for the identification and discrimination of the vibrational spectra of pharmaceutical compounds. This approach is crucial as it provides a basis for the applications of both quantum chemical calculations and vibrational spectroscopy in pharmaceutical analysis.

Several key research papers have successfully demonstrated the potential of Raman spectroscopy for studies in polymorphism, particularly in investigating the transformation of pharmaceuticals in various environments (Hu et al. 2007; Amado et al. 2007b; Aaltonen et al. 2007a and Anquetil et al. 2003). Thermal analysis methods provide information about the bulk temperature-dependent physical properties of materials. However, it is not always possible to gain information about the molecular chemical changes associated with changes in temperature by using standard thermal analysis equipment alone. The combination of thermal analysis with Raman spectroscopy presents a complete picture of the chemical and physical changes

occurring in thermal processes. This thesis also explores the application of *in situ* Raman spectroscopy and differential scanning calorimetry in the preliminary investigation of the polymorphic transformations of pharmaceutical systems.

## **1.2. Aims**

The aims of this research project were:

- 1- To assess the suitability of vibrational spectroscopy (Raman, FT-IR and FT-NIR) as a means of identifying and differentiating several drugs used in the management of respiratory disorders which include budesonide, fluticasone propionate, salbutamol hemisulfate, terbutaline hemisulfate, ipratropium bromide, the polymorphic forms of salmeterol xinafoate and two polymorphic forms of sulfathiazole. Differentiation of these materials is of great importance to the quality control analysis of pharmaceutical processes.
- 2- To assess the potential application of quantum chemical calculations to provide a better understanding of the vibrational spectra of selected drugs and deduce a molecular approach for identification of key molecular vibrational band signatures.
- 3- To investigate the dependence of the Raman spectra of salmeterol xinafoate polymorphs with laser excitation wavelengths ranging from the visible to the near infrared regions of the electromagnetic spectrum.
- 4- To investigate the use of near-infrared spectroscopy for the non-invasive *in situ* identification of several pharmaceutical excipients which include potassium sorbate, sodium starch glycollate, calcium ascorbate, calcium carbonate, candelilla wax, maltosextrin and monohydrated and anhydrous lactose inside USP vials.
- 5- To develop simultaneous *in situ* Raman spectroscopy and differential scanning calorimetry and apply the instrumentation to investigations of the polymorphic

transformation of salmeterol xinafoate polymorphs and two polymorphic forms of sulfathiazole.

### **1.3. Thesis structure**

This thesis has been divided into eight chapters. This chapter (Chapter One) provides the context and aims of this project. Chapter Two introduces Raman and infrared spectroscopy and gives a brief introduction to the quantum chemical techniques used in this work. Chapter Three gives a comprehensive review on the pharmaceutical applications of Raman spectroscopy. Chapters Four to Seven are divided into two parts. Part I (Chapters Four to Six) presents a comprehensive study of the vibrational spectroscopy for the characterisation of selected drugs that are used in the management of respiratory disorders leading to full assignment of the spectra supported by quantum chemical calculations. Part I also includes the dependence of the Raman spectra of salmeterol xinafoate polymorphs upon laser excitation wavelength and an evaluation of near-infrared spectroscopy for the non-invasive *in situ* identification of several pharmaceutical excipients. Part II (Chapter Seven) concerns the development of simultaneous *in situ* Raman spectroscopy and differential scanning calorimetry for the preliminary investigation of the polymorphic transformation of salmeterol xinafoate polymorphs and two polymorphic forms of sulfathiazole. Chapter eight provides the conclusions of this research and recommendations for further work.

## 2.1. Vibrational spectroscopy

Raman and IR spectroscopy are techniques that yield complementary information in order to characterise and identify the molecular structure of materials. These vibrational spectroscopic techniques, however, are governed by different selection rules (Grasselli et al., 1981). An overview of the origin of both the Raman effect and infrared absorption will now be provided.

## 2.2. Molecular vibrations

The position of a molecule in three-dimensional space can be described using x, y and z co-ordinates for each atom relating to the three mutually orthogonal independent axes in space. Thus, each molecule containing N atoms has  $3N$  degrees of freedom. Molecular motions consist of combinations of translations, rotations and vibrations; three of these fundamentals are pure translations that involve moving atoms simultaneously in the same direction, hence there is no change in the shape of the molecule and its bond lengths. Linear molecules have two rotational fundamental motions around the three orthogonal axes of the molecules (again, not altering any distances between the atoms) and non-linear molecules have three. Thus, each non-linear molecule has  $3N-6$  vibrational degrees of freedom and each linear molecule has  $3N-5$ , giving rise to the fundamental vibrations of the molecule (Hendra et al., 1991). The number of stretching modes is equal to the number of bonds in the molecule; since acyclic molecules have  $N-1$  bonds, there will be  $N-1$  bond stretching modes and the remaining vibrations are bending modes. The stretching and bending modes comprise the vibrational spectrum of the molecule and for which all atoms move in-phase and with the same vibrational frequency. The numbers of fundamental bands observed are dependent upon the degeneracy of the vibrations and their positions in the spectrum are

governed by the vibrational frequencies. Overtone and combination vibrations may produce bands which are less intense than the fundamental vibrations in the Raman and IR spectra (Jee, 2004).

### **2.3. The Raman effect**

When a sample is illuminated with a monochromatic beam of radiation (typically, from a laser), the radiation is transmitted, absorbed or scattered by the molecules (Tu, 1982). The scattered radiation contains photons with the same frequency as the incident radiation. This form of scattering is referred to as elastic scattering or Rayleigh scattering. A very small proportion of photons (approximately one in  $10^8$  to  $10^{10}$ ) are scattered inelastically with frequencies different to that of the incident radiation; the phenomenon of inelastic collisions between incident photons and the molecule is known as the Raman effect (Raman and Krishnan, 1928) and the wavelength-shifted frequency is called Raman scattering. The differences in frequencies between the incident and the inelastic scattered radiation correspond to the frequency of the molecular vibrations present in the molecules of the sample.

When electromagnetic radiation is incident on the system of atoms in a molecule, the interaction distorts the electron cloud of the molecule and induces an electric dipole moment. This induced dipole then radiates scattered light, with or without exchanging energy with vibrations in the molecule.

The magnitude of the induced polarization,  $P$  is proportional to the intensity of the electric field,  $E$ , of the electromagnetic wave and to the molecular polarizability,  $\alpha$ , as given by:

$$P = \alpha E$$

The molecular polarizability is related to properties of a molecule which depend on its structure, the nuclear positions in the molecule and on the nature and direction of its chemical bonds (Hendra et al., 1991). The time-dependent amplitude of the electric field varies according to the equation:

$$E = E_0 \cos 2\pi\nu_0 t$$

where  $E_0$  is the maximum electric field amplitude,  $\nu_0$  is the frequency and  $t$  is the time. Hence;

$$P = \alpha E_0 \cos 2\pi\nu_0 t$$

In the case of Rayleigh scattering, the induced dipole emits electromagnetic radiation at the same frequency as the incident radiation (i.e.  $\nu_0$ ). However, if a molecular vibration causes a change in the molecular polarizability, the induced dipole and the magnitude of the emitted radiation will also change. The change is described by the polarizability derivative,  $\delta\alpha/\delta q$ . According to the Raman selection rule, to be Raman-active, only vibrations that change the polarizability will yield Raman scattering (Pelletier, 1999), Hence

$$\left[ \frac{\delta\alpha}{\delta q} \neq 0 \right]$$

where  $q$  is the normal-co-ordinate (bond length or bond angle) describing the motions of the atoms during a normal vibration. The Raman band intensity is a function of the magnitude of the change in the polarizability (Schrader, 1995).

The polarizability of electrons in the molecule will be modulated by the molecular vibration ( $\nu_m$ ) so that (McCreery, 2000),

$$\alpha = \alpha_0 + \sin \nu_m$$

### 2.3.1. Quantum theory

If a molecule interacts with an electromagnetic field, a transfer of energy from the field to the molecule can occur. According to quantum theory, molecular motion can only have certain discrete energy states, for which a change in state is accompanied by the gain or loss of one or more quanta of energy (Turrell, 1996). A quantum of energy is described by Planck's equation,  $\Delta E = h\nu$ , where  $h$  is Planck's constant and  $\nu$  is the classical frequency of the molecular motion.

The interaction of a molecule with electromagnetic radiation can be analyzed in terms of an energy mechanism. A vibrating molecule will be instantaneously polarized as a photon of incident radiation collides with it and its energy will be raised by  $h\nu_0$  (the energy being immediately lost again by scattering). The scattered radiation consists of two types; the Rayleigh scattering is strong and has the same frequency as the incident beam,  $\nu_0$ , with no net energy loss and the other type of scattering is called Raman scattering and very weak.

Molecules in the ground state give rise to Raman scattering at frequencies  $\nu_0 - \nu_{\text{vib}}$ , where  $\nu_{\text{vib}}$  is the frequency at which the molecule vibrates, given that a change in polarizability occurs during the vibration. If the molecule happens to be in an excited vibrational state when an incident photon is irradiated, the photon may gain energy when scattered, giving a Raman effect at frequencies  $\nu_0 + \nu_{\text{vib}}$ . These are known as the Stokes and anti-Stokes Raman scattering, respectively (Pelletier, 1999). The differences between the incident frequency of radiation and inelastic scattered frequencies correspond to the frequency of molecular vibrations present in the molecules of the sample. The excited states are not real and are described as virtual. The Stokes and anti-Stokes Raman peaks are symmetrically positioned about the Rayleigh peak but their

intensities are very different. The vibrational energy transitions that can occur and which give rise to fundamental modes of vibrations are presented in Figure 2.1.

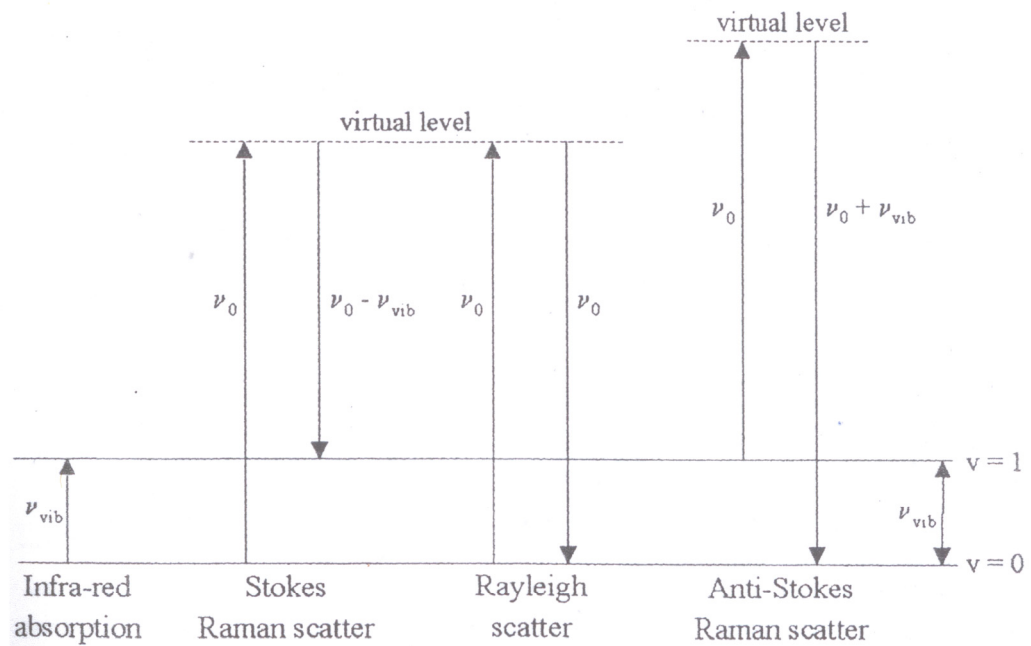


**Figure 2.1. An energy level diagram showing transitions equivalent to Raman and Rayleigh scattering and IR absorption (Day, 2002).**

The ratio of Stokes to anti-Stokes intensity is governed by the temperature. According to the Boltzmann distribution, at ambient temperature most molecules are in their vibrational ground state (Bugay and Smith, 2004). The anti-Stokes lines therefore are less intense than the Stokes line because these transitions arise from higher vibrational energy levels that contain fewer molecules. Hence, Stokes Raman scattering is generally used for the Raman spectrum. A Raman spectrum is normally represented as a plot of Raman scattering intensity versus wavenumber shift or Raman shift. The frequency of the exciting radiation is set to zero and the wavenumber of the Raman shift represents the shift in frequency of a photon from this point. Thus, the Raman shift is independent of the frequency of the incident exciting laser.

### 2.3.2. Raman intensity

The Raman band intensities are proportional to:

$$\nu^4 \sigma_{\nu} I C$$

where  $\nu$  is the frequency of the incident radiation,  $\sigma_{\nu}$  is the Raman cross section,  $I$  is the irradiance of the radiation ( $\text{Wm}^{-2}$ ) and  $C$  is the sample concentration. The intensity of Raman scattering, therefore, depends on several factors such as the laser power and the wavelength or frequency of the incident laser as well as the polarizability of the molecule (Schrader, 1995).

### 2.4. Infrared spectroscopy

Infrared (IR) spectroscopy is a technique based on the absorption of the electromagnetic radiation in the infrared region (Figure 2.2). The IR spectrum can be divided into three sub-regions, namely near-IR (NIR;  $12500 - 4000 \text{ cm}^{-1}$ ), mid-IR ( $4000 - 400 \text{ cm}^{-1}$ ) and far-IR ( $400 - 10 \text{ cm}^{-1}$ ). Photon energies of IR radiation are not high enough to excite electrons, but may excite molecular vibrations (and the associated molecular rotations) of covalently bonded atoms and groups.

At room temperature, a molecule is generally in its ground electronic state where it sits in its ground vibrational state. The absorption occurs when the energy of the incident photons exactly matches that of a vibrational energy transition in the molecule (Drake, 2004). The absorption of energy occurs to excite the molecule to a particular higher vibrational state. A change in the dipole moment of molecule during a vibration is also necessary to induce the absorption process, i.e.  $\delta\mu/\delta q \neq 0$  ( $\delta\mu/\delta q =$  change of the dipole moment  $\mu$  with distortion of the normal co-ordinate  $q$ ).

When a bond with an electric dipole moment is exposed to IR radiation, it will increase its amplitude of vibration. Bonds with a dipole moment that oscillate at discrete

resonant frequencies when exposed to IR radiation are called IR-active. If the resonant frequency of the bond matches the frequency of the incident radiation, interaction will occur leading to absorption.

An IR absorption spectrum of a sample is obtained by passing the IR radiation through the sample and the fraction of the radiation absorbed at each frequency is determined. The frequency at which any peak in the absorption spectrum appears corresponds to the frequency of a normal mode of bond vibration in the molecule (Banwell, 1972). The fundamental vibrational modes are most often observed in the mid-IR region of the spectrum ( $4000 - 400 \text{ cm}^{-1}$ ).

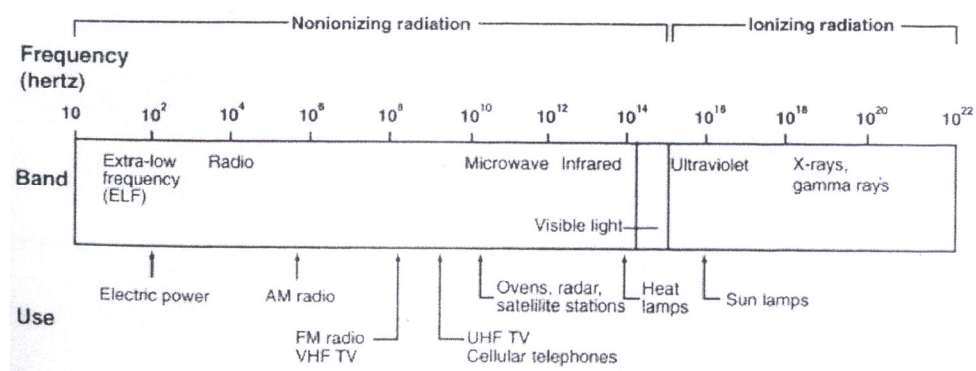


**Figure 2.2. Electromagnetic spectrum (Lang, 1995).**

### 2.4.1. Infrared selection rules

An overall change in the dipole moment of the molecule must occur for it to be IR active. The dipole moment is determined by the magnitude of the difference of charge and the distance between two centres of charge. The absorption will be high if the dipole moment associated with the bond vibration is large (as with highly polar groups of atoms with different electronegativities) and vice versa. A vibration which retains the centre of symmetry of a non-vibrating molecule (e.g. that found in homonuclear species such as O<sub>2</sub>) is termed IR inactive. IR active vibrations are categorised into two types of

vibrations, namely bending and stretching vibrational modes, which are classified depending upon the change of the molecular shape during the vibration with respect to its centre of symmetry. A stretching mode involves a change in the bond length, whereas the bending modes are characterised by the change in the angle of the bond.

Anharmonicity of the vibrations in the IR can cause the occurrence of overtone and combination bands. Overtones (the excitation of a vibration to a double or higher frequency) and combinations that are the sum or difference of two or more fundamental bands are observed in the near-IR region of the spectrum (12500 – 4000  $\text{cm}^{-1}$ ). These features however are less intense than the corresponding fundamental vibrational modes in the mid-IR region of the spectrum.

#### 2.4.2. Quantitative infrared measurements

The absorption of radiation can be calculated through the Beer-Lambert law (Drake, 2004):

$$A = \log (I_0/I_t) = \epsilon.c.l$$

where:

A = Absorbance

$I_0$  = intensity of incident radiation

$I_t$  = intensity of radiation transmitted by the sample

$l$  = path length of the sample

$c$  = molar concentration

$\epsilon$  = molar extinction coefficient/absorption coefficient

The various vibrational modes have different tendencies to absorb with different molar extinction coefficients and therefore they have different intensities in the IR spectrum.

## 2.5. Raman versus IR spectroscopy

Both IR and Raman spectroscopic techniques are complementary rather than supplementary because of their different selection rules. They provide information on molecular structure with regard to molecular vibrations and rotations (for which observation is only possible in the gas phase). In IR spectroscopy, a sample is exposed to IR radiation which it absorbs at only specific energies (one-photon direct process). Raman spectroscopic excitation on the other hand is usually performed at a single wavelength (two-photon scattering process i.e. laser photon and Raman photon). Vibrational modes can be strong in the Raman and weak in the IR and vice versa. To be IR active, a change in the dipole moment of a molecule is required, whereas in Raman spectroscopy, a change in polarizability is necessary. Polar bonds such as carbonyl groups produce the most intense bands in an IR spectrum, whereas non-polar bonds such as C=C tend to be stronger in the Raman spectrum.

Raman spectroscopy has some distinct advantages over IR spectroscopy, mainly due to the fact that it is non-destructive and non-invasive which is particularly very suitable for pharmaceutical studies as it requires minimal or no sample preparation and hydrated specimens, for example, can be analysed without desiccation as normally required for IR spectroscopy. Water and glass are weak Raman scatterers, but they absorb in the IR which favours the use of Raman spectroscopy in the analysis of aqueous solutions and glass can be simply used as a sample container. This allows the analysis of a wide range of sample types (solids, liquids and gases). A Raman spectrometer can be coupled to a probe via an optical fibre for *in situ* and remote analyses.

Fluorescence is a major issue in Raman spectroscopy which frequently arises from the analyte or sample impurities. This phenomenon is associated with the absorption and subsequent emission (approximately  $10^{-8}$ s) of a photon with energy equal to the

difference between two electronic energy levels in the molecule. Non-radiative decay processes occur in the electronically excited state prior to emission. These processes result in a reduction of energy of the emitted photon, in which the frequency of fluorescence emission may coincide with that of the Raman Stokes scattering. Since fluorescence has a higher ( $\times 10^6$ ) quantum yield than Raman scattering, the Raman signal can be easily swamped by a broad fluorescence background signal. Sample fluorescence can be reduced by a careful selection of the laser excitation wavelength used.

Attenuated total reflectance (ATR) IR spectroscopy is also a non-destructive and non-invasive technique but it requires contact with the sample. ATR-IR normally works well with specimens having flat surfaces, whereas Raman spectroscopy can be used to analyse samples with rough surfaces.

In pharmaceutical polymorphic studies, it is essential that the technique is robust and non-destructive to preserve the identity of the specimens. Raman spectroscopy, Fourier Transform ATR and near-IR (NIR) spectroscopy, therefore, were considered to be appropriate spectroscopic techniques for pharmaceuticals in this work.

## **2.6. X-ray powder diffraction**

X-rays lie in the electromagnetic spectrum between the UV and gamma radiation and have approximate wavelengths of 0.1-100 Å. They are generated when electrons are accelerated by an electric field and directed against a metal target, which slows them by multiple collisions. Most of the electrons are not brought to a total stop by a single collision and so a continuum of radiation is formed. X-rays are scattered in various directions by the atomic electrons in the material.

X-rays are reflected from crystals only when the angle between the X-ray and the planes in the crystal fulfil the Bragg equation (van Grieken and Markowicz, 1993) (Figure 2.3):

$$n\lambda = 2d \sin \theta$$

Where  $d$  is the perpendicular spacing between the lattice planes,  $\theta$  is the complement of the angle of incidence of the X-ray beam, also known as Bragg angle and  $n$  is the order of diffraction. If  $n = 1$ , the difference is one wavelength and the diffraction is said to be of first order. If  $n = 2$ , the difference is two wavelengths and the diffraction is second order and so on (Figure 2.3).

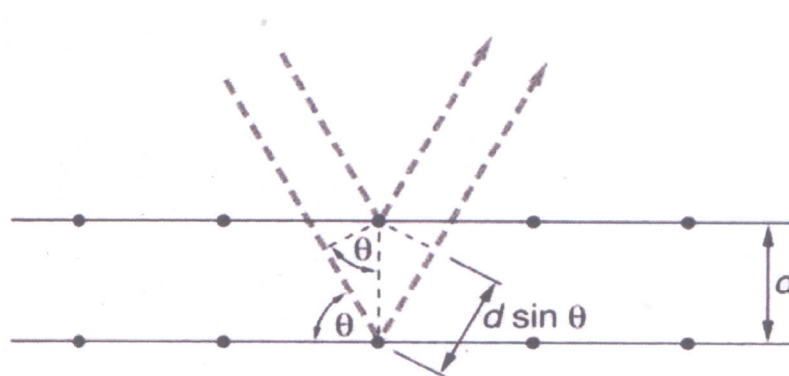


**Figure 2.3. Diagram of Bragg theory of X-ray diffraction showing the Bragg angle  $\theta$ .**

There are many number of diffraction planes possible through the crystal lattice, but only a limited number which give reflections within the range:  $2 < \theta/\text{degrees} < 180$ . Every molecular repetition will give a unique set of reflections and so generate a unique diffraction pattern. Therefore, any polymorph will give a distinctive X-ray powder pattern, making X-ray crystallography of great value for identifying and distinguishing polymorphs.

## **2.7. Differential scanning calorimetry (DSC)**

DSC is used to measure heat flow changes in materials as a function of temperature. As the temperature is raised, phase transformations occur which may be endothermic or

exothermic. The technique may be considered as complementary to TGA (thermogravimetric analysis, concerned with measuring the change in mass of a sample as it is heated, so it is a quantitative rather than a qualitative technique, determining weight loss profiles against temperature or time, in controlled atmospheres). Since many of the changes that are observed do not coincide with weight loss processes, e.g. crystallisation and melting. The industrial uses of DSC are extensive, particularly for polymers, polymorphism, degradation, sublimation and melting point characterisation. Experienced thermal analysts can correctly infer many changes taking place from the breadth, position and intensity of heat flow peaks. However, not all transitions are simple to interpret, and as will be mentioned later in section 2.8.5, complementary molecular information about the heat-induced transitions taking place in a sample should be available through the coupling of DSC with FT-IR and Raman spectroscopy.

## **2.8. Instrumentation**

### **2.8.1. Raman spectrometers**

In general, there are two types of Raman spectrometers, dispersive and non-dispersive. Both differ in the way in which the Raman scattered radiation is analysed. A non-dispersive instrument analyses the Raman scattered radiation in an interferometer, where the beam is split into two components creating a path difference between the source and the signal beam, which interfere when recombined to create an interferogram. The interferogram is then subjected to a Fourier-transform operation to produce the Raman spectrum. In a dispersive instrument, the Raman scattered radiation is spatially separated and dispersed into its constituent wavelengths before reaching the detector. Both types of Raman spectrometers were used during the course of this project and these are discussed in the following sections.

### **2.8.1.1. Fourier-Transform (FT) Raman spectrometer**

A Bruker Fourier-Transform IFS66 optical bench instrument with an FRA 106 Raman module accessory was used in this work (Figures 2.4a and 2.4b). The Nd<sup>3+</sup>/YAG (neodymium-doped yttrium-aluminium-garnet) solid-state continuous wave laser produced a NIR source of excitation wavelength at 1064 nm. At this wavelength, the laser can produce the maximum output of 1 W. The components drawn in broken lines are used only for FT-IR spectroscopy and are not discussed. Spectra were obtained from macroscopic samples placed in the sample holder; an open aluminium sample cup was used for powdered and small-sized samples. The spectral resolution and number of scans required were selected using the instrument software package (Bruker OPUS). To ensure the optimal performance is achieved, the alignment and frequency scale of the instrument were checked before the experiment is undertaken by obtaining a spectrum of sulphur and also routinely corrected using white light produced by a tungsten lamp. Raman spectra were normally recorded in the range 3200 – 50 cm<sup>-1</sup>

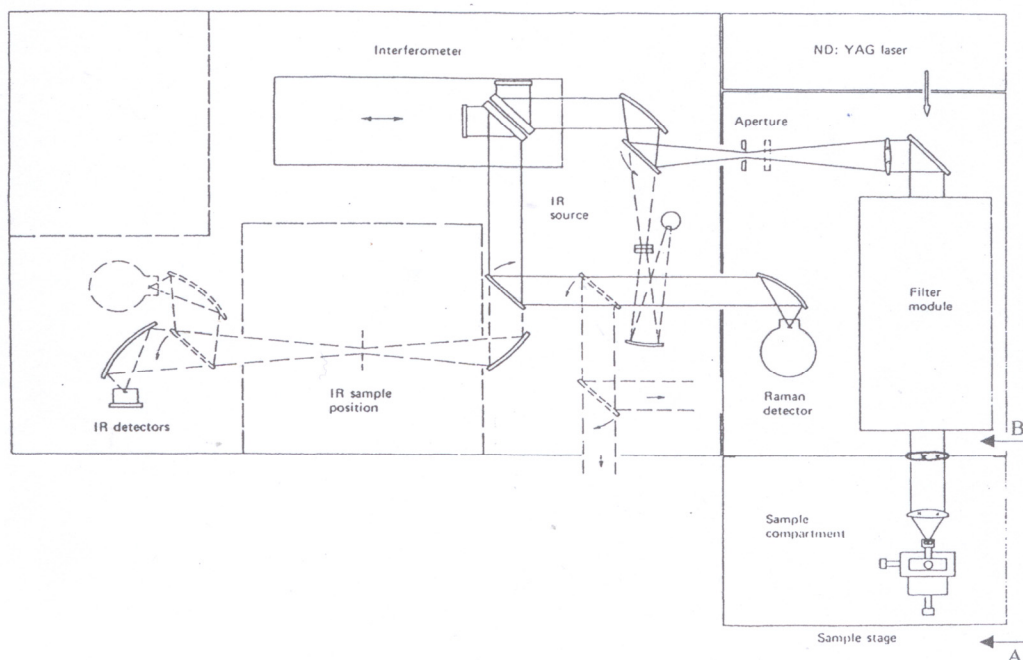


Figure 2.4a. Optical diagram of the Bruker IFS66 spectrometer optical bench with FRA 106 Raman module accessory (Brody, 2000) (Modified from Bruker).

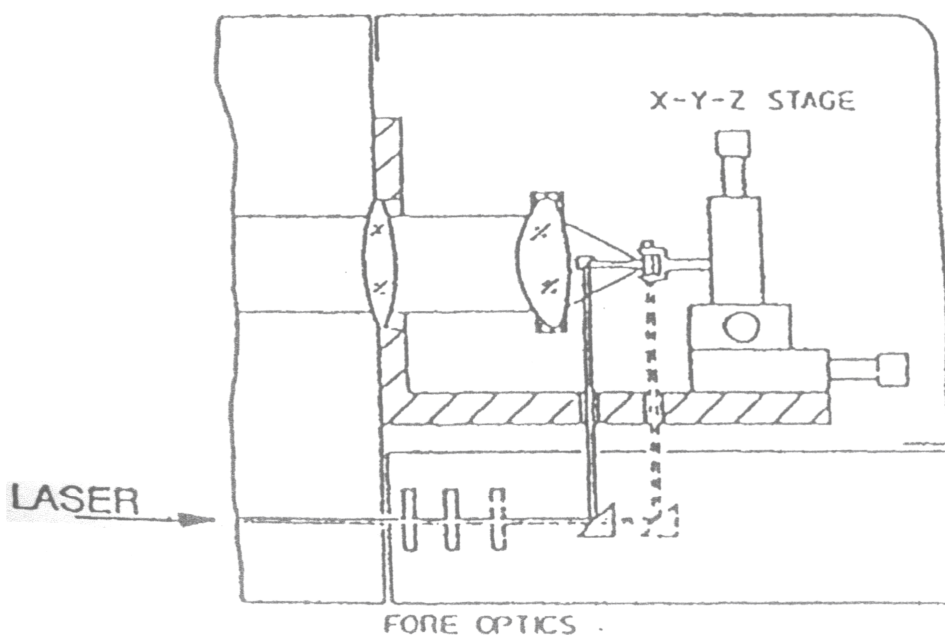


Figure 2.4b. Diagram of the fore-optics-section A-B on Figure 2.4a (Brody, 2000), (Modified from Bruker).

#### **2.8.1.1.1. Standard operation**

The main components of a conventional FT-Raman instrument comprise the laser, collection optics and filters, interferometer and detection system (Chase and Rabolt, 1994). The laser provides a beam of intense, monochromatic radiant energy, which is polarized and coherent (in-phase). In the macroscopic mode, the laser passes parallel to the fore-optics through the base of the FRA 106 bench. The fore-optics contain prisms which turn the laser beam through  $180^\circ$  (known as ‘backscattered’ collection), but since the system is flexible, the collection of  $90^\circ$  scattering from the sample is also permissible. The laser provides a focussed spot diameter of approximately  $100\ \mu\text{m}$  at the sample. The collected scattered radiation from the sample then passes through a filter module which removes the unshifted Rayleigh scattered radiation (i.e. that at  $1064\ \text{nm}$ ). The collection optics and filter are optimized to be optically efficient, as this will control the amount of scattered radiation that will reach the detector.

The filtered radiation passes to an interferometer (Michelson or modified Michelson) where it is modulated. The interferometer splits the radiation beam into paths, which travel different distances. When recombined, the two beams interfere, producing either a constructive or destructive interference pattern. The modulated radiation leaving the interferometer is reflected back into the FRA 106 Raman module and to the FT-Raman detector (a liquid-nitrogen cooled extended range germanium detector), which measures variations in the intensity of the emergent beam as a function of the difference in path lengths. The interferogram, which comprises a number of sinusoidal signals added together, is converted into a Raman spectrum of signal intensity against wavenumber shift by the Fourier-Transform operation.

### **2.8.1.2. Dispersive Raman spectrometers**

Two types of dispersive Raman spectrometers were used in this research; a Renishaw *In Via* confocal Raman microscope and a Renishaw portable Raman analyzer (RX210).

#### **2.8.1.2.1. Renishaw *In Via* confocal Raman microscope**

A Renishaw *In Via* confocal Raman microscope has a variety of laser excitation wavelengths, ranging from the UV to the NIR region of the electromagnetic spectrum, depending upon the installed grating and filters. The excitation sources used during the course of this research were an argon-ion ( $\text{Ar}^+$ ) gas laser (488 and 514 nm), a helium-neon (He-Ne) gas laser (633 nm) and a gallium-aluminium-arsenide (GaAlAs) stabilised diode laser (785 nm). The alignment and frequency scale calibration of the instrument were checked before the experiment as a routine set-up by obtaining a spectrum of a silicon wafer (reference band at  $520 \text{ cm}^{-1} \pm 1 \text{ cm}^{-1}$ ). Samples on glass or steel slides were placed on the microscope stage and the area of interest was focused with the objective lens. Raman spectra were acquired at  $2 \text{ cm}^{-1}$  spectral resolution and recorded normally in the range  $3200 - 100 \text{ cm}^{-1}$ . The required parameters such as spectral frequency range, exposure time of the charged coupled device (CCD) detector and number of spectra to be accumulated were selected using instrument software (Renishaw WiRE<sup>TM</sup>). This software automatically switches the spectrometer to the required excitation wavelength. The filter wheel is rotated if saturation of the CCD detector occurred to reduce the laser intensity at the sample. The use of a confocal microscope can increase the spatial resolution up to  $1 \mu\text{m}$  diameter, which is beneficial for the analysis of a small spot within the specimen.

#### **2.8.1.2.2. Charge-coupled device (CCD) detection**

In the early 1990s the charge-coupled device (CCD) detector was created (Pelletier, 1999). This development greatly increased the speed at which a complete Raman spectrum could be collected but CCD detectors are most suited for lasers with wavelengths of less than 1000 nm, due to the silicon being essentially transparent above 1100 nm. The detector is made up of thousands of pixels, each of which store charge proportional to the number of photons that hit it. Each pixel can only take a limited charge so sometimes the photons overflow, creating peak shape distortion in the spectrum.

#### **2.8.1.2.3. Standard operation**

A schematic diagram of the instrument is shown in Figure 2.5. Laser radiation passes through a filter wheel (1), which can be used to minimise the incident laser power to 50%, 25%, 10% or 1%. The beam is then spectrally (2) and spatially (3) filtered. Once filtered, the laser radiation is directed into the Olympus metallurgical microscope using mirrors (4 and 5) and two holographic notch filters (both labelled 6), as a beam splitter. The laser radiation is focused onto the sample through the objective lens (20x and 50x were used in this project, giving a spot diameter of approximately 3 and 2  $\mu\text{m}$ , respectively, at the sample). The scattered radiation is collected by the objective lens (180° backscattered geometry) and the intense Rayleigh scattered radiation is rejected by two holographic notch filters (6) to prevent it from entering the spectrograph.

The Raman scattered radiation is analysed using a spectrograph, which contains a holographic grating (typically 1200 or 2400 grooves/mm). This scattered radiation is focused through the spectrograph entrance slit (7) and passed via a reflecting prism (8)

to a diffraction grating (9) which disperses the radiation into its constituent wavelengths before reflecting them back to the prism (8) and then onto the CCD detector (10).

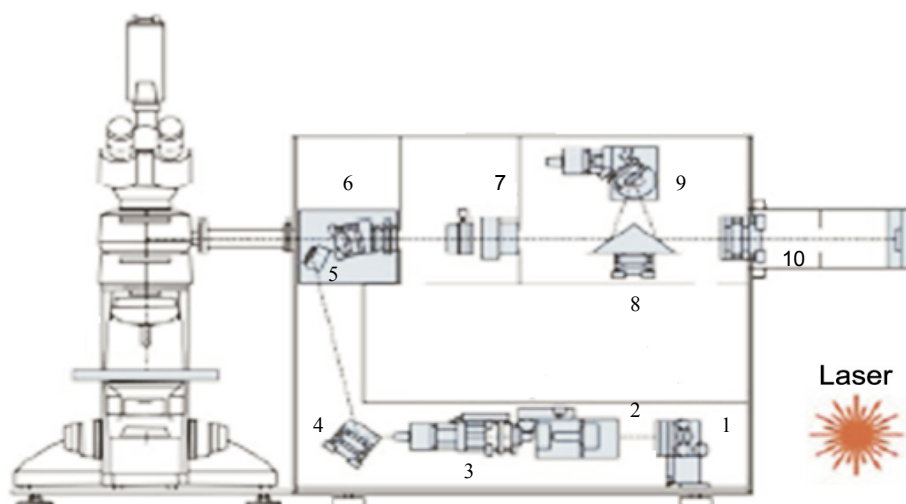


**Figure 2.5. A schematic diagram of Renishaw *In Via* confocal Raman microscope (Source: Renishaw Plc.)**

#### **2.8.1.2.4. Portable Raman analyser**

A Renishaw portable Raman Analyser (RX210) (Figure 2.6) gives a rapid, non-destructive analysis by Raman spectroscopy in a compact portable unit. This instrument is also known as the prototype RIAS or ‘Raman In A Suitcase’. Because of its portability, versatility and real-time analysing capability it can be used in conjunction with other analytical instruments for pharmaceutical applications. The Renishaw RX210 spectrometer operates at 785 nm in the NIR region, produced by a diode laser with a spectrograph coupled to a thermoelectrically cooled CCD detector and holographic grating (Figure 2.6). An attached fibre-optic probe was equipped with an x20 objective lens. The diffraction grating (1000 lines/mm) limits the spectral range to  $\sim 2100$ - $100$   $\text{cm}^{-1}$  with a spectral resolution of  $10$   $\text{cm}^{-1}$ . The maximum output power of the diode laser at the source is 500 mW and  $\sim 50$  mW at the sample. Daily wavenumber

calibration is required and is achieved by recording the Raman spectrum of silicon (1 accumulation, 10 s) for static mode. If necessary, an offset correction is performed to ensure that the position of the silicon band is  $520.5 \pm 0.10 \text{ cm}^{-1}$ . Spectra were recorded with a single scan, 10s exposure. To avoid the interference from white light (i.e. room light), the system was covered with a shroud. Spectra were not corrected for the instrument response. The spectrometer was controlled by a portable PC with commercial instrument control software (Renishaw WiRE 2 Service Pack 8).

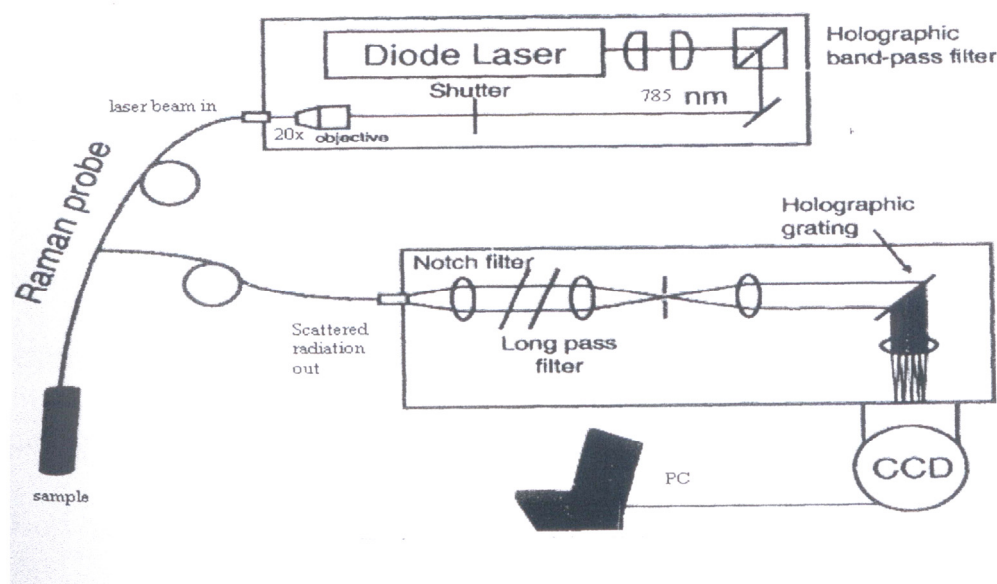


**Figure 2.6. A schematic diagram of Renishaw portable Raman analyser (RX210) (Source: Renishaw Plc.)**

### 2.8.1.3. Dispersive versus non-dispersive Raman spectrometers

The use of either a dispersive or non-dispersive Raman spectrometer is not just a matter of choice since both instruments depend on many factors such as the nature of the sample to be analysed, e.g. fluorescent or non-fluorescent and the time scale for the analysis. Both systems fundamentally give the same spectrum from a given sample but may differ in the quality of the spectra obtained. The careful selection of the instrument

type which can give optimal performance therefore, is necessary prior to performing an experiment in order to obtain a high quality Raman spectrum.

A non-dispersive FT-Raman spectrometer normally uses 1064 nm laser excitation, whereas a dispersive Raman spectrometer uses multiple laser excitation wavelengths ranging from the UV to NIR. With 1064 nm excitation, the energy of the radiation is lower than that of electronic transitions from the ground state in most molecules; therefore the electronic excited state is rarely populated. In contrast, at the lower wavelengths of excitation used in dispersive instruments, the high energy of photon/radiation involved can initiate fluorescence, which is more intense than the Raman signal, as well as resulting in the possibility of sample photodegradation. Sample heating in the FT-Raman system may also interfere with the Raman spectrum but this normally occurs when higher laser power levels are used.

Higher Raman spectral intensities can be collected by decreasing the wavelength (increasing the frequency) since the band intensity is directly proportional to the fourth power of the frequency of the incident radiation. Therefore, the more intense spectrum, i.e. larger Raman scattering, is generally obtained within shorter acquisition times using the dispersive Raman spectrometer. It also offers higher sensitivity with the use of low noise CCD detectors in contrast to the relatively high noise level and low sensitivity of the germanium detector. The scattered radiation is dispersed by the diffraction grating across an array of pixels on the CCD detector and the intensities of radiation incident at all frequencies on the CCD is analysed simultaneously (multichannel advantage).

In non-dispersive spectrometers, with no slits, fewer optical elements and the use of the interferometer, the scattered radiation is not spatially separated (multiplex/Fellgett advantage) as it is in dispersive instruments, in which a spectrograph with a diffraction grating separates the radiation into individual wavelengths. This allows a high

throughput of scattered radiation to the detector (known as the Jacquinot advantage) (Hendra et al., 1991). The simultaneous measurement offered over the whole spectral range results in an improved signal-to-noise ratio. The FT-system also offers a constant spectral resolution over the whole spectral range covered.

With dispersive instruments, frequency precision and accuracy depend on the calibration being effected with external standards and the ability of the electromechanical mechanisms to uniformly move gratings and slits during and between scans, where, during this process, displacement error can sometimes occur due to mechanical wear, resulting in band shape distortion and low signal-to-noise ratios. In contrast, the interferometer has an internal frequency standard provided. As a result, the wavenumber calibration of the interferometer is more accurate as well as having longer term stability than that of the dispersive instruments. This is known as the Connes advantage (Hendra et al., 1991).

Since, both types of spectrometers were available during the course of this research, a range of pharmaceutical samples were analysed using several instruments at various excitation wavelengths.

### **2.8.2. Infrared spectroscopy**

Two types of IR instruments were used in this research, namely a Scimitar series Digilab UMA-400 FT-IR spectrometer and Bruker Optics MPA<sup>TM</sup> FT-NIR spectrometer.

### **2.8.2.1. Scimitar series Digilab UMA-400 FT-IR spectrometer**

The Varian Scimitar series FT-mid-IR spectrometer's components comprise the radiation source, interferometer and detector. The interferometer (Michelson) consists of three active components, a moving mirror, a fixed mirror and a beam splitter. Radiation from the broadband IR source is directed into the interferometer, and imaged on the beam splitter. At the beam splitter, half the IR beam is transmitted to the fixed mirror and the remaining half is reflected to the moving mirror. After the separated beams are reflected from the two mirrors, they are recombined at the beam splitter. Due to changes in the relative position of the moving mirror to the fixed mirror, an interference pattern is generated. The resulting beam then passes through the sample and is focused on the Mercury Cadmium Telluride (MCT) detector.

When the mirror is moved at constant velocity, the intensity of radiation reaching the detector varies in a sinusoidal manner to produce the interferogram. The interferogram is the record of the interference signal. If the sample happens to absorb at this frequency, the amplitude of the sinusoidal wave is reduced by an amount proportional to the amount of sample in the beam. The interferogram contains information over the entire IR region to which the detector is responsive. Fourier-transformation converts the interferogram into the final IR spectrum.

For attenuated total reflectance (ATR) measurements, the Varian 400 UMA microscope is attached to the spectrometer and Specac Silver Gate™ single reflection germanium crystal ATR is used with the depth of penetration of 0.7  $\mu\text{m}$ . ATR technique relies on total internal reflection which sample is brought into direct contact with the crystal (known as internal reflection element, IRE), which has a higher refractive index than that of the sample. When the angle of incidence of the light from the IRE to the sample exceeds the critical angle, total internal reflection takes place, allowing the light

to penetrate slightly into the sample, producing an absorbance-like spectrum. A simplified optical layout of a typical ATR-FTIR is represented in Figure 2.7. In this work, both transmission and ATR techniques were used and this system was controlled by the instrument software (Digilab Win-IR Pro 3.4). The software was set to remove the absorption peak of CO<sub>2</sub> and a background spectrum was collected prior to the experiments being conducted. Spectra were recorded in the range 4000 – 400 cm<sup>-1</sup>.

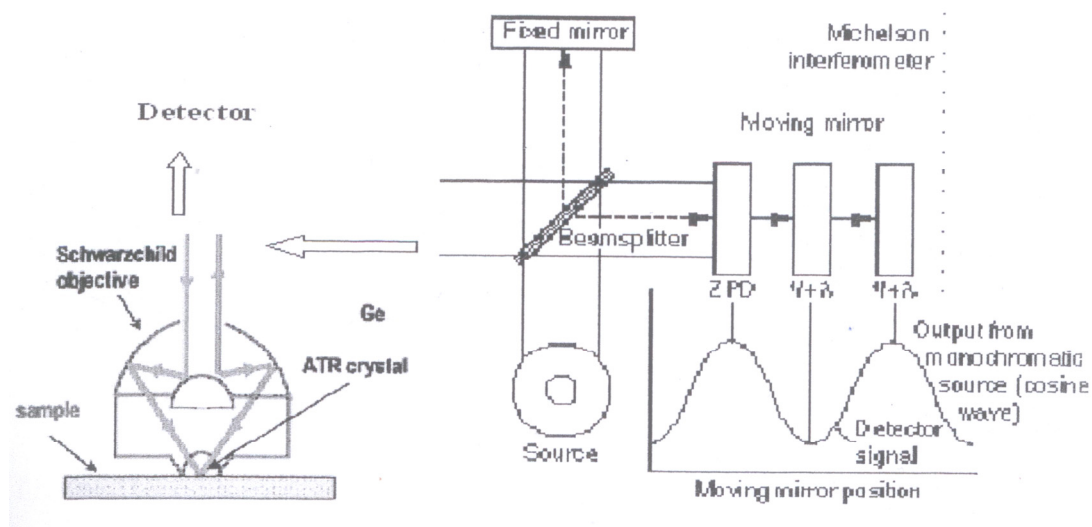


**Figure 2.7. A simplified optical layout of a typical ATR-FTIR spectroscopy (modified from (Sherman Hsu, 1997)).**

### 2.8.2.2. Bruker Optics MPA<sup>TM</sup> FT-NIR spectrometer

A Bruker Optics MPA (Figure 2.8) is a multi-purpose analyser, combining flexibility and the power of FT-NIR spectroscopy. The spectrometer allows both transmission and diffuse reflectance measurements to be carried out. It comprises filter, grating and interferometer, which is equipped with gold-coated optics and an indium gallium arsenide (InGaAs) detector. A thirty-position sample wheel can be used for automated sampling and an optical fibre probe is also available for remote analysis. For instrument calibration, the background spectrum was routinely collected before the experiment was undertaken. The spectral resolution and number of scans required were

optimized using the instrument software package (Bruker OPUS). In this work, samples were inside USP vials, placed on the sample stage and analysed in diffuse reflectance mode. Spectra were recorded in the range  $12500 - 4000 \text{ cm}^{-1}$  ( $2500 - 800 \text{ nm}$ ).



**Figure 2.8. Bruker optics MPA<sup>TM</sup> FT-NIR spectrometer (Source: The Bruker Optics Inc.)**

### **2.8.3. X-ray powder diffractometer**

Powder *X*-ray diffraction data were recorded with a Bruker D8 diffractometer (Figure 2.9) with Cu-K $\alpha_{1,2}$  radiation ( $1.5418 \text{ \AA}$ ) and a secondary curved graphite monochromator. The *X*-ray tube was operated at 40 kV and 30 mA. Samples were scanned in a vertical Bragg-Brentano ( $\theta/2\theta$ ) geometry (flat reflection mode) from  $5-40^\circ$  ( $2\theta$ ) using a  $0.005^\circ$  step width and a 1.5 s count time at each step. The receiving slit was  $1^\circ$  and the scattering slit was  $0.2^\circ$ . Data were analysed with Bruker AXS Topas 2.1 software including a correction for axial divergence. Background coefficients, cell parameters, sample displacement error and phase fractions were optimised parameters.

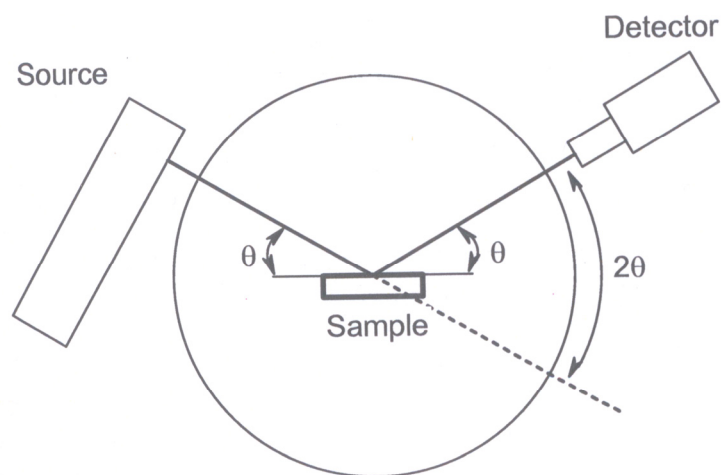


**Figure 2.9. Schematic diagram of a typical X-ray powder diffractometer.**

#### **2.8.4. Differential scanning calorimeter**

DSC profiles were generated in the range of 50 to 220°C using a TA Instrument, DSC Q2000 apparatus operating in the PCA mode with an RSC90 cooling unit. Temperature calibration was performed using an indium metal standard at the respective heating rate. Accurately weighed samples (1.5 – 2.5 mg) were placed in Tzero aluminium pans using a similar empty pan as a reference. A scanning speed of 10 °C min.<sup>-1</sup> was employed.

#### **2.8.5. The simultaneous *in situ* Raman –DSC set up**

In this research work, an assembly of the fibre-optic coupled portable Raman spectrometer and DSC instrument was used (Figure 2.10) for the simultaneous *in situ* investigation of the solid-state polymorphic transformation of salmeterol xinafoate and sulfathiazole polymorphs.

For establishing thermal treatments, 1.5 – 2.5 mg of the samples was placed in Tzero aluminium pans. The sample and reference pans were run in an open configuration without the use of lids and the cell of the instrument was covered with specially

engineered lids and a quartz window to allow the acquisition of the Raman signals simultaneously.

Following thermal preparation, Raman spectra were collected with samples held isothermally for 1 minute at the temperatures of interest. DSC melting curves were run simultaneously with Raman spectral scanning. The probe laser radiation could have a heating effect on the sample but the emerging lower power of 25 mW laser beams from the fibre-optic probe is divergent, giving a greatly reduced power density spread over the sample surface. Raman spectra collected during the temperature-transformation experiments showed changes coincident with changes in DSC heating curves, confirming that any heating effect arises from the bulk of the sample and not from just the surface layer.



**Figure 2.10. An assembly of the fibre-optic coupled portable Raman and DSC.**

## **2.9. Spectral conversion and manipulation**

Several spectral manipulation methods were employed to the vibrational spectra in this work. Spectral manipulation refers to mathematical transformation of the original

spectra by using specific software. All vibrational spectra were exported to the Galactic\*.SPC format using GRAMS AI (Galactic Industries, Salem, NH, Version 8.0). Several techniques of spectral manipulation were used; the principal ones being baseline correction, smoothing, deconvolution and integration of peak areas which have been done using GRAMS AI package.

### **2.9.1. Baseline correction**

Background in vibrational spectra is common and arises from either luminescence processes (fluorescence), non-laser-induced emissive processes (room lights) or Raman scattering from optics or solvents (Shaver, 2001). The background can be removed by employing baseline correction, i.e. by selecting multiple points through which a straight line or curve is drawn. The resulting curve is then subtracted from the original spectrum.

### **2.9.2. Smoothing**

‘Noise’ in a spectrum can be diminished by a smoothing process. After a spectrum is smoothed, it becomes similar to the result of an experiment carried out at a lower spectral resolution. A smoothing function is basically a convolution between the spectrum and a vector whose points are determined by the degree of smoothing applied. The Savitzky-Golay smoothing algorithm was used in this research with seven smoothing points and a second order polynomial. The algorithm is based on performing a least squares linear regression fit of a polynomial around each point in the spectrum to smooth the data.

### **2.9.3. Deconvolution**

Deconvolution is the process of compensating for the intrinsic line widths of bands in order to resolve overlapping bands (Kauppinen et al., 1981). This technique yields spectra that have much narrower bands and is able to distinguish closely spaced features. The instrumental resolution is not increased, but the ability to differentiate spectral features can be significantly improved.

### **2.9.4. Integration of peak areas**

The band area integration is performed using the trapezoidal rules. The area under the peak is separated into trapezoids; the ends are made equal by the use of baseline correction.

## **2.10. Computational chemistry**

Computational chemistry encompasses not only quantum mechanics, but also molecular mechanics, minimisation, simulations, conformational analysis and other computer-based methods for understanding and predicting the behaviour of molecular systems (Leach, 2001). In this work, we are interested in molecular properties such as vibrational spectra so we will focus on the use of quantum chemical calculations applicable to these types of problems.

Hartree-Fock (HF) methods increase the accuracy of prediction for vibrational spectra but scale as a function of the number of electrons in the system and become unwieldy for large systems (Young, 2001). Density functional theory (DFT) calculations improve on the accuracy of HF methods but are similarly unwieldy for many-atom (>100 atoms) systems.

Fundamentally, the calculations try to determine the energetics of the molecular conformations. HF is an *ab initio* method that accomplishes this by getting as close as possible to a solution of the Schrödinger equation for the molecular system of interest. The Schrödinger equation is given as:

$$\hat{H}\Psi = E\Psi$$

This equation states that the energy of the system (E) is derived from the operation of the Hamiltonian operator ( $\hat{H}$ ) on the wave function ( $\Psi$ ), a function of the nuclei and electrons in the system. An advantage of the quantum methods is that they provide insight into electronic structure in the sense of electron distributions; these are often very important in terms of reactivity of the system of interest. The output of the calculations describes the electronic structure in terms of molecular orbitals. The orbitals are constructed from mathematical functions, called basis functions, which when grouped for the purposes of the calculation are called a basis set. The more functions present in the basis set the better the representation of the orbitals. However, the greater the number of functions in the calculation, the greater the resources required to accomplish the output. In fact, calculations scale as the number of basis functions to the fourth power – thus the more basis functions employed, the more resources the calculation requires (Jensen, 2007). The Hamiltonian operator ( $\hat{H}$ ) yields the energy by considering the energy in a molecule to be made up of a series of interactions:

$\hat{H} =$  - Kinetic energy of electron

- Potential energy between electrons and nuclei

+ Potential energy between electrons

+ Potential energy between nuclei

The attractive forces are negative and the repulsive forces are positive in this equation. The HF method, however, has an intrinsic weakness in its approach. This lies

in the way in which the potential energy between electrons (a repulsive force) is determined. HF methods use the central field approximation, which takes an advantage for the electron-electron repulsion and uses that value in  $\hat{H}$  and does not determine the specific electron-electron interactions. This is clearly not physically realistic. The situation where the electrons are far from each other should be more probable as the electron-electron repulsion is less; the consideration of the explicit interactions between electrons is called electron – electron correlation. The absence of this correlation means that HF methods always carry an intrinsic error.

A more practical approach to improving accuracy of calculations for the medium-to-large systems is density functional theory (DFT) (Jensen, 2007). In such calculations some aspects of electron – electron correlation are included. DFT has come to dominate computational chemistry of medium-to-large molecules, including pharmaceuticals (Young, 2001) so it has been used throughout this work.

In determining geometries, the molecule is varied until a local or global energy minimum is obtained. Once the structure is calculated it is possible to test if the calculation is accurate. One way to do this is to compare the calculated structure with a known crystal structure. Generally, DFT and HF methods perform well in structural comparisons with experimental data. Another way is to use the information from the calculation to evaluate other observables, such as the dipole moment or vibrational spectra of the compound of interest. The vibrational spectra are useful observables because they are relatively easy to measure on samples for which crystallographic data may be absent (Foresman and Frisch, 1996).

Vibrational spectroscopy offers a good method of determining how accurate a calculation is for a number of reasons. Firstly, the values for the band frequencies are evaluated through the gradients of the energy (E) of the nuclear potential energy

surfaces (PES) for the vibrational modes of the molecule ( $q$ ), which is  $\delta E / \delta q$ . For this to correlate with experimental data, the calculation must reproduce the stiffness of the bonds in the molecule. Secondly, the relative intensities of vibrational spectra are related to the PES and its interaction with external electric fields and geometry changes caused by vibrational motion. For example the IR intensities are determined by the change in the dipole moment ( $\mu$ ) with vibrational mode ( $\delta\mu/\delta q$ ). To calculate this correctly the modelling must not only accurately predict the dipole but also how it changes with vibrational modes (e.g. bond stretching). For Raman spectroscopy, the Raman intensity is related to the change in polarizability ( $\alpha$ ) with vibrational mode ( $\delta\alpha/\delta q$ ). The polarizability of the molecule is related to the elasticity of the electron field in the system. These are related to the energy of the system in the following ways (Jensen, 2007). For IR intensity  $(\delta\mu/\delta q)^2 = (\delta^2 E / \delta R \delta F)^2$ , where R is the change in geometry and F is the electric field strength. For Raman intensity  $(\delta\alpha/\delta q)^2 = (\delta^3 E / \delta R \delta F^2)^2$ , thus the Raman intensities require the energy of the system to be known with respect to geometry change and the effect of the external electric field. Importantly, if there is good correlation between the calculated properties, such as electronic potentials and molecular orbitals (MOs), may also be good representations and thus provide predictive power to the analyst examining these data. The nature of the MOs and electrostatic potentials are important parameters used to study pharmaceuticals and the properties of such compounds.

### **3.1. Introduction**

Raman spectroscopy is experiencing renewed interest in pharmaceutical applications, with a wide field of applications ranging from the characterization of drug formulations to on-line process analysis encompassing qualitative, quantitative and physical analysis. Physical analysis has involved the identification of polymorphism, hydrates and amorphous mixtures. Characterisation of simple powders has been extended to complex pharmaceutical formulations, including tablets, capsules, injection solutions and suspensions. Formulations have also been analysed through their packaging. The characteristics of the Raman spectroscopic technique make it ideal for process monitoring and it has been used to quantify changes *in situ* during pharmaceutical unit operations. These areas are described in the following subsections, with potential future uses of Raman spectroscopy also indicated. The literature contains several reviews on the uses of Raman spectroscopy in the pharmaceutical field (Angel et al., 1999; Bugay et al., 2007; Chalmers and Dent, 2006; Fini, 2004; Pfeffer-Hennig and Bellus, 2004; Pinzaru et al., 2004; Sandler et al., 2007; Vankeirsbilck et al., 2002; Wartewig and Neubert, 2005; Williams, 2001).

### **3.2. Characterisation and detection of pharmaceuticals**

A wide range of applications of Raman spectroscopy is evident for the characterisation of drug molecules either alone or in various dosage forms, in complexation with various metals and  $\beta$ -cyclodextrin derivatives, as co-crystals and using quantum chemical calculations have been presented in the literature.

The absence of the need for sample preparation and short spectral acquisition times make Raman spectroscopy particularly suitable for high-throughput identity verification of pharmaceutical compounds. Recently, quantum chemical calculations in conjunction

with Raman spectroscopy have been used in studying pharmaceutical systems. One reason to combine computational methods with spectroscopic data is that spectroscopy provides a method of testing the efficacy of the calculations. The accurate prediction of the frequency and intensity of vibrational bands suggests a well modelled potential energy surface. This in turn provides more confidence for the assignment of other predicted parameters. In this way it is possible for quantum chemical calculations to assist quality control development in the same way that it has facilitated drug discovery for many years. Table 3.1 presents a list of pharmaceutical systems studied by Raman spectroscopy and computational methods, within the Table, the pharmaceutical compound is presented along with the methods utilized, and a citation.

Raman spectra can be obtained noninvasively from solids and liquids inside vials or blister packs. McCreery et al. have reported the use of NIR Raman spectroscopy for identification of pharmaceuticals inside amber USP vials. Although the amber glass greatly attenuates the signal, spectra of sufficient quality were obtained for the determination of vial contents with 1-60 s integration. Identification was performed using a library of spectra and ranged in accuracy from 88% to 96%. Most of the errors were due to fluorescent emission in the samples. When these samples were omitted, a marked improvement in accuracy of the search algorithm resulted (McCreery et al., 1998). This work has demonstrated the potential of Raman spectroscopy for on-line process monitoring.

The superior ability of Raman spectroscopy to characterize the stretching modes of the C-H bond compared with IR spectroscopy has been demonstrated for several compounds of pharmaceutical interest (Cutmore and Skett, 1993). Raman spectra can be recorded directly from TLC plates with no need for special treatment of either the samples or the plates (Petty and Cahoon, 1993).

Raman spectroscopy has been used to investigate the metal complexes of ibuprofen, naproxen, tolmetin, diclofenac sodium (Trincherro et al., 2004), allopurinol (Torreggiani et al., 2003), suprofen (Williams, 2000), cimetidine (Baranska and Proniewicz, 1999), piroxicam (Santi et al., 1993; Wagner and Baran, 1999), insulin-mimetic complex (Muglia and Baran, 2000), the  $\beta$ -cyclodextrin inclusion complexes of tolbutamide (Ueda and Nagai, 1981; Veiga et al., 2001; Veiga et al., 1996) and the anti-inflammatory drug loxoprofen (Choi et al., 2001) and the hydroxypropyl-  $\beta$ -cyclodextrin inclusion complexes of sertaconazole (Rodriguez-Perez et al., 2006), and progesterone (Zoppetti et al., 2007). The characterisation of the indomethacin-saccharin (Basavoju et al., 2008), norfloxacin-isonicotinamide (Basavoju et al., 2006) and carbamazepine-nicotinamide (Rodriguez-Hornedo et al., 2006; Seefeldt et al., 2007) cocrystals by Raman spectroscopy have also been reported.

### **3.3. Solid-state properties**

One clear advantage of Raman spectroscopy for the study of the solid-state forms of pharmaceuticals is that the technique can probe the low frequency lattice vibrations (100 to 150  $\text{cm}^{-1}$ ) that are associated with molecules in the crystalline state. Many drugs exhibit polymorphism, different molecular arrangements within a crystal lattice. Different polymorphic forms have different lattice energies with consequent deviations in properties such as melting point, solubility, dissolution rate, and bioavailability. Thus, the characterisation of polymorphism in new chemical entities (and in some existing therapeutic agents) is of great importance. Although X-ray data remains the prime method for deducing the presence of polymorphs, Raman spectroscopy can provide rapidly some valuable complementary information. It is worth emphasizing that X-ray data are time-consuming to collect and are clearly an off-line method, whereas

Raman spectroscopy has the potential of providing relevant information *in situ* or in at-line analysis. Table 3.2 presents a list of polymorphic systems studied by Raman spectroscopy; within the Table, the pharmaceutical compound is presented along with a brief comment, and a citation.

With some crystalline solids, solvent in the surrounding medium may become incorporated into the crystal lattice of the compound in stoichiometric proportions. These molecular adducts are termed solvates. Hydrates are formed when water is the solvent of crystallization. Incorporation of the solvent molecules into the crystal lattice produces a new unit cell different from that of the anhydrate and, consequently, the physical properties of the solvate may differ from those of the anhydrate. To distinguish solvates from polymorphs, the term pseudopolymorphs has been applied to solvates (Giron, 1995). Raman spectroscopy has been used to identify and characterize the anhydrate and monohydrate forms of baclofen (Mirza et al., 2007), the anhydrate form of norfloxacin (Info et al., 2006), paroxetine hydrochloride hemihydrate (Thorley et al., 2006), the non-stoichiometric hydrates of ester type local anesthetics (Schmidt and Schwarz, 2006), the two anhydrous phases and water:DMSO solvate of olanzapine (Polla et al., 2005), the hydrated and anhydrous crystal forms of amlodipine besylate (Rollinger and Burger, 2002), amoxicillin trihydrate (Cutmore and Skett, 1993), five solvates of spironolactone (Beckstead et al., 1993), griseofulvin and its solvates (Bolton and Prasad, 1981), risedronate hemi-pentahydrate (Lester et al., 2006), and the mono and sesquihydrates of pantoprazole sodium (Zupancic et al., 2005).

Amorphous forms, where the drug molecules show minimal order, are also of considerable importance because these systems show more rapid dissolution than crystalline forms. Additionally, there are issues concerning stability where the amorphous system may be hygroscopic and the presence of moisture could induce re-

crystallization of the material to provide a crystalline form of the drug. Raman spectroscopy has been used to study the amorphous forms of blends of paracetamol and citric acid (Pekka et al., 2007), indomethacin (Savolainen et al., 2007a) and lactose (Katainen et al., 2005).

Salt selection for a pharmaceutical compound is a critical component of drug development because the selection of the wrong salt can lead to chemical and physical stability issues as well as formulation problems. Raman spectroscopy has been used to study the molecular nature of the organic salts of norfloxacin with succinic acid, malonic acid and maleic acid (Basavoju et al., 2006) and the salts crystallized from a salbutamol base (Edwards et al., 1993a), where variations in vibrational frequencies due to electron withdrawing or donating substituents were clearly evident; for example, the C-C-O stretching vibration shifted from  $776\text{ cm}^{-1}$  in the free base to  $756\text{ cm}^{-1}$  in the benzoate salt. The C=C stretching frequency also shifted from  $1610$  to  $1603\text{ cm}^{-1}$  with the benzoate ion but showed an increase to  $1616\text{ cm}^{-1}$  with sulfate ion. Clearly the choice of salt affects the molecular nature of the drug with obvious implications for its physico-chemical properties.

### 3.4. Quantitative applications of Raman spectroscopy in various pharmaceutical systems

Raman scattering is proportional to the concentration of the scattering substance, and this provided the basis for quantitative Raman spectroscopy. The intensity of spontaneous Raman scattering in an ideal (non-absorbing) system during a particular vibration can be defined as:

$$L = P_D \beta D K$$

where  $L$  is the specific intensity of the Raman scattering ( $\text{photons sr}^{-1} \text{ cm}^{-2} \text{ sec}^{-1}$ ),  $P_D$  is the power density of the incident laser radiation ( $\text{photons cm}^{-2} \text{ sec}^{-1}$ ),  $\beta$  is the differential Raman scattering cross-section per  $\text{cm}^3$  and  $K$  is a geometric factor that depends on the observation geometry (incident and detection angles) (McCreery, 2000). The most important feature of the previous equation in this context is that the intensity of Raman scattering of a particular mode is directly proportional to the vibrating species concentration (described by  $D$ ). Although the Raman scattering occurs over the bandwidth of the mode and hence a frequency range, proportionality is maintained at a single Raman shift as described by McCreery (McCreery, 2000). This relationship provides the basis for quantitative Raman spectroscopy.

In solid-state analysis, peak intensities, or peak areas were determined for quantification after baseline correction (Kontoyannis, 1995). When chemometric methods based on Partial Least Squares (PLS) regression and multivariate calibration were developed for quantitative determination, a better accuracy of prediction became possible. For multivariate calibration not only one data point but a complete spectral structure is used for calibration and modelling. Compared to univariate calibration characteristic peaks are dispensable. Thus, in recent years this technique has become popular (Dyrby et al., 2002; Szostak and Mazurek, 2004). Further advances were

achieved by Principal Component Analysis by which only reduced spectral information is used for calibration (Mazurek and Szostak, 2006b; Pratiwi et al., 2002; Szostak and Mazurek, 2002).

Quantitative Raman spectroscopy has been used in diverse applications in pharmaceutical analysis. An exhaustive review by Strachan et al (Strachan et al., 2007b) provided good survey of the quantitative Raman spectroscopic analysis of pharmaceutical solids. Table 3.3 presents a list of pharmaceutical compounds studied by quantitative Raman spectroscopy, within the Table, the pharmaceutical compound is presented along with a brief comment, and a citation. Chemical applications have mainly involved quantifying active pharmaceutical ingredients, while physical characterisation has covered polymorphism, hydrate formation and crystallinity. Initially, simple binary powder mixtures were quantified but this has since extended to complex formulations, including tablets, capsules, microspheres, ointments, injection solutions and suspensions as in Table 3.3.

### **3.5. Process pharmaceutical applications**

As far as industrial applications are concerned, the Raman spectroscopic technique is really promising because the spectrometers traditionally used in the laboratory may be displaced to the industrial environment in a remote manner through the use of fibre-optic probes. *In situ* measurements can thus be ensured for a number of applications. Moreover, Raman techniques are well suited for measurements through glass or plastic media and can be performed within inhomogeneous media, which avoids difficulties and uncertainties related to sampling for off-line analysis.

Rantanen (Rantanen, 2007) has reviewed the process analytical applications of Raman spectroscopy, where different applications of Raman spectroscopy in the field of

process analysis of pharmaceutical solid dosage forms are summarized. In addition, the pitfalls associated with interfacing to the process environment and challenges within data management are discussed. Févotte (Févotte, 2007) has reviewed the real-time use of Raman spectroscopy for monitoring solid pharmaceutical elaboration processes with a particular attention on the in-line monitoring of crystallization processes.

NIR absorption spectroscopy is characterised by strong OH absorption so that solid state transitions cannot always easily be identified when using this technique in the presence of water. On the contrary, water is a weak Raman scatterer, which makes the technique attractive for many pharmaceutical applications involving aqueous media such as the monitoring of wet granulation of theophylline and caffeine (Jørgensen et al., 2002), and the freeze drying processes of mannitol (Romero-Torres et al., 2007).

Spray coating is an important unit operation in the pharmaceutical industry. El Hagrasy et al. have utilized a noncontact Raman fibre-optic probe for the in-line monitoring of the progress of coating from process measurements (El-Hagrasy, 2006). Romero-Torres et al. have quantitatively characterized the coating variation in tablets using Raman spectroscopy with a revolving laser focus combined with PLS multivariate analysis (Romero-Torres et al., 2005) and created a predictive tablet coating thickness quantification models in the presence of a strong broad-band fluorescence interference (Romero-Torres et al., 2006). The Raman spectra of a set of coated acetaminophen tablets were analyzed for the purpose of calibrating the spectra to tablet coating thickness (Kauffman et al., 2007).

There is a very wide range of process pharmaceutical applications of Raman spectroscopy available in literature ranging from monitoring of solvent-mediated polymorphic transitions to quantitative reaction monitoring, in Table 3.4, the various pharmaceutical systems that have been studied by Raman spectroscopy as a PAT

technique with a brief comment on the special role achieved by Raman spectroscopy have been presented.

### **3.6. Interactions**

Interactions between drugs and excipients play an important role during the development of a new pharmaceutical formulation. The problem of chemical or physical interactions exists for all dosage forms. Raman spectroscopy has been proven to be an important tool in evaluating the drug and excipient interactions. Flemming and Picker-Freyer have studied the compaction of spray dried lactose or anhydrous lactose with acetylsalicylic acid, nicotinamide and thiaminchloride hydrochloride (Flemming and Picker-Freyer, 2008). The drug-excipient interaction in ketoprofen with lactose and polyvinylpyrrolidone was reported, these interactions were found to involve mainly the central carbonyl group and the terminal methyl-carboxylic moieties of the ketoprofen molecule, this being reflected in particular vibrational modes, such as the methyl torsion, the out-of-plane C-OH bending, and the inter-ring C=O stretching. (de Carvalho et al., 2006). A Raman spectroscopic study of diclofenac sodium and  $\beta$ -cyclodextrin interaction was also reported (Iliescu et al., 2004).

The use of Raman spectroscopy to study drug polymer interactions has been reported. The interactions of diclofenac sodium with ammonio methacrylate (Sipos et al., 2008), clotrimazole with polyethylene oxide (Todica et al., 2007), indomethacin with polyvinylpyrrolidone (Taylor and Zografi, 1997), sulfthiazole with povidone (Bolton and Prasad, 1984) and probucol with polymers (Broman et al., 2001) have been presented. Hendra et al. have studied the interactions of diclofenac sodium and sympathomimetic amines with biomedical polymers (Hendra et al., 1990), and promethazine, diclofenac, theophylline and indomethacin in polymeric diluents based

on polyethylene oxide, sodium alginate and hydroxypropylmethyl cellulose (Davies et al., 1990).

Raman spectroscopy has been used to study the interactions of the antimalarial drugs, chloroquine and mefloquine with hematin (Cinta-Pinzaru et al., 2006), antimicrotubular agent with cysteine (Bouchaour, 1986), lecithin with cholesterol (Tantipolphan et al., 2006) and sugar ester and hydroxypropylmethyl cellulose with cefditoren pivoxil (Yokoi et al., 2005).

Raman spectroscopy has been used as method to probe the solid-state form of active substances present in various dosage forms. Taylor and Langkilde (Taylor and Langkilde, 2000) have obtained Raman spectra from intact tablets and capsules containing enalapril maleate, prednisolone, form I and II polymorphs of rantidine, anhydrous and monohydrated theophylline and warfrin sodium clathrate, phase transitions from anhydrous and monohydrate forms could be specially determined. Okumura and Otsuka have evaluated the microcrystallinity of indomethacin in a pharmaceutical model tablet based on FT-Raman spectroscopy (Okumura and Otsuka, 2005). Severdia and Siek have identified and differentiated between dosage strengths of an active drug in white opaque hard gelatine capsules (Severdia and Siek, 2002). Compton and Compton have demonstrated that FT-Raman spectroscopy can be used to examine pharmaceutical preparations contained in polymeric packages (Compton and Compton, 1991). Recently, Matousek and Parker have reported that, the largely neglected transmission Raman geometry is ideally suited for the non invasive probing of pharmaceutical capsules and tablets, reducing substantially capsule and tablet shell Raman and fluorescence signals that often hamper similar measurements in the conventional backscattering Raman geometry (Matousek and Parker, 2006; Matousek and Parker, 2007).

Pharmaceutical counterfeiting is becoming a serious problem in developed and developing countries. Because of its ability to record spectra without sample preparation with short collection times, Raman spectroscopy is a useful method to detect counterfeit drugs. The use of Raman spectroscopy to study pharmaceutical counterfeiting has been reviewed (Deisingh, 2005; Olsen and Kiehl, 2006). Raman spectroscopy is proposed as a fast and reliable method for the detection of counterfeit Viagra tablets (de Veij et al., 2008) and artesunate anti-malarial tablets, (de Veij et al., 2007; Hall et al., 2006; Ricci et al., 2007). Eliasson and Matousek described the application of spatially offset Raman spectroscopy (SORS) in the identification of counterfeit pharmaceutical tablets and capsules through different types of packaging (Eliasson and Matousek, 2007). SORS uses conventional Raman spectroscopy, but rather than detect the Raman signal directly at the point of laser illumination, SORS detects the signal at a distance from the incident position.

Raman spectroscopy has been used to study the composition of pharmaceutically relevant medicinal plants. Edwards et al have reported that FT-Raman spectroscopy has the ability to discriminate between ginseng specimens according to the country of origin (Edwards et al., 2007). Raman spectroscopy has been used in the identification of Chinese traditional medicines (Mao and Xu, 2006) and medicinal and aromatic plants (Schulz, 2005). The determination of alkaloids in capsules, milk and ethanolic extracts of poppy by FT-Raman spectroscopy was also reported (Schulz et al., 2004).

Edwards et al. have studied extensively skin and the drug-skin interactions. They have reported the interactions between the human stratum corneum and the penetration enhancer (DMSO) (Edwards et al., 1995a; Edwards et al., 2002), verrucae and salicylic acid (Edwards et al., 1998), oxybenzone oxidation following solar irradiation of the skin (Edwards et al., 1996b), and the drug distribution in a transdermal drug delivery device

(Edwards et al., 1996a). They have also reported the FT-Raman spectra of mammalian, reptilian (Edwards et al., 1994), human skin (Edwards et al., 1992), and human stratum corneum in vitro and in vivo (Edwards et al., 1993b) for pharmaceutical drug delivery experiments on diffusion across the skin membranes. Caspers et al. have also presented in vitro and in vivo Raman spectra of human skin (Caspers et al., 1998). Zhang et al. have utilized confocal Raman spectroscopy to track dephosphorylation of resveratrol triphosphat in skin (Zhang et al., 2007a) and image the prodrug-to-drug transformation of a 5-fluorouracil derivative in skin (Zhang et al., 2007b). A confocal Raman microprobe has been used in the screening of glycerol-based hydration cream of human skin (Chrit et al., 2006). Raman spectroscopy has been used to study the crystallization of  $\beta$ -estradiol in acrylic transdermal drug delivery system (Variankaval et al., 1999) and to investigate the bioadhesive tetracaine local anaesthetic formulations (Dennis et al., 2004). Raman spectra of the human lens in relation to the anticataract effect of bendaline have been reported (Bertoluzza et al., 1986).

### **3.7. Chemical imaging and mapping**

Chemical imaging is an emerging platform technology that integrates conventional imaging and spectroscopy to attain both spatial and spectral information from an object. Vibrational spectroscopic methods, such as near-IR and Raman spectroscopy, combined with imaging are particularly useful for analysis of pharmaceutical forms (Bell et al., 2008).

Chemical images are made up of hundreds of contiguous wavebands for each spatial position of a target studied. Consequently, each pixel in a chemical image contains the spectrum of that specific position. The resulting spectrum acts like a fingerprint, which can be used to characterise the composition of that particular pixel. The spectroscopic

chemical imaging technique relies on the interface of an optical microscope equipped with a motorized stage to a Raman spectrometer. The operator is able to visually focus upon a sample of interest and optical observations about the sample are made. Subsequently, the same visual area (two-dimensional) is defined for spectroscopic analysis. Utilizing a raster pattern involving the stepwise movement of the motorized stage along the  $x$ - and  $y$ -axes, individual spectra are acquired for each spatial location within the two dimensional area. Spatial resolution is typically defined by the technique as about  $\sim 1 \mu\text{m}$ . Once the individual spectra are obtained for the two-dimensional area, the intensity of a specific spectral feature within each spectrum can be plotted versus the spatial position. In this manner, one is able to obtain a contour plot showing the spatial position of a chemical entity.

Bell et al (Bell et al., 2008), recently published a review documenting the applications of chemical imaging to pharmaceutical process monitoring and quality control. Belu et al. (Belu et al., 2008) have utilized scanning confocal Raman microscopy for chemical imaging of rapamycin eluting coatings. Šašić has reported the application of Raman imaging technique for determining the spatial distribution of all components in a common type of pharmaceutical tablet manufactured in two different ways (Šašić, 2007a), chemical imaging of pharmaceutical granules (Šašić, 2008) and alprazolam in alprazolam/xanax tablets (Šašić, 2007b). Multivariate data analysis for Raman imaging of a model pharmaceutical tablet (Zhang et al., 2005), comparison of Raman chemical images produced by univariate and multivariate data processing (Šašić et al., 2004), confocal Raman microimaging of coated pellets of remoxipride hydrochloride monohydrate (Ringqvist et al., 2003), Raman imaging for the study of the subcellular distribution of the anticancer agent paclitaxel in living breast cancer cells

(Ling et al., 2002) and emulsion systems (Andrew et al., 1998) have been presented in the literature. Confocal Raman spectroscopy was successfully applied to determine the state of ibuprofen in a solid matrix showing equivalence to physical solution (Breitenbach et al., 1999).

Raman micro-spectroscopic mapping is utilized to investigate pharmaceutical tablets containing a low concentration of active pharmaceutical ingredient (Henson and Zhang, 2006), tablets containing chloramphenicol palmitate polymorphs (Lin et al., 2006), pharmaceutical bead formulations (Šašić et al., 2005b), pharmaceutical products by sample-sample two-dimensional correlation (Šašić et al., 2005a), in vitro deposition of combination pressurized metered-dose inhalers containing salbutamol and beclometasone dipropionate (Steele et al., 2004), the subcellular distribution of zinc phthalocyanines (Freeman et al., 1998), pharmaceutical tablets and powder blends (Šašić and Clark, 2006) and surface domains of amorphous sorbitol (Ward et al., 2005). Clarke et al. have applied the chemical image fusion approach which is the development of a novel sample referencing approach that allows data to be acquired from exactly the same area of the sample using both Raman and FT-NIR microscopies, the optimum images for the components are then overlaid which gives rise to a combined chemical image that visually describes the entire formulation, for a more complete visualization of pharmaceutical formulations (Clarke et al., 2001a; Clarke et al., 2001b).

### **3.8. Hyphenated techniques**

Aaltonen et al. (Aaltonen et al., 2007b) have utilized Hyphenated NIR/Raman spectroscopy combined with principal component analysis as fast and comprehensive method of solid phase analysis. NIR spectroscopy was effective in separating the hydrate form (II) from the hydrates ( $\alpha$  and  $\beta$ ) of nitrofurantoin, while Raman

spectroscopy provided accurate information from the differences between the anhydrates (Aaltonen et al., 2007b). Taylor and Gift have reported the hyphenation of Raman spectroscopy with gravimetric analysis to interrogate water solid interaction in pharmaceutical systems containing sulfaguanidine, cromolyn sodium, amorphous sucrose, ranitidine HCl, and silica gel (Gift and Taylor, 2007). Cimpoiu et al. have separated and identified eight hydrophilic vitamins using TLC and Raman spectroscopy without using standards of vitamins (Cimpoiu et al., 2005).

### **3.9. Future pharmaceutical uses of Raman spectroscopy**

Raman spectroscopy continues to grow in popularity both among analytical chemists and in other fields and it has become a standard method for the characterisation of drugs and for industrial process monitoring. Raman spectroscopy is being developed as a detection mechanism in many hyphenated techniques, and it is expected that this field will continue to develop in the next few years.

While Raman spectroscopy in the backscattering collection mode is limited to probing shallow, semitransparent media, the spatial offset Raman spectroscopy (SORS) improves the penetration depth (Matousek, 2006). The SORS method is based on the collection of Raman spectra from spatially offset region away from the point of illumination on the sample surface. The laterally offset Raman spectra contain different relative contributions from sample layers located at different depths. This difference is brought about by a wider lateral diffusion of photons emerging from greater depths. The offset spectra can either contain acceptably low Raman contributions from the surface layer, or if a considerable signal is still present then this can be further removed using a scaled subtraction of spectra obtained at different spatial offsets. Alternatively, the separation of Raman signals originating from different layers in the sample can be

accomplished using multivariate data analysis applied to a set of spatially offset Raman spectra. The SORS approach is also capable of effectively suppressing the interfering fluorescence if it originates from the surface layer of the probed medium. Clearly, SORS will broaden the pharmaceutical application of Raman spectroscopy.

The future for Raman spectroscopy within the pharmaceutical field appears bright. The technique has developed rapidly, with instrumental advances providing flexible equipment that is capable of obtaining good quality rapid data from a variety of sample forms and states.

**Table 3.1. Listing of different pharmaceutical compounds characterised by Raman spectroscopy and computational methods.**

Pharmaceutical compound	Raman spectroscopy	Computational method	References
Fluticasone propionate	X	X	(Ali et al., 2009a)
Artemisinin	X	X	(Moroni et al., 2008)
Ibuprofen	X	X	(Bondesson et al., 2007; Vueba et al., 2008)
Thalidomide	X	X	(Cipriani and Smith, 2008)
Paracetamol,oxcarbazepine, chloropropamide and olanzapine	X	X	(Ayala, 2007)
Platinum II anticancer drug (Cimpoiu et al., 2005)	X	X	(Amado et al., 2007a)
Uracilyl-pyridinium mesomeric betaine	X	X	(Schmidt et al., 2007)
Budesonide	X	X	(Ali et al., 2007)
$\gamma$ -crystalline and amorphous indomethacin	X	X	(Strachan et al., 2007a)
Isoniazid	X	X	(Akalin and Akyuz, 2007; Gunasekaran, 2005a)
Clavulanic acid	X	X	(Miani et al., 2007)
Nevirapine	X	X	(Ayala et al., 2007)
Aspirin, caffeine and ibuprofen	X	X	(Bondesson et al., 2007)
Atorvastatin calcium	X		(Gunasekaran et al., 2007a)
Diazepam,phenytoin, phenobarbitone	X	X	(Gunasekaran et al., 2006b)
Indomethacin-cyclodextrin inclusion complex	X	X	(Rossi et al., 2006)
Glibendamide, rosiglitazone maleate	X		(Gunasekaran et al., 2007b)
Metformin	X	X	(Gunasekaran et al., 2006a)
Salmeterol xinafoate and fluticasone propionate	X		(Theophilus et al., 2006)
4-Thiocarbamoylpyridine	X	X	(Wysokinski et al., 2006b)

**Table 3.1. (Continued)**

Pharmaceutical compound	Raman spectroscopy	Computational method	References
5-para-fluoro-benzilidene-thiazolidine-2-thione-4-one	X	X	(Baias, 2006)
Pyrazinamide, atenolol, metoprolol, pindolol and verapamil	X	X	(Cozar et al., 2006)
Carboplatin	X	X	(Wysokinski et al., 2006a)
Non steroidal anti-inflammatory drugs (ibuprofen, naproxen and tolmetin)	X	X	(Jubert et al., 2006)
Cyanocobalamin (vitamin B12)	X		(Gunsekaran and Sankari, 2005)
5-Fluorouracil	X	X	(Pavel et al., 2005; Rastogi et al., 2000)
Sulfonamides	X		(Rama et al., 2005)
Falicaine HCl and isomorphous dyclonine HCl	X		(Schmidt, 2005c)
Benzocaine	X	X	(Gunasekaran, 2005b)
Fluoroquinolones (naldixic acid, oxolinic acid, cinoxacin, flumequine, norfloxacin, ciprofloxacin, lomefloxacin, ofloxacin, enoxacin, sarafloxacin and moxifloxacin)	X	X	(Neugebauer et al., 2005)
Caffeine, theobromine and theophylline	X		(Edwards et al., 2005)
Platinum II anticancer drugs	X	X	(Michalska and Wysokinski, 2005)
Plumbagin	X	X	(Sajan et al., 2005)
Combretastatin-A4	X	X	(Binoy et al., 2004)
Carbamazepine polymorphs	X	X	(Strachan et al., 2004a)
Carvedilol	X	X	(Marques et al., 2002)
9-β-D-arabinofuranosyladenine-5'-monophosphate	X	X	(Hernandez et al., 2002)

**Table 3.1. (Continued)**

Pharmaceutical compound	Raman spectroscopy	Computational method	References
Cimetidine	X	X	(Baranska and Proniewicz, 1999)
Amantadine	X	X	(Rivas et al., 1999)
5-iodo-2'-deoxyuridine	X	X	(Bailey et al., 1999)
Aminoglutethimide	X	X	(Glice et al., 1998)
Arabino nucleoside	X	X	(Hernandez et al., 1998)
Frozen glucose solution	X		(Taylor et al., 1997)
Lansoprazole	X		(Curin, 1997)
Sanocrysin	X		(Tobön-Zapata et al., 1997)
Heparin	X	X	(Atha et al., 1995; Atha et al., 1996)
Salbutamol base and salts	X	X	(Ali et al., 2009b; Edwards et al., 1993a; Ticehurst et al., 1994)
Aged flurazepam mono and dihydrochloride salts	X		(Neville et al., 1994)
A promising drug in AIDS therapy	X		(Baran, 1993)
Flucloxacillin and sodium cephalothin	X		(Cutmore and Skett, 1993)
Acridine	X	X	(Butler and Cooney, 1993)
Antineoplaston A10	X	X	(Michalska, 1993)
Phenethylamine, tyramine, dopamine and tyrosine	X	X	(Choi and Lubman, 1992)
Primaquine diphosphate and its cation radical	X		(De Faria and Santos, 1991)
Sulfa drug molecules	X		(Prabakaran and Mohan, 1990)
Dapsone	X		(D'Cunha, 1983)
New anticancer inorganic ring systems	X		(Manfait et al., 1982a; Manfait et al., 1982b)
Barium sulphate in parenteral solution	X		(Boddapati et al., 1980)

**Table3.1. (Continued)**

Pharmaceutical compound	Raman spectroscopy	Computational method	References
Benzodiazepines	X		(Bass, 1978a)
Sympathomimetic amines	X		(Bass, 1978b)
Phenothiazines	X		(Hosomi et al., 2004; Kure and Morris, 1976)
Palladium-5-nitofurylthiosemicarbazone complex	X	X	(Gambino et al., 2007)
Lamivudine	X	X	(Pereira et al., 2007)
Deflazacort	X		(Cuffini et al., 2007)
Microcrystalline cellulose and powder cellulose	X		(Fechner et al., 2003)
Krypton solution	X	X	(Durig et al., 2004)
Iodixanol	X		(Priebe et al., 1995)
Complex for magnesium supplementation	X		(Wagner et al., 1999)
Nystatin	X		(Colline et al., 1985)
Anthopleurin A	X		(Ishizaki et al., 1979)

**Table 3.2. Listing of different pharmaceutical polymorphic systems studied by Raman spectroscopy.**

Pharmaceutical polymorph	Comments	References
Salmeterol xinafoate	Characterisation and polymorphic transformation by simultaneous <i>in situ</i> Raman spectroscopy and DSC	(Ali et al., 2008)
Nimodipine	In its solid dispersions in polyethylene glycol	(Docoslis et al., 2007)
Carbamazepine	Cocrystals with nicotinamide and saccharin The influence of various excipients on its conversion kinetics in aqueous suspensions Quantitative analysis of polymorphic mixtures	(Porter, 2008) (Tian et al., 2007) (Strachan et al., 2004b)
Oxybuprocaine HCl	Three polymorphic forms	(Info et al., 2008)
Tamoxifen citrate	Three polymorphic forms	(Gamberini et al., 2007)
Salicylanilide	Three forms (polymorph I,II and the amorphous form)	(De Spiegeleer et al., 2007)
Risperidone	In tablets	(Karabas et al., 2007)
Bicalutamide	Two crystal forms and an amorphous phase	(Vega et al., 2007)
Sulphathiazole	Five polymorphic forms	(Zeitler et al., 2006)
Norfloxacin	Enantiotropic relationship between polymorphs A and B	(Barbas et al., 2006)
Chloramphenicol palmitate	Three polymorphic forms	(Gamberini et al., 2006)
Celecoxib	A novel polymorphic form (form IV)	(Lu et al., 2006)
Rantidine	Form I and II	(Thorley et al., 2006)
Paracetamol	Form II Monoclinic and orthorhombic forms	(Thorley et al., 2006) (Moynihan and O'Hare, 2002)
Local anaesthetic drugs	24 local anaesthetics have been characterized	(Schmidt, 2005a)
Chloroprocaine HCl	Two polymorphic crystal forms	(Schmidt, 2005b)
Felodipine and nitrendipine		(Vassou et al., 2005)
Benzimidazole drug	In complex finished formulation	(De Spiegeleer et al., 2005)

**Table 3.2. (Continued)**

Pharmaceutical polymorph	Comments	References
Chlorpropamide, diflunisal, furosemide, piroxicam, ritonavir and other 9 pharmaceutical compounds	Statistical analysis of differences in Raman spectra of polymorphs	(Mehrens et al., 2005)
Hydroxyprocaine HCl	Two polymorphic and a pseudopolymorphic crystal form	(Schmidt and Schwarz, 2005)
Prilocaine HCl	Two polymorphic forms, a dioxane solvate and the amorphous form	(Schmidt et al., 2004)
Nifedipine	One amorphous and three crystalline phases	(Chan et al., 2004)
A novel sodium ion channel blocker	Two polymorphic forms A and B	(Cheung et al., 2003)
Pramocaine base and HCl	Two crystal forms of the Base and three crystal modifications of the salt	(Schmidt et al., 2003a)
Various drugs and excipients	Potential of carrageenans to protect drugs from polymorphic transformation	(Schmidt et al., 2003b)
Roxifiban	Two polymorphic forms	(Maurin et al., 2002)
Cilostazol	Three forms A, B and C	(Stowell et al., 2002)
CNS active drug Org 13011	Four forms A, B, C and D	(van Hoof et al., 2002)
17 $\beta$ -estradiol	In transdermal drug delivery system	(Variankaval, 2002)
D-mannitol	Four different crystal forms (EA, EC, ED and EM) Three modifications In binary mixture with NaCl	(Variankaval et al., 2000) (Burger et al., 2000) (Telang et al., 2003)
Diprophylline	Two polymorphic forms	(Griesser, 1999)
Acetazolamide	Two modifications I and II	(Griesserx, 1997)

**Table 3.2. (Continued)**

Pharmaceutical polymorph	Comments	References
Nimodipine	Two polymorphic forms	(Grunenberg et al., 1995)
Spirolactone	Differentiation of polymorphic samples	(Neville et al., 1992)
Ampicillin and griseofulvin	Two polymorphs and a trihydrate form	(Bellows et al., 1977)
Lactose	A definitive guide to polymorph determination	(Kirk et al., 2007)
Buspirone HCl	Two forms 1 and 2	(Sheikhzadeh et al., 2006)
Salicaine base and HCl		(Schmidt et al., 2006)
Benzocaine, butambene and isobutambene	Each drug exists in two polymorphic crystal forms	(Schmidt, 2005d)
Acetaminophen, sulfamethoxazole, carbamazepine and a pharmaceutical intermediate	Control of crystal polymorphism through the use of polymer heteronuclei	(Price et al., 2005)
Tranilast	Five polymorphic forms	(Vogt et al., 2005)
Torasemide	Three crystal forms I and II and a pseudopolymorphic crystal form (form A)	(Rollinger et al., 2002)
Piroxicam	Three different forms (alpha, beta and monohydrate)	(Taddei et al., 2001)
Stavudine	Three forms I, II and III	(Gandhi et al., 2000)
DuP 747	Two polymorphic forms	(Raghavan et al., 1994)

**Table 3.3. Listing of different pharmaceutical compounds studied by quantitative Raman spectroscopy.**

Pharmaceutical compound	Comments	References
Ticlopidine HCl	In tablets	(Markopoulou et al., 2008)
Sulfathiazole and sulfanilamide	As a pharmaceutical powder using a simple univariate calibration model	(López-Sánchez et al., 2008)
Phenacetin and salophen	In solid binary mixtures with caffeine	(Koleva et al., 2008)
Atorvastatin calcium	Polymorph in tablets	(Skorda and Kontoyannis, 2008)
Pharmaceutical tablets and capsules	Using transmission Raman spectroscopy	(Johansson et al., 2007)
Ambroxol	In an intact capsule formulation In tablets	(Kim et al., 2007a) (Hwang et al., 2005; Szostak and Mazurek, 2004)
Amiodarone HCl	In Angoron liquid formulation	(Orkoula et al., 2007)
Acetaminophen	In a turbid pharmaceutical suspension	(Park et al., 2007)
Medroxyprogesterone acetate	In a pharmaceutical suspension	(De Beer et al., 2007b; De Beer et al., 2004)
Povidone	In a commercial eyewash solution by direct measurement through a plastic bottle	(Kim et al., 2007b)
Salicylic acid	Influence of particle size on its quantitative determination in a pharmaceutical ointment	(De Beer et al., 2007a)
Spray dried lactose	Determination of the amorphous content	(Lehto et al., 2006)
Diclofenac sodium and aminophylline	In injection solutions	(Mazurek and Szostak, 2006b)
Captopril and prednisolone	In tablets	(Mazurek and Szostak, 2006a)
Illicit drug mixtures	On paper currency	(Noonan et al., 2005)
Ahydrate/hydrate powder mixtures	Using nitrofurantoin, theophylline, caffeine and carbamazepine	(Rantanen et al., 2005)
Carbamazepine	Polymorphic mixtures	(Strachan et al., 2004b)

**Table 3.3. (Continued)**

Pharmaceutical compound	Comments	References
Corn starch and lactose monohydrate	Two-component powders and tableted mixtures	(Virágh, 2003)
Sorbitol, mannitol, famotidine, acemetacin, carbamazepine, meprobamate and phenylbutazone	Polymorphic forms in drug formulations	(Auer et al., 2003)
Dipyrrone	In tablets	(Izolani et al., 2003)
Acyclovir	In pharmaceutical solid dosage forms through their poly(vinyl chloride) blister package	(Skoulika and Georgiou, 2003)
Rantidine HCl	Polymorphic mixtures	(Pratiwi et al., 2002)
Vitamin C	In food and pharmaceutical products	(Yang and Irudayaraj, 2002)
Diltiazem HCl	In tablets	(Vergote et al., 2002)
Active substance (containing CN)	In a pharmaceutical tablet	(Dyrby et al., 2002)
Mannitol polymorphs	Binary mixtures containing beta and delta mannitol	(Campbell Roberts et al., 2002)
Acetylsalicylic acid and acetaminophen	In tablets	(Szostak and Mazurek, 2002)
Ciprofloxacin	In solid pharmaceutical dosage forms	(Skoulika and Georgiou, 2001)
A radiosensitizer, 5-iodo-2'-deoxyuridine	Within biodegradable polymeric microspheres	(Geze et al., 1999)
Isosorbide-5-mononitrate	In a tablet	(Jedvert et al., 1998)
Bucindolol	In intact gel capsules	(Niemczyk et al., 1998a; Niemczyk et al., 1998b)
Two crystal forms of a pharmaceutical compound		(Langkilde et al., 1997)
Cortisone acetate	Polymorphs	(Deeley, 1991)

**Table 3.3. (Continued)**

Pharmaceutical compound	Comments	References
Sulfasalazine-containing polymeric microspheres		(Watts et al., 1991)
Phenylpropanolamine HCl and acetaminophen	In pharmaceutical preparations	(King et al., 1985)
Indomethacin	Ternary mixtures of different solid-state forms	(Heinz et al., 2007)
Diphenhydramine HCl	In liquid formulations	(Orkoula et al., 2006)
Etoricoxib	Investigating the hydrate conversion propensity	(Dalton et al., 2006)
Vitamin A	Degradation	(Failloux et al., 2003)
Monoclinic and orthorhombic paracetamol	In powder mixtures	(Al-Zoubi et al., 2002)
Aspirin	Tablets	(Wang et al., 1997)
Calcium carbonate and glycine	In antacid tablets	(Kontoyannis, 1995)

**Table 3.4. Listing of different process pharmaceutical applications of Raman spectroscopy.**

Pharmaceutical system	Comments	References
Flufenamic acid	Estimation of the transition temperature for the enantiotropic polymorphic system from the transformation kinetics	(Hu et al., 2007)
Magnesium stearate	Monitoring in blends and tablets	(Aguirre-Mendez, 2007)
Active pharmaceutical ingredient's hydrate form	Online Raman spectroscopy in a complex wet drying process	(Liang, 2007)
Potential pharmaceutical materials	Fluidised bed characterization	(Bell et al., 2007)
Theophylline	Probing pseudomorphic transitions in pharmaceutical solids	(Amado et al., 2007b)
	Effect of excipients on hydrate formation in wet masses	(Airaksinen et al., 2003)
$\alpha$ -lactose monohydrate and amorphous lactose and trehalose	Determination of amorphous content in the pharmaceutical process environment	(Savolainen et al., 2007b)
Theophylline and nitrofurantoin	<i>In situ</i> measurement of solvent-mediated phase transformations during dissolution testing	(Aaltonen et al., 2006)
Theophylline monohydrate	In-line monitoring of solid-state transitions during fluidisation	(Aaltonen et al., 2007a)
Ibuprofen and xanthan gum	Quantitative in-line monitoring of the homogenization process of a pharmaceutical suspension	(De Beer et al., 2006)
Taltirelin and timepidium bromide	Monitoring of solvent-mediated polymorphic transitions	(Kobayashi et al., 2006)

**Table 3.4. (Continued)**

Pharmaceutical system	Comments	References
Carbamazepine	Solvent-mediated phase transformations kinetics of an anhydrate/dehydrate system <i>In situ</i> Raman spectroscopic polymorphic analysis of optically trapped microcrystals in a microliter fluid volumes <i>In situ</i> FT-Raman spectroscopy to study the kinetics of the polymorphic transformation Monitoring the solubility and stability of anhydrate/hydrate in ethanol-water mixtures	(Qu et al., 2006b) (Anquetil et al., 2003) (O'Brien et al., 2004) (Qu et al., 2006a)
Pharmaceutical tablet	On-line content uniformity determination of tablets using low-resolution Raman spectroscopy	(Wikström et al., 2006)
Erythromycin A dihydrate	Thermally induced phase transformations	(Miroshnyk et al., 2006)
Risedronate	Use of a TG/DTA/Raman system to monitor dehydration and phase conversions On-line Raman spectroscopy for characterizing relationships between drug hydration state and tablet physical stability	(Kern et al., 2005) (Hausman et al., 2005a)
Powder blends	Comparison of sampling techniques for in-line monitoring	(Wikström et al., 2005)
Theophylline anhydrous	In-line monitoring of hydrate formation during wet granulation	(Wikstroem et al., 2005)
Diltiazem HCl	In-line monitoring of a pharmaceutical blending process	(Vergote et al., 2004)
Pharmaceutical polymorph	Robust polymorph isolation using <i>in situ</i> Raman spectroscopy	(Zhou et al., 2002)

**Table 3.4. (Continued)**

Pharmaceutical system	Comments	References
Carbopol ultrez and tefose	Raman spectroscopy as a PAT during formulations of topical gels and emulsions	(Islam et al., 2004)
Compound A	Evaluation of drug physical form during granulation, tableting and storage	(Williams et al., 2004)
A multipolymorphic compound (MK-A)	The use of <i>in situ</i> Raman spectroscopy to determine the rate of polymorph turnover	(Starbuck et al., 2002)
Theophylline and caffeine	Monitoring of hydrate formation during wet granulation	(Jørgensen et al., 2002)
Ibuprofen	<i>In situ</i> study of impregnation of ibuprofen into PVP	(Kazarian and Martirosyan, 2002)
Muro 128 (dehydrating agent)	Drug induced corneal hydration changes monitored in vivo by confocal Raman spectroscopy	(Erckens et al., 2001)
Ethyl acetate and acetylsalicylic acid	Quantitative reaction monitoring	(Shackman et al., 2000)
Paracetamol and lufenuron	<i>In situ</i> characterization of polymorphic forms	(Szelagiewicz et al., 1999)
Polycyanoacrylates	Raman spectroscopic monitoring of the polymerization of cyanoacrylate	(Urlaub, 1998)
Acetaminophen	<i>In situ</i> identification in a fatal overdose case	(Pestaner et al., 1996)
Hydrate forms of Piroxicam and carbamazepine	In situ analysis to reveal the multiple solid-state forms that appear during isothermal dehydration	(Kogermann et al., 2007)
Mannitol	Monitoring of phase behaviour during freeze-drying	(Romero-Torres et al., 2007)
Azimilide dihydrochloride	On-line monitoring of low dose blend uniformity	(Hausman et al., 2005b)
Lovastatin	Monitoring the stability in solid state in the presence of gallic acid	(Orkoula et al., 2004)
Metoprolol	Monitoring of the synthesis	(Svensson et al., 2000)

#### 4.1. Introduction

The purpose of this study is to provide a group of case studies that illustrate how quantum chemistry may be used in studying pharmaceutical systems to provide viable structural information when considering the complexation, interactions and solid-state analysis of a number of commonly used respiratory drugs, namely, budesonide, fluticasone propionate, salbutamol hemisulphate, terbutaline hemisulphate and ipratropium bromide, and how they have been studied using quantum chemistry. Importantly, the focus is on existing and well-established quantum methods to support vibrational spectroscopic molecular assignments.

We are particularly interested in trying to model the properties of molecules, such as structure and vibrational spectra; for these properties there are an array of methods and commercial programme packages available to researchers (Young, 2001). For example, there are comparatively simple molecular mechanics and semi-empirical methods that may be applied to large molecular systems. These methods have been successful in many areas, e.g., a review by Taskinen and Yliruusi (Taskinen and Yliruusi, 2003) highlighted the use of semi-empirical calculations to predict the octanol-water partition coefficients for a variety of compounds. Calculations may be used to screen tens of thousands of compounds for the purpose of drug design as exemplified in the study of ligands for the retinoic acid receptor by Silva et al (Silva et al., 2005). However, as we are interested in molecular properties such as vibrational spectra it is often necessary to use more sophisticated and more limited computational methods than those offered by semi-empirical approaches. For this reason we will focus on the use of quantum chemical calculations applicable to these types of problems.

#### 4.1.1. Budesonide

Budesonide (BUD) is a relatively new non-halogenated potent glucocorticoid that has been designed to express high topical activity with reduced systemic side effects. This has been achieved by incorporating features into the drug molecule that generate a pronounced hepatic metabolism resulting in low oral bioavailability and high hepatic clearance (Spencer and McTavish, 1995). Because of these design features, BUD has been very successful in the topical treatment of asthma via inhalation administration (Hvizdos and Jarvis, 2000). The use of BUD has also been extended to the local therapy of other diseases. It is evaluated in the treatment of chronic inflammatory bowel disease in the form of enteric-coated pellets insoluble in gastric juice, rectal foams and enemas (Hamedani et al., 1997).

Structurally, BUD is a  $16\alpha$ ,  $17\alpha$ -acetal prepared by reaction of the  $16\alpha$ ,  $17\alpha$ -dihydroxysteroid ( $16\alpha$ -hydroxyprednisolone) with *n*-butyraldehyde. Due to the introduction of the alkyl chain at the  $C_{22}$  atom, BUD is a mixture of two epimers ( $22R$  and  $22S$ ) (Figure 4.1) (Albertsson et al., 1978). Both epimers appear to have similar pharmacological effects; however, *in vitro* studies have suggested that the *R*-epimer is two to three times more potent with respect to its anti-inflammatory effects (Brattsand et al., 1982). The only pharmacopoeial monograph for BUD appears in the British and European Pharmacopoeias (Pharmacopoeia, 2001; Pharmacopoeia, 1997) which state that the *R/S* epimer ratio should be within the range of 60 ~ 49/40 ~ 51.



### 4.1.3. Salbutamol hemisulfate

Salbutamol hemisulfate (SB) (synonym: albuterol hemisulfate) is a relatively selective  $\beta_2$ -adrenergic agonist and is used as a bronchodilator. The chemical name of SB (Figure 4.3) (Ganjali et al., 2005; Oliva et al., 2005; Yamini et al., 2006) is 1-(4-hydroxy-3-hydroxymethylphenyl)-2-(*tert*-butylamino) ethanol sulphate (2:1) (salt). SB is indicated for the prevention and relief of bronchospasm with reversible obstructive airway disease (asthma), and for the prevention of exercise induced bronchospasm. SB acts by stimulating the adenylyl cyclase enzyme, which catalyzes the formation of cyclic-3', 5'-adenosine monophosphate (cyclic AMP) from adenosine triphosphate (ATP). The cyclic AMP thus formed, mediates the cellular responses. The increased cyclic AMP levels are associated with relaxation of bronchial smooth muscles. SB is effective by both oral and inhalation routes of administration so it has been used in tablets, syrups, metered dose inhalers, and nebulised inhalation solutions.

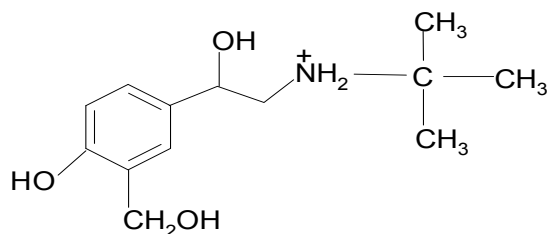


**Figure 4.3. The chemical structure of SB.**

SB, like other  $\beta_2$ - agonists are misused by athletes for their potential to improve muscular strength via their significant anabolic effects (Clarkson and Thompson, 1997). SB is often illegally used as feed additives for their potential role in increasing muscular mass and reducing body fat in animal species (Moloney et al., 2003). However, SB is a steady substance, so it can be easily deposited in both human and the edible animal tissues. When used at higher or long-term dose, it is found to have severe poisoning side effects (Vale, 2003). The misuse of SB by athletes has been demonstrated and banned

by the World Anti-Doping Agency (WADA). Its usage as feed additives for growth promotion in livestock growth, which has resulted in a number of reports of human food poisoning (Ramos et al., 2003) has also been prohibited in many countries.

#### 4.1.4. Terbutaline hemisulfate

Terbutaline hemisulfate (TBS), 1-(3,5-dihydroxyphenyl)-2-(*tert*butylamino) ethanol sulphate (2:1) (salt) (Figure 4.4) belongs to the class of  $\beta_2$ -agonist drugs as SB and used for the treatment of pulmonary disorders particularly in the treatment of bronchial asthma in humans (Ramos et al., 2003). As a therapeutic agent, low doses of TBS can be administered directly to the lung airways via inhalation in order to minimize negative side effects and maximize efficiency (Votion et al., 1997). It has been pharmacologically proven to be able to increase muscle protein, reduce total body fat due to lipid removal from fat deposits, and promote muscle growth. In animals, in addition to its regulatory role in veterinary medicine as a bronchodilator and tocolytic agents, increases the ratio of lean meat to fat (re-partitioning) and improve feed conversion efficiency (Kuiper et al., 1998).

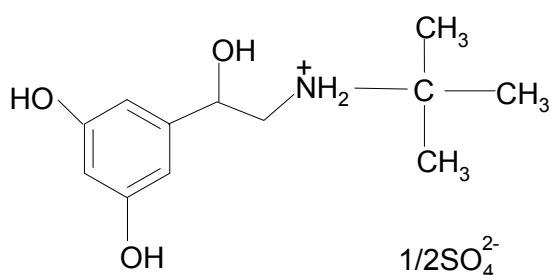


**Figure 4.4. The chemical structure of TBS.**

TBS is known to exist in at least two anhydrous modifications (A and B), a monohydrate and an acetic acid solvate. A higher hydrate, supposedly a trihydrate (which has also been denoted as terbutaline hemisulfate sesquihydrate), has also been

reported (Hickel et al., 1982). All five modifications have been structurally characterized by thermogravimetric analysis, differential scanning calorimetry, X-ray powder diffraction and solid-state NMR (Harris et al., 2008).

The crystal structures of anhydrate B and the acetic acid solvate are known (Harris et al., 2008; Sengupta and Dattagupta, 1996) and are contained in the Cambridge Crystal Structure Database (CSD) with codes ZIVKAQ and ZIVKAQ01, respectively. The crystal structure of terbutaline hemisulfate sesquihydrate also appears in the CSD, under code BECVIO.

#### 4.1.5. Ipratropium bromide

Ipratropium bromide (IPRA), chemically known as, 8-isopropyl-nor-atropine-methylbromide, a quaternary ammonium compound with antimuscarinic properties, is used as a bronchodilator for the maintenance and treatment of bronchospasms associated with chronic obstructive pulmonary disease (Martindale, 2005) (Figure 4.5).

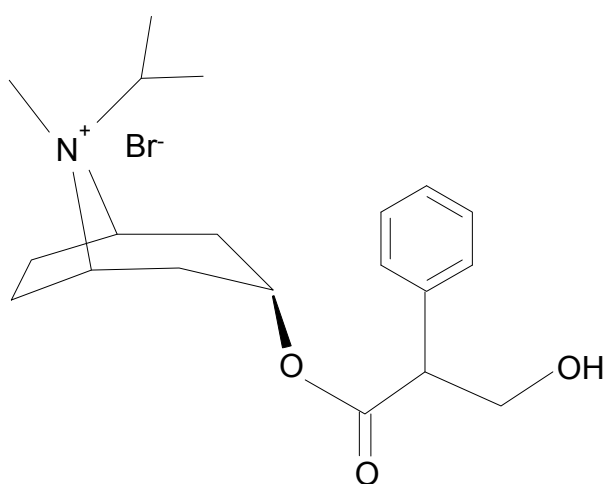


**Figure 4.5. The chemical structure of IPRA.**

## **4.2. Experimental**

### **4.2.1. Materials**

A specimen of BUD was obtained from Mallincrodt and specimens of FP, SB, IPRA and TBS were obtained from Sigma-Aldrich. All specimens were used without further purification.

### **4.2.2. Raman spectroscopy**

Fourier-transform Raman spectroscopy for all the drugs studied was carried out using a Bruker IFS 66 instrument with an FRA 106 Raman module attachment and a Nd<sup>3+</sup> /YAG laser operating at 1064 nm in the near infrared. The powdered specimens were examined in aluminium cups. The spectra were recorded at 4 cm<sup>-1</sup> spectral resolution and 500 spectral scans accumulated to improve signal-to-noise ratios. Laser powers were maintained at 100 mW at the sample in case of FP, SB and TBS and at 200 mW in case of BUD and IPRA.

### **4.2.3. Infrared spectroscopy**

The IR spectra of the all studied drugs were recorded as KBr discs (1:200) using a Digilab Scimitar Series spectrometer. The spectra were recorded in the range of 400-4000 cm<sup>-1</sup> at 4 cm<sup>-1</sup> spectral resolution with the accumulation of 512 spectral scans.

### **4.2.4. X-ray powder diffractometry**

Powder X-ray diffraction (PXRD) data for BUD and TBS were recorded with a Bruker D8 diffractometer with Cu-K $\alpha_{1,2}$  radiation (1.5418 Å) and a secondary curved graphite monochromator. The X-ray tube was operated at 40 kV and 30 mA. Samples were scanned in vertical Bragg-Brentano ( $\theta/2\theta$ ) geometry (flat reflection mode) from 5-

40° (2 $\theta$ ) using a 0.005° step width and a 1.5 s count time at each step in the case of BUD and from 5-50° (2 $\theta$ ) using a 0.01° step width and a 1.0 s count time at each step in the case of TBS . The receiving slit was 1° and the scattering slit was 0.2°. Data were analysed with Bruker AXS Topas 2.1 software including a correction for axial divergence. Background coefficients, cell parameters, sample displacement error and phase fractions were optimised parameters.

#### **4.2.5. Calculation details**

Calculations for all the drugs studied were performed using GAMESS-UK (Guest et al., 2005) and ORCA programmes (Neese, 2004). Geometry optimisation was initially performed using a semi-empirical PM3 Hamiltonian and then further refined using BLYP density functional theory with a 6-31G\* basis set (Becke, 1988; Lee et al., 1988; Neese, 2004). IR and Raman spectra were calculated using the quasi-harmonic approximation, through diagonalisation of the mass-weighted Hessian matrix. Intensities were calculated using the dipole-moment derivatives and the polarisability derivatives of the normal modes.

#### **4.3. Results and discussion**

Prior to the vibrational spectroscopic analysis, it is worth noting that the computed vibrational frequencies are sensitive to the theoretical method used and are generally shifted with respect to the experimental values. The hybrid BLYP functional has been used throughout this work because it shows the best performance with a minimum error (Jensen, 2007). At the basis set limit, the deviations from the experimental harmonic frequencies are 20-30 cm<sup>-1</sup>.

The crystal structures, conformations and comparisons between the experimental and the calculated vibrational spectra of certain drugs will be presented as representative examples.

The IR and Raman spectra of the all studied drugs have been recorded over the wavenumber range 4000-400  $\text{cm}^{-1}$  and 3600-100  $\text{cm}^{-1}$ , respectively, using both transmission and attenuated total reflectance modes of operation for the former and 1064 nm laser wavelength for the later technique.

The OH stretching modes observed near 3500  $\text{cm}^{-1}$  in the IR spectra are not observed in the Raman spectra, whereas bands in the low wavenumber region that are normally characteristic of polymorphic crystalline pharmaceutical forms are not recorded in the IR spectra of the all studied drugs.

### **4.3.1. Budesonide**

#### **4.3.1.1. X ray powder Diffractometry**

The crystal structures of BUD were taken from the Cambridge Structure Database (CDS) as collection codes RHBUXP10 and SHBUXP10 for *R*- and *S*-epimers, respectively.

The composition of BUD sample was investigated by PXRD. All peaks in the pattern coincided with theoretical patterns for *R*- and *S*-epimer forms generated from single crystal studies (Figure 4.6) (Albertsson et al., 1978). Notably, no halo attributable to amorphous content in the sample was apparent. Peaks in the pattern were significantly broadened and pattern-fitting using the Rietveld approach indicated the presence of only two components underpinning the major peaks in the pattern. The broadening was hence attributed to the mixture of epimers in the sample. Quantitative Rietveld analysis, based on the single crystal structures, indicated the mixture to be composed of epimers

in the ratio *R*:*S* of 36:64. The two epimers of BUD are known to form solid solutions in the mixtures over the composition range 0-95%. (Albertsson et al., 1978). Inclusion of both epimers in the same crystal is likely to induce significant disorder which manifests as peak broadening in the diffraction pattern (James, 1982). Refinement of cell dimensions in conjunction with quantitative Rietveld analysis resulted in cell parameters (*R*-form:  $a = 8.510(2)$ ,  $b = 9.175(2)$ ,  $c = 29.027(9)$  Å; *S*-form:  $a = 8.552(2)$ ,  $b = 9.228(2)$ ,  $c = 29.1106(9)$  Å) corresponding to those reported for epimer mixtures with a predominance of the *S*-epimer, again these observations suggest that the material corresponds with the range of continuous solid solutions described by Albertsson *et al* (Albertsson et al., 1978).

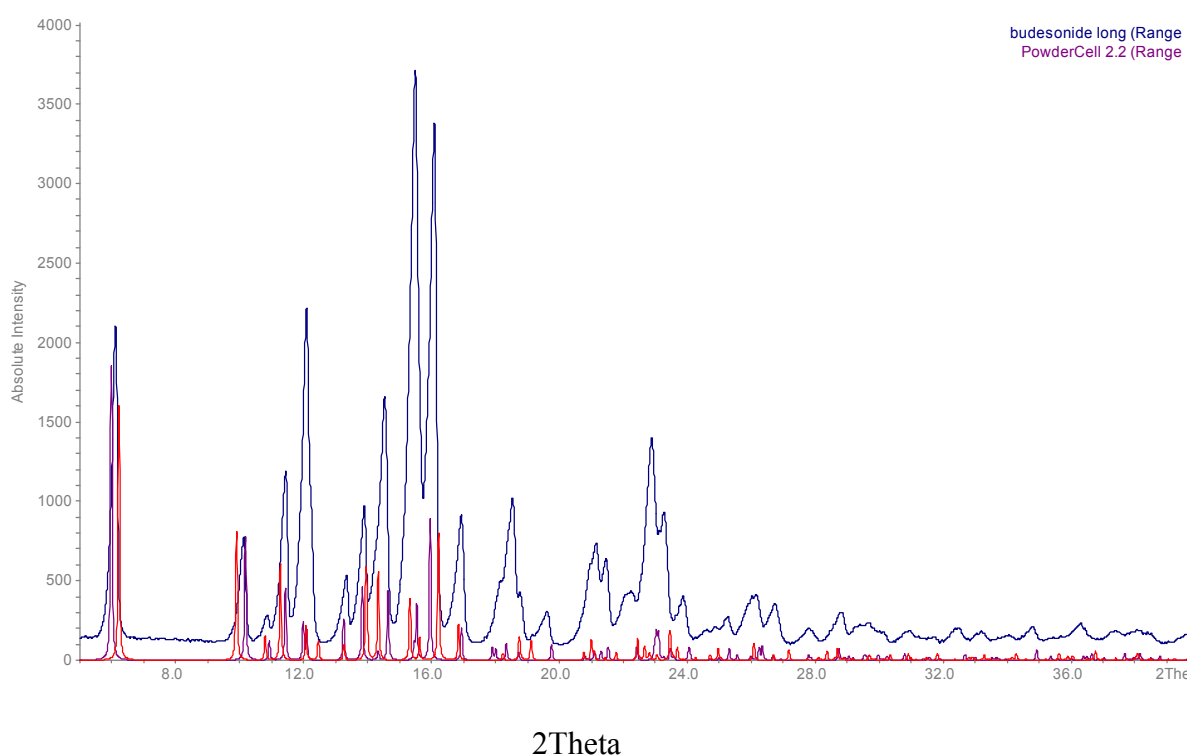


**Figure 4.6. PXRD pattern of BUD epimers (the red is 22R and the blue is 22S).**

### 4.3.1.2. Infrared and Raman Spectroscopy

The BUD conformation (Figure 4.7) has been used in the calculation of its vibrational spectra.

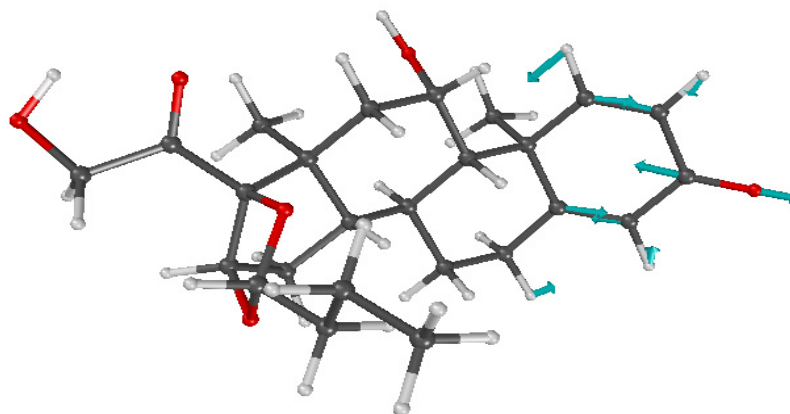


**Figure 4.7. The BUD conformation**

The IR and FT-Raman spectra of BUD are shown in Figures 4.8- 4.13; these spectra illustrate clearly the complexity of structural information that is provided from IR and Raman analysis.

#### 4.3.1.2.1. 4000– 2600 $\text{cm}^{-1}$ region

Although the IR spectrum of BUD is reported in the FDM, Electronic Handbook of FTIR Spectra, (FDM), this does not identify the epimeric content and does not provide spectral band assignments. Bandi et al (Bandi et al., 2004) have reported the IR spectrum of BUD and its complex with hydroxypropyl- $\beta$ -cyclodextrin (HPBCD) citing the spectral band assignments to indicate the possibility of the molecular interaction with excipients, other additives and combinations of drugs. However, no recognition is made in this paper of the BUD epimers and a detailed analysis of the  $\nu$  (C=O) stretching region of its complex with HPBCD does not clarify the molecular interaction between the BUD and the HPBCD.

The  $\nu$  (OH) stretching band (Figure 4.8) in the IR spectrum at  $3488\text{ cm}^{-1}$  suggests that external hydrogen bonding occurs in the crystalline BUD. The CH stretching region comprises several features in the wavenumber range  $3100\text{--}2800\text{ cm}^{-1}$  (Figures 4.8 and 4.9 for the IR and Raman spectra, respectively); the CH stretching bands of the unsaturated, aromatic component of BUD are more clearly shown in the Raman spectrum rather than in the IR spectrum (Table 4.1) and can be assigned to bands at  $3043$  and  $3010\text{ cm}^{-1}$  in the Raman spectrum. The CH aliphatic stretching bands comprise both  $\text{CH}_3$  and  $\text{CH}_2$  symmetric and asymmetric stretching modes assigned to the medium-strong features between  $2990$  and  $2871\text{ cm}^{-1}$ . A weak feature at  $2755\text{ cm}^{-1}$  in the IR spectrum (Figure 4.8) is assignable to a combination band arising from the  $\text{CH}_3\text{CH}_2$  – end group of the aliphatic chain attached to the heterocyclic five-membered ring (Edwards et al., 1995b).

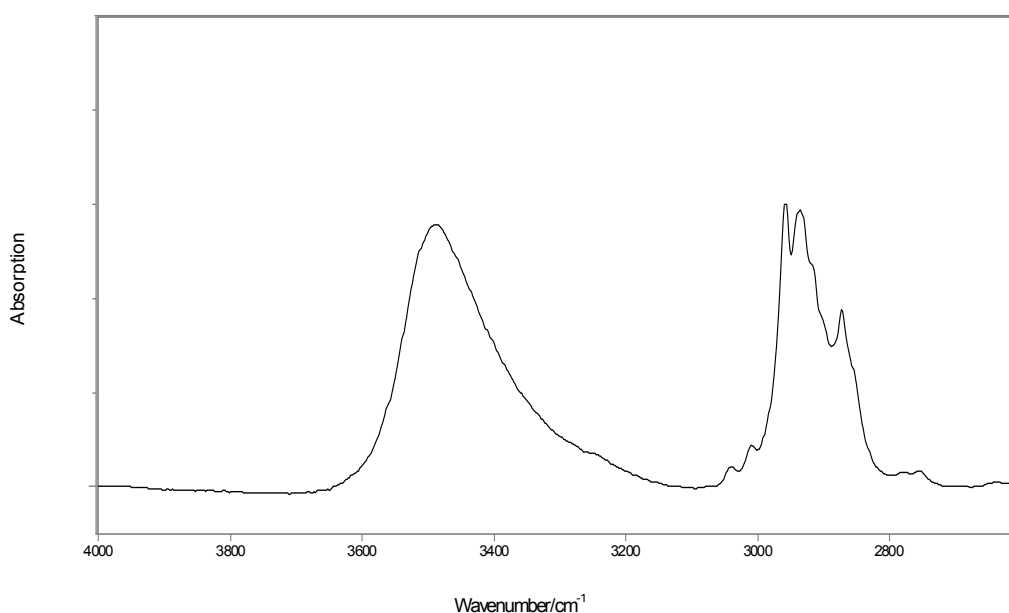


**Figure 4.8. The IR spectrum of BUD,  $2600 - 4000\text{ cm}^{-1}$  region.**

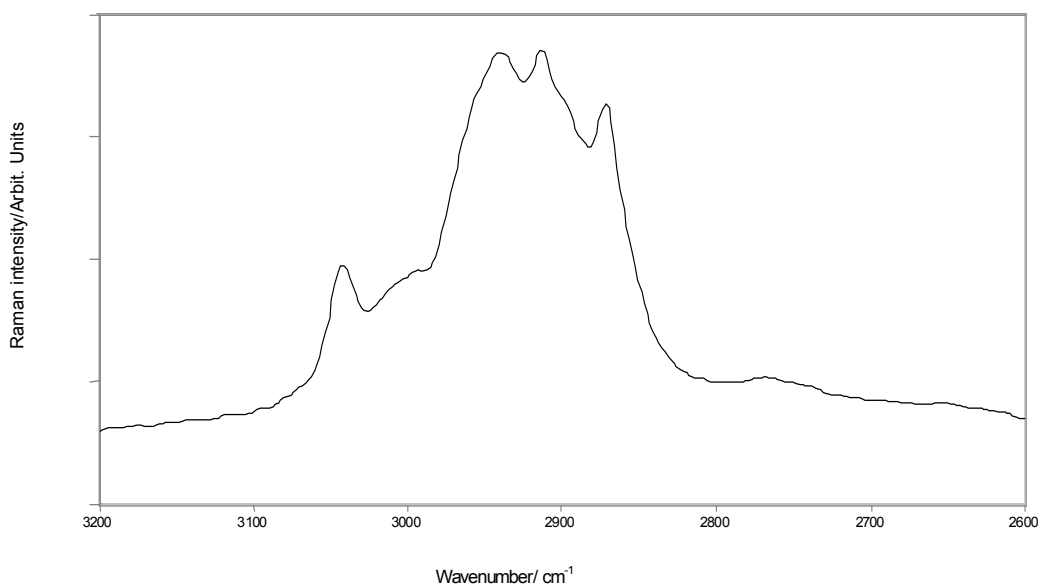


**Figure 4.9. The Raman spectrum of BUD, 2600 – 3200  $\text{cm}^{-1}$  region.**

#### **4.3.1.2.2. 1780 – 1580 $\text{cm}^{-1}$ region**

This is a very important spectroscopic region for structural studies, particularly for the C=O and C=C groups in this molecule. Expanded wavenumber regions of the IR and Raman spectra are shown in Figures 4.10 and 4.11, respectively. The IR spectrum has two very strong bands at 1721 and 1668  $\text{cm}^{-1}$  compared with a single strong Raman band at 1656  $\text{cm}^{-1}$ . Close inspection of Figures 4.10 and 4.11 reveals that the strong IR band at 1721  $\text{cm}^{-1}$  has a weak shoulder at 1715  $\text{cm}^{-1}$  and that at 1668  $\text{cm}^{-1}$  has a weak shoulder at 1656  $\text{cm}^{-1}$ ; whereas the Raman band at 1656  $\text{cm}^{-1}$  has a weak shoulder at 1668  $\text{cm}^{-1}$  and two components are identifiable for a weak broad band at 1714 and 1721  $\text{cm}^{-1}$ . There are two other bands clearly seen in this spectral region at 1625, 1603 and 1627, 1602  $\text{cm}^{-1}$  in the IR and Raman spectra, respectively. The strong band at 1721  $\text{cm}^{-1}$  in the IR can be attributed to the carbonyl attached to the aliphatic ring (*cf.* literature values for 5-membered aliphatic ring at 1750–1700  $\text{cm}^{-1}$ , and dimethyl ketone at 1715  $\text{cm}^{-1}$ ) (Colthup et al., 1975) whereas that at 1668  $\text{cm}^{-1}$  can be attributed to the quinonoid aromatic C=O (*cf.* benzophenone at 1660  $\text{cm}^{-1}$ ). para -Substitution in an

aromatic ring decreases their mode further in wavenumber. In contrast, the strong Raman spectral feature at  $1656\text{ cm}^{-1}$  can be attributed to C=C stretching in the quinonoid aromatic ring. Figure 4.10 and 4.11 also show the curve-resolved spectral region accomplished using the GRAMS8 package which contain the components of the C=O and C=C modes discussed above.

The  $1714\text{ cm}^{-1}$  band in the doublet is reliably assigned to the intramolecular hydrogen bonded C=O group which with the evidence from the OH stretching region, can be associated with the OH group on the side chain of the 5-membered aliphatic ring. Another possible assignment of the carbonyl bands at  $1720$  and  $1714\text{ cm}^{-1}$  is a monomer/dimer structure but this can be excluded here on the basis of the PXRD evidence. Considerable spectroscopic attention focuses on the closeness in wavenumber between the aromatic C=O at  $1668\text{ cm}^{-1}$  (strong in the IR and weak in the Raman) and the C=C band at  $1656\text{ cm}^{-1}$  (strong in the Raman and weak in the IR); close coupling between the conjugated C=C and C=O in the aromatic ring is suggested and the quantum chemical calculations confirm this.

The remaining two vibrational bands in this wavenumber region at  $1627$  and  $1602\text{ cm}^{-1}$  (Raman),  $1625$  and  $1603\text{ cm}^{-1}$  (IR) can be assigned on the basis of the quantum chemical calculations to molecular vibrations that involve both C=C and C=O groups in an asymmetric ring vibrations.

It is appropriate here to consider the results from our interpretation of the C=O and C=C stretching region of BUD in comparison with the previously reported IR spectrum (FDM). Firstly, Bandi et al (Bandi et al., 2004) did not consider the R&S epimers of BUD. Secondly, they have calculated that the molecular interaction between BUD and HPBCD should have produced a band wavenumber shift in the IR of  $11\text{ cm}^{-1}$ , from which they proposed that there is a possible change in the environment of the BUD

band of the quinonoid C=O group. They observed that there is a change in the spectrum with a shift from 1673 to 1662  $\text{cm}^{-1}$ . Our Raman and IR structural analysis here can now be applied to the data of Bandi et al. and we can confirm the assignment of 1668  $\text{cm}^{-1}$  band as a quinonoid structure. It is interesting also that the 11  $\text{cm}^{-1}$  shift reported on molecular complexation by Bandi et al now brings their modes into almost exact coincidence with the C=C Raman mode, when the close ring coupling between the C=C and C=O is supported from our calculations.

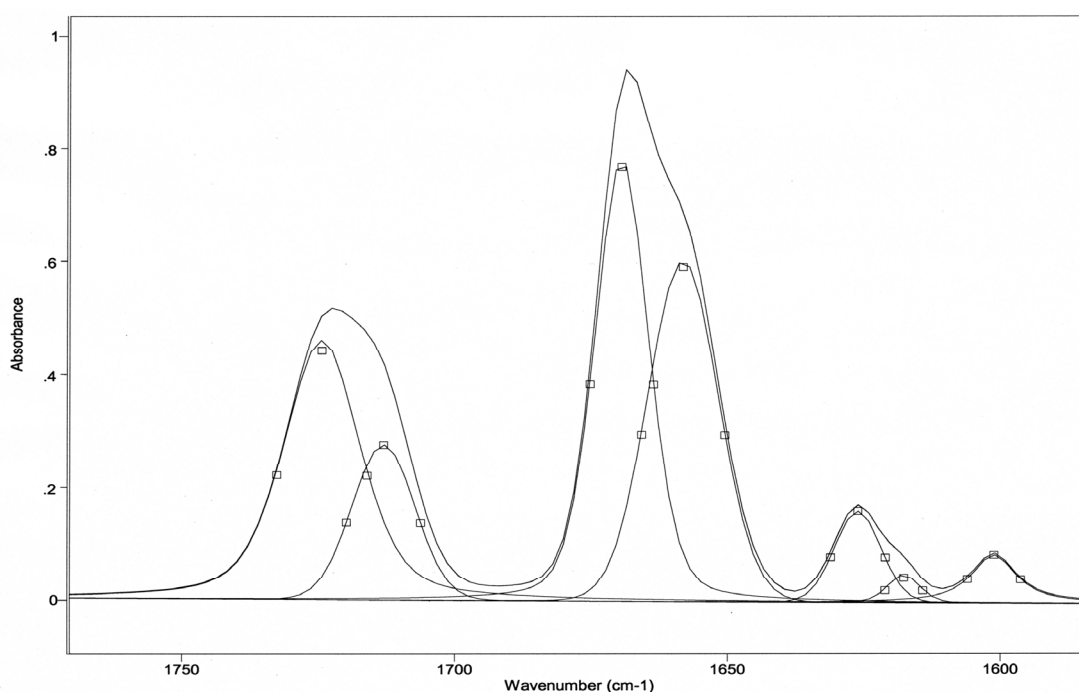


**Figure 4.10. Expanded wavenumber region of the IR spectrum of BUD (1580 – 1780  $\text{cm}^{-1}$ ), showing observed (-) and curve resolved ( $\square$ ) component spectra.**

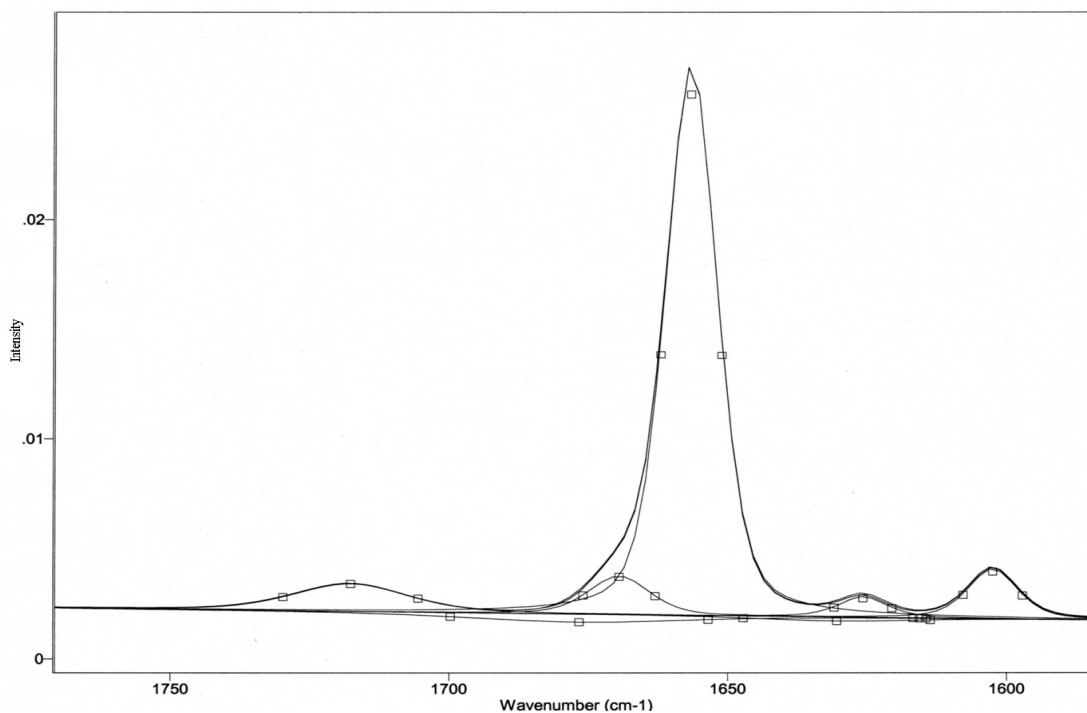


**Figure 4.11. Expanded wavenumber region of the Raman spectrum of BUD (1580 – 1780  $\text{cm}^{-1}$ ), showing observed (-) and curve resolved ( $\square$ ) component spectra.**

#### 4.3.1.2.3. 1800 – 100 $\text{cm}^{-1}$ region

The IR and Raman spectra over this wavenumber range are shown in Figures 4.12 and 4.13, respectively; the IR comprises a rich spectrum from the C=O and C=C functionalities, which have already been discussed in some detail above, along with many bands of medium and strong intensities, whereas the Raman spectrum consists mainly of the strong C=C features and relatively few, weaker features. In the range 1450 – 1300  $\text{cm}^{-1}$  we expect  $\text{CH}_3$  and  $\text{CH}_2$  aliphatic bending vibrations to occur with CHO deformations around 1375 – 1410  $\text{cm}^{-1}$ . Lower in wavenumber, we expect to find the COC ether stretching modes at 1140/1130  $\text{cm}^{-1}$  and 1050/1040  $\text{cm}^{-1}$  strong in the IR, and at 870/850  $\text{cm}^{-1}$  of medium intensity in the Raman spectrum. CCO stretching occurs between 1150-1075 and 1075-1000  $\text{cm}^{-1}$  for primary and secondary alcohols, with strong bands in the IR spectrum and medium bands in the Raman spectrum. COH bending occurs over a wide range between 1430 and 1200  $\text{cm}^{-1}$ , weak in intensity in the

IR spectrum and of medium weak intensity in the Raman spectrum. The CH<sub>2</sub> scissoring and wagging modes occur near 1250 cm<sup>-1</sup>.

Then, in the 1100 – 900 cm<sup>-1</sup> region we can expect modes arising from CCH bending and C–O stretches in primary and secondary alcohols near 1060 cm<sup>-1</sup> and C–C stretching modes in the aliphatic chains and alicyclic moieties. Methyl rocking and CH<sub>2</sub> rocking modes extend over the region 970 – 760 cm<sup>-1</sup>.

Finally, complex ring modes of CCO and COCOC vibrations and deformations in the range between 660 and 500 cm<sup>-1</sup> occur in the low wavenumber region; in this region, we should expect the aromatic quinonoid ring deformations near 600 cm<sup>-1</sup>. In the weak bands observed in the Raman spectrum below 400 cm<sup>-1</sup>, the methyl torsional mode at 265 cm<sup>-1</sup> of medium weak intensity can be noted.

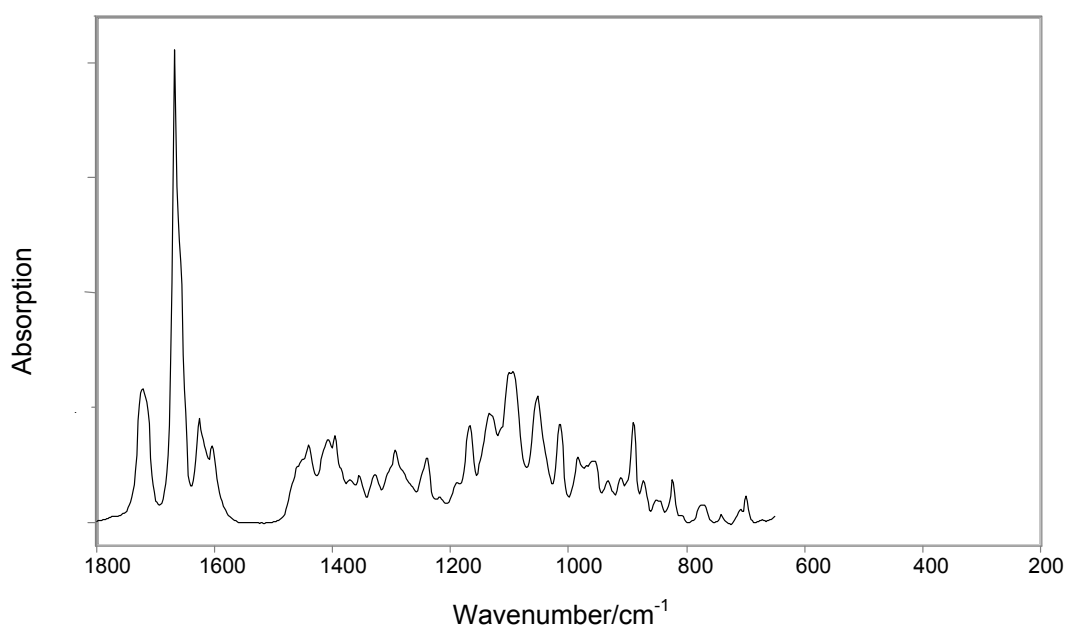


**Figure 4.12. Expanded wavenumber region of the IR spectrum of BUD (100 – 1800 cm<sup>-1</sup>).**

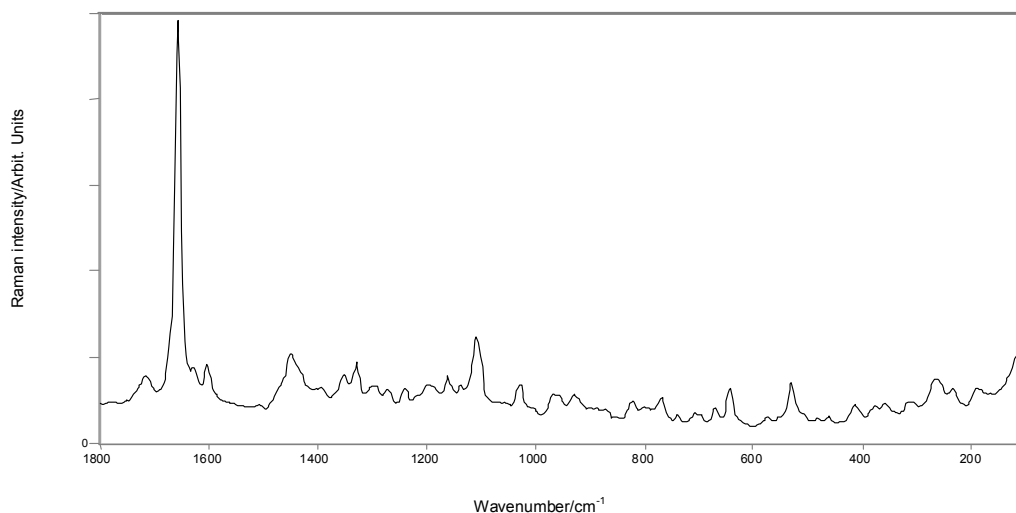


**Figure 4.13. Expanded wavenumber region of the Raman spectrum of BUD (100 – 1800  $\text{cm}^{-1}$ ).**

The key Raman spectral features of BUD are the aromatic  $\nu(\text{CH})$  band at  $3043 \text{ cm}^{-1}$ , the  $\nu_{\text{as}}(\text{CH}_2)$  band at  $2940 \text{ cm}^{-1}$ , the  $\nu(\text{CH}_2)$  bands at  $2914$  and  $2871 \text{ cm}^{-1}$  and the  $\nu(\text{C}=\text{C})$  band at  $1656 \text{ cm}^{-1}$ , while its key IR spectral features are the hydrogen bonded  $\nu(\text{OH})$  band at  $3488 \text{ cm}^{-1}$ , the  $\nu_{\text{as}}(\text{CH}_2)$  band at  $2936 \text{ cm}^{-1}$ , the  $\nu(\text{CH}_2)$  band at  $2873 \text{ cm}^{-1}$ , the  $\nu(\text{C}=\text{O})$  band at  $1721 \text{ cm}^{-1}$ , the  $\nu(\text{C}=\text{C})$  band at  $1668 \text{ cm}^{-1}$ , the in-plane  $\delta(\text{CH})$  band at  $1407 \text{ cm}^{-1}$ , the  $\nu(\text{C}-\text{C})$  band at  $1292 \text{ cm}^{-1}$ , the  $\nu(\text{C}-\text{OH})$  bands at  $1051$  and  $1014 \text{ cm}^{-1}$  and the CCH aromatic deformation band at  $888 \text{ cm}^{-1}$ .

Molecular vibrational assignments for the observed IR and Raman bands are given in Table 4.1.

**Table 4.1. Vibrational wavenumbers/cm<sup>-1</sup> of BUD.**

Observed		Calculated	Proposed Assignment
Raman	IR		
-	3488, br, s	3419	OH stretching, H-bonded
3043 m	3040 w	3032	aromatic CH stretching
3010 mw	3009 w	3007	(C=CH) stretching
2990 mw	-	2994	$\nu_{as}$ CH <sub>3</sub> stretching
-	2958	2964	$\nu_{as}$ CH <sub>3</sub> , $\nu_{as}$ CH <sub>2</sub> stretching
2940 s	2936 s	2946	$\nu_{as}$ CH <sub>2</sub> stretching
2914 s	2915 m, sh	2929	$\nu$ CH <sub>2</sub> stretching
2902 w, sh	2900 w, sh	2900	$\nu$ CH <sub>3</sub> stretching
2871 s	2873 s	2875	$\nu$ CH <sub>2</sub> stretching
2755 mw	2755 w		(CH <sub>3</sub> -CH <sub>2</sub> -) end group; combination band
1721 w, sh	1721 s	1687	$\nu$ (C=O)
1714 mw, br	1715 w, sh		$\nu$ (C=O)
1668 w, sh	1668 s	1665	$\nu$ (C=O)
1656 vs	1656 mw, sh		$\nu$ (C=C)
1627 mw	1625 ms	1632	
1602 mw	1603 ms	1597	
1451 mw	1450 mw, sh		CH <sub>3</sub> symmetric deformation
	1440 m	1429	
	1407 ms	1403	CH deformation/ in plane
	1394 ms	1401	
	1369 mw	1367	
1352 w	1353 mw	1354	
1329 mw	1327 mw	1330	
1296 w	1292 m	1285	$\nu$ (C-C)
1240 w	1239 m	1239	
	1217 w	1225	
1162 w	1166	1152	
1130 w	1133 m	1141	
1109 mw	1110 m	1112	
	1092 m	1097	
1029 w	1051 m	1067	C-OH stretching
		1030	
	1014 m	1018	C-OH stretching
970 w	982 mw	987	CH <sub>3</sub> rocking
	956 mw	957	CH <sub>3</sub> rocking
	932 w	933	
	910 w	916	
	888 ms	892	CCH aromatic deformation
	872 mw	866	CCH aromatic deformation
	849 m, br	847	
823 w	821 m	821	
768 w	769 mw		CH <sub>2</sub> rocking
	739 w		

**Table 4.1. (Continued)**

Observed		Calculated	Proposed Assignment
Raman	IR		
	696 mw		CH wagging
671 w			
643 mw			
531 mw		538	
414 w			
312 w			
265 mw			CH <sub>3</sub> τ

### 4.3.2. Fluticasone propionate

An initial structure (code DAXYUX) (Figure 4.14) for the geometry optimisation was taken from the CSD optimised using BLYP density functional theory (Becke, 1988; Lee et al., 1988).

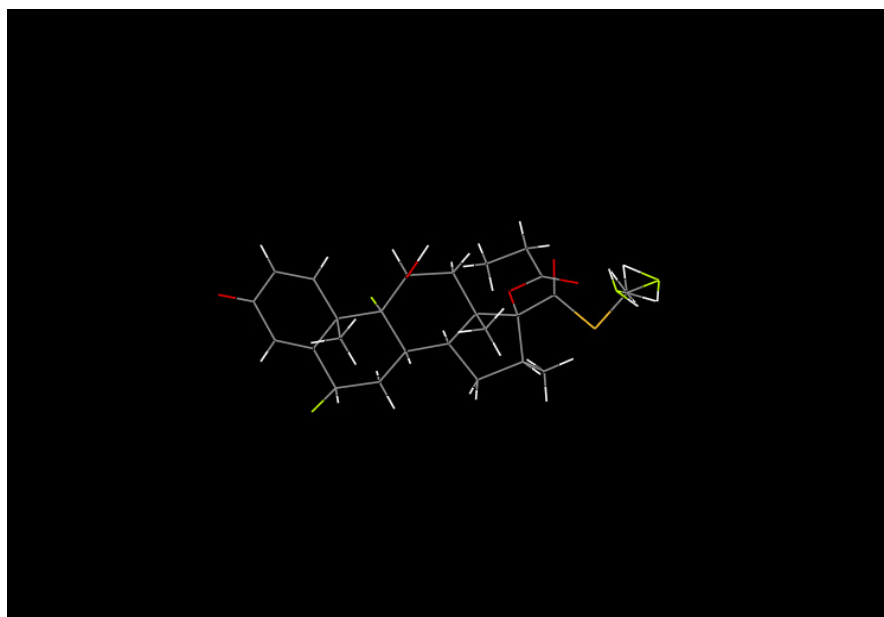


**Figure 4.14. The crystal structure of FP (code DAXYUX).**

The IR and FT-Raman spectra are shown in Figures 4.15-4.17. A complete assignment of the experimental vibrational features was carried out (Table 4.2) in the light of both the theoretical results presently performed and the vibrational spectroscopic data. Several calculated modes have been matched with the experimentally observed bands in the IR and Raman spectra, and these modes have been described. The vibrational spectra illustrate clearly the complexity of structural information that is provided from the IR and Raman analysis.

#### **4.3.2.1. 3700 – 2600 cm<sup>-1</sup> region**

Although the IR and Raman spectra have been reported previously (Guo-feng et al., 2007; Theophilus et al., 2006), but these reports provide neither spectral band assignments nor vibrational spectroscopic characterisation in conjunction with the quantum chemical calculations.

The profile of the  $\nu$  (OH) stretching band (Figure 4.15) in the IR spectrum at 3336 cm<sup>-1</sup> suggests that external hydrogen bonding occurs in the crystalline FP. The CH stretching region comprises several features in the wavenumber range 3100 – 2800 cm<sup>-1</sup> (Figure 4.15) for the IR and Raman spectra; the CH stretching bands of the unsaturated, component of FP are shown more clearly in the Raman spectrum rather than in the IR spectrum (Table 4.2) and can be assigned to the bands at 3075 and 3058 cm<sup>-1</sup> in the Raman spectrum in addition to, the CH stretching band of the five membered ring at 3023 cm<sup>-1</sup>. The CH aliphatic stretching bands comprise both CH<sub>3</sub> and CH<sub>2</sub> symmetric and asymmetric stretching modes which have been assigned to the medium intensity features between 2878 and 2965 cm<sup>-1</sup>.

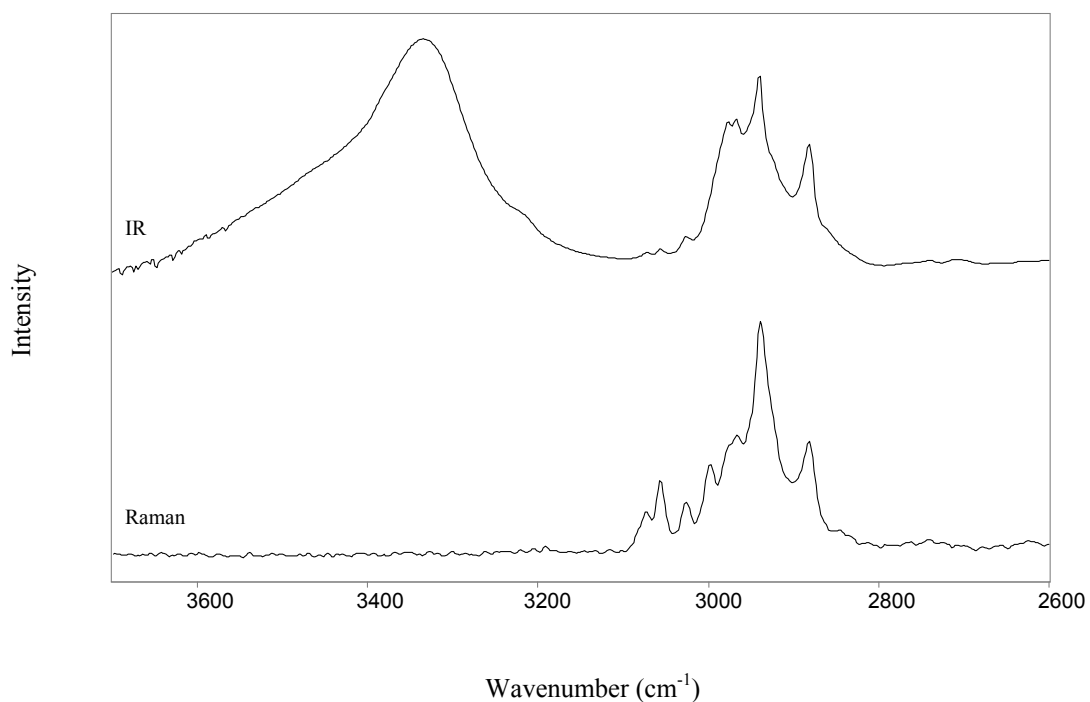


**Figure 4.15. FT-Raman and IR spectral stackplot of FP in the 2600 – 3700  $\text{cm}^{-1}$  region.**

#### 4.3.2.2. 1800 – 1550 $\text{cm}^{-1}$ region

This is a very important spectroscopic region for structural studies, particularly for the C=O and C=C groups in the molecule. Expanded wavenumber regions of the IR and Raman spectra are shown in Figure 4.16. The IR spectrum has one very strong band at 1661  $\text{cm}^{-1}$  and four strong bands at 1744, 1699, 1616 and 1611  $\text{cm}^{-1}$  compared to one very strong band at 1663  $\text{cm}^{-1}$ , one medium band at 1606  $\text{cm}^{-1}$ , medium shoulder band at 1611  $\text{cm}^{-1}$  and two weak bands at 1742 and 1698  $\text{cm}^{-1}$  in the Raman spectrum. The strong bands at 1744 and 1699  $\text{cm}^{-1}$  in the IR spectrum and the weak Raman spectral features at 1742 and 1698  $\text{cm}^{-1}$  can be attributed to the carbonyl attached to the aliphatic ring (*cf.* literature values for a five membered aliphatic ring at 1750 – 1700  $\text{cm}^{-1}$ , and dimethyl ketone at 1715  $\text{cm}^{-1}$ ) (Colthup et al., 1975) and carbonyl attached to sulfur respectively, this shift occurs because of force constant changes in the carbonyl bond

(Lin-Vien et al., 1991), whereas that at 1661 and 1616  $\text{cm}^{-1}$  can be attributed to the C=O and C=C stretching vibration in the quinonoid aromatic ring (*cf.* benzophenone at 1660  $\text{cm}^{-1}$ ), which couples together in the same moiety. This coupling explains the observed strength in both Raman and IR bands at 1663 and 1661  $\text{cm}^{-1}$  respectively.

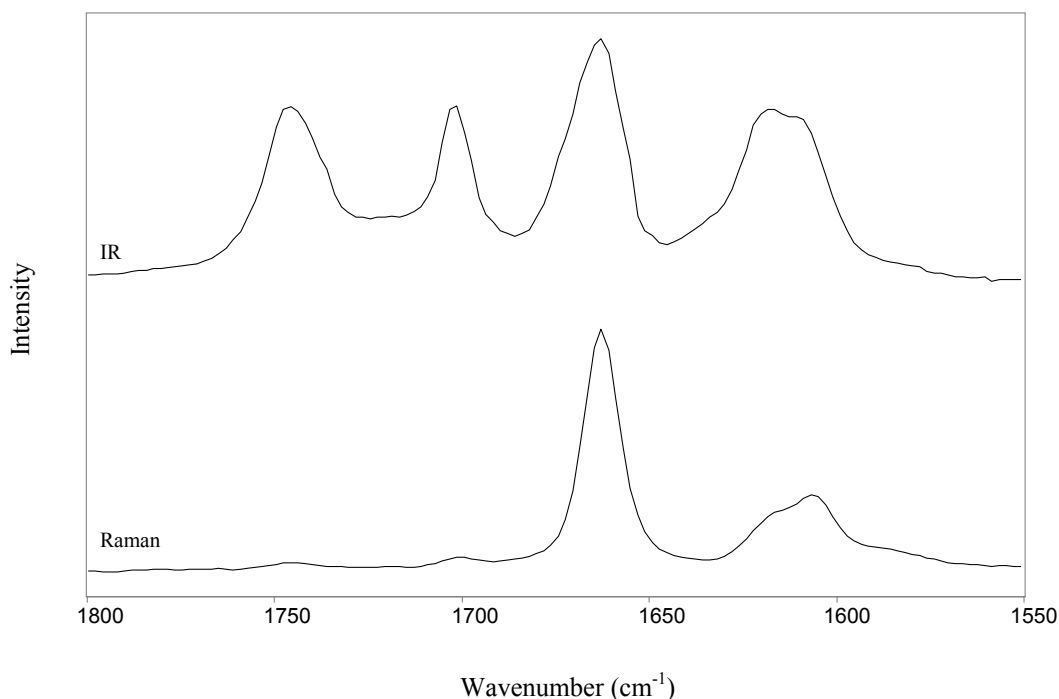


**Figure 4.16.** FT-Raman and IR spectral stackplot of FP in the 1550 – 1800  $\text{cm}^{-1}$  region.

#### 4.3.2.3. 1800 – 100 $\text{cm}^{-1}$ region

The IR and Raman spectra over this wavenumber region are shown in Figure 4.17; the IR region comprises a rich spectrum from the C=O and C=C functionalities, which have been already discussed in some detail above, along with several bands of medium and strong intensities, whereas the Raman spectrum consists mainly of the strong C=C features and other weaker features. In the range 1530 – 1330  $\text{cm}^{-1}$ , we expect  $\text{CH}_3$ ,  $\text{CH}_2$  and CH aliphatic deformation vibrations to occur. Lower in wavenumber, we expect to

find the aliphatic C-F stretching vibrations at 1271 and 1233  $\text{cm}^{-1}$ , of medium intensity in the IR spectrum and of weak intensity in the Raman spectrum. The in-plane  $\delta(\text{CH})$  vibration occurs at 1226  $\text{cm}^{-1}$  in the IR spectrum of medium intensity and at 1194  $\text{cm}^{-1}$  in the Raman spectrum of medium weak intensity and the  $\nu(\text{F-C-S})$  band occurs at 1027  $\text{cm}^{-1}$  in the IR spectrum of medium intensity and at 1023  $\text{cm}^{-1}$  in the Raman spectrum of weak intensity.

Methyl rocking and  $\text{CH}_2$  rocking modes extend over the range 970 – 995  $\text{cm}^{-1}$ , the CCH aromatic deformation mode extends over the range 870 – 900  $\text{cm}^{-1}$ , the (O=C-O-C) stretching mode occurs at 843  $\text{cm}^{-1}$ , the CH wagging mode occurs near 700  $\text{cm}^{-1}$  and the C-S stretching mode occurs in the range of 616 – 650  $\text{cm}^{-1}$ .

Finally, the complex ring modes of CCO and COCOC vibrations and deformations in the range between 600 and 500  $\text{cm}^{-1}$  occur. In the low wavenumber region the methyl torsional mode at 234 and 264  $\text{cm}^{-1}$  of weak intensity can be noted.

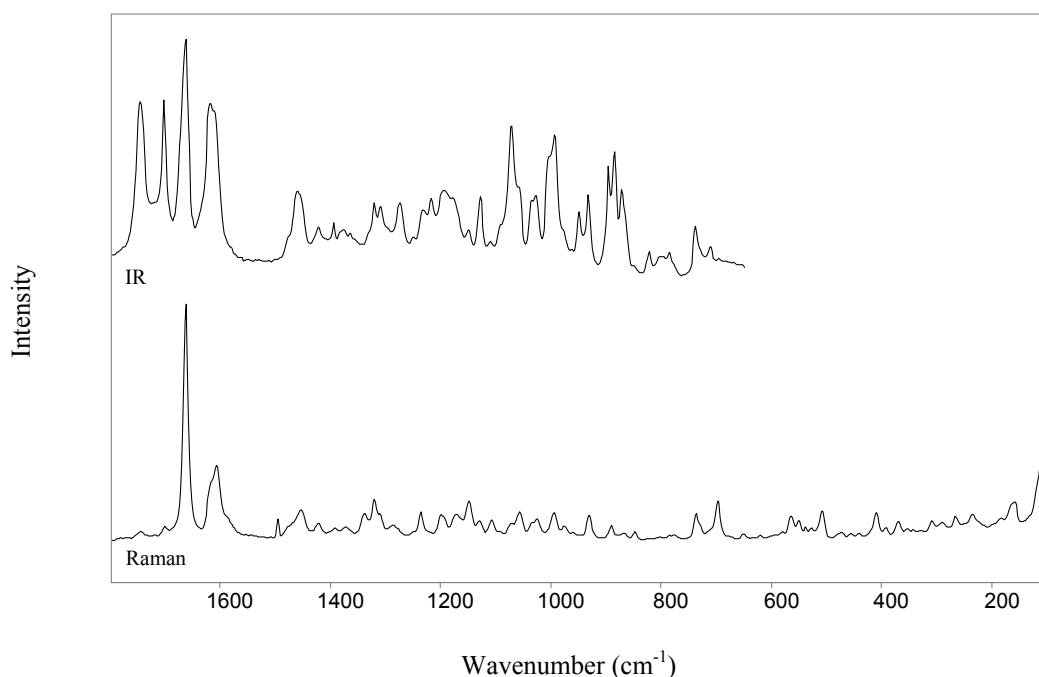


**Figure 4.17. FT-Raman and IR spectral stackplot of FP in the 100 – 1800  $\text{cm}^{-1}$  region.**

The key Raman spectral features of FP are the  $\nu_{as}(\text{CH}_2)$  band at  $2935\text{ cm}^{-1}$ , the  $\nu(\text{C}=\text{O})$  band at  $1663\text{ cm}^{-1}$  and the  $\delta(\text{CH}_3)$  band at  $1606\text{ cm}^{-1}$ , while the key IR spectral features are the  $\nu(\text{OH})$  band at  $3336\text{ cm}^{-1}$ , the  $\nu(\text{C}=\text{CH})$  band at  $2975\text{ cm}^{-1}$ , the  $\nu_{as}(\text{CH}_3)$ ,  $\nu_{as}(\text{CH}_2)$  bands at  $2964$ ,  $2942$  and  $2881\text{ cm}^{-1}$ , the  $\nu(\text{C}=\text{O})$  bands at  $1744$  and  $1661\text{ cm}^{-1}$ , the  $\nu(\text{S}-\text{C}=\text{O})$  band at  $1699\text{ cm}^{-1}$ , the  $\nu(\text{C}=\text{C})$  band at  $1616\text{ cm}^{-1}$ , the  $\delta(\text{CH}_3)$  band at  $1455\text{ cm}^{-1}$ , the  $\nu(\text{C}-\text{C})$  band at  $1304\text{ cm}^{-1}$ , the  $\nu(\text{C}-\text{F})$  band at  $1271\text{ cm}^{-1}$ , the in-plane  $\delta(\text{CH})$  band at  $1226\text{ cm}^{-1}$ , the  $\nu(\text{F}-\text{C}-\text{S})$  band at  $1027\text{ cm}^{-1}$ , the  $r(\text{CH}_3)$  band at  $993\text{ cm}^{-1}$ , the  $\delta(\text{C}-\text{C}-\text{C})$  band at  $944\text{ cm}^{-1}$  and the CCH aromatic deformation bands at  $895$ ,  $884$  and  $873\text{ cm}^{-1}$ .

**Table 4.2. The observed and calculated vibrational wavenumbers/ $\text{cm}^{-1}$  of FP. The calculated Raman and IR intensities ( $I_{\text{Raman}}$  and  $I_{\text{IR}}$ ) are relative to that of  $\nu(\text{C}=\text{O})$  at  $1667\text{ cm}^{-1}$ , set arbitrarily equal to 1.**

Observed		Calculated			Proposed Assignment
Raman ( $\text{cm}^{-1}$ )	IR ( $\text{cm}^{-1}$ )	$\nu$	$I_{\text{Raman}}$	$I_{\text{IR}}$	
	3336 m	3567	0.513	0.030	$\nu(\text{OH})$
3075 w	3069 vw	3123	0.186	0.035	$\nu(\text{CH})$
3058 mw	3051 vw	3082	0.465	0.069	$\nu(\text{CH})$
3023 mw	3024 vw	3027	0.229	0.120	$\nu(\text{CH})$ of the five membered ring
3005 mw	2975 m	2999	0.291	0.119	$\nu(\text{C}=\text{CH})$
2965 mw	2964 m	2968	0.138	0.080	$\nu_{as}(\text{CH}_3)$ , $\nu_{as}(\text{CH}_2)$
2935 m	2942 m	2944	0.308	0.155	$\nu_{as}(\text{CH}_2)$
2878 mw	2881 m	2933	0.356	0.102	$\nu_s(\text{CH}_2)$
1742 w	1744 s	1737	0.684	0.047	$\nu(\text{C}=\text{O})$
1698 w	1699 s	1695	0.118	0.525	$\nu(\text{S}-\text{C}=\text{O})$
1663 vs	1661 vs	1667	1.000	1.000	$\nu(\text{C}=\text{C})$
	1616 s	1639	0.036	0.155	$\nu(\text{C}=\text{C})$
1611 sh,m	1611 s				
1606 m		1607	0.054	0.039	$\delta(\text{CH}_3)$
1492 mw	1530 vw	1493	0.071	0.019	$\delta(\text{CH}_3)$
1453 mw	1455 m	1445	0.027	0.058	$\delta(\text{CH}_3)$
1422 w	1421 mw	1425	0.004	0.024	Ring stretching
1387 w	1395 mw	1399	0.041	0.017	$\delta(\text{CH}_2)$
1369 w	1376 mw	1372	0.028	0.045	
1334 w	1365 mw	1357	0.019	0.002	$\delta(\text{CH})$
1321 m	1319 m	1323	0.074	0.034	
1281 w	1304 m	1298	0.081	0.059	$\nu(\text{C}-\text{C})$
1233 mw	1271 m	1267	0.035	0.074	$\nu(\text{C}-\text{F})$

**Table 4.2. (Continued)**

Observed		Calculated			Proposed Assignment
Raman (cm <sup>-1</sup> )	IR (cm <sup>-1</sup> )	$\nu$	$I_{\text{Raman}}$	$I_{\text{IR}}$	
	1248 m	1244	0.018	0.055	
1194 mw	1226 m	1223	0.097	0.052	In-plane $\delta(\text{CH})$
	1214 m	1217	0.015	0.016	
1168 mw	1188 m	1177	0.017	0.022	
1146 mw	1147 w	1147	0.004	0.397	
1126 w	1124 m	1124	0.167	0.046	
1106 w		1109	0.021	0.016	
1067 w	1064 s	1070	0.039	0.090	
1058 w		1058	0.018	0.055	
1023 w	1027 m	1020	0.023	0.480	$\nu(\text{F-C-S})$
992 w	993 s	993	0.097	0.196	$r(\text{CH}_3)$
970 w		972	0.004	0.053	$r(\text{CH}_3)$
953 w	944 m	953	0.047	0.257	$\delta(\text{C-C-C})$
931 w	933 m	936	0.015	0.124	
887 w	895 ms	904	0.028	0.135	CCH aromatic deformation
	884 ms	877	0.011	0.094	CCH aromatic deformation
869 w	873 m	863	0.016	0.110	CCH aromatic deformation
843 w		835	0.033	0.028	$\nu(\text{O=C-O-C})$
	816 w	816	0.022	0.046	
799 vw	797 w	802	0.002	0.014	
773 vw	782 w	776	0.021	0.032	$r(\text{CH}_2)$
733 m	734 mw	751	0.008	0.009	
698 vw	707 w	706	0.003	0.013	CH wagging
650 vw		655	0.005	0.037	$\nu(\text{C-S})$
616 vw		626	0.015	0.012	$\nu(\text{C-S})$
584 w		581	0.005	0.016	
562 w		558	0.034	0.015	
549 w		541	0.004	0.084	
532 w		524	0.022	0.009	
519 w		512	0.019	0.012	Out-of-plane $\delta(\text{CC})$
505 w		508	0.002	0.014	
470 vw		484	0.019	0.016	
448 vw		448	0.008	0.004	
435 vw		425	0.009	0.007	
409 w		408	0.013	0.033	
387 vw		387	0.014	0.018	
370 w		372	0.015	0.025	
348 vw		348	0.013	0.014	
330 vw		324	0.007	0.203	
308 w		311	0.019	0.008	
286 vw		282	0.011	0.08	
264 w		264	9.6e-4	0.018	$\text{CH}_3\tau$
234 w		237	0.013	0.026	$\text{CH}_3\tau$
159 w		156	0.010	0.011	

### 4.3.3. Salbutamol hemisulfate

Calculations were performed on the SB cation (Figure 4.18) and its molecular structure used for geometry optimisation, using the BLYP density functional with a 6-31G\* basis set (Becke, 1988; Lee et al., 1988), was taken from Cambridge Crystal Structure Database (CSD) with code SALBUT, Figure 4.19.

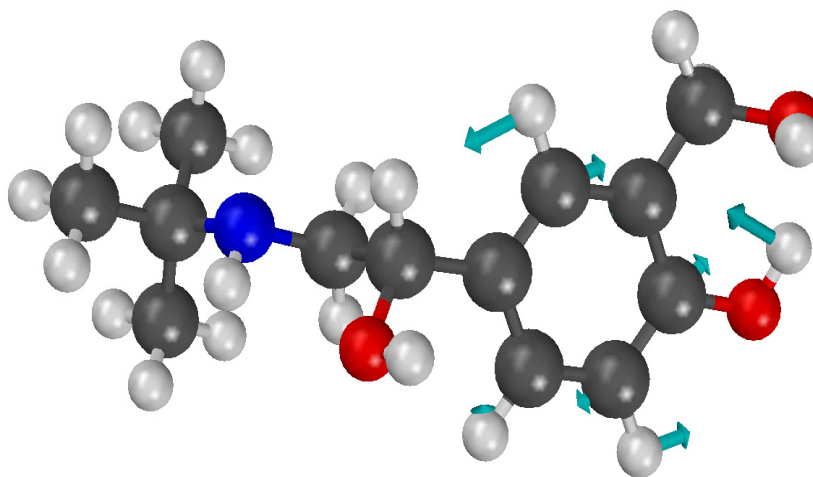


Figure 4.18. The SB conformation

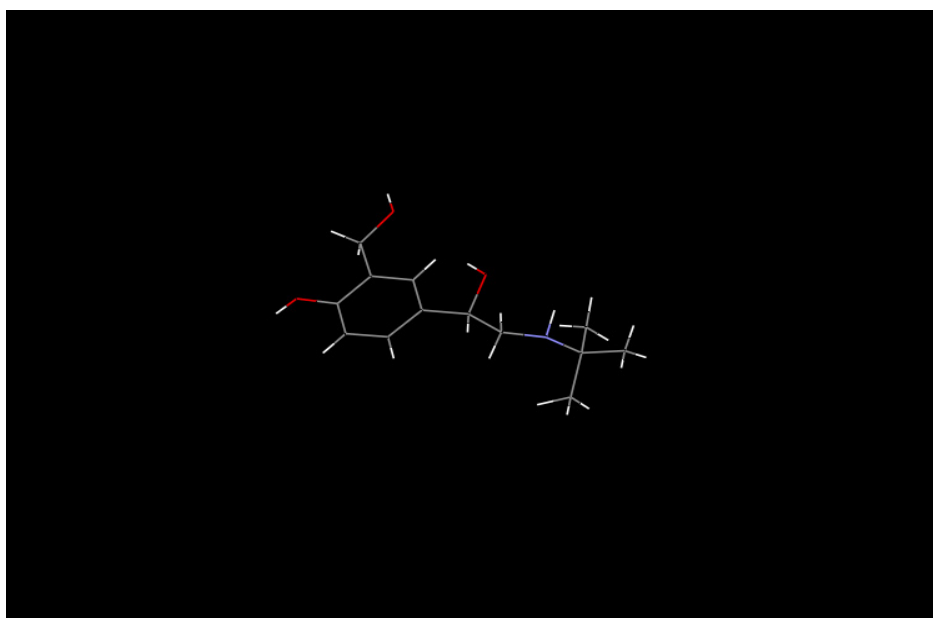
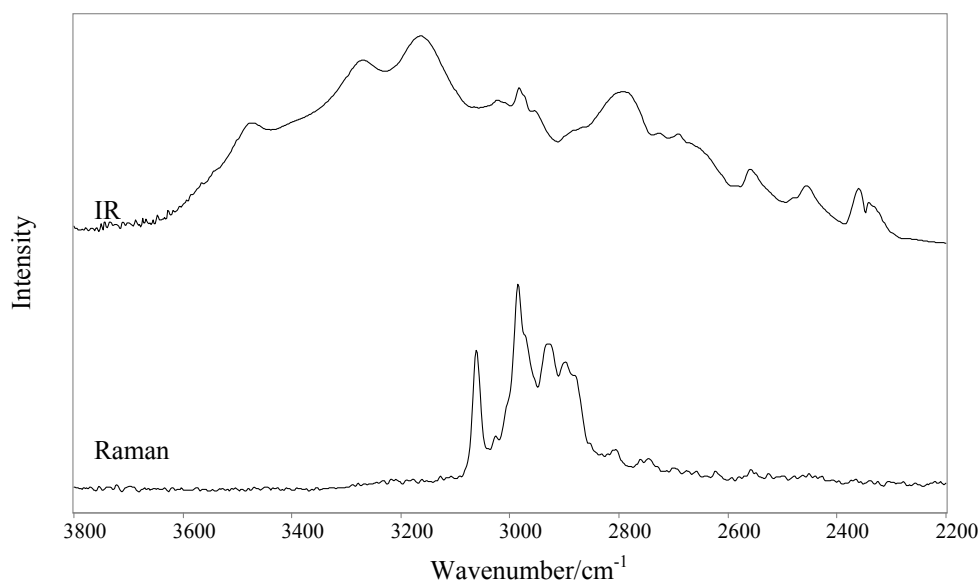


Figure 4.19. The crystal structure of SB (code SALBUT).

The observed IR and Raman spectroscopic wavenumbers are listed in Table 4.3 along with the calculated values; assignment of the major experimental vibrational features was carried out in the light of the theoretical results and the vibrational spectroscopic data previously reported (Corrigan et al., 2006; Edwards et al., 1993a; FDM; Ticehurst et al., 1994). Several calculated modes have been matched with experimentally observed bands in the IR and Raman spectra, and these modes have been described; very weak features in the observed spectra cannot be reliably assigned on the basis of the quantum chemical calculations.

#### **4.3.3.1. 3800 – 2200 cm<sup>-1</sup> region**

The broad rather diffuse  $\nu$  (OH) stretching band (Figure 4.20) in the IR spectrum at 3474 cm<sup>-1</sup> suggests that hydrogen bonding occurs in the crystalline SB. The  $\nu$  (NH) stretching band is observed in the IR spectrum in the range 3280 – 3160 cm<sup>-1</sup> (Figure 4.16). The CH stretching region comprises several features in the wavenumber range 3130 – 2800 cm<sup>-1</sup> (Figure 4.20) for the IR and Raman spectra; the CH stretching bands of the aromatic component of SB are shown in the Raman spectrum (Table 4.3) and can be assigned to the bands at 3127, 3107 and 3093 cm<sup>-1</sup>. The CH aliphatic stretching bands of CH<sub>3</sub> symmetric and asymmetric stretching modes are shown in the both Raman and IR spectra, and can be assigned to the medium strong features at 3025 and 2982 cm<sup>-1</sup> and the medium feature at 2954 cm<sup>-1</sup> in the IR spectrum, the weak feature at 3027 cm<sup>-1</sup>, the medium strong feature at 2985 cm<sup>-1</sup>, the medium shoulder feature at 2973 cm<sup>-1</sup> and the medium feature at 2880 cm<sup>-1</sup> in the Raman spectrum. The broad medium band at 2927 cm<sup>-1</sup> and the medium band at 2899 cm<sup>-1</sup> in the Raman spectrum can be attributed to  $\nu$  (CH) and  $\nu$  (CH<sub>2</sub>) attached to aliphatic (OH), respectively, and the weak feature at 2623 cm<sup>-1</sup> can be assigned to  $\nu$  (CC)<sub>ring</sub>.



**Figure 4.20. FT-Raman and IR spectral stack plot of SB in the 2200 – 3800  $\text{cm}^{-1}$  region.**

#### 4.3.3.2. 1800 – 1100 $\text{cm}^{-1}$ region

This is a very important spectroscopic region for structural studies, particularly for the C=C group in this molecule. Expanded wavenumber regions of the IR and Raman spectra are shown in Figure 4.21. It is worth noting that, the calculated band of  $\delta(\text{NH}_2^+)$  at 1643  $\text{cm}^{-1}$  was observed in neither IR nor Raman spectra and this may be attributed to the presence of sulfate anion which may hinder this feature. The IR region comprises a rich spectrum from the C=C functionality, along with several bands of medium and strong intensities, whereas the Raman spectrum consists mainly of the strong C=C features and several other weaker features. The  $\nu(\text{C}=\text{C})$  band occurs at 1616  $\text{cm}^{-1}$ , of medium strong intensity in both the Raman and IR spectra. The bands at 1616 and 1205  $\text{cm}^{-1}$  in both Raman and IR spectra and the band at 1558  $\text{cm}^{-1}$  in the IR spectrum can be assigned on the basis of quantum chemical calculations as hydrogen bonded C-OH angle coupled to a phenyl ring vibration. Again, it is worth noting that the calculated methyl deformation vibrational bands at 1569, 1563 and 1552  $\text{cm}^{-1}$  have not been

observed in the experimental vibrational spectra which may be due to the presence of the sulfate anion which may hinder the observation of some of the methyl deformation features. The very weak feature at  $1539\text{ cm}^{-1}$  and the medium strong feature at  $1507\text{ cm}^{-1}$  in the IR spectrum can be assigned to  $\nu(\text{CC})_{\text{ring}}$  and  $\delta(\text{CH}_2)_{(\text{sciss.})}$  modes, respectively. The medium intensity band in the Raman spectrum and the medium weak band in the IR spectrum at  $1468\text{ cm}^{-1}$  can be assigned to  $\delta(\text{CH}_2\text{-N})$ . In the  $1360 - 1390\text{ cm}^{-1}$  range in the IR spectrum we have observed three bands at  $1386$ ,  $1379$  and  $1362\text{ cm}^{-1}$  which can be assigned on the basis of quantum chemical calculations as mixed modes associated with  $\delta(\text{NH}_2^+)$ ,  $\delta(\text{CH}_2)$  and  $\delta(\text{CHOH})$  groups. In the range  $1470 - 1250\text{ cm}^{-1}$ , we expect  $\text{CH}_3$ ,  $\text{CH}_2$  and  $\text{CH}$  aliphatic bending vibrations bands to occur. Lower in wavenumber we have observed the  $\nu(\text{S=O})$  band at  $1156\text{ cm}^{-1}$  in the Raman spectrum and the  $\delta(\text{COH})$  and  $\delta(\text{CH}_2\text{OH})$  bands at  $1126\text{ cm}^{-1}$  and the very strong band at  $1112\text{ cm}^{-1}$  in the IR spectrum which can be assigned on the basis of quantum chemical calculations to hydrogen bonded  $\text{CH-OH}$  angle coupled to the phenyl ring vibration.

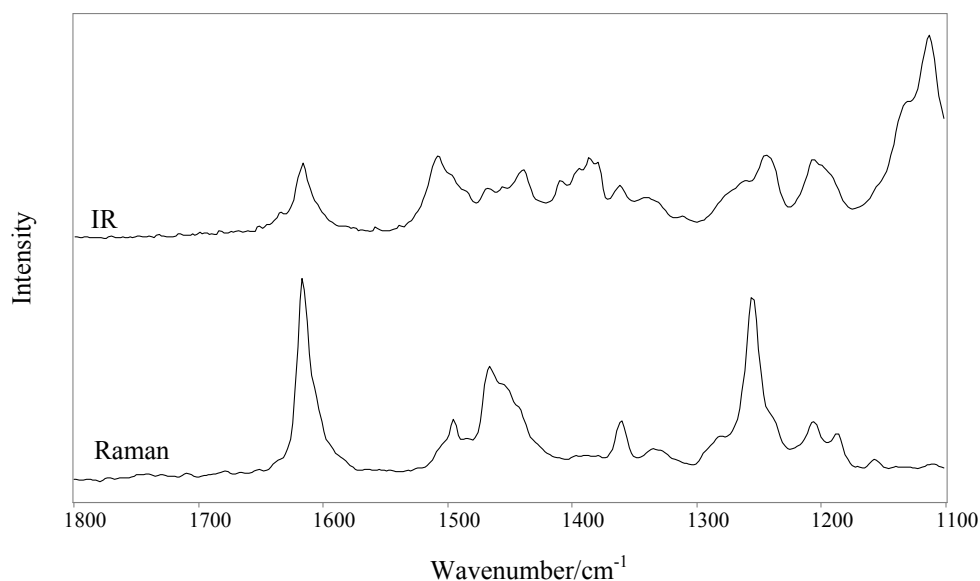


**Figure 4.21. FT-Raman and IR spectral stack plot of SB in the 1100 – 1800 cm<sup>-1</sup> region.**

#### 4.3.3.3. 1100 – 50 cm<sup>-1</sup> region

IR and Raman spectra over this wavenumber range are presented in Figure 4.22. The strong band in the IR spectrum at 1084 cm<sup>-1</sup> can be assigned on the basis of quantum chemical calculation to hydrogen bonded CH-OH & CH<sub>2</sub>OH angle coupled to phenyl ring vibration and the very strong band at 1029 cm<sup>-1</sup> can be assigned to r (CH<sub>3</sub>) mode. The three ν<sub>as</sub>(C-OH) bands of the three OH groups of SB are more clearly shown in the IR spectrum of medium intensity at 988 and 978 cm<sup>-1</sup> and weak intensity at 947 cm<sup>-1</sup> as well as the ν<sub>as</sub>(CN) and the ν<sub>as</sub>(CN) attached to the quaternary carbon bands at 916 and 840 cm<sup>-1</sup> respectively. Lower in wavenumber, we expect to find the ν(C-C-O) band at 780 cm<sup>-1</sup> in the Raman spectrum and at 773 cm<sup>-1</sup> in the IR spectrum and the CH wagging bands at 648 cm<sup>-1</sup> in the Raman spectrum and at 668 and 647 cm<sup>-1</sup> in the IR spectrum.

Finally, the complex ring modes of CCC and CCN deformations in the range between 300 and 550 cm<sup>-1</sup> occur. The very weak feature in the Raman spectrum at 404

$\text{cm}^{-1}$  can be assigned on the basis of quantum chemical calculations to  $\delta(\text{OH})$ . The methyl torsional band is observed in the Raman spectrum at  $264 \text{ cm}^{-1}$  of weak intensity. The skeletal mode extends over the region of  $80$  to  $150 \text{ cm}^{-1}$  in the Raman spectrum.

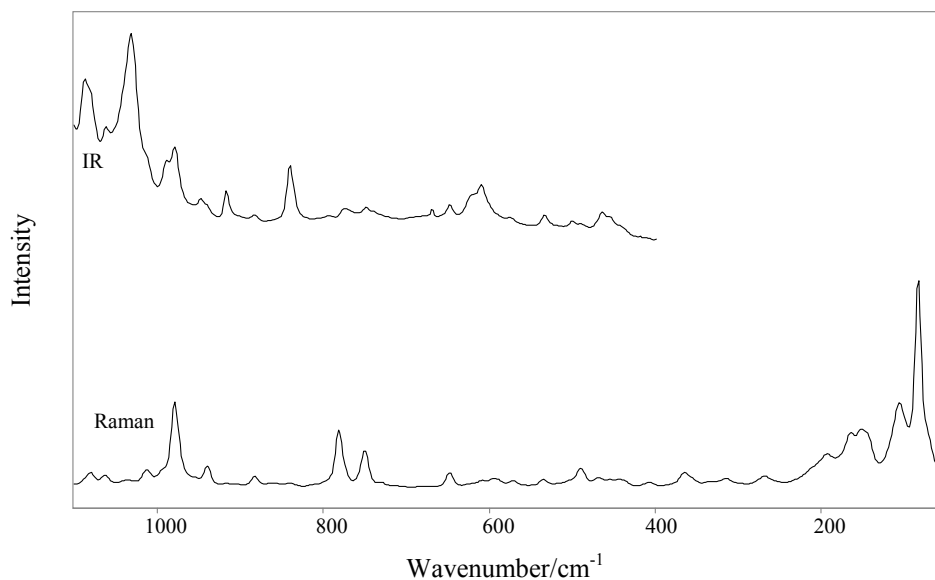


**Figure 4.22. FT-Raman and IR spectral stack plot of SB in the  $50 - 1100 \text{ cm}^{-1}$  region.**

The key Raman spectral features of SB are the  $\nu(\text{NH})$  band at  $3160 \text{ cm}^{-1}$ , the  $\nu(\text{CH}_2)$  and  $\nu(\text{CH}_3)$  bands at  $3062 \text{ cm}^{-1}$ , the  $\nu_{\text{as}}(\text{CH}_3)$  band at  $2985 \text{ cm}^{-1}$ , the  $\nu(\text{CH})$  attached to aliphatic (OH) band at  $2927 \text{ cm}^{-1}$ , the  $\nu(\text{CH}_2)$  attached to aliphatic (OH) band at  $2899 \text{ cm}^{-1}$ , the  $\nu(\text{CH}_3)$  band at  $2880 \text{ cm}^{-1}$ , the  $\nu(\text{C}=\text{C})$  band at  $1616 \text{ cm}^{-1}$ , the  $\delta(\text{CH}_2\text{-N})$  band at  $1466 \text{ cm}^{-1}$ , the  $\delta(\text{CH})$  band at  $1255 \text{ cm}^{-1}$ , the  $\nu_{\text{as}}(\text{C-OH})$  band at  $978 \text{ cm}^{-1}$ , the  $\nu(\text{C-C-O})$  band at  $780 \text{ cm}^{-1}$  and the skeletal mode bands at  $150$ ,  $101$  and  $81 \text{ cm}^{-1}$ , while its key IR spectral features are the  $\nu(\text{OH})$  band at  $3474 \text{ cm}^{-1}$ , the  $\nu(\text{NH})$  bands at  $3272$  and  $3162 \text{ cm}^{-1}$ , the  $\nu_{\text{as}}(\text{CH}_2)$  attached to (OH) band at  $3025 \text{ cm}^{-1}$ , the  $\nu_{\text{as}}(\text{CH}_3)$  bands at  $2982$  and  $2954 \text{ cm}^{-1}$ , the  $\nu(\text{C}=\text{C})$  band at  $1616 \text{ cm}^{-1}$ , the  $\delta(\text{CH}_2)_{(\text{sciss.})}$  band at  $1507 \text{ cm}^{-1}$ , the mixed modes associated with  $\delta(\text{NH}_2^+)$ ,  $\delta(\text{CH}_2)$  and  $\delta(\text{CHOH})$  at  $1386$  and  $1379 \text{ cm}^{-1}$ , the

hydrogen bonded C-OH angle coupled to phenyl ring vibration bands at 1205 and 1112  $\text{cm}^{-1}$ , the hydrogen bonded CH-OH & CH<sub>2</sub>OH angle coupled to phenyl ring vibration band at 1084  $\text{cm}^{-1}$ , the  $\nu(\text{CH}_3)$  band at 1029  $\text{cm}^{-1}$ , the  $\nu_{\text{as}}$  (C-OH) bands of the three (OH) groups at 988, 978 and 947  $\text{cm}^{-1}$  and the  $\nu_{\text{as}}(\text{CN})$  attached to the quaternary carbon band at 840  $\text{cm}^{-1}$

**Table 4.3. The observed and calculated vibrational wavenumbers/cm<sup>-1</sup> of SB. The calculated IR intensities (I<sub>IR</sub>) are relative to that of δ(COH) and δ(CH<sub>2</sub>OH) at 1187 cm<sup>-1</sup>. The calculated Raman intensities (I<sub>Raman</sub>) are relative to that of ν<sub>as</sub>(CH<sub>3</sub>) at 2997 cm<sup>-1</sup>.**

Observed		Calculated			Proposed Assignment
Raman (cm <sup>-1</sup> )	IR (cm <sup>-1</sup> )	ν	I <sub>Raman</sub>	I <sub>IR</sub>	
	3474 ms	3573	0.450	0.250	ν(OH)
	3272 s	3344	0.158	0.141	ν(NH)
3190 vw					ν(NH)
3177 vw					ν(NH)
3160 vs	3162 s	3208	0.345	0.452	ν(NH)
3127 w		3120	0.384	0.504	ν(CH) <sub>ring</sub>
3107 vw		3103	0.255	0.335	ν(CH) <sub>ring</sub>
3093 vw		3091	0.400	0.057	ν(CH) <sub>ring</sub>
3062 m		3058	0.261	0.342	ν(CH <sub>2</sub> ) & ν(CH <sub>3</sub> )
3027 w	3025 ms	3037	0.235	0.308	ν <sub>as</sub> (CH <sub>2</sub> ) attached to (OH)
2985 ms	2982 ms	2997	1.000	0.010	ν <sub>as</sub> (CH <sub>3</sub> )
2973 m,sh		2992	0.115	0.046	ν <sub>as</sub> (CH <sub>3</sub> )
	2954 m	2984	0.202	0.048	ν <sub>as</sub> (CH <sub>3</sub> )
2927 br,m		2925	0.216	0.161	ν(CH) attached to aliphatic (OH)
2899 m		2920	0.622	0.237	ν(CH <sub>2</sub> ) attached to aliphatic (OH)
2880 m					ν(CH <sub>3</sub> )
2854 w					
2833 vw					
2821 vw					
2808 w,br					
	2793 ms,br				
2760 w					
2745 w,br					
2728 vw	2726 m				
2711 vw					
2702 w,br					
	2691 m				
2676 w					
2659 w					
2641 vw					
2623 w					ν(CC) <sub>ring</sub>
	2584 mw				
	2560 mw				
	2483 w				
	2457 mw				
	2360 mw				
	2341 w				
		1643	0.032	0.219	δ(NH <sub>2</sub> <sup>+</sup> )
1616 ms	1616 ms	1625	0.259	0.177	Hydrogen bonded C-OH angle coupled to phenyl ring vibration & (C=C)

**Table 4.3. (Continued)**

Observed		Calculated			Proposed Assignment
Raman (cm <sup>-1</sup> )	IR (cm <sup>-1</sup> )	$\nu$	I <sub>Raman</sub>	I <sub>IR</sub>	
	1558 vw	1580	0.111	0.059	Hydrogen bonded C-OH angle coupled to phenyl ring vibration
		1569	0.036	0.052	$\delta(\text{CH}_3)$
		1563	0.069	0.172	$\delta(\text{CH}_3)$
		1552	0.033	0.027	$\delta(\text{CH}_3)$
	1539 vw	1527	0.014	0.391	$\nu(\text{CC})_{\text{ring}}$
	1507 ms				$\delta(\text{CH}_2)_{(\text{sciss.})}$
1494 mw		1489	0.062	0.031	
1468 m	1468 mw	1475	0.052	0.064	$\delta(\text{CH}_2\text{-N})$
	1455 mw	1456	0.052	0.054	
	1438 m	1429	0.083	0.049	Ring stretch
	1409 mw	1419	0.029	0.183	Hydrogen bonded C-OH angle coupled to phenyl ring vibration
1395 vw	1395 m	1395	0.016	0.919	
	1386 m	1376	0.085	0.167	Mixed modes associated with $\delta(\text{NH}_2^+)$ , $\delta(\text{CH}_2)$ and $\delta(\text{CHOH})$
	1379 m	1371	0.009	0.135	Mixed modes associated with $\delta(\text{NH}_2^+)$ , $\delta(\text{CH}_2)$ and $\delta(\text{CHOH})$
1360 w	1362 mw	1355	0.076	0.038	Mixed modes associated with CH <sub>2</sub> and CH-OH vibrations
	1340 w	1344	0.006	0.290	Ring stretch
1331 vw					In-plane $\delta(\text{CH})$
	1309 vw	1299	0.028	0.014	
1283 vw		1290	0.009	0.119	$\nu(\text{C-C})$ of the <i>t</i> - Butyl group
1255 m	1261 m,sh	1268	0.017	0.327	$\delta(\text{CH})$
	1244 m	1249	0.018	0.129	
1205 w	1205 m	1219	0.065	0.032	Hydrogen bonded C-OH angle coupled to phenyl ring vibration
1187 w					
1156 vw					$\nu(\text{S=O})$
	1126 ms,sh	1187	0.029	1.000	$\delta(\text{COH})$ and $\delta(\text{CH}_2\text{OH})$
	1112 vs	1106	0.031	0.141	Hydrogen bonded CH-OH angle coupled to phenyl ring vibration
1080 w	1084 s	1097	0.007	0.418	Hydrogen bonded CH-OH & CH <sub>2</sub> OH angle coupled to phenyl ring vibration
1062 w	1060 ms	1067	0.017	0.008	
1034 vw	1029 vs	1033	0.014	0.124	$r(\text{CH}_3)$
1011 w	988 m	1012	0.060	0.446	$\nu_{\text{as}}(\text{C-OH})$
978 s	978 m	965	0.010	0.188	$\nu_{\text{as}}(\text{C-OH})$
	947 w	944	0.040	0.076	$\nu_{\text{as}}(\text{C-OH})$
937 mw		924	0.026	0.008	Out-of-plane $\delta(\text{CH})$

**Table 4.3. (Continued)**

Observed		Calculated			Proposed Assignment
Raman ( $\text{cm}^{-1}$ )	IR ( $\text{cm}^{-1}$ )	$\nu$	$I_{\text{Raman}}$	$I_{\text{IR}}$	
917 vw	916 mw	912	0.137	0.376	$\nu_{\text{as}}(\text{CN})$
881 w	882 w	910	0.073	0.102	$\delta(\text{CH})_{\text{ring}}$
859 vw		869	0.026	0.074	$\delta(\text{CC})_{\text{ring}}$
841 vw	840 m	835	0.041	0.121	$\nu_{\text{as}}(\text{CN})$ attached to the quaternary carbon
	792 vw	796	0.013	0.137	Out-of-plane $\delta(\text{CH})_{\text{ring}}$
780 ms	773 w	775	0.010	0.020	$\nu(\text{C-C-O})$
747 m	747 w	750	0.092	0.022	Ring vibration
729 vw		728	0.005	0.026	Out-of-plane $\delta(\text{CC})_{\text{ring}}$
	668 w	670	0.003	0.006	CH wagging
648 w	647 w	651	0.006	0.006	CH wagging
609 vw	616 mw,sh	635	0.006	0.091	$\delta(\text{CCC})$
	610 m	593	0.006	0.066	Ring deformation
589 w		577	0.010	0.071	Out-of-plane $\delta(\text{CCC})_{\text{ring}}$
569 vw	575 vw				In-plane $\delta(\text{CCN})$
533 w	534 w	520	0.033	0.011	Out-of-plane $\delta(\text{CC})$
487 mw	487 vw	472	0.009	0.014	
465 vw	464 w	457	0.002	0.124	$\delta(\text{CC})_{\text{chain}}$
404 vw		409	0.017	0.664	$\delta(\text{OH})$
360 w		362	0.006	0.008	Out-of-plane (CCC) skeletal deformation
338 vw		333	0.004	0.126	Out-of-plane (CCC) skeletal deformation
312 w		318	0.013	0.250	In-plane (CCC) skeletal deformation
264 w		257	0.004	0.016	$\text{CH}_3\tau$
193 m		203	0.013	0.032	
165 ms		165	0.007	0.010	
150 ms		142	0.017	0.010	Skeletal mode
101 s		101	0.004	0.015	Skeletal mode
81 vs		92	0.001	0.015	Skeletal mode

#### 4.3.4. Terbutaline hemisulfate

The PXRD pattern of TBS is presented in Figure. 4.23. The diffraction pattern of TBS has been used to establish the solid-phase identity of the sample under investigation. All peaks in the pattern coincided with the theoretical patterns for terbutaline hemisulfate sesquihydrate as appears in CSD, under code BECVIO (Figure 4.24). The calculations were performed on the terbutaline cation.

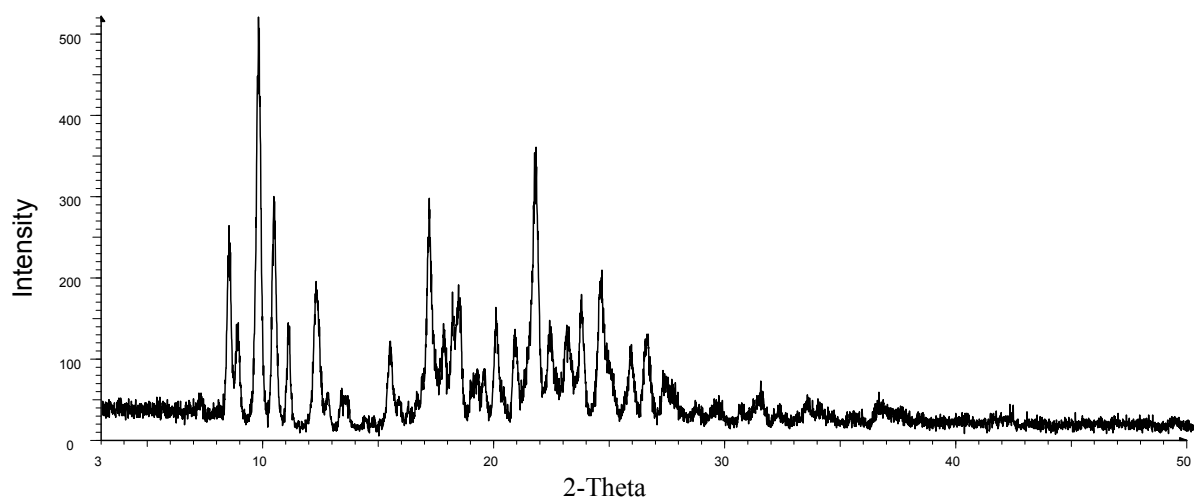


Figure 4.23. The PXRD pattern of TBS.

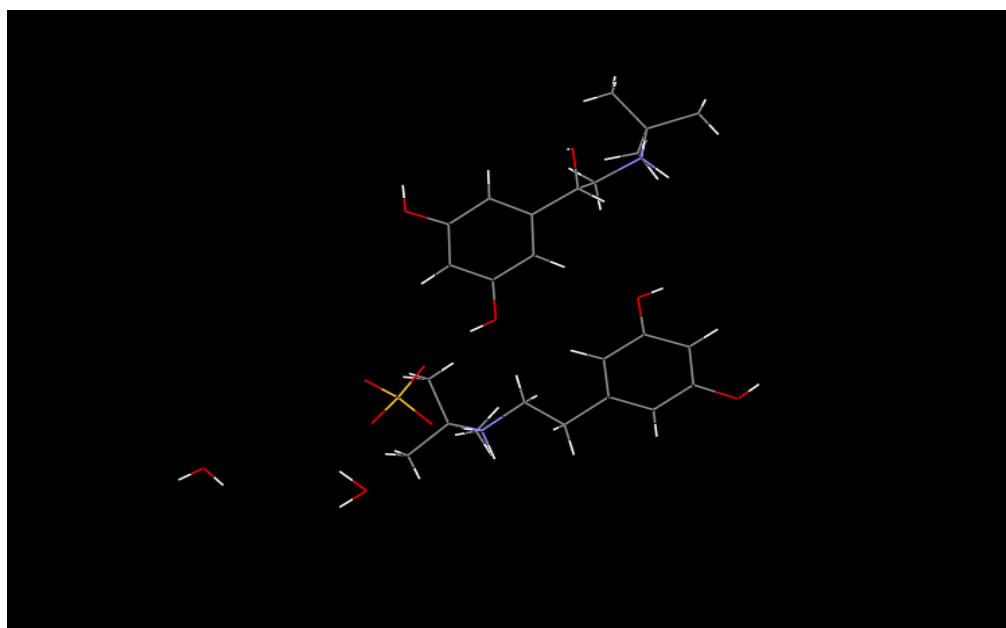
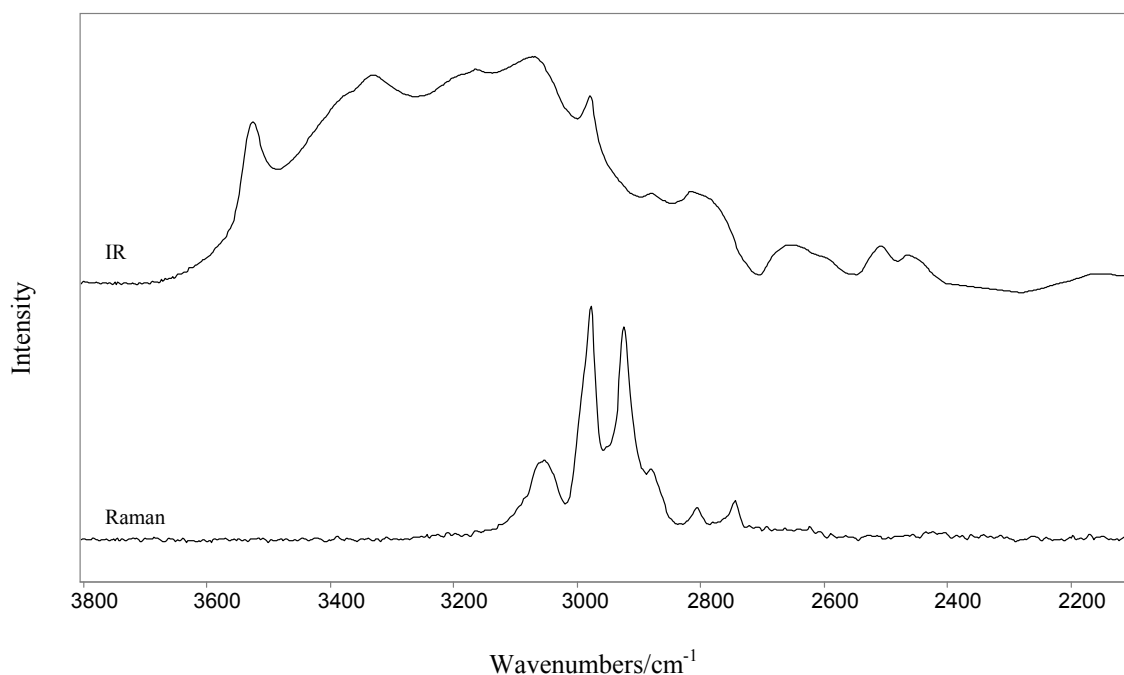


Figure 4.24. The crystal structure of terbutaline hemisulfate sesquihydrate (code BECVIO).

The observed IR and Raman spectroscopic wavenumbers are listed in Table 4.4 along with the calculated values; assignment of the major experimental vibrational features was carried out in the light of the theoretical results performed and the spectroscopic Raman data and the previously reported IR data (Agatonovic-Kustrin and Alany, 2001; FDM). Several calculated modes have been matched with experimentally observed bands in the IR and Raman spectra, and these modes have been described; only very weak features in the observed spectra cannot be reliably assigned on the basis of the quantum chemical calculations.

#### **4.3.4.1. 3800 – 2100 cm<sup>-1</sup> region**

The  $\nu$  (OH) stretching band (Figure 4.25) in the IR spectrum at 3527 cm<sup>-1</sup> suggests that hydrogen bonding occurs in the crystalline TBS. The  $\nu$  (NH) stretching bands are observed in the IR spectrum in the range 3500 – 3100 cm<sup>-1</sup> (Figure 4.25) which are much more broader than the  $\nu$  (OH) band. The CH stretching region comprises several features in the wavenumber range 3100 – 2800 cm<sup>-1</sup> (Figure 4.25) for the IR and Raman spectra; the CH stretching bands of the aromatic component of TBS are shown in both the Raman and IR spectra (Table 4.4) and can be assigned to the bands at 3057 and 3069 cm<sup>-1</sup> in the Raman and IR spectra respectively. The CH aliphatic stretching bands of CH<sub>3</sub> symmetric and asymmetric stretching modes are more clearly shown in the Raman spectrum rather than the IR spectrum and can be assigned to the medium feature at 2978 cm<sup>-1</sup> and to the medium weak feature at 2881 cm<sup>-1</sup>.



**Figure 4.25. FT-Raman and IR spectral stackplot of TBS in the 2100 – 3800  $\text{cm}^{-1}$  region.**

#### **4.3.4.2. 1800 – 1100 $\text{cm}^{-1}$ region**

This is a very important spectroscopic region for structural studies, particularly for the C=C group in this molecule. Expanded wavenumber regions of the IR and Raman spectra are shown in Figure 4.26. A comparison between the experimental and calculated IR and Raman spectra (Figures 4.27 and 4.28) are also presented to show the overall agreement between them as a representative example. The IR spectral region comprises a rich spectrum from the C=C functionality, along with several bands of medium and strong intensities, whereas the Raman spectrum consists mainly of the strong C=C features and several other weaker features. The  $\nu(\text{C}=\text{C})$  band occurs at 1604  $\text{cm}^{-1}$ , of medium intensity in the Raman spectrum and strong intensity in the IR spectrum. It is worth noting that, the calculated methyl deformation vibrational bands at 1549, 1558 and 1568  $\text{cm}^{-1}$  have not been observed in the experimental spectra that is due to the presence of sulfate anion may hinder some of the methyl deformation

features. The  $\delta$  ( $\text{NH}_2^+$ ) band is observed at  $1624\text{ cm}^{-1}$  of medium intensity in the Raman spectrum and medium strong intensity in the IR spectrum. In the range  $1490 - 1300\text{ cm}^{-1}$ , we expect  $\text{CH}_3$ ,  $\text{CH}_2$  and  $\text{CH}$  aliphatic bending vibrations bands to occur. Lower in wavenumber we expect to find the  $\nu(\text{C-C})$  and  $\nu(\text{C-N})$  bands of weak intensities in the Raman spectrum at  $1292$  and  $1195\text{ cm}^{-1}$  respectively and the  $\nu(\text{C-OH})$  band at around  $1235\text{ cm}^{-1}$  of medium intensity in the IR spectrum and weak intensity in the Raman spectrum. The  $\nu(\text{S=O})$  band is observed at around  $1155\text{ cm}^{-1}$  of strong intensity in the IR spectrum and weak intensity in the Raman spectrum.

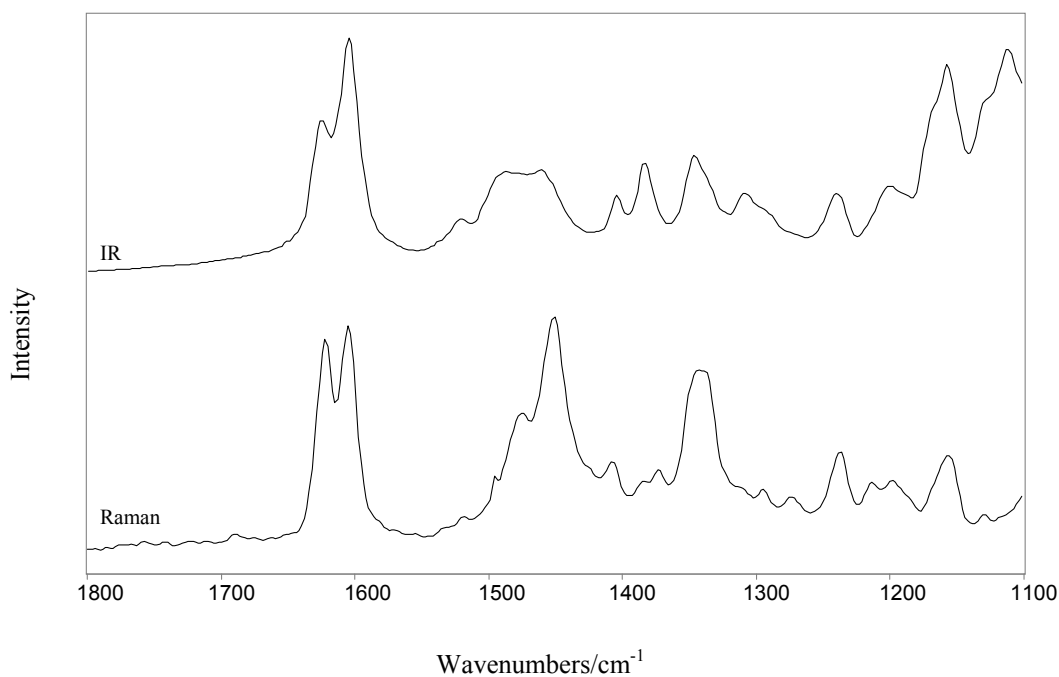


**Figure 4.26. FT-Raman and IR spectral stackplot of TBS in the  $1100 - 1800\text{ cm}^{-1}$  region.**

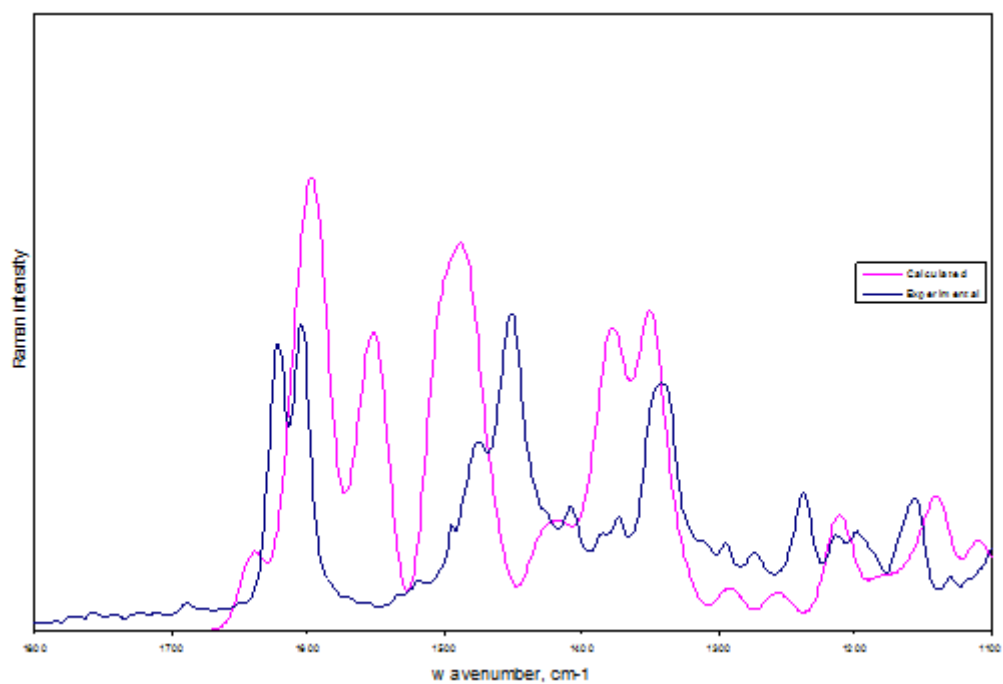


**Figure 4.27.** A comparison between the calculated and experimental Raman spectra of TBS 1100 – 1800  $\text{cm}^{-1}$  region.

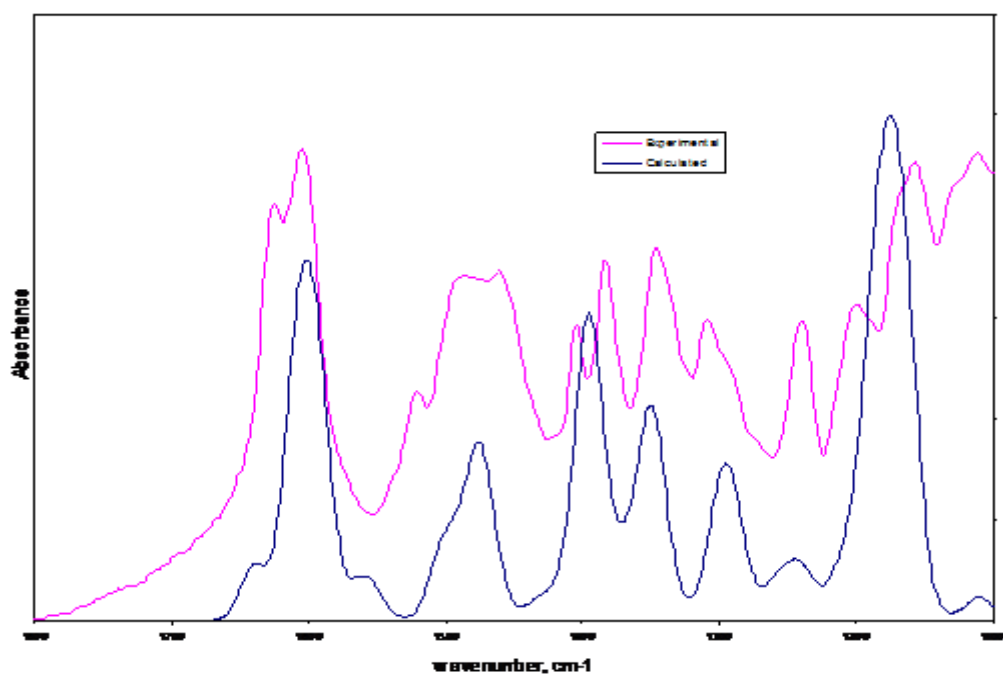


**Figure 4.28.** A comparison between the calculated and experimental IR spectra of TBS 1100 – 1800  $\text{cm}^{-1}$  region.

#### 4.3.4.3. 1100 – 100 cm<sup>-1</sup> region

Raman and IR spectra over this wavenumber range are presented in Figure 4.29.

In the 973 – 997 cm<sup>-1</sup> region we can expect modes arising from  $\nu_{as}(\text{C-OH})$ . Lower in wavenumber we expect to find the CH wagging bands at 759 and 784 cm<sup>-1</sup> in the Raman spectrum and at 760 and 689 cm<sup>-1</sup> in the IR spectrum.

Finally, the complex ring modes of CCC deformations in the range between 400 and 550 cm<sup>-1</sup> occur. The methyl torsional band is observed in the Raman spectrum at 271 cm<sup>-1</sup> of weak intensity.

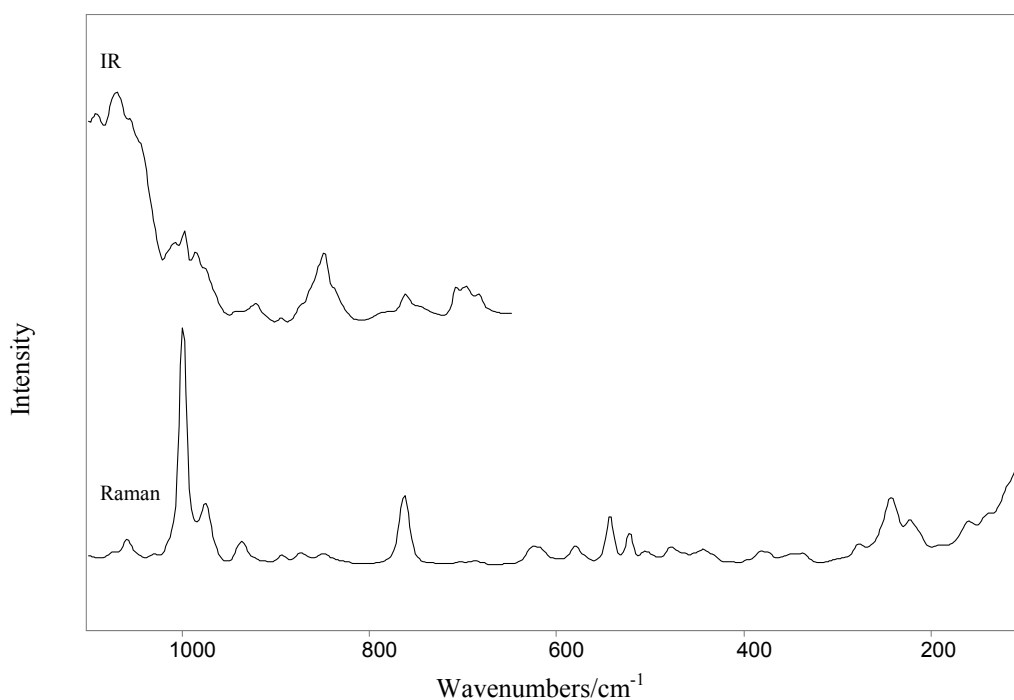


**Figure 4.29. FT-Raman and IR spectral stackplot of TBS in the 100 – 1100 cm<sup>-1</sup> region.**

The key Raman spectral features of TBS are the  $\nu_{\text{as}}(\text{CH}_3)$  band at  $2978\text{ cm}^{-1}$ , the  $\nu(\text{CH})$  attached to the aliphatic (OH) band at  $2922\text{ cm}^{-1}$ , The  $\delta(\text{NH}_2^+)$  band at  $1624\text{ cm}^{-1}$ , the  $\nu(\text{C}=\text{C})$  band at  $1604\text{ cm}^{-1}$ , the  $\delta(\text{CH}_3)$  band at  $1450\text{ cm}^{-1}$ , the  $\delta(\text{CH})$  band at  $1341\text{ cm}^{-1}$ , the (C-OH) stretching bands of the three (OH) groups at  $1232$ ,  $992$  and  $973\text{ cm}^{-1}$ , and the out of plane (CH) wagging band at  $759\text{ cm}^{-1}$  while its key IR spectral features are the  $\nu(\text{OH})$  band at  $3527\text{ cm}^{-1}$ , the  $\nu(\text{NH})$  bands at  $3332$  and  $3171\text{ cm}^{-1}$ , the aliphatic  $\nu(\text{CH})$  band at  $3069\text{ cm}^{-1}$ , the  $\nu_{\text{as}}(\text{CH}_3)$  band at  $2983\text{ cm}^{-1}$ , the  $\delta(\text{NH}_2^+)$  band at  $1624\text{ cm}^{-1}$ , the  $\nu(\text{C}=\text{C})$  band at  $1605\text{ cm}^{-1}$ , the  $\delta(\text{CH}_3)$  band at  $1458\text{ cm}^{-1}$ , the  $(\text{CH}_2)\&(\text{NH}_2)$  and (CH) deformation bands at  $1380$  and  $1346\text{ cm}^{-1}$ , respectively, the (C-OH) stretching bands of the three (OH) groups at  $1237$ ,  $997$  and  $982\text{ cm}^{-1}$  and the  $\nu(\text{S}=\text{O})$  band at  $1154\text{ cm}^{-1}$ .

**Table 4.4. The observed and calculated vibrational wavenumbers/cm<sup>-1</sup> of TBS. The calculated IR intensities (I<sub>IR</sub>) are relative to that of δ (NH<sup>+</sup><sub>2</sub>) at 1396 cm<sup>-1</sup>. The calculated Raman intensities (I<sub>Raman</sub>) are relative to that of ν (CH) at 3075 cm<sup>-1</sup>.**

Observed		Calculated			Proposed Assignment
Raman (cm <sup>-1</sup> )	IR (cm <sup>-1</sup> )	ν	I <sub>Raman</sub>	I <sub>IR</sub>	
	3527 m	3583	0.805	0.026	ν(OH)
	3332 m	3326	0.272	0.030	ν(NH)
	3171 m	3229	0.889	0.059	ν(NH)
3057 mw	3069 m	3075	1.000	0.103	Aromatic ν(CH)
2978 m	2983 m	2979	0.225	0.102	ν <sub>as</sub> (CH <sub>3</sub> )
2922 m		2908	0.379	0.069	ν(CH) attached to the aliphatic OH
2881 mw	2878 mw			0.133	ν(CH <sub>3</sub> )
2802 w	2819 mw			0.087	
2749 w				0.040	
	2653 w			0.449	
	2510 w			0.856	
	2461 w			0.133	
	2153 vw				
	2078 vw			0.033	
1624 m	1624 ms	1639	0.039	0.016	δ(NH <sup>+</sup> <sub>2</sub> )
1604 m	1604 s	1608	0.107	0.049	ν(C=C)
		1593	0.180	0.021	ν(CC) <sub>ring</sub>
		1569	0.031	0.015	δ(CH <sub>3</sub> )
		1558	0.033	0.038	δ(CH <sub>3</sub> )
		1549	0.120	0.002	δ(CH <sub>3</sub> )
	1518 w	1505	0.117	0.029	
1472 m,sh	1485 m	1486	0.104	0.051	δ(CH <sub>3</sub> )
1450 m	1458 m	1463	0.036	0.063	δ(CH <sub>3</sub> )
1409 w	1402 m	1391	0.014	0.047	Ring stretch
		1396	0.024	1.000	ν(NH <sup>+</sup> <sub>2</sub> )
1371 w	1380 m	1378	0.119	0.052	δ(CH <sub>2</sub> )& δ(NH <sub>2</sub> )
1341 m	1346 m	1349	0.149	0.045	δ(CH)
	1304 m	1327	0.031	0.019	In-plane δ(CH)
1292 w		1299	0.007	0.340	ν(C-C)
1266 w		1258	0.018	0.039	δ(CH)
1232 w	1237 m	1212	0.057	0.014	ν(C-OH)
1213 w					
1195 w	1195 m	1195	0.005	0.077	ν(C-N)

**Table 4.4. (Continued)**

Observed		Calculated			Proposed Assignment
Raman (cm <sup>-1</sup> )	IR (cm <sup>-1</sup> )	$\nu$	I <sub>Raman</sub>	I <sub>IR</sub>	
1157 w	1154 s				$\nu(\text{S}=\text{O})$
1131 w	1113 s	1139	0.063	0.168	
1097 w	1087 s	1110	0.043	0.045	
1067 w	1064 s	1066	0.006	0.220	
1056 mw				0.106	$\nu(\text{CC})$ aromatic
1030 w		1026	0.026	0.183	
992 s	997 m	1004	0.029	0.317	$\nu_{\text{as}}(\text{C}-\text{OH})$
973 m	982 m	986	0.023	0.112	$\nu_{\text{as}}(\text{C}-\text{OH})$
932 mw	921 w	943	0.017	0.136	
891 w	895 w	912	0.192	0.327	
872 w		873	0.028	0.110	
842 w	846 m	822	0.012	0.039	
759 ms	760 mw	766	0.010	0.102	Out of plane(CH) wagging
703 w	707 mw	721	0.063	0.039	
684 w	689 mw	674	0.002	0.026	CH wagging
620 w		632	0.014	0.002	
581 w		548	0.021	0.028	
541 m		561	0.006	0.002	In-plane $\delta(\text{CCN})$
519 mw		532	0.076	0.005	Out-of-plane $\delta(\text{CC})$
505 w		509	0.027	0.007	
475 w		475	0.004	0.041	
439 w		450	0.047	0.024	Out-of-plane $\delta(\text{CC})_{\text{chain}}$
373 w		384	0.023	0.389	
342 w		352	0.004	0.028	
271 w		265	0.005	0.074	$\text{CH}_3\tau$
236 ms		233	0.017	0.056	
222 mw		220	0.015	0.021	
152 mw		161	0.007	0.040	

### 4.3.5. Ipratropium bromide

Calculations were performed on the IPRA cation (Figure 4.30). Two conformations of the IPRA cation were investigated. As can be seen in Figure 4.30, the hydroxyl group is able to form an intramolecular hydrogen bond (conformer IPRA2). This conformation would be expected to be the most stable in the gas phase. In the solid state the hydroxyl group is able to form intramolecular hydrogen bonds and the conformation depicted in Figure 4.30 (conformer IPRA1) may be important. For both conformers full geometry optimisation was carried out, followed by the determination of the predicted vibrational frequencies.

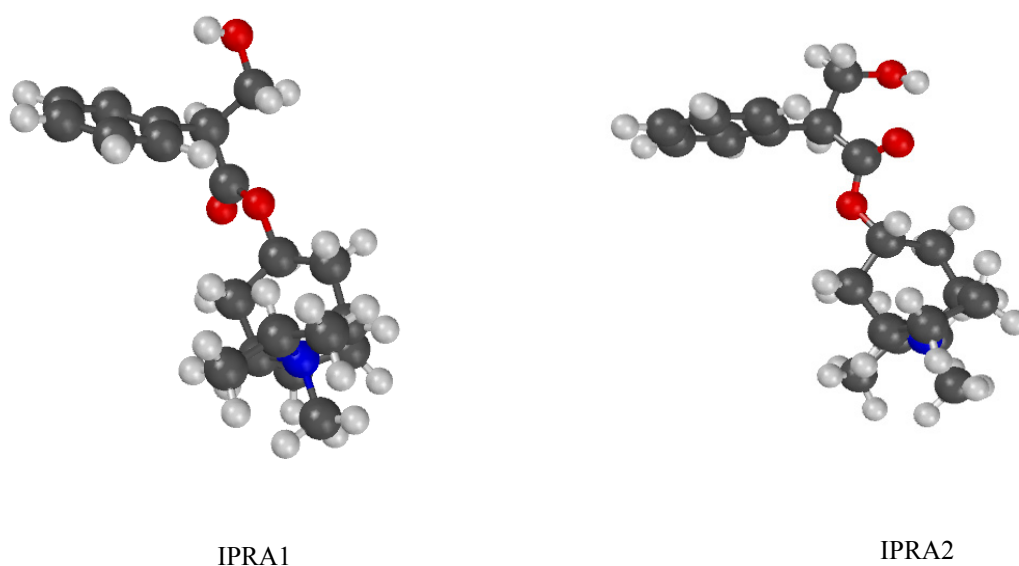


**Figure 4.30.** The calculated conformations of the IPRA cation; IPRA1 has no intramolecular hydrogen bond and IPRA2 with an intramolecular hydrogen bond.

#### 4.3.5.1. Computational studies

The predicted IR spectra of the conformations IPRA1 and IPRA2 over the region 0-2000  $\text{cm}^{-1}$  are compared in Figure 4.31. The simulated spectra were generated by using the computed frequencies and intensities and applying a Gaussian broadening to each transition of 10  $\text{cm}^{-1}$ . There is a clear shift in the C=O stretching at 1743  $\text{cm}^{-1}$  (IPRA1)

to  $1716\text{ cm}^{-1}$  (IPRA2) resulting from the intramolecular hydrogen bonding. The strong absorption at  $1134\text{ cm}^{-1}$  (IPRA1) shifts to  $1110\text{ cm}^{-1}$  (IPRA2) corresponds to a coupled stretching of the C-O and C=O of the ester linkage.

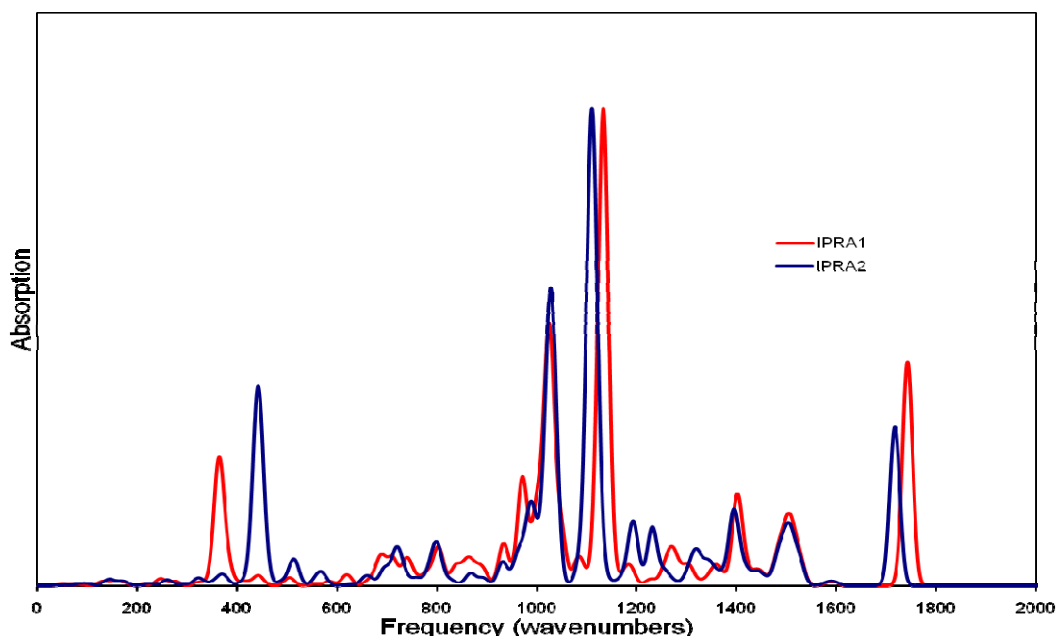


**Figure 4.31. The calculated IPRA cation IR conformational shifts in the region 0-2000  $\text{cm}^{-1}$ .**

The predicted Raman spectra of both IPRA1 and IPRA2 are dominated by the CH stretching bands; the region from 0-2000  $\text{cm}^{-1}$  is shown in Figure 4.32. The simulated spectra were generated by using the computed frequencies and intensities and applying a Gaussian broadening to each peak of  $5\text{ cm}^{-1}$ . The most intense scattering, apart from the CH and OH region, is seen at  $1595\text{ cm}^{-1}$  (IPRA1) and  $1596\text{ cm}^{-1}$  (IPRA2). This is a stretching mode in the phenyl group. It is only seen with a very weak intensity in the predicted IR spectra. The small shift in frequency between the two conformations reflects the small influence from the internal hydrogen bond on this vibrational mode.

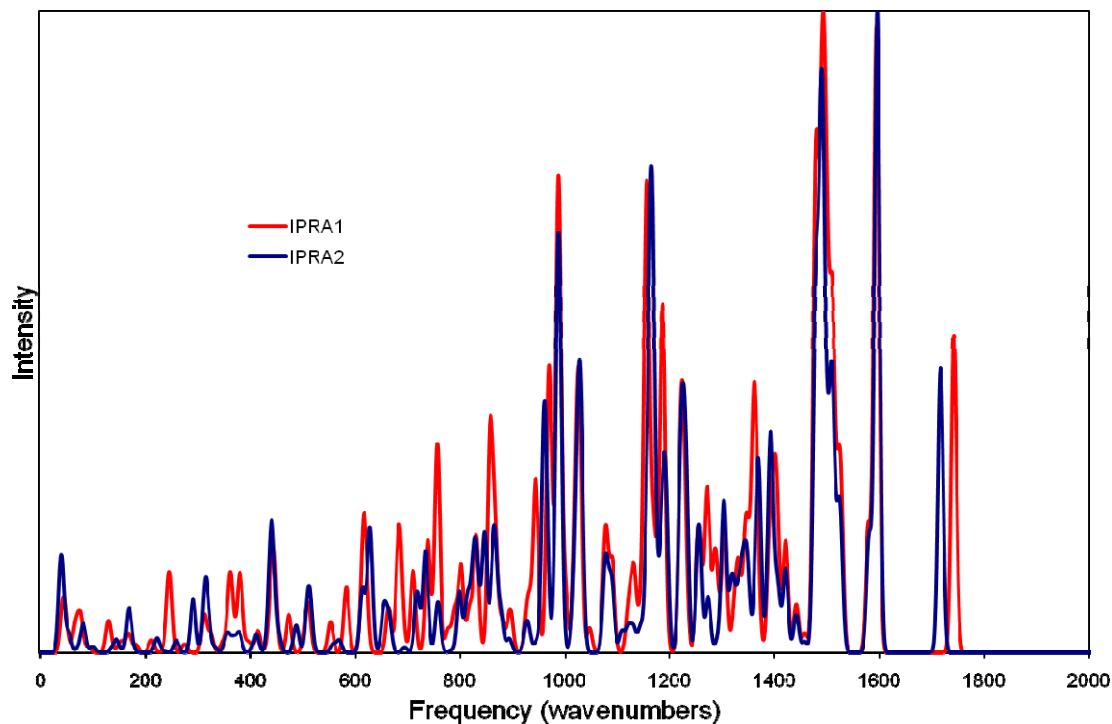


**Figure 4.32.** The calculated IPRA cation Raman conformational shifts in the region 0-2000  $\text{cm}^{-1}$ .

The predicted Raman spectra are complex and are difficult to interpret in terms of conformational changes. The shifts observed in the predicted IR spectra of the two conformers are more straightforward to interpret and are summarised in comparison with the observed bands of IPRA in Table 4.5. It can be noted that, the observed IR spectral features comprise the calculated IR spectral features of both IPRA1 and IPRA2. The very strong calculated bands at  $1134 \text{ cm}^{-1}$  and  $1109 \text{ cm}^{-1}$  of IPRA1 and IPRA2 respectively are recorded in the observed IR spectrum at  $1246$  and  $1228 \text{ cm}^{-1}$  and the strong calculated bands at  $1743$  and  $1716 \text{ cm}^{-1}$  of IPRA1 and IPRA2, respectively, are recorded in the observed IR spectrum at  $1726$  and  $1712 \text{ cm}^{-1}$ . These data suggest that the conformation in the solid state crystalline structure could be a mixture of IPRA1 and IPRA2.

**Table 4.5. The key calculated IR spectral features of IPRA1 and IPRA2 in comparison with the observed bands of IPRA in the range of 600 – 1800 cm<sup>-1</sup>.**

Observed	IPRA1	Observed	IPRA2
700 m	698 w	667 w	669 w
741 m	745 mw		724 mw
804 w	800 mw	804 w	802 mw
852 w	849 w		874 w
868 vw	869 w	894 vw	891 vw
894 vw	891 w	934 w	936 mw
934 w	937 mw	989 vw	991 m
974 m	973 m	1029 w	1029 s
1029 w	1022 s	1228 s	1109 vs
1246 s	1134 vs	1327 w	1324 w
1273 w	1275 w	1348 w	1347 mw
1310 vw	1306 mw	1402 w	1397 m
1360 vw	1355 w	1452 ms	1450 w
1402 w	1403 m		1508 m
1452 ms	1450 w	1601 w	1595 w
	1508 m	1712 vs	1716 s
1601 w	1595 w		
1726 m,sh	1743 s		

#### 4.3.5.2. Vibrational spectroscopic analysis

The IR and Raman spectra of IPRA were shown in Figures 4.33 - 4.35. Experimental IR and Raman wavenumbers are listed in Table 4.6 along with the calculated values; assignment of the major experimental vibrational features was carried out in the light of the computational results and the Raman spectrum, reported for this first time in this study, and the IR spectroscopic data reported previously (FDM). It is shown here that the major features in the observed spectra can be reliably assigned on the basis of the quantum chemical calculations.

##### 4.3.5.2.1. 3800 – 2600 cm<sup>-1</sup> region

The broad rather diffuse  $\nu$  (OH) stretching band (Figure 4.33) in the IR spectrum at 3492 cm<sup>-1</sup> suggests that hydrogen bonding occurs in the crystalline IPRA. The CH stretching region comprises several features in the wavenumber range 3100 – 2800 cm<sup>-1</sup>

(Figure 4.33) for the IR and Raman spectra; the CH stretching bands of the unsaturated, aromatic component of IPRA are more clearly shown in the Raman spectrum rather than in the IR spectrum (Table 4.6) and can be assigned to the bands at 3067 and 3057  $\text{cm}^{-1}$  in the Raman spectrum. The strong bands in the Raman spectrum at 2992 and 2968  $\text{cm}^{-1}$  could be attributed to  $\nu(\text{CH}_2\text{-O-})$  and  $\nu_{\text{as}}(\text{CH}_2\text{-OH})$ , respectively.

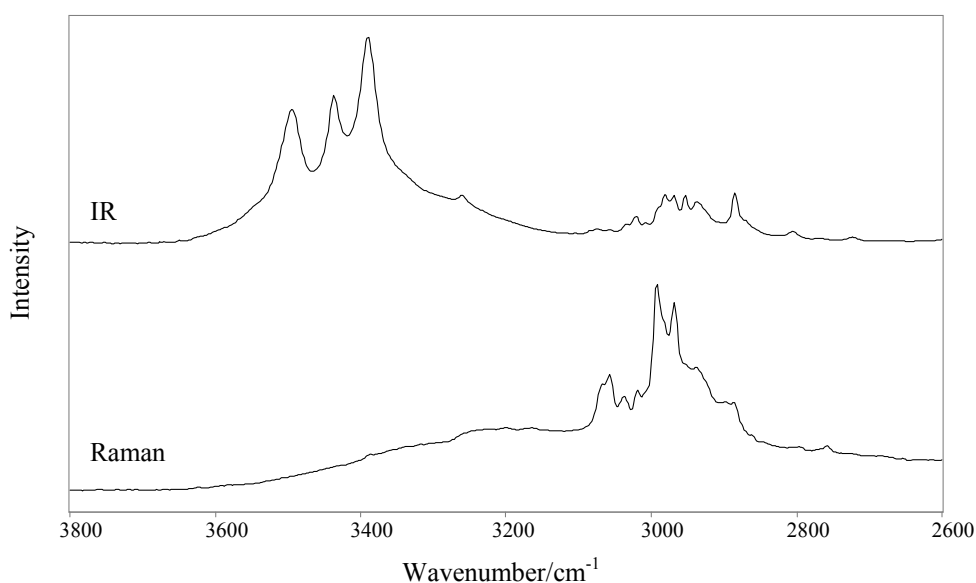


**Figure 4.33. FT-Raman and IR spectral stackplot of IPRA in the 2600 – 3800  $\text{cm}^{-1}$  region.**

#### 4.3.5.2.2. 1750 – 1550 $\text{cm}^{-1}$ region

Expanded wavenumber regions of the IR and Raman spectra are shown in Figure 4.34. The observed IR spectrum has a medium shoulder at 1726  $\text{cm}^{-1}$  which can be assigned to  $\nu(\text{C=O})$  which is not involved in the hydrogen bonding, and a very strong band at 1712  $\text{cm}^{-1}$ , consequent upon the participation of the carbonyl group in the hydrogen bonding can be assigned to the carbonyl of the ester linkage. These features suggest that IPRA specimen could be a mixture of the two conformations, IPRA1 and IPRA2. The medium intensity band at 1603  $\text{cm}^{-1}$  in the Raman spectrum can be

attributed to  $\nu$  (CC)<sub>ring</sub>. There are several other features clearly seen in this wavenumber region at 1672, 1639, 1601, 1582  $\text{cm}^{-1}$  and 1712, 1649, 1583  $\text{cm}^{-1}$  in the IR and Raman spectra, respectively; these features can be assigned on the basis of the quantum chemical calculations to molecular vibrations that involve both C=C and C=O groups and symmetric and asymmetric ring vibrations.

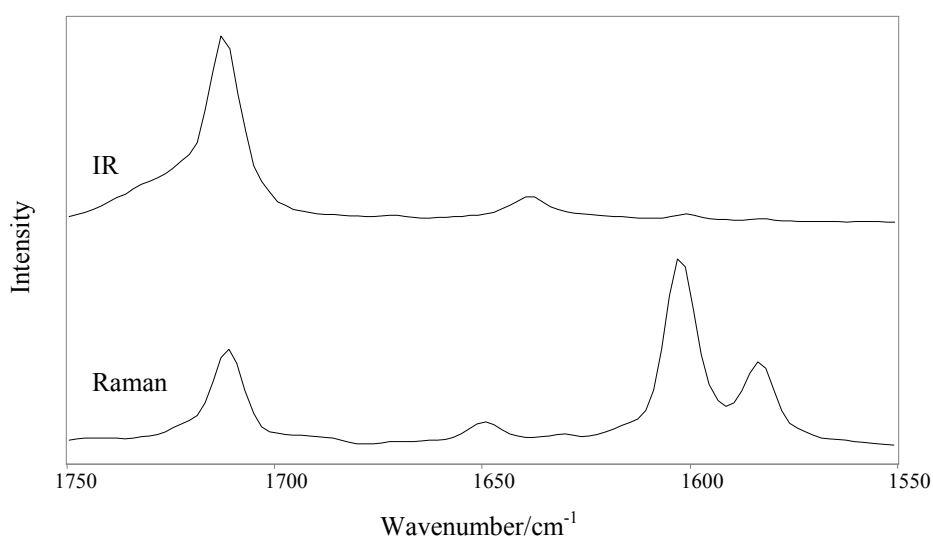


**Figure 4.34. FT-Raman and IR spectral stackplot of IPRA in the 1550 – 1750  $\text{cm}^{-1}$  region.**

#### 4.3.5.2.3. 1800 – 100 $\text{cm}^{-1}$ region

The IR and Raman spectra over this wavenumber range are presented in Figure 4.35; the IR spectral region comprises a rich spectrum from the C=O and C=C functionalities, which have already been discussed in some detail above, along with several bands of medium and strong intensities, whereas the Raman spectrum consists mainly of the strong C=C features and several other weaker features. In the range 1470 – 1300  $\text{cm}^{-1}$ , we expect  $\text{CH}_3$  and  $\text{CH}_2$  aliphatic bending vibrations to occur with  $\nu$ (C-N) at around 1310  $\text{cm}^{-1}$ .

At lower wavenumber, there is additional indication that the IPRA sample is a mixture of the two conformations IPRA1 and IPRA2. The two strong calculated bands at 1134 and 1109  $\text{cm}^{-1}$  (25  $\text{cm}^{-1}$  shift) for the IR spectrum were observed in the experimental IR spectrum at 1246 and 1228  $\text{cm}^{-1}$  (18  $\text{cm}^{-1}$  shift). These two bands were assigned on the basis of quantum chemical calculations as the coupled stretching of the C-O and C=O of the ester linkage.

In the 1050 – 850  $\text{cm}^{-1}$  region, assignment of a series of bands to modes arising from  $\nu(\text{C-OH})$  of the primary alcohols and CCH aromatic deformation modes near 1040  $\text{cm}^{-1}$  can be made. The  $\nu(\text{C-N-C})$  band is observed at around 850  $\text{cm}^{-1}$ .

Finally, the complex ring modes of CCC deformations in the range between 690 and 500  $\text{cm}^{-1}$  occur. The weak skeletal deformation bands are observed in the Raman spectrum below 440  $\text{cm}^{-1}$  and the methyl torsional mode at 267  $\text{cm}^{-1}$  of weak intensity can be noted.

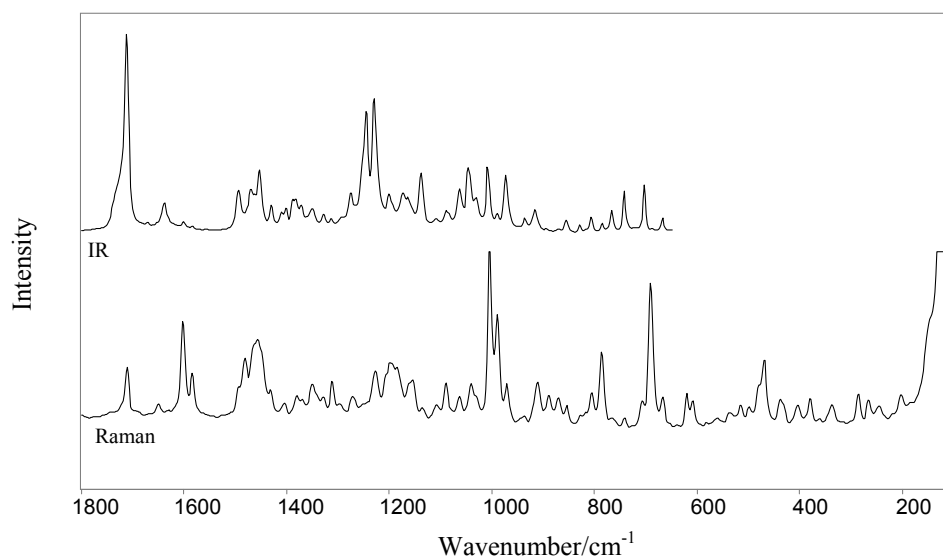


**Figure 4.35. FT-Raman and IR spectral stackplot of IPRA in the 100 – 1800 cm<sup>-1</sup> region.**

The key Raman spectral features observed for IPRA are: the  $\nu(\text{CH})$  bands at 3057 and 3067 cm<sup>-1</sup>; the  $\nu(\text{CH}_2\text{-O-})$  band at 2992 cm<sup>-1</sup>; the  $\nu_{\text{as}}(\text{CH}_2\text{O-H})$  band at 2968 cm<sup>-1</sup>; the  $\nu(\text{CC})_{\text{ring}}$  band at 1603 cm<sup>-1</sup>; the ring vibration band at 1006 cm<sup>-1</sup>; the ring breathing band at 990 cm<sup>-1</sup>; the out-of-plane  $\delta(\text{CH})_{\text{ring}}$  band at 785 cm<sup>-1</sup> and the out-of-plane  $\delta(\text{CCC})$  band at 690 cm<sup>-1</sup>.

In contrast, key IR spectral features include: the  $\nu(\text{OH})$  band at 3492 cm<sup>-1</sup>; the  $\nu(\text{C=O})$  band at 1712 cm<sup>-1</sup>; the  $\delta(\text{CH})_{\text{ring}}$  and  $\delta(\text{CH}_2)_{\text{(sciss.)}}$  bands at 1492 cm<sup>-1</sup>; the  $\delta(\text{CH}_3)$  band at 1468 cm<sup>-1</sup>; the ring stretching band at 1452 cm<sup>-1</sup>; the coupled stretching of the C-O and C=O of the ester linkage bands at 1246 and 1228 cm<sup>-1</sup>; the  $\nu(\text{C-OH})$  band at 1045 cm<sup>-1</sup>; the ring vibration bands at 1006 and 741 cm<sup>-1</sup>; the out-of-plane  $\delta(\text{CH})$  band at 970 cm<sup>-1</sup> and the  $\delta(\text{COC})$  band at 700 cm<sup>-1</sup>.

#### 4.4. Conclusions

The Raman spectra of BUD, TBS and IPRA have been recorded for the first time and coupled with the predictions of quantum chemical calculations. A good overall agreement was obtained between the experimental and calculated frequency values for the all five studied drugs (Figures 4.27 and 4.28 and Tables 4.1,2,3,4 and 6); however, even with the support of quantum chemical calculations, it is difficult to be certain about the assignments of some of these molecular vibration in the mid-low wavenumber range because of the complexities of mode mixing of the drugs studied; nevertheless, it is clear that the major vibrational spectroscopic features of the all studied drugs have been reasonably assigned in this study.

Raman, IR and quantum chemical calculations, have been used to explain the presence of the observed spectroscopic complexity in the C=C and C=O stretching region which provide useful structural information when considering the complexation of BUD and FP.

Vibrational spectroscopy and quantum chemical calculations have been applied to the investigation of SB and TBS. As a result of the comparison of the experimental and calculated frequencies, the vibrational modes associated with the atoms involved in the hydrogen bonding were identified. As such, this study could be viable for examining the way in which these drugs interact with their target molecules.

The calculated vibrational modes of non-intramolecular hydrogen-bonded and hydrogen-bonded IPRA conformations, IPRA1 and IPRA2, provided insight into the

solid state analysis of IPRA. In particular it was possible to indicate that IPRA specimens in the solid state could be a mixture of the two conformations IPRA1 and IPRA2 without and with intramolecular hydrogen bonding, respectively. Quantum chemical calculations offer great potential to improve understanding of the structural properties of solid-state pharmaceuticals and these are of particular importance in the absence of more detailed structural information, as is the case for this system.

**Table 4.6. The observed vibrational frequencies of IPRA and those calculated for IPRA cation. For calculated data, relative intensities for IPRA1 and IPRA2 were normalised such that the most intense band in the calculated spectra is 1.**

Observed		calculated		Proposed assignment
Raman, cm <sup>-1</sup>	IR, cm <sup>-1</sup>	IPRA1 $\nu$ (cm <sup>-1</sup> ) (Raman, IR Int.)	IPRA2 $\nu$ (cm <sup>-1</sup> ) (Raman, IR Int.)	
	3492 ms 3437 ms 3390 s 3258 w	3552 (0.201,0.045)	3589 (0.230, 0.049)	$\nu(\text{OH})$
3067 m	3073 vw	3131 (1.000, 0.037)	3137 (1.000, 0.049)	Aromatic $\nu(\text{CH})$
3057 m	3057 vw	3059 (0.527, 0.023)	3058 (0.157, 0.002)	$\nu(\text{CH})$
3038 mw	3034 vw	3043 (0.169, 0.061)	3040 (0.322, 0.045)	$\nu_{\text{as}}(\text{CH}_2)$
3017 mw	3020 w	3026 (0.155, 0.020)	3025 (0.113, 0.013)	$\nu_{\text{as}}(\text{CH}_2)$
2992 s	3007 vw	3009 (0.141, 0.018)	3004 (0.756, 0.004)	$\nu(\text{CH}_2\text{-O-})$
	2979 w	3003 (0.014, 0.016)	2989 (0.067, 0.047)	$\nu_{\text{as}}(\text{CH}_2)\& \nu_{\text{as}}(\text{CH}_3)$
2968 s	2968 w	2933 (0.159, 0.164)	2969 (0.285, 0.059)	$\nu_{\text{as}}(\text{CH}_2\text{-O-H})$
2952 w	2952 w			$\nu_{\text{as}}(\text{CH}_2)$
2938 w	2937 w			$\nu(\text{CH}_3)$
2896 vw				$\nu(\text{CH}_3)$
2886 w	2885 w			
	2871 sh,w			$\nu(\text{CH}_2)$
2861 w				
	2804 vw			
2757 w				
	2723 vw			
	1726 m,sh	1743 (0.061, 0.662)		$\nu(\text{C=O})$

**Table 4.6. (Continued)**

Observed		calculated		Proposed assignment
Raman, cm <sup>-1</sup>	IR, cm <sup>-1</sup>	IPRA1 $\nu$ (cm <sup>-1</sup> ) (Raman, IR Int.)	IPRA2 $\nu$ (cm <sup>-1</sup> ) (Raman, IR Int.)	
1712 mw	1712 vs 1672 vw		1716 (0.081, 0.360)	$\nu(\text{C}=\text{O})$
1649 vw	1639 mw			$\nu(\text{C}=\text{C})_{\text{chain}}$
1603 m	1601 w	1594 (0.120, 0.009)	1596 (0.183, 0.008)	$\nu(\text{CC})_{\text{ring}}$
1583 w	1582 vw	1579 (0.024, 0.005)	1580 (0.033, 0.007)	
1493 sh,w	1492 m	1495 (0.006, 0.032)	1494 (0.049, 0.001)	$\delta(\text{CH})_{\text{ring}}$ & $\delta(\text{CH}_2)_{(\text{sciss.})}$
1481 mw		1482 (0.004, 0.071)	1482 (0.005, 0.048)	$\delta(\text{CH}_3)$
	1468 m	1478 (0.089, 0.005)	1478 (0.097, 0.004)	$\delta(\text{CH}_3)$
1456 br,m	1452 ms	1458 (0.004, 0.019)	1457 (0.003, 0.013)	Ring stretch
1431 w	1429 w	1421 (0.021, 0.035)	1421 (0.024, 0.026)	
1406 w	1408 w	1406 (0.015, 0.045)	1406 (0.018, 0.032)	In-plane $\delta(\text{CH}_3)$
	1402 w	1400 (0.026, 0.221)	1394 (0.038, 0.113)	$\delta(\text{OH})$ & $\delta(\text{CH}_2)$
	1386 w	1391 (0.023, 0.013)	1390 (0.029, 0.048)	$\delta(\text{CH}_3)$ & $\delta(\text{CH})_{\text{chain}}$
1380 w	1381 w			$\delta(\text{CH}_3)$
1370 sh,w	1372 w	1368 (0.013, 0.017)	1370 (0.029, 0.003)	
	1360 vw	1361 (0.035, 0.001)	1364 (0.011, 0.014)	
1348 w	1348 w	1355 (0.005, 0.028)	1348 (0.011, 0.009)	
1327 w	1327 w	1327 (0.006, 0.003)	1328 (0.007, 0.003)	$\delta(\text{CH})$
1312 w	1310 vw	1304 (0.025, 0.054)	1318 (0.018, 0.068)	$\nu(\text{C}-\text{N})$ & $\delta(\text{CH}_3)$
1294 vw	1291 w,sh	1286 (0.016, 0.023)	1291 (0.003, 0.002)	$\delta(\text{OH})$ & $\delta(\text{CH}_2)$
1271 w	1273 w	1273 (0.018, 0.036)	1273 (0.016, 0.008)	$\delta(\text{CH}-\text{N})$

**Table 4.6. (Continued)**

Observed		calculated		Proposed assignment
Raman, cm <sup>-1</sup>	IR, cm <sup>-1</sup>	IPRA1 $\nu$ (cm <sup>-1</sup> ) (Raman, IR Int.)	IPRA2 $\nu$ (cm <sup>-1</sup> ) (Raman, IR Int.)	
	1246 s	1134 (0.004, 1.000)		Coupled stretching of the C-O and C=O of the ester linkage
1226 w	1228 s		1110 (0.006, 1.000)	Coupled stretching of the C-O and C=O of the ester linkage
1196 br,w 1185 w	1199 w			
	1173 w			
1162 w 1155 w	1161 w			
1137 vw	1137 m			
1110 vw	1105 vw			
1090 w	1088 w	1091 (0.017, 0.029)	1090 (0.018, 0.048)	
1063 w	1060 mw	1078 (0.022, 0.009)	1077 (0.024, 0.003)	
1040 w	1045 m	1047 (0.005, 0.161)	1032 (0.026, 0.323)	$\nu$ (C-OH)
	1029 w	1027 (0.036, 0.037)	1029 (0.031, 0.120)	$\nu$ (C-OH)
1006 ms	1006 m	1001 (0.011, 0.213)	1017 (0.008, 0.099)	Ring vibration
990 m	989 vw	988 (0.091, 0.017)	988 (0.106, 0.017)	Ring breathing
970 w	974 m	970 (0.053, 0.316)	968 (0.007, 0.011)	Out-of-plane $\delta$ (CH)
938 vw	934 w	933 (0.006, 0.113)	934 (0.001, 0.002)	
911 w	913 w	927 (0.005, 0.003)	926 (0.006, 0.002)	$\delta$ (CH <sub>3</sub> )
889 w	894 vw	897 (0.007, 0.007)	892 (0.001, 0.016)	CCH aromatic deformation
870 w	868 vw	867 (0.022, 0.033)	869 (0.002, 0.003)	

**Table 4.6. (Continued)**

Observed		calculated		Proposed assignment
Raman, cm <sup>-1</sup>	IR, cm <sup>-1</sup>	IPRA1 $\nu$ (cm <sup>-1</sup> ) (Raman, IR Int.)	IPRA2 $\nu$ (cm <sup>-1</sup> ) (Raman, IR Int.)	
854 w	852 w	858 (0.040, 0.048)	847 (0.034, 0.002)	$\nu$ (C-N-C)
828 vw	826 w	831 (0.022, 0.002)	826 (0.021, 0.011)	Out-of-plane $\delta$ (CH) <sub>ring</sub>
816 vw		819 (0.008, 0.004)	815 (0.015, 0.003)	Skeletal vibrations
805 w	804 w	802 (0.017, 0.109)	799 (0.017, 0.091)	Skeletal vibrations
785 m	783 w	790 (0.008, 0.009)	784 (5.9e-4, 0.027)	Out-of-plane $\delta$ (CH) <sub>ring</sub>
764 vw	766 mw	757 (0.040, 0.019)	758 (0.014, 0.017)	Out-of-plane $\delta$ (CH) <sub>ring</sub>
742 vw	741 m	739 (0.022, 0.079)	735 (0.029, 0.020)	Ring vibration
708 w		711 (0.016, 0.079)	719 (0.017, 0.081)	Ring vibration
	700 m			$\delta$ (COC)
690 m	686 vw	690 (0.005, 0.051)	695 (0.002, 0.039)	Out-of-plane $\delta$ (CCC)
669 w	667 w	684 (0.022, 0.040)	665 (0.009, 0.012)	
639 vw		665 (0.009, 0.016)	656 (0.013, 0.012)	
621 w		621 (0.021, 0.023)	629 (0.036, 0.002)	Ring deformation
608 w		616 (0.018, 0.011)	614 (0.018, 0.001)	$\delta$ (CCC) <sub>ring</sub>
538 vw		554 (0.006, 0.006)	559 (0.002, 0.015)	$\delta$ (C-N)
515 vw		512 (0.009, 0.001)	514 (0.013, 0.044)	
499 vw		504 (0.003, 0.024)	510 (0.008, 0.018)	
479 sh,w		474 (0.007, 0.001)	489 (0.008, 0.009)	
470 mw		447 (0.010, 0.004)	455 (0.005, 0.031)	
438 w		439 (0.007, 0.019)	438 (0.014, 0.196)	In-plane (CCC) <sub>ring</sub> skeletal deformation
405 w		405 (0.001, 0.002)	405 (0.001, 2.3e-4)	In-plane (CCC) skeletal deformation
380 w		382 (0.015, 0.050)	380 (0.005, 0.005)	$\delta$ (OH)

**Table 4.6. (Continued)**

Observed		calculated		Proposed assignment
Raman, cm <sup>-1</sup>	IR, cm <sup>-1</sup>	IPRA1 $\nu$ (cm <sup>-1</sup> ) (Raman, IR Int.)	IPRA2 $\nu$ (cm <sup>-1</sup> ) (Raman, IR Int.)	
362 vw		360 (0.003, 0.011)	359 (0.005, 5.6e-4)	Skeletal deformation  (CH <sub>3</sub> ) $\tau$
337 w		326 (0.004, 0.010)	333 (0.001, 0.003)	
285 w		276 (0.002, 0.013)	292 (0.015, 0.004)	
267 w		249 (0.002, 0.003)	260 (0.004, 0.014)	
240 w		247 (0.012, 0.017)	242 (1.1e-4, 4.3e-4)	

## 5.1. Introduction

A major problem with the analysis of pharmaceutical compounds by Raman spectroscopy is the fluorescence caused by either the sample itself or by the presence of a small amount of impurity. The fluorescence emission of aromatic molecules such as salmeterol xinafoate (SX), generally occurs in the near-UV to visible region (300-700 nm) and therefore can interfere with the Raman signal if it is located within that spectral region (Berlman, 1971). This type of fluorescence can usually be avoided if the Raman signal is located in the far UV or NIR part of the spectrum. The Raman signal is generally located (spectrally) near the excitation wavelength so the fluorescence can be avoided by choosing a laser of an appropriate wavelength. With a NIR laser, the fluorescence signal may be avoided or minimised as the resultant Raman spectrum is in a lower energy region of the electromagnetic spectrum than the emitted fluorescence. In, addition, the NIR laser photon generally does not have sufficient energy to excite the fluorophore by single photon excitation, thus reducing the total amount of fluorescence produced. In contrast, excitation with a UV laser can still excite visible fluorescence but the Raman spectrum is located in the relatively fluorescence-free UV region of the electromagnetic spectrum (Asher and Johnson, 1984).

There are two disadvantages associated with moving to NIR excitation. The Raman intensity is inversely proportional to the fourth power of the laser wavelength, so the intensity of the Raman signal is weaker than with visible excitation (McCreery, 2000). Hence, practically, the spectral data acquisition time is increased. In addition, the efficiency of the typical silicon based CCD detector falls off in the NIR region (Delhaye et al., 1996). The benefits of avoiding the fluorescence emission, however, often outweigh these disadvantages of NIR laser excitation.

In this study, we describe experiments that explore the effects of using a variety of laser wavelengths from 488 nm to 1064 nm on the Raman spectra of SX polymorphs (see section 7.1.1 for details about the structure of SX).

## **5.2. Experimental**

### **5.2.1. Materials**

See section 7.2.1 for details.

### **5.2.2. Raman spectroscopy**

Raman spectra were recorded using a Bruker IFS66 with an FRA106 Raman spectrometer module operating at 1064 nm, laser powers were maintained at 200 mW at the samples and a Renishaw InVia Raman microscope operating at 785, 633, 514 and 488 nm with approximately 25 mW laser power at the sample (see sections 2.8.1.1 and 2.8.1.2 for details)

## **5.3. Results and discussion**

### **5.3.1. Characterisation of SX polymorphs**

Different polymorphs of the same molecule each have a different crystalline form and, hence, a unique Raman spectrum (Yu et al., 1998). Analysis of SX polymorphs I & II by Raman spectroscopy yielded spectra with excellent signal to noise ratios, with the two polymorphs exhibiting differences in both peak positions and intensities. The presence of the xinafoate ion has been considered, since it is common to both polymorphs, hence, the spectral characteristics are due to the polymorphic forms of salmeterol itself. The Raman spectra of both polymorphs are shown in Figures 5.1 and

5.2. The wavenumbers and proposed assignments of the Raman bands are given in Table 5.1.

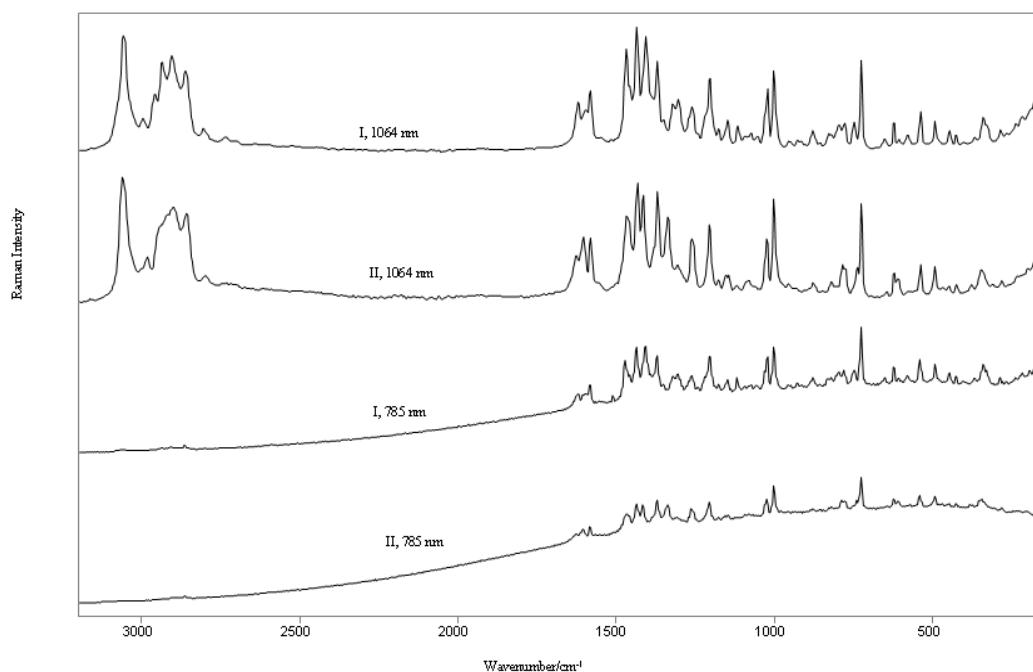


**Figure 5.1. Raman spectra of SX (forms I and II) at 1064 and 785nm.**

The main Raman spectral features common to both polymorphs studied were the  $\nu(\text{CH})$  band at  $3060\text{ cm}^{-1}$ , the  $\nu(\text{CH}_2)$  bands at  $2998$  and  $2862\text{ cm}^{-1}$ , the  $\nu_{\text{as}}(\text{CH}_2)$  band at  $2937\text{ cm}^{-1}$ , the  $\nu(\text{CH})_{\text{ring}}$  band at  $2905\text{ cm}^{-1}$ , the ring stretching vibrations at  $1621$ ,  $1602$  and  $1581\text{ cm}^{-1}$ , the  $(\text{CH})$  deformation bands at  $1466$ ,  $1434$  and  $1260\text{ cm}^{-1}$ , the  $\delta(\text{OCH}_2)$  band at  $1369\text{ cm}^{-1}$ , the in-plane  $\delta(\text{CH})$  band at  $1304\text{ cm}^{-1}$ , the  $\nu(\text{CN})$  band at  $1203\text{ cm}^{-1}$ , the  $\delta(\text{CH})_{\text{ring}}$  band at  $1178\text{ cm}^{-1}$ , the symmetric ring stretching bands at  $1021$  and  $1000\text{ cm}^{-1}$ , the skeletal stretching band at  $822\text{ cm}^{-1}$ , the out-of-plane  $\delta(\text{CH})_{\text{ring}}$  band at  $779\text{ cm}^{-1}$ , the  $r(\text{CH}_2)$  band at  $726\text{ cm}^{-1}$ , the out-of-plane  $\delta(\text{COC})$  band at  $538\text{ cm}^{-1}$  and the in-plane  $\delta(\text{CC})_{\text{chain}}$  band at  $494\text{ cm}^{-1}$ .

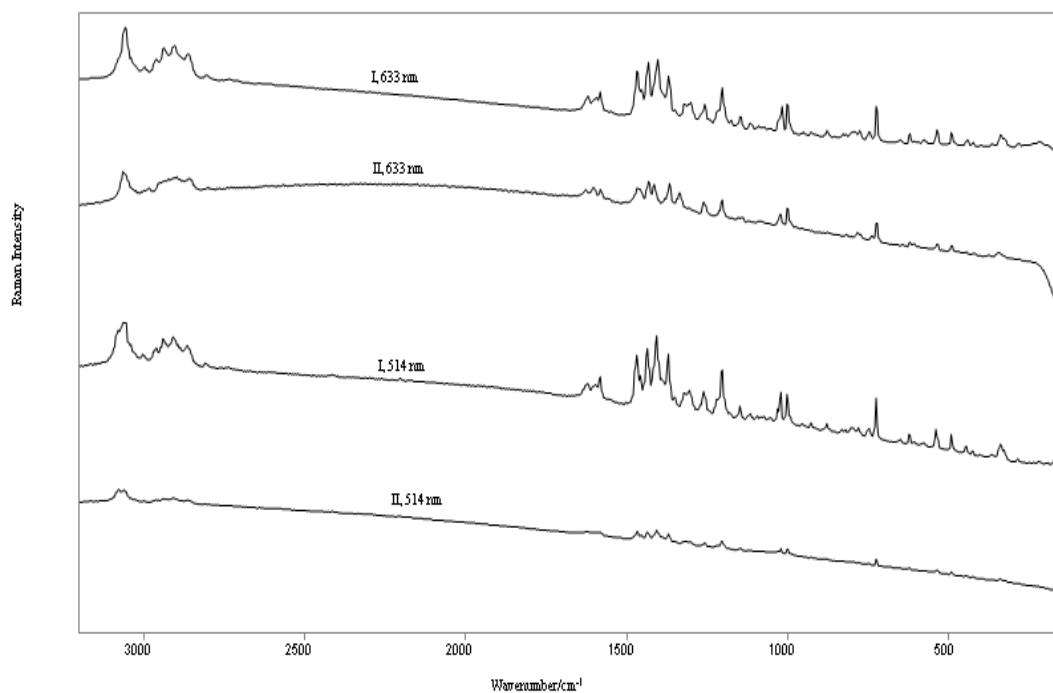


**Figure 5.2. Raman spectra of SX (forms I and II) at 633 and 514 nm.**

Despite the generally common Raman spectral features (Table 5.1), both forms under study were found to give rise to distinctive Raman patterns, which allow them to be identified through this spectroscopic technique. Form I is characterised by the  $\nu_{as}(\text{CH}_2)$  band at  $2959\text{ cm}^{-1}$ , the ring stretching bands at  $1594$  and  $1405\text{ cm}^{-1}$ , the  $\delta(\text{CH})$  bands at  $1457$  and  $1350\text{ cm}^{-1}$ , the ring vibration bands at  $1323$ ,  $1054$  and  $749\text{ cm}^{-1}$ , the symmetric ring stretching band at  $1029\text{ cm}^{-1}$ , the out-of-plane  $\delta(\text{CH})_{\text{chain}}$  band at  $927\text{ cm}^{-1}$ , the out-of-plane  $\delta(\text{CH})_{\text{ring}}$  bands at  $829$  and  $796\text{ cm}^{-1}$ , the in-plane  $\delta(\text{CCN})$  band at  $578\text{ cm}^{-1}$ , the  $\delta(\text{COC})$  band at  $482\text{ cm}^{-1}$ , the in-plane skeletal deformation band at  $400\text{ cm}^{-1}$ , the out-of-plane skeletal deformation band at  $238\text{ cm}^{-1}$  and the skeletal deformation bands at  $220$ ,  $193$  and  $167\text{ cm}^{-1}$ . Form II, in turn, is readily identified by the weak band due to  $\nu(\text{CH}_2)$  at  $2984\text{ cm}^{-1}$ , the strong ring stretching band at  $1415\text{ cm}^{-1}$ , the  $\delta(\text{CH}_2)_{\text{chain}}$  band at  $1382\text{ cm}^{-1}$ , the  $\delta(\text{CH})$  band at  $1338\text{ cm}^{-1}$ , the  $\nu(\text{CC})$  band at  $1157$

$\text{cm}^{-1}$ , the weak ring breathing band at  $976 \text{ cm}^{-1}$ , the out-of-plane  $\delta(\text{CH})_{\text{ring}}$  band at  $784 \text{ cm}^{-1}$ , the ring vibration band at  $738 \text{ cm}^{-1}$  and the very weak feature at  $466 \text{ cm}^{-1}$  ascribed to out-of-plane  $\delta(\text{COC})$ . These Raman differences can be attributed to the differences in intermolecular interactions and different modes of packing of the two crystalline polymorphs.

Several Raman peaks have been observed to be common to both forms but with small shifts in wavenumbers. The  $\nu_{\text{as}}(\text{C-NH})$  band at  $1149 \text{ cm}^{-1}$  in the spectrum of form I is shifted to  $1143 \text{ cm}^{-1}$  in the spectrum of form II with decreased intensity. The in-plane  $\delta(\text{CC})$  bands at  $1097$  and  $1074 \text{ cm}^{-1}$  of form I are shifted to  $1090$  and  $1079 \text{ cm}^{-1}$ , respectively in the spectrum of form II. This is due to the fact that when molecules are packed together in different arrangements in the crystal (i.e. polymorphism) the vibrational modes involving less rigid bonds will be affected more than those of rigid structures. Additionally, the  $\nu(\text{CNC})$ , out-of-plane  $\delta(\text{CH})_{\text{ring}}$  and  $\delta(\text{C-C-C long chain})$  bands at  $880$ ,  $855$  and  $341 \text{ cm}^{-1}$  in the spectrum of the form I are shifted to  $875$ ,  $848$  and  $346 \text{ cm}^{-1}$ , respectively, in the spectrum of the form II.

The present study allowed the assignment of specific Raman spectral features, characteristic of each of the polymorphic form of SX investigated. Therefore, these results will be very useful for the identification and possible discrimination of these polymorphs.

### **5.3.2. Dependence of the Raman spectra upon laser excitation wavelength**

Figures 5.1, 5.2 and 5.3 show the Raman spectra obtained from the both polymorphs with the five different excitation wavelengths used ( $488$ ,  $514$ ,  $633$ ,  $785$  and  $1064 \text{ nm}$ ). The wavenumbers and proposed assignments of the Raman bands are given in Table 5.1, from which, it is noted that, with decreasing the excitation wavelength from  $1064$

nm to 514 nm there is a reduction in the intensities of the Raman bands of form II except for the  $\nu(\text{CH})_{\text{ring}}$  and symmetric ring stretching bands at 3079 and 1029  $\text{cm}^{-1}$ , respectively, and at 488 nm, there is very high fluorescence background and accordingly Raman spectra could not be obtained for both forms (Figure 5.3).

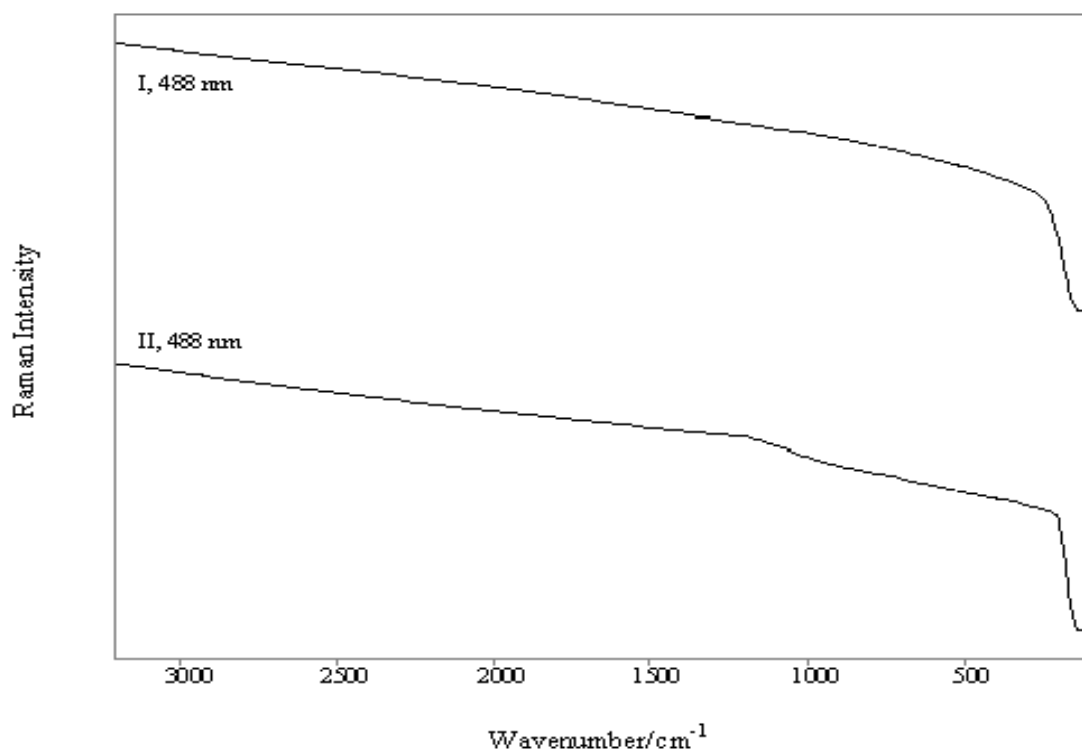


**Figure 5.3. Raman spectra of SX (forms I and II) at 488 nm.**

There are several spectral features common to both polymorphs which disappear in the Raman spectra of form II with decreasing the excitation wavelength to both 633 and 514 nm which are the out-of-plane  $\delta(\text{CC})_{\text{ring}}$ , in-plane skeletal deformation and chain expansion bands at 648, 445 and 425  $\text{cm}^{-1}$  respectively, and to 514 nm, which are the in-plane  $\delta(\text{CC})$  bands at 1090 and 1079  $\text{cm}^{-1}$ , the  $\nu(\text{CH}_2)$  band at 955  $\text{cm}^{-1}$ , the ring deformation band at 621  $\text{cm}^{-1}$  and the in-plane  $\delta(\text{CCC})$  band at 605  $\text{cm}^{-1}$ . In turn, there are several distinctive patterns of form II which disappear with decreasing the excitation wavelength to both 633 nm and 514 nm, which is the out-of-plane  $\delta(\text{COC})$  band at 466  $\text{cm}^{-1}$ , and to 514 nm, where the ring stretching band at 1415  $\text{cm}^{-1}$ , the ring breathing

band at  $976\text{ cm}^{-1}$  and the out-of-plane  $\delta(\text{CH})_{\text{ring}}$  band at  $784\text{ cm}^{-1}$  are all absent from its Raman spectrum. From our observations, it is clear that SX form II generally has a higher fluorescence background level so we can conclude that, on examining the dosage forms containing SX by Raman spectroscopy, it is better to use NIR laser excitation, if available, rather than the visible excitation to avoid the higher fluorescence background of the form II and to ease the possible identification and discrimination of both forms under study.

#### **5.4. Conclusions**

The Raman spectrum of SX polymorph II is reported for the first time. From the Raman spectroscopic analysis carried out in this study it is possible to identify the key Raman characteristic bands of SX polymorphs (I&II). The effect of using different laser excitation wavelengths in the range from visible to NIR when carrying out Raman spectroscopic analysis on these polymorphs has been studied. It can be concluded that, on examining the dosage forms containing SX by Raman spectroscopy, it is better to use NIR laser excitation if available rather than visible excitation to avoid the higher fluorescence background of the form II and to ease the possible identification and discrimination of both forms.

The present study clearly demonstrates that Raman spectroscopy is useful as a tool for assessing the polymorphic purity of SX materials and possibly other polymorphic forms showing similar behaviour.

**Table 5.1. Raman spectral wavenumbers and proposed assignments for SX polymorphs I&II at the selected wavelengths (514, 633, 785 and 1064 nm).**

1064 nm		785 nm		633 nm		514 nm		Proposed Assignment
I	II	I	II	I	II	I	II	
3079 w,sh	-	3079 w,sh	-	3079 w,sh	-	3079 mw	3079 m	$\nu(\text{CH})_{\text{ring}}$
3060 m	3060 m	3060 m	3060 w	3060 m	3060 m	3060 m	3060 m	$\nu(\text{CH})$
3037 w,sh	-	3037 w,sh	-	3037 w,sh	-	3037 w,sh	-	$\nu_{\text{as}}(\text{CH}_2)_{\text{chain}}$
2998 w	2998 w	2998 w	2998 vw	2998 w	2998 w	2998 w	2998 w	$\nu(\text{CH}_2)$
-	2984 w	-	2984 vw	-	2984 w	-	2984 w	$\nu(\text{CH}_2)$
2959 mw	-	2959 mw	-	2959 mw	-	2959 mw	-	$\nu_{\text{as}}(\text{CH}_2)$
2937 m	2937 mw,br	2937 m	2937 vw,br	2937 m	2937 mw,br	2937 m	2937 w	$\nu_{\text{as}}(\text{CH}_2)$
2905 m	2905 mw,br	2905 m	2905 vw,br	2905 m	2905 mw,br	2905 m	2905 w	$\nu(\text{CH})_{\text{ring}}$
2862 m	2862 mw	2862 m	2862 mw	2862 m	2862 w	2862 m	2862 w	$\nu(\text{CH}_2)$
-	2802 vw	-	2802 w	-	2802 w	-	2802 vw	-
1621 m	1621 m	1621 m	1621 m	1621 m	1621 w	1621 m	1621 w	Ring stretch
1602 m	1602 m	1602 m	1602 m	1602 m	1602 w	1602 m	1602 w	Ring stretch
1594 m	-	1594 m	-	1594 m	-	1594 m	-	Ring stretch
1581 m	1581 m	1581 m	1581 m	1581 m	1581 w	1581 m	1581 w	Ring stretch
1466 s	1466 ms	1466 s	1466 ms	1466 s	1466 m	1466 s	1466 m	$\delta(\text{CH})$
1457 m,sh	-	1457 m,sh	-	1457 m,sh	-	1457 m,sh	-	$\delta(\text{CH})$
1434 s	1434 s	1434 s	1434 s	1434 s	1434 m	1434 s	1434 w	$\delta(\text{CH})$
-	1415 s	-	1415 s	-	1415 m	-	-	Ring stretch
1405 s	-	1405 s	-	1405 s	-	1405 s	-	Ring stretch
-	1382 w,sh	-	1382 w,sh	-	1382 w,sh	-	1382 w,sh	$\delta(\text{CH}_2)_{\text{chain}}$
1369 ms	1369 s	1369 ms	1369 s	1369 ms	1369 m	1369 ms	1369 w	$\delta(\text{OCH}_2)$
1350 w	-	1350 w	-	1350 w	-	1350 w	-	$\delta(\text{CH})$

**Table 5.1. (Continued)**

1064 nm		785 nm		633 nm		514 nm		Proposed Assignment
I	II	I	II	I	II	I	II	
-	1338 s	-	1338 m	-	1338 m	-	1338 w	$\delta$ (CH)
1323 m	-	1323 m	-	1323 m	-	1323 m	-	Ring vibration
1304 m	1304 w	1304 m	1304 vw	1304 m	1304 vw	1304 m	1304 vw	In-plane $\delta$ (CH)
1266 w,sh	-	1266 w,sh	-	1266 w,sh	-	1266 w,sh	-	In-plane $\delta$ (CH)
1260 m	1260 ms	1260 m	1260 m	1260 m	1260 m	1260 m	1260 w	$\delta$ (CH)
1243 vw	-	1243 vw	-	1243 vw	-	1243 vw	-	-
1218 m,sh	-	1218, m,sh	-	1218 m,sh	-	1218 m,sh	-	$\delta$ (CH) <sub>ring</sub>
1203 s	1203 s	1203 s	1203 m	1203 s	1203 m	1203 s	1203 w	$\nu$ (CN)
1178 w	1178 w	1178 w	1178 vw	1178 w	1178 vw	1178 w	1178 vw	$\delta$ (CH) <sub>ring</sub>
-	1157 mw	-	1157 w	-	1157 w	-	1157 vw	$\nu$ (CC)
1149 m	1143 mw	1149 m	1143 w	1149 m	1143 w	1149 m	1143 vw	$\nu_{as}$ (C-NH)
1097 w	1090 w	1097 w	1090 vw	1097 w	1090 vw	1097 w	-	In-plane $\delta$ (CC)
1074 vw	1079 w	1074 vw	1079 vw	1074 vw	1079 vw	1074 vw	-	In-plane $\delta$ (CC)
1054 vw	-	1054 vw	-	1054 vw	-	1054 vw	-	Ring vibration
1029 m,sh	-	1029 m,sh	-	1029 m,sh	-	1029 m,sh	1029 w,sh	Symmetric ring stretch
1021 s	1021 ms	1021 s	1021 ms	1021 s	1021 m	1021 m	1021 w	Symmetric ring stretch
1000 s	1000 s	1000 s	1000 s	1000 s	1000 m	1000 m	1000 w	Symmetric ring stretch
-	976 w	-	976 w	-	976 vw	-	-	Ring breathing
955 vw	955 w	955 vw	955 w	955 vw	955 vw	955 vw	-	r (CH <sub>2</sub> )
927 vw	-	927 vw	-	927 vw	-	927 vw	-	Out-of-plane $\delta$ (CH) <sub>chain</sub>

**Table 5.1. (Continued)**

1064 nm		785 nm		633 nm		514 nm		Proposed Assignment
I	II	I	II	I	II	I	II	
880 w	875 w	880 w	875 w	880 w	875 w	880 w	875 w	$\nu(\text{CNC})$
855 vw	848 vw	855 vw	848 vw	855 vw	848 vw	855 vw	848 vw	Out-of-plane $\delta(\text{CH})_{\text{ring}}$
829 w	-	829 w	-	829 w	-	829 vw	-	Out-of-plane $\delta(\text{CH})_{\text{ring}}$
822 w	822 w	822 w	822 vw	822 w	822 vw	822 vw	822 vw	Skeletal stretch
796 w	-	796 w	-	796 w	-	796 w	-	Out-of-plane $\delta(\text{CH})_{\text{ring}}$
-	784 m	-	784 mw	-	784 w	-	-	Out-of-plane $\delta(\text{CH})_{\text{ring}}$
779 mw	779 m	779 mw	779 mw	779 mw	779 w	779 mw	779 w	Out-of-plane $\delta(\text{CH})_{\text{ring}}$
749 mw	-	749 mw	-	749 mw	-	749 mw	-	Ring vibration
-	738 mw	-	738 mw	-	738 w	-	738 vw	Ring vibration
726 s	726 s	726 s	726 ms	726 s	726 m	726 s	726 w	$r(\text{CH}_2)$
648 w	648 w	648 w	648 vw	648 w	-	648 w	-	Out-of-plane $\delta(\text{CC})_{\text{ring}}$
621 mw	621 w	621 mw	621 w	621 mw	621 vw	621 mw	-	Ring deformation
605 vw	605 w	605 vw	605 w	605 vw	605 vw	605 vw	-	In-plane $\delta(\text{CCC})$
578 w	-	578 w	-	578 w	-	578 w	-	In-plane $\delta(\text{CCN})$
538 m	538 w	538 m	538 w	538 m	538 w	538 m	538 vw	Out-of-plane $\delta(\text{COC})$
494 mw	494 w	494 mw	494 w	494 mw	494 w	494 mw	494 vw	In-plane $\delta(\text{CC})_{\text{chain}}$
482 w,sh	-	482 w,sh	-	482 w,sh	-	482 w,sh	-	$\delta(\text{COC})$
-	466 vw	-	466 vw	-	-	-	-	Out-of-plane $\delta(\text{COC})$
445 w	445 vw	445 w	445 vw	445 w	-	445 w	-	In-plane skeletal deformation
425 w	425 vw	425 w	425 vw	425 w	-	425 w	-	Chain expansion
400 vw	-	400 vw	-	400 vw	-	400 vw	-	In-plane skeletal deformation

**Table 5.1. (Continued)**

1064 nm		785 nm		633 nm		514 nm		Proposed Assignment
I	II	I	II	I	II	I	II	
-	378 vw	-	378 vw	-	378 vw	-	378 vw	-
368 vw	-	368 vw	-	368 vw	-	368 vw	-	-
341 mw	346 w	341 mw	346 w	341 mw	346 w	341 mw	346 vw	$\delta$ (C-C-C long chain)
327 w	-	327 w	-	327 w	-	327 w	-	-
284 vw	284 w	284 vw	284 w	284 vw	-	284 vw	-	-
269 vw	-	269 vw	-	269 vw	-	269 vw	-	-
238 w	-	238 w	-	238 w	-	238 w	-	Out-of-plane skeletal deformation
220 w	-	220 w	-	220 w	-	220 w	-	Skeletal deformation
193 vw	-	193 vw	-	193 vw	-	193 vw	-	Skeletal deformation
167 m	-	167 m	-	167 vw	-	167 w	-	Skeletal deformation

br,m, s, sh, v and w stand for broad, medium, strong, shoulder, very and weak respectively. as, r, v, and  $\delta$  stand for asymmetric, rocking, stretching and deformation respectively.

## 6.1. Introduction

The identification of excipients is an important task in the cGMP manufacture of drug products within the pharmaceutical industry. A positive test is required to release the excipient batches for use in the production of clinical trial or commercial batches. The identification of excipients is performed according to the various pharmacopoeias, for the European Pharmacopoeia, which includes tests for identification (Pharmacopoeia, 1997). These tests are often wet chemical in nature, with additional tests required for providing evidence of functional groups such as aldehydes or ketones within the excipient structure. These mostly laborious compendial identification methods afford an opportunity to improve the analyses for both time and quality and one technique that meets these requirements is NIR spectroscopy.

NIR absorption bands in the NIR spectral region (800-2500 nm) exist because the vibration of a chemical bond is not a simple harmonic motion. Due to the nonideal nature of a chemical bond, weaker overtones of bond vibrations occur at about one-half, one-third, one-quarter, and one-fifth the wavelength (or twice, three times, four times, and five times the frequency) of the fundamental vibration. The overtones of the stretching vibrations are generally stronger than bending or rocking modes (Weyer and Lo, 2002). The overtones observed primarily in the NIR region involve small hydrogen atoms coupled with larger atoms. There are two main reasons of this. One is that these vibrations are more anharmonic than those between atoms of similar size, and therefore have stronger overtones. The other is that the fundamental stretching vibrations of the C-H, O-H and N-H bonds occur at the short-wavelength (high-frequency) end of the mid-IR spectrum due to lower reduced mass. The relatively high wavenumbers of these fundamentals means that their first overtones will occur in the NIR, while the first overtones of other vibrations occur within the mid-IR region.

In addition to the overtone bands, the NIR region also contains groups of combination bands of diminished intensity. These bands involve hydrogenic vibrations almost exclusively, again because anharmonicity is important to both their existence and strength. These bands appear at frequencies that represent approximately the sum of the two vibrations. The stronger combination bands involve good coupling between the two vibrations (Weyer and Lo, 2002). Good coupling is most likely to occur when the frequencies of the two vibrations are very similar or when they are bound together by a double bond or a ring. The first and strongest set of combination bands appear in the region of about 1900 to 2500 nm region of the NIR spectrum.

The low intensity of the NIR spectral features is largely compensated by the notable advances in the instrumentation associated with modern NIR spectrometers. The use of non-moving components in the construction of NIR spectrometers has also imparted the robustness and portability necessary for field or process operation and use in less restrictive ambient conditions.

NIR spectroscopy combined with multivariate data analysis opens many interesting perspectives in pharmaceutical analysis, both qualitatively and quantitatively. Fast, non destructive NIR measurements and their compatibility with fibre optics and glass containers without any sample pre-treatment being necessary have increased the analytical throughput significantly. The special feature of combined physical and chemical information allows for the assessment of a “spectral signature” of raw materials, intermediates and final dosage forms, which in turn offers the possibility of a simultaneous determination of several sample characteristics. The basic principles and pharmaceutical applications of NIR spectroscopy has been reviewed recently (Reich, 2005) and several papers have been reported on the feasibility of NIR identification of both active ingredients and excipients (Sulub et al., 2008; Chalus et al., 2005; Roggo et

al., 2004; Krämer and Ebel, 2000; Beckenkamp et al., 2001; Thosar et al., 1999; Gustafsson et al., 2003; Burneau and Carteret, 2000; Blanco et al., 1999)

The current work was undertaken to evaluate FT-NIR spectroscopy for the *in situ* identification of solid pharmaceutical excipients inside USP vials.

## **6.2. Experimental**

### **6.2.1. Materials**

The following pharmaceutical excipients were studied: potassium sorbate, sodium starch glycollate, calcium ascorbate, calcium carbonate, candelilla wax, maltodextrin, lactose monohydrate, anhydrous and unknown lactose sample.

These substances are used in the manufacture of solid dosage forms as binders, diluents, disintegrate or lubricants. All the samples in each class (excipient) were obtained from the warehouse of a pharmaceutical company. The samples came from different excipient batches and occasionally from different suppliers. Multiple excipient grades within certain classes were considered, but the primary aim of this study is to identify the pharmaceutical excipients inside USP vials and, not their specific grades.

### **6.2.2. FT-NIR spectroscopy**

NIR spectra for each powder sample were collected in triplicate using a Bruker Optics *MPA* FT-NIR spectrometer (see section 2.8.2.2 for details). Individual sample vials were rotated between triplicate scans to ensure representative spectra. Triplicate scans were averaged to obtain one spectrum for each powder sample.

### 6.3. Results and discussion

Common glasses (borosilicate, soda, etc.) are virtually transparent to NIR radiation and powdered samples may be measured in glass sample bottles using the reflectance mode. The effect of sampling through the transparent vials is illustrated in Figures 6.1 to 6.8 for the studied pharmaceutical excipients as open powders and inside USP vials.

#### 6.3.1. Non-invasive *in situ* identification of potassium sorbate, sodium starch glycollate, calcium ascorbate, calcium carbonate, candelilla wax and maltodextrin.

The NIR spectra of the above pharmaceutical excipients in the range of 800 to 2500 nm are shown in Figures 6.1-6.6 as open powders and inside USP vials. It should be noted that the NIR spectra obtained from specimens inside vials are almost the same as those obtained from open powder specimens.

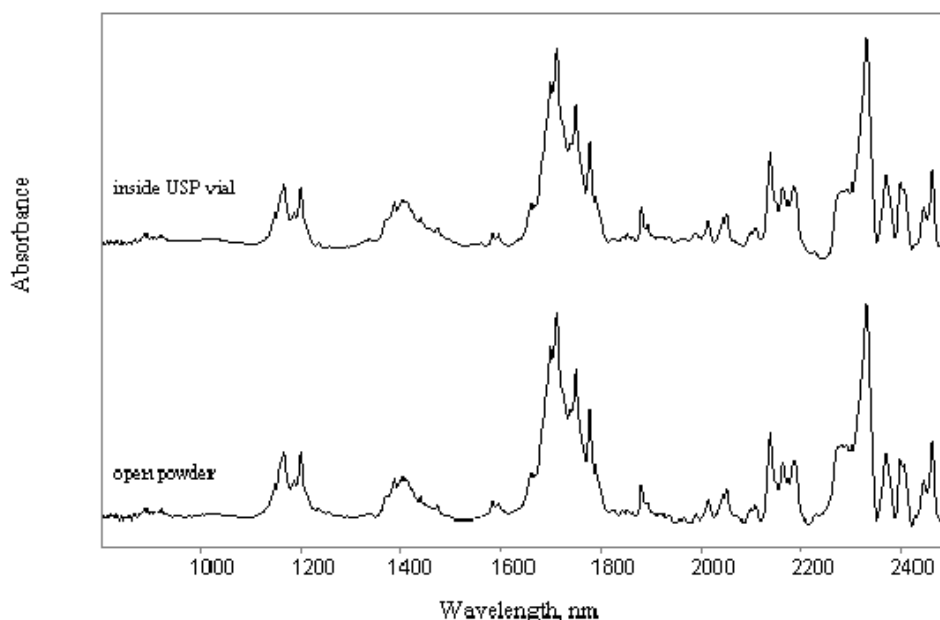


**Figure 6.1. NIR spectra of potassium sorbate obtained inside a USP vial and as an open powder.**

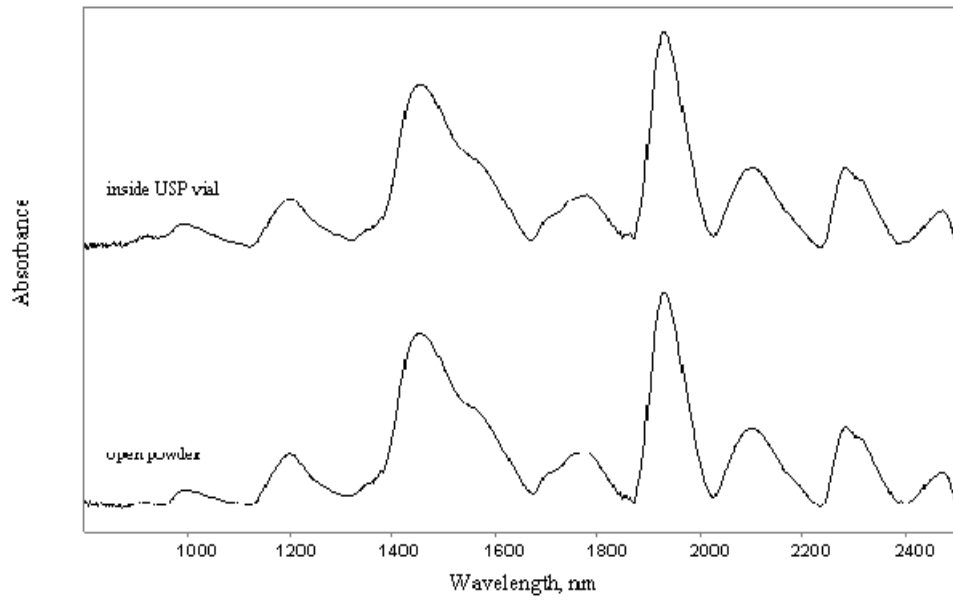


**Figure 6.2. NIR spectra of sodium starch glycolate obtained inside a USP vial and as an open powder.**

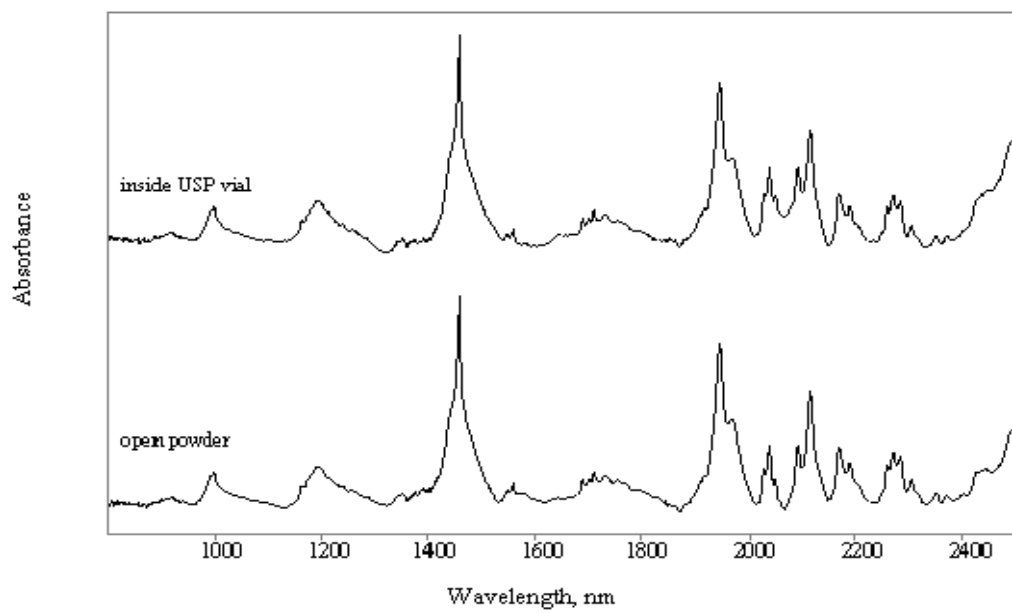


**Figure 6.3. NIR spectra of calcium ascorbate obtained inside a USP vial and as an open powder.**

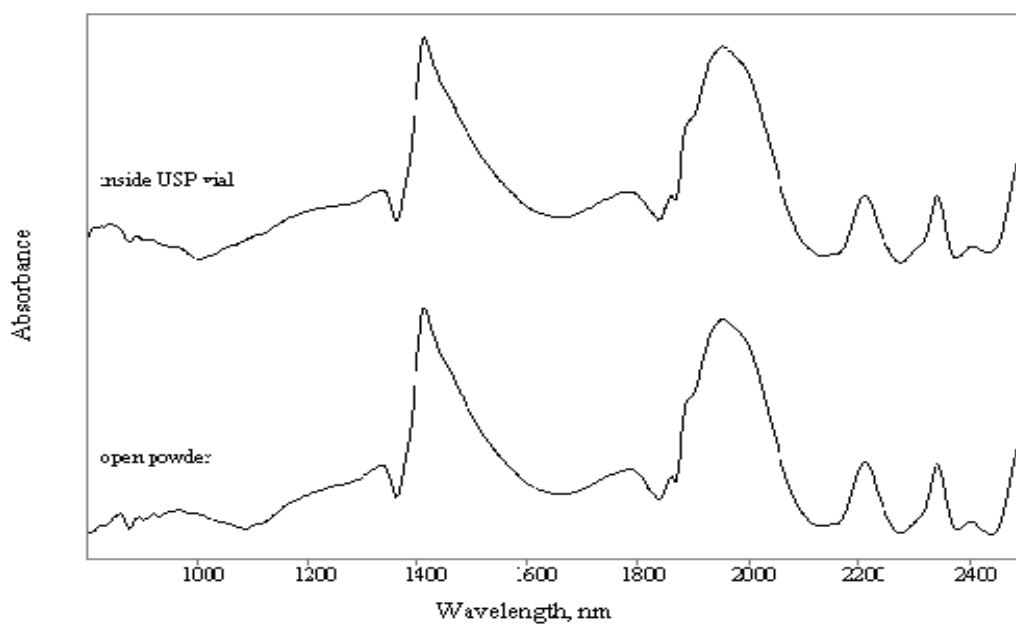


**Figure 6.4. NIR spectra of calcium carbonate obtained inside a USP vial and as an open powder.**

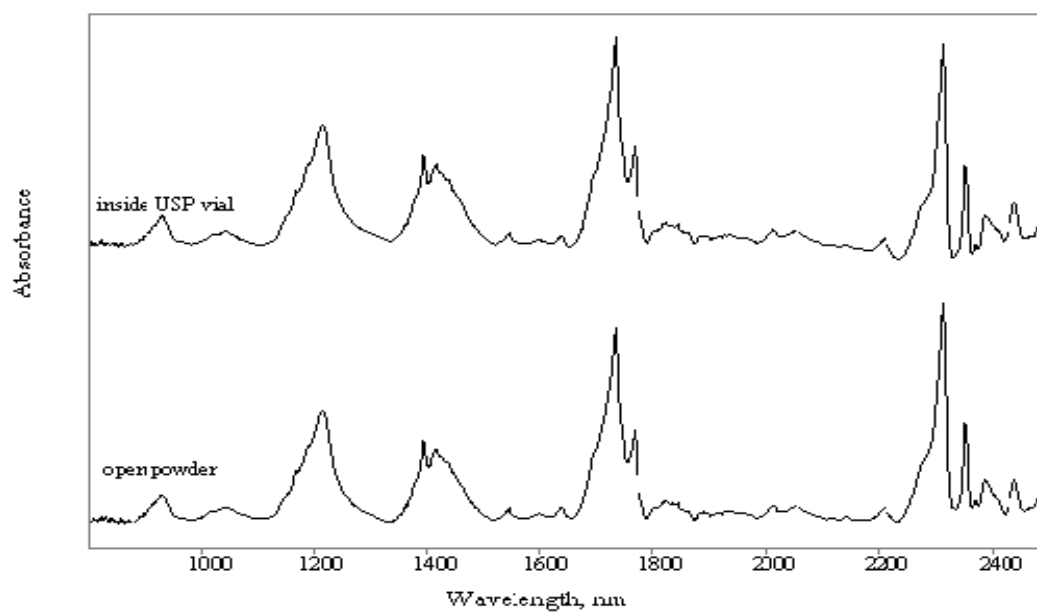


**Figure 6.5. NIR spectra of candelilla wax obtained inside a USP vial and as an open powder.**

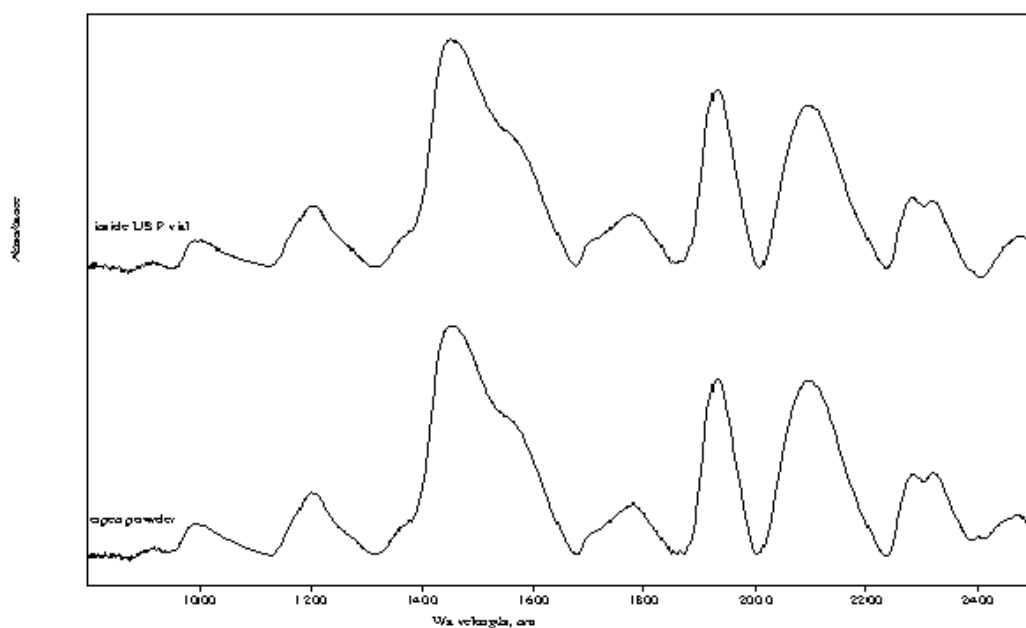


**Figure 6.6. NIR spectra of maltodextrin obtained inside a USP vial and as an open powder.**

NIR spectral wavelengths (nm) and proposed assignments for the pharmaceutical excipients under study are presented in Table 6.1. From the NIR spectroscopic analysis carried out in the present work, it is observed that the NIR spectra of potassium sorbate and calcium ascorbate are much richer than the NIR spectra of sodium starch glycollate, calcium carbonate, candelilla wax and maltodextrin; this is due to the fact that compounds with long aliphatic chains, such as hydrocarbons, stearates and waxes, are difficult to distinguish as the spectra become dominated by the  $-CH_2$  groups. Starches and related compounds, such as maltodextrins, gums and other materials with polysaccharide groupings, are also difficult to distinguish from one another reliably.

Water is a particularly strong absorber in the NIR region, with the O-H first overtone of the stretching vibration occurring near 1450 nm in the case of sodium starch glycollate and maltodextrin (Figures 6.2 and 6.6). Sodium starch glycollate, calcium ascorbate and maltodextrin in the NIR spectra have a very intense water absorption in the

region 1900 to 1940 nm assigned to the combination band between the fundamental stretching and deformation vibrations of the O-H bond, whereas this strong water band is not observed in the NIR spectra of potassium sorbate, calcium carbonate and candelilla wax (Figures 6.1-6.6).

Pharmaceutical excipients screening using NIR spectroscopy is truly a timesaving process, although it is not an absolute method. This approach provides an improvement for rapid *in situ* analysis of pharmaceutical excipients in the case of large number of samples contained in USP vials.

**Table 6.1. NIR spectral wavelengths, nm and proposed assignments for potassium sorbate, sodium starch glycollate, calcium ascorbate, calcium carbonate, candelilla wax and maltodextrin.**

Potassium sorbate	Sodium starch glycollate	Calcium ascorbate	Calcium carbonate	Candelilla wax	Maltodextrin	Proposed assignment
888			860			Third overtone C-H stretching
918		917		930		Third overtone C-H stretching
	985	998		1042	996	Second overtone O-H stretching
1164		1162		1190, sh		Second overtone C-H stretching
1185	1197	1193			1201	Second overtone C-H stretching
1199				1215		Second overtone C-H stretching
1235						
		1345				Combination C-H stretching
1335		1353	1337			Combination C-H stretching
1337, sh		1367		1394		Combination C-H stretching
1387		1377	1414	1416		Combination C-H stretching
1404		1392				Combination C-H stretching
1439	1455				1455	First overtone O-H stretching
1457		1457				First overtone O-H stretching
1473	1556, sh	1548		1542	1554, sh	
1582		1558				
1596		1639		1637		
1662		1690				First overtone C-H stretching
1698		1700			1717, sh	First overtone C-H stretching
1710	1725, sh	1708		1733		First overtone C-H stretching
1739		1733		1765		First overtone C-H stretching

**Table 6.1. (Continued)**

Potassium sorbate	Sodium starch glycollate	Calcium ascorbate	Calcium carbonate	Candelilla wax	Maltodextrin	Proposed assignment
1749	1773	1755	1792		1780	First overtone C-H stretching
1780				1802		First overtone C-H stretching
1816						
1826						
1843						
1853						
1865			1861			
1883						
1895			1899, sh			
1918						
1928						
1936	1932	1944	1954		1932	
1962		1969				
1991		2031				
2015		2037		2013		Combination O-H stretching
2052		2048		2056		Combination O-H stretching
2101	2102	2092			2099	Combination O-H stretching
2109		2115		2117		Combination O-H stretching
2141		2169		2143		Combination O-H stretching
2167		2190		2171		Combination O-H stretching
2186						Combination O-H stretching
2230		2261	2208			Combination C-H stretching
2295, sh	2285	2273			2286	Combination C-H stretching
2332	2316, sh	2285	2344	2314	2320	Combination C-H stretching
2371		2308		2352		Combination C-H stretching
2401		2352	2405	2370		Combination C-H stretching

**Table 6.1. (Continued)**

Potassium sorbate	Sodium starch glycollate	Calcium ascorbate	Calcium carbonate	Candelilla wax	Maltodextrin	Proposed assignment
2446		2372		2387		Combination C-H stretching
		2403				Combination C-H stretching
		2427		2439		Combination C-H stretching
2462	2490	2490	2462		2484	

### 6.3.2. Non-invasive *in situ* identification of lactose anhydrous and monohydrate

The NIR spectra of lactose anhydrous and monohydrate in the range of 800-2500 nm are shown in Figures 6.7 and 6.8 as an open powder and inside USP vials. Again, it can be noted that NIR spectra inside vials are almost identical with those obtained as open powders, with no loss of spectral quality.

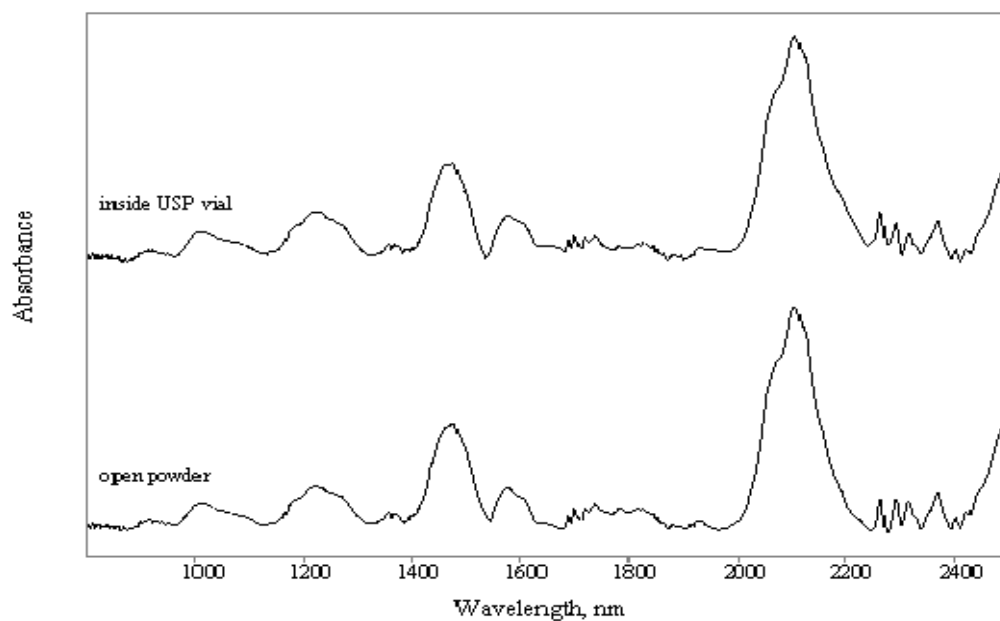


**Figure 6.7. NIR spectra of lactose anhydrous obtained inside a USP vial and as an open powder.**

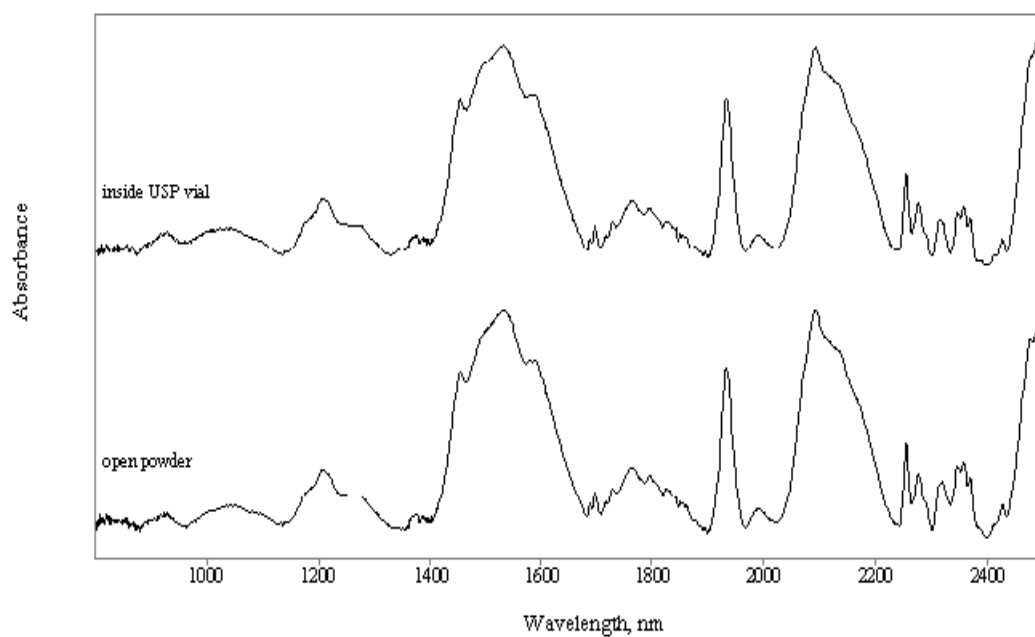


**Figure 6.8. NIR spectra of lactose monohydrate obtained inside a USP vial and as an open powder.**

An unknown lactose sample inside a USP vial was analysed using NIR spectroscopy, and could be identified as anhydrous lactose (Figure 6.9). NIR spectral wavelengths (nm) and proposed assignments for lactose anhydrous and monohydrate are presented in Table 6.2.

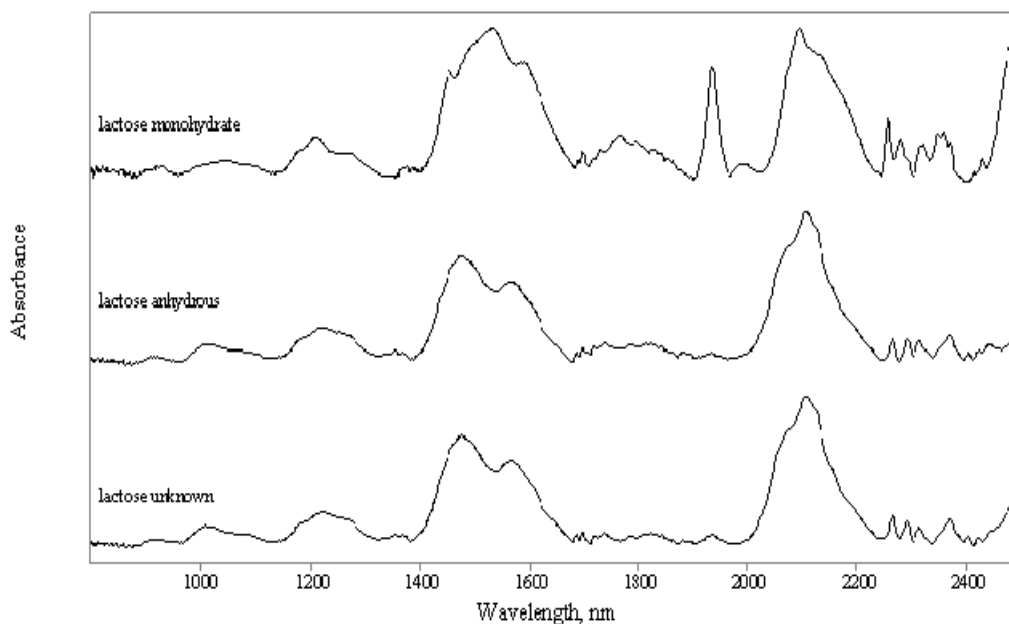


**Figure 6.9. NIR spectra of lactose monohydrate, anhydrous and unknown obtained inside a USP vial.**

Despite some common spectral features between lactose anhydrous and monohydrate (Table 6.2), both forms were found to give rise to distinctive NIR patterns, which allow them to be readily and noninvasively identified inside USP vials through this spectroscopic technique. By careful inspection of Figures 6.7 and 6.8, it can be noted that the first overtone O-H stretching band at 1454 nm is characteristic of lactose monohydrate along with the O-H deformation combination band at 1934 nm, which is very strong in the lactose monohydrate NIR spectrum and weak in the lactose anhydrous NIR spectrum. It can be concluded that even the lactose anhydrous sample has absorbed some moisture, as indicated by the presence of the weak O-H deformation combination band at 1934 nm in the NIR spectrum of the anhydrous form; however NIR spectroscopy is still able to differentiate between the anhydrous and monohydrate forms of lactose.

**Table 6.2. NIR spectral wavelengths, nm and proposed assignments for lactose anhydrous and monohydrate.**

Lactose anhydrous	Lactose monohydrate	Proposed assignment
914	926	Third overtone C-H stretching
1010	1040	Second overtone O-H stretching
	1180, sh	Second overtone C-H stretching
1221	1207	Second overtone CH <sub>2</sub> stretching
	1268	
	1454	First overtone O-H stretching
1475		First overtone O-H stretching
	1536	Symmetric and antisymmetric stretching of water species with at least three hydrogen bonds
1577		
1601, sh	1593	
1656		First Overtone C-H stretching
1689	1690	First Overtone C-H stretching
1699	1698	First Overtone C-H stretching
1720	1719	First overtone of CH <sub>2</sub> antisymmetric stretching
1739	1731	First Overtone C-H stretching
1784	1763	First Overtone C-H stretching
1934	1934	Combination band between the fundamental stretching and deformation vibrations of the OH bond
	1991	
2082, sh	2095	Combination O-H stretching
2107	2123, sh	Combination O-H stretching
2265	2259	Combination C-H stretching
	2280	Combination C-H stretching
2292	2291	Combination C-H stretching
2316	2318	Combination of CH <sub>2</sub> asymmetric stretching and bending vibrations
2324, sh		
	2348	Combination of CH <sub>2</sub> symmetric stretching and bending vibrations
	2361	Combination C-H stretching
2371	2371	Combination C-H stretching
2402		Combination C-H stretching
2421	2421, sh	Combination C-H stretching
	2430	Combination C-H stretching
	2479	
2489	2491	

NIR spectroscopy can be used in real time to follow the changes in the solid state, the onset of crystallization and the changes between different forms of lactose which accompany the onset of crystallization. The fact that NIR is non-invasive and that the spectra are measured *in situ* at room temperature in a rapid and easy manner, makes it very valuable tool to use in conjunction with other physical methods to study transitions in pharmaceuticals. There are significant advantages in the use of the NIR technique, which is isothermal at room temperature, over the use of differential scanning calorimetry where crystallization processes and transitions are induced due to heating, making it difficult to be certain of the properties of the starting material.

#### **6.4. Conclusions**

The current work establishes that NIR spectra can be obtained noninvasively and rapidly through USP vials. Pharmaceutical excipients can be readily identified *in situ* by NIR spectroscopy, although several samples of different manufacturers and physical properties were studied. The discrimination of lactose anhydrous and monohydrate forms can be done reliably inside USP vials by studying the regions of the NIR spectrum corresponding to the combination and first overtone stretching frequencies of water. After clustering the NIR spectra of various samples, XRPD and complementary methods can be applied to the verification of the pharmaceuticals. This approach provides a timesaving improvement for the pharmaceutical analysis of excipients in the case of large number of samples.

Further studies will target to the construction of a spectral library of reference pharmaceutical materials using NIR spectroscopy as a rapid, non-invasive technique for the identification of compounds relevant to pharmaceutical preparations.

## 7.1. Introduction

Polymorphism is the tendency of a substance to crystallise in different crystalline states. The solid forms of the same compounds are called polymorphs or crystalline modifications. Polymorphs show the same properties in the liquid or gaseous state but they behave differently in the solid state. The best known example of polymorphism is carbon, which can exist in the form of graphite or as diamond.

In the solid states, the atoms of a molecule may be arranged in one of seven fundamental crystalline forms: triclinic, monoclinic, orthorhombic, tetragonal, trigonal, hexagonal or cubic. The amorphous state is characterised by crystallisation in a non-ordered, random system, related to the liquid state.

Differences in the morphological appearance of a substance do not necessarily reflect polymorphism. Crystallisation of the base cells may occur in three different directions. A compound can produce crystals with different morphologies (habits) without changing the crystalline structure by preferentially growing in different directions.

Like many other chemical compounds, however, certain hydrates (See section 3.3 for details) may themselves exhibit polymorphism, as in the case of fluprednisolone monohydrate, succinyl sulfathiazole monohydrate and nedocromil sodium monohydrate (Khankari and Grant, 1995).

Because all the physicochemical characteristics of the solid state are implied in polymorphism and pseudopolymorphism, the pharmaceutical industry is confronted with this behaviour. The main properties affected are melting and sublimation temperatures, heat capacity, conductivity, volume, density, viscosity, crystal hardness, crystal shape, colour, refractive index, solubility, dissolution rate, stability, hygroscopicity and solid state reactions.

The effect of polymorphism on bioavailability is the most important consequence if the bioavailability is mediated via the dissolution (Giron, 1995). The polymorphism of excipients (Giron, 1995) may also play an important role in bioavailability as demonstrated by the loss of bioavailability of suppositories due to polymorphic transformation of the excipient during storage. The process of transformation of one polymorph into another is a phase transition, which may occur also on storage or during processing. If the phase transition is reversible, the two polymorphs are enantiotropic. If the phase transition is irreversible, the two polymorphs are monotropic.

In the case of monotropy, the higher melting form is always the thermodynamically stable form. In the case of enantiotropy, the lower melting form is the thermodynamically stable form at temperatures below the transition point and the higher melting form is the thermodynamically stable form at temperatures above the transition point.

For enantiotropic polymorphs, the transition temperature is important since it defines the temperature at which the stability between the two forms becomes inverted. There are several methods currently available to experimentally determine or estimate this value (Hu et al., 2007; Zhang et al., 2002; Urakami et al., 2002; Tong et al., 2001; Gu and Grant, 2001; Wenslow et al., 2000; Carlton et al., 1996; Yu, 1995; Behme and Brooke, 1991; Lagas and Lerk, 1981; Kanke and Sekiguch, 1973).

The manufacture of different polymorphic forms, the determination of the stable modification and the knowledge of monotropy or enantiotropy are the initial studies in pre-formulation work.

Previously, simultaneous Raman spectroscopy and DSC have been used to study the solid state transition mechanisms of ammonium nitrate (Harju et al., 1991; Harju, 1993; Sprunt and Jayasooriya, 1997) and the structural polymorphs of the triglyceride 1,3-

distearoyl-2-oleoylglycerol (Sprunt et al., 2000). However, to date, simultaneous Raman spectroscopy and DSC have not been used in investigations involving drug polymorphs and pharmaceuticals.

In this study, we have utilized both Raman and near IR spectroscopy to characterise and provide molecular structural information about salmeterol xinafoate polymorphs and certain sulfathiazole polymorphs (I and III) and we have monitored preliminarily the solid-state polymorphic conversion of salmeterol xinafoate polymorph I into polymorph II and sulfathiazole polymorph III into I using simultaneous *in situ* portable Raman spectroscopy and DSC to unambiguously characterise the polymorphic form of a sample analysed *in situ*.

### 7.1.1. Salmeterol xinafoate (SX)

Salmeterol or [(RS)-5{1-hydroxy-2-[6-(4-phenylbutoxy)-hexylamino]ethyl}salicyl alcohol (Figure 7.1) is the first of a class of long acting  $\beta$ -adrenergic receptor agonists with both bronchodilator and anti-inflammatory actions. It is prepared as the 1:1 salt of salmeterol and 1-hydroxy-2-naphthoic acid (Martindale, 2005).

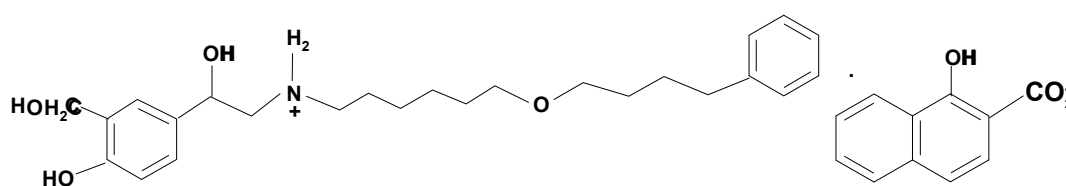


**Figure 7.1. The chemical structure of SX.**

SX is known to exist in two crystalline polymorphic forms with form I being the stable and form II the metastable polymorph under ambient conditions (Beach et al., 1999). These polymorphs have been characterized using differential scanning calorimetry, X-ray powder diffractometry, thermogravimetric analysis and inverse gas

chromatography (Tong et al., 2001; Tong et al., 2003). Commercial SX is a micronized form with the same crystal structure as that of form I. However, the commercial drug can contain traces of the form II polymorph which is formed during the pharmaceutical manufacturing processes.

### 7.1.2. Sulfathiazole (SZ)

The antibiotic drug sulfathiazole (N<sup>1</sup>-2-thiazolylsulfanilamide), Figure 7.2, and its crystalline properties have been extensively described and studied since the 1940s (Apperley et al., 1999). SZ has been identified as a classic four polymorphic system by Burger and Dialer (Burger and Dialer, 1983). The structure of a fifth polymorph has only been recently determined (Hughes et al., 1997; Hughes et al., 1999). A number of different techniques have been used for the physical characterization of these polymorphic forms including thermal analysis, vibrational spectroscopy, X-ray and terahertz pulsed spectroscopy (Zeitler et al., 2006; Lagas and Lerk, 1981; Apperley et al., 1999; Burger and Dialer, 1983; Chan et al., 1999; Anwar et al., 1989; Aaltonen et al., 2003).

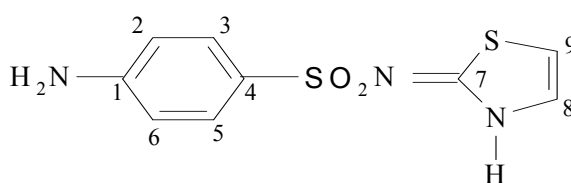


**Figure 7.2. The chemical structure of SZ.**

## 7.2. Experimental

### 7.2.1. Materials

SX polymorph I was obtained from Apin Chemicals Co., the polymorphic form being confirmed by PXRD. SX polymorph II was crystallized as a fine powder using a

Solution Enhanced Dispersion by Supercritical Fluids (Tong et al., 2001). Quantitative conversion from type I to type II polymorphic structures was confirmed by PXRD.

SZ form III was obtained from Alfa Aesar, Lancashire, UK. The polymorphic form was confirmed by PXRD.

### **7.2.2. X- Ray powder diffractometry**

PXRD patterns were recorded for SX and SZ samples with a Bruker D8 diffractometer with Cu-K $\alpha_{1,2}$  radiation (1.5418 Å) and a secondary curved graphite monochromator. The X-ray tube was operated at 40 kV, 30 mA. Samples were scanned in a vertical Bragg-Brentano ( $\theta/2\theta$ ) geometry (flat reflection mode) from 5-40° ( $2\theta$ ) using a 0.005° step width and a 1.5 second count time at each step. The receiving slit was 1° and the scattering slit was 0.2°.

### **7.2.3. Differential scanning calorimetry (DSC)**

DSC profiles of SX and SZ were generated in the range of 0 to 150°C and 50 to 220°C in the case of SX and SZ respectively by the use of TA instruments, DSC Q2000 apparatus using the PCA mode with RSC90 cooling unit. Temperature calibration was performed using indium metal standard supplied with the instrument at the respective heating rate. Accurately weighed samples (1.5 – 2.5 mg) were placed in Tzero aluminium pans using similar empty pans as reference. A scanning speed of 10°C min.<sup>-1</sup> was employed.

#### 7.2.4. Raman Spectroscopy

Raman spectra of both SX and SZ were obtained using a Renishaw portable Raman analyser RX210 ‘Raman-In-A-Suitcase’ (RIAS) equipped with a diode laser emitting at 785 nm and a thermoelectrically cooled CCD detector (see section 2.8.1.2.4 for details).

#### 7.2.5. Near-infrared Spectroscopy

A Bruker Optics *MPA* FT-NIR spectrometer with an integrating sphere and auto-sampler along with a fibre optic powder probe was used for these measurements of both SX and SZ (see section 2.8.2.2 for details).

#### 7.2.6. The simultaneous *in situ* Raman –DSC method

An assembly of the fibre-optic coupled portable Raman spectrometer and DSC instrument was used (Figures 2.10 and 7.3) for the simultaneous *in situ* investigation of the solid-state polymorphic transformation of SX form I to II and SZ form III to I (see section 2.8.5. for details).



**Figure 7.3. DSC head before optical access by the probe.**

## 7.3. Results and discussion

### 7.3.1. Salmeterol xinafoate

#### 7.3.1.1. X- Ray powder diffractometry

The PXRD patterns (Figure 7.4) show significant differences between the diffraction patterns of the two polymorphs which have been used to establish the solid-phase identity of these samples.

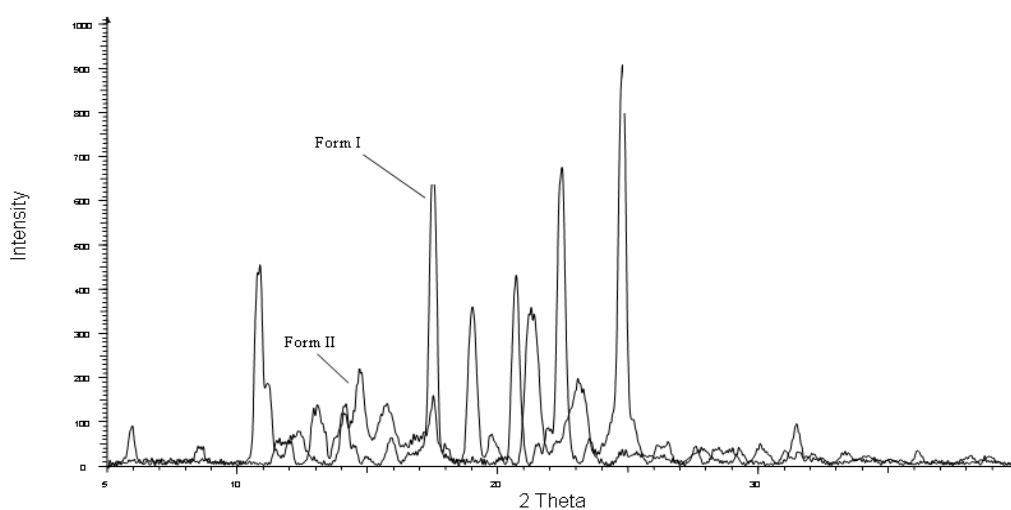


**Figure 7.4. The PXRD patterns of SX polymorphs I&II.**

#### 7.3.1.2. Differential scanning calorimetry

The DSC sample arrangement has been modified to accommodate the fibre-optic probe; it is therefore important to compare the DSC data with and without encapsulation. Figure 7.5 shows that the onset melting points of 124°C for form I and 138°C for form II are very similar for each form and agree well with the previously published data (Beach et al., 1999).

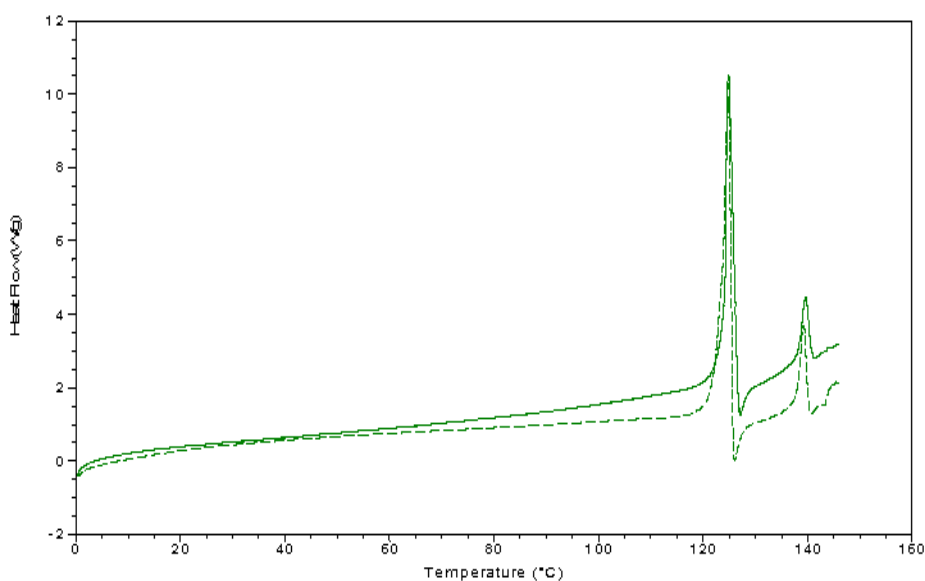


**Figure 7.5. DSC melting curves of SX, (-) for encapsulated and (- -) for unencapsulated specimens.**

### 7.3.1.3. Raman spectroscopy

Different polymorphs of the same molecule each have a different crystalline form and, hence, a unique Raman spectrum (Yu et al., 1998). Analysis of SX polymorphs I & II by Raman spectroscopy yielded spectra with excellent signal to noise ratios, with the two polymorphs exhibiting differences in both peak positions and intensities (see chapter 5 for details).

### 7.3.1.4. Near infrared Spectroscopy

As NIR spectra arise, for the most part, from the overtone bands of fundamental groups containing C-H, O-H and N-H bonds, organic molecules with this functionality can be investigated using this approach. NIR spectroscopy can be an attractive option for the characterisation of the SX polymorphic system because of ease of sampling. The NIR spectra of SX polymorphs are shown in Figure 7.6. The wavelengths and proposed

assignments of the NIR bands are given in Table 7.1. From the NIR spectroscopic analysis carried out in the present work, there are several spectral bands present which can be used for the differentiation between polymorphic forms I and II of SX. The NIR spectral bands at 2393, 2364, 1743 and 1706 nm are characteristic of polymorph I, whereas bands at 2143, 2101, 2065, 1576 and 1501 nm are characteristic of polymorph II. There are several observed peak shifts from 2467, 2416, 2271, 2258, 2212, 2157, 1757, 1723 and 1176 nm of polymorph I to 2460, 2408, 2280, 2265, 2219, 2161, 1752, 1719 and 1181 nm of polymorph II, respectively.

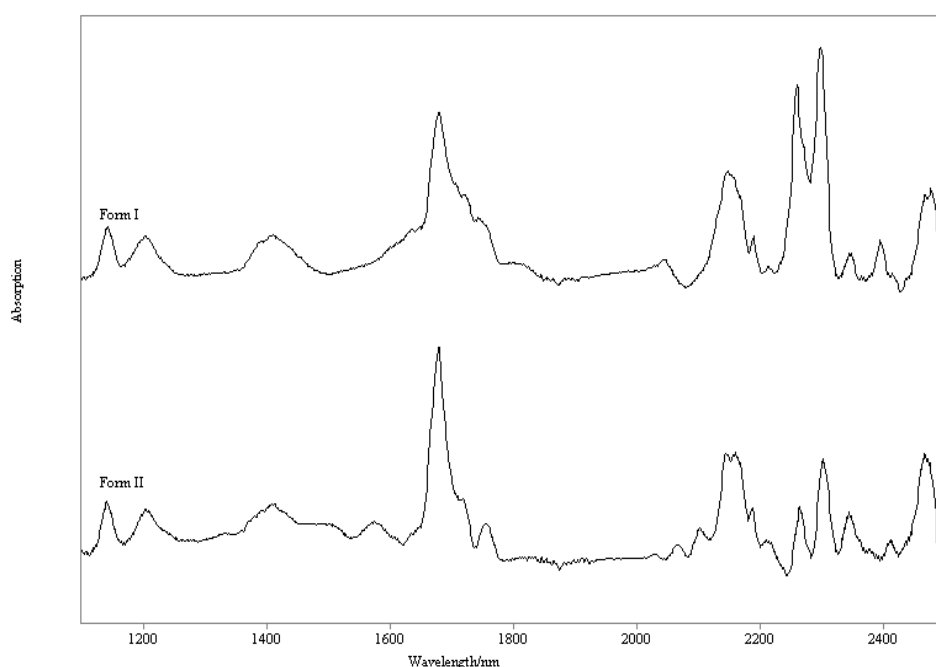


**Figure 7.6. NIR spectra of SX (forms I and II).**

**Table 7.1. NIR spectral wavelengths/nm and proposed assignments for SX polymorphs I&II.**

Form I	Form II	Proposed Assignment
2477 m	2476 m	Combination C-H stretching
2467 m	2460 m	Combination C-H stretching
2416 w,sh	2408 w	Combination C-H stretching
2393 m	-	Combination C-H stretching
2364 w	-	Combination C-H stretching
2345 m	2343 m	Combination C-H stretching
2298 s	2301 s	Combination C-H stretching
2271 m,sh	2280 ms	Combination C-H stretching
2258 ms	2265 vw	Combination C-H stretching
2212 w	2219 vw	Combination C-H stretching
2188 m	2187 mw	Combination N-H stretching, Combination O-H stretching
2157 m	2161 m	Combination N-H stretching, Combination O-H stretching
-	2143 m	Combination N-H stretching, Combination O-H stretching
-	2101 w	Combination N-H stretching, Combination O-H stretching
-	2065 w	Combination N-H stretching, Combination O-H stretching
1757 w	1752 w	First overtone C-H stretching
1743 w	-	First overtone C-H stretching
1723 w	1719 w	First overtone C-H stretching
1706 w,sh	-	First overtone C-H stretching
1679 s	1678 s	First overtone C-H stretching
1646 w	1646 w,sh	
1634 w	1634 w,sh	
-	1576 w,br	
-	1501 w,br	
1408 w,br	1410 w,br	First overtone N-H stretching, first overtone O-H stretching
1389 w,br	1389 w,br	Combination C-H stretching
1199 w,br	1202 w,br	Second overtone CH stretching
1176 mw	1181 mw	Second overtone CH stretching
1142 m	1141 m	Second overtone CH stretching

### 7.3.1.5. The simultaneous *in situ* Raman –DSC method

The DSC melting curves for SX obtained simultaneously with the Raman spectra confirm the identity of each polymorph (Figure 7.5). Therefore, this provides an unambiguous assignment of the Raman spectrum to a certain polymorph.

The polymorphic transformation from form I to form II was monitored *in situ* at the following temperatures 0, 50, 100, 110, 115°C and from 118 to 140°C at 1 degree interval. Typical spectral results are shown in Figures 7.7 and 7.8. Several changes in the collected spectra were observed during the thermal transformation of polymorph I to polymorph II, with the relative intensities and positions of a number of peaks changing. The Raman spectra of polymorph I change systemically with increasing temperature until the steady state is reached; at this stage the crystals are identified as polymorph II. This was verified by X-ray powder diffraction patterns collected on the sample. The detection of the difference can be accounted for in part by the baseline shifts due to the change in shape of the crystals during the conversion, as well from the inherent differences in polymorph I and II noted in the Raman spectral regions defined in Table 5.1.

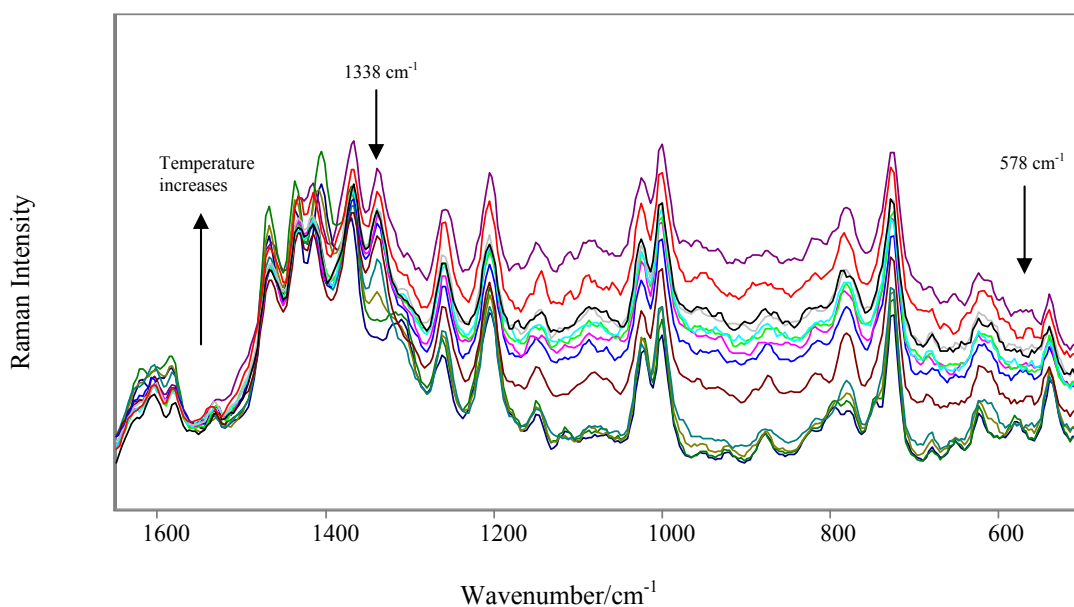


**Figure 7.7.** Typical Raman spectra collected during conversion of SX polymorph I into polymorph II on heating at 115°C then from 118 to 130 °C at 1 degree interval, (500 cm<sup>-1</sup> – 1650 cm<sup>-1</sup>).

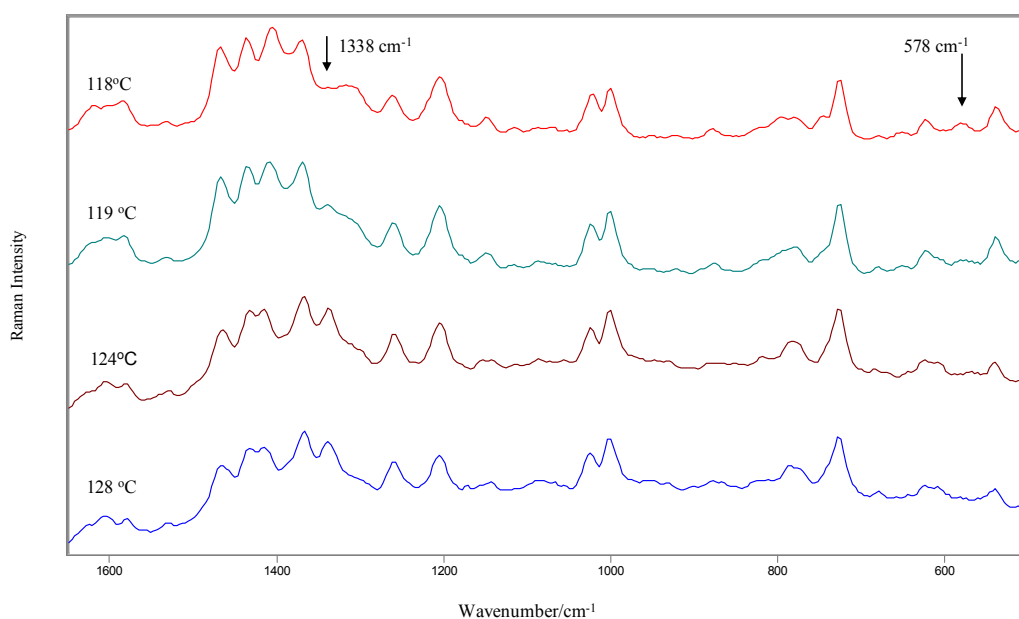


**Figure 7.8. Typical Raman spectra collected during conversion of SX polymorph I into polymorph II on heating at 118, 119, 124 and 128°C.**

The peak areas of in-plane  $\delta$  (CCN) band at  $578\text{ cm}^{-1}$ , characteristic of form I and  $\delta(\text{CH})$  band at  $1338\text{ cm}^{-1}$ , characteristic of form II, (indicated by arrows in Figures 7.7 and 7.8), have been plotted against the temperature degrees (Figure 7.9). Clearly, Raman spectroscopy reveals that the polymorph I is the only form that presents from 0 to  $118^\circ\text{C}$ , when it starts to melt and its characteristic peak at  $578\text{ cm}^{-1}$  starts to disappear, at the same time the  $\delta(\text{CH})$  band characteristic of form II starts to appear at  $119^\circ\text{C}$  and reaches its maximum at  $128^\circ\text{C}$  after the complete melting of form I, then starts to decrease until the complete melting of form II is observed at  $138^\circ\text{C}$ . Therefore, we can deduce that the transition temperature of the polymorphic conversion from form I to form II is  $\sim 119^\circ\text{C}$ .

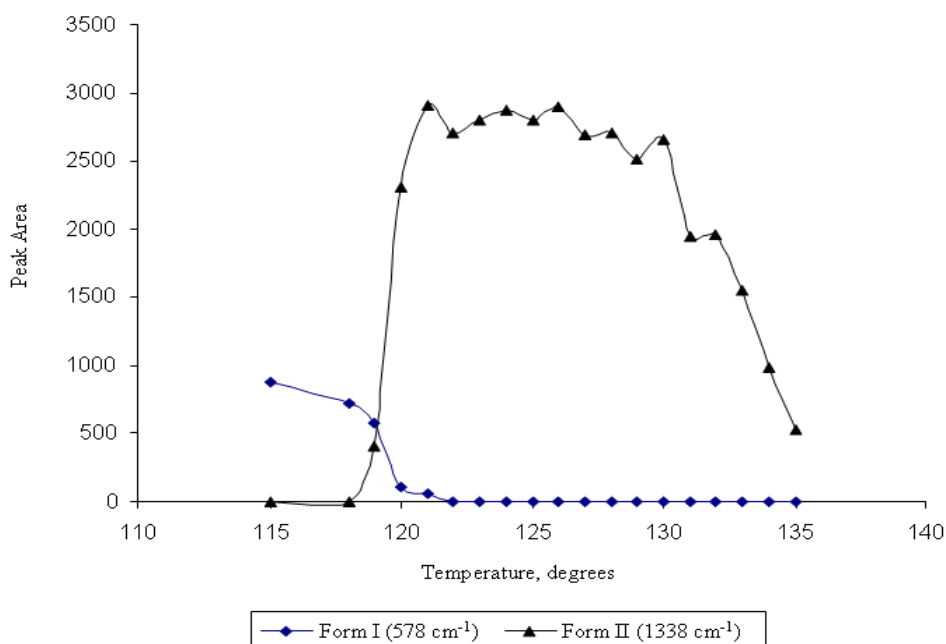


**Figure 7.9. Temperature dependence of the peak areas of SX polymorphs.**

The two polymorphs are related enantiotropically (Tong et al., 2001), the lower melting form (form I) is the thermodynamically stable form at temperatures below the transition point and the higher melting form (form II) is the thermodynamically stable form at temperatures above the transition point (Giron, 1995). The transition temperature of this polymorphic system was previously reported using the van't Hoff solubility-temperature plot as ( $\sim 99^{\circ}\text{C}$ ) (Tong et al., 2001) and estimated from the DSC curve from a vigorously ground form I ( $\sim 109^{\circ}\text{C}$ ) (Tong et al., 2001). This discrepancy in the estimation of the transition temperature from ( $\sim 99^{\circ}\text{C}$ ) to ( $\sim 119^{\circ}\text{C}$ ) is perhaps not surprising, considering the fact that neither technique is free from limitations or drawbacks. The solubility method has both experimental and theoretical constraints while the accuracy of the DSC technique is limited by its dynamic nature and the material-dependent resistance to solid-solid phase transitions at the transition

temperature. However, the combined approach of the current study using both DSC and Raman methods is the ideal complement to thermal analysis for correct interpretation of DSC thermal events. Changes of structure during the heating of the sample, for which no DSC thermal event is detectable, have been demonstrated in this combined DSC and Raman study as shown in Figures 7.7 and 7.8.

### **7.3.2. Sulfathiazole**

#### **7.3.2.1. X-Ray powder diffractometry**

The PXRD pattern (Figure 7.10) of form III has been used to establish the solid-phase identity of the solid sample prior to the Raman/DSC experiments.

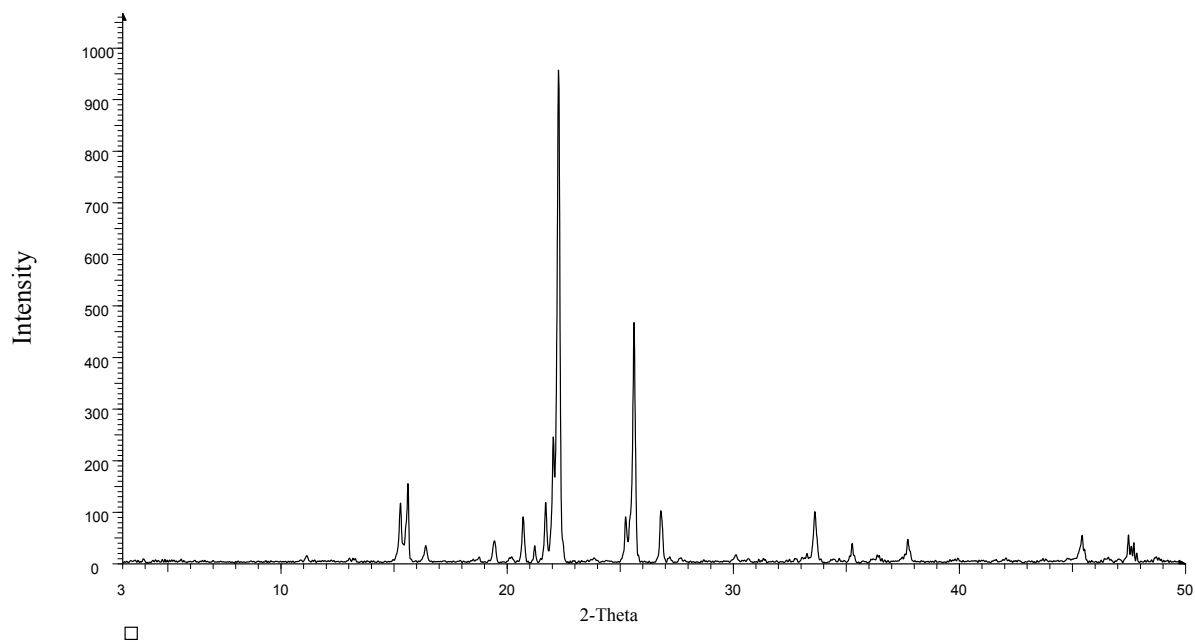


**Figure 7.10. The PXRD pattern of SZ polymorph III.**

### **7.3.2.2. Differential scanning calorimetry**

The onset melting points of 168°C for polymorph III and 202°C for polymorph I of SZ agree well with the previously published data (Anwar et al., 1989; Lagas and Lerk, 1981; Zeitler et al., 2006) (Figure 7.11).

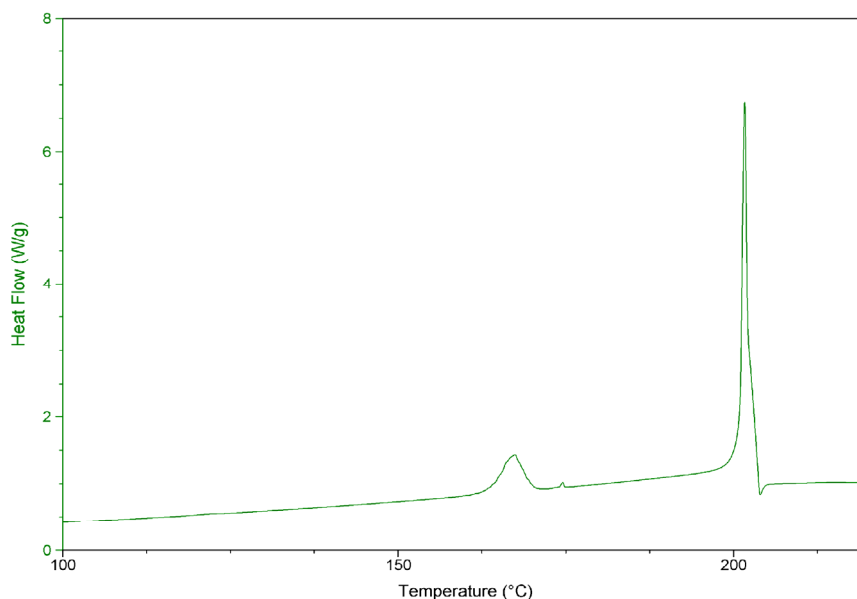


**Figure 7.11. DSC melting curve of SZ, shows the onset melting points of 168°C for polymorph III and 202°C for polymorph I.**

### 7.3.2.3. Raman spectroscopy

The Raman spectra of both polymorphs are shown in Figure 7.12. The wavenumbers and proposed assignments of the Raman bands are given in Table 7.2.

The strongest Raman bands of both polymorphs are the  $\nu$  ( $\text{SO}_2$ ) and ring deformation modes at 1132, 628 and 1128, 629  $\text{cm}^{-1}$  for the polymorphic forms III and I, respectively. Since the ring structure is relatively rigid, only a small shift was observed for the two different polymorphs. Polymorph I has one more strong band assigned to the  $\delta$  ( $\text{NH}_2$ ) mode at 1595  $\text{cm}^{-1}$ .

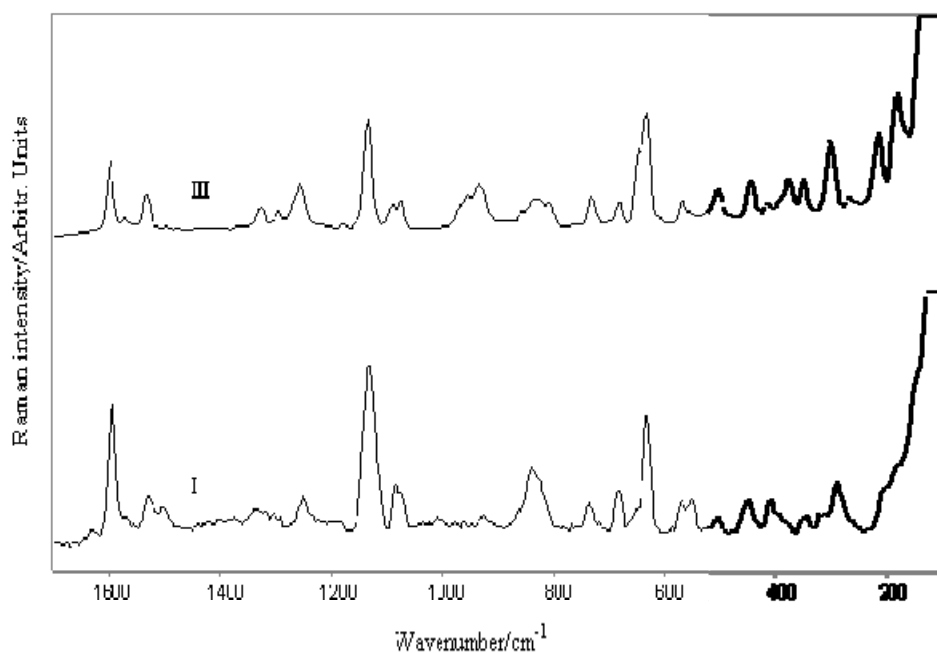


**Figure 7.12. Raman spectra of SZ polymorphs III and I at 785nm.**

Despite the common Raman spectral features (Table 7.2.); both forms under study were found to give rise to distinctive Raman spectral patterns, which allow them to be easily identified through this spectroscopic technique. Polymorph III is characterised by the in-plane  $\delta(\text{CH})_{\text{ring}}$  band at  $1290\text{ cm}^{-1}$ , the  $\delta(\text{CH})$  band at  $1175\text{ cm}^{-1}$ , the out-of-plane  $\delta(\text{CH})_{\text{chain}}$  band at  $934\text{ cm}^{-1}$ , the in-plane  $\delta(\text{CC})_{\text{ring}}$  bands at  $879$  and  $805\text{ cm}^{-1}$  and the out-of-plane (CCC) skeletal deformation band at  $376\text{ cm}^{-1}$ . Polymorph, I, in turn, is readily identified by the  $\delta(\text{NH}_2)$  band at  $1630\text{ cm}^{-1}$ , the  $\nu(\text{C}=\text{N})$  band at  $1499\text{ cm}^{-1}$ , the  $\nu_{\text{as}}(\text{SO}_2)$  band at  $1317\text{ cm}^{-1}$ , the in-plane  $\delta(\text{CC})_{\text{ring}}$  band at  $1007\text{ cm}^{-1}$ , the in-plane  $\delta(\text{CH})_{\text{chain}}$  band at  $976\text{ cm}^{-1}$ , the out-of-plane  $\delta(\text{CH})_{\text{chain}}$  band at  $921\text{ cm}^{-1}$ , the out-of-plane  $\delta(\text{CC})_{\text{ring}}$  band at  $780\text{ cm}^{-1}$  and the in-plane  $\delta(\text{CCC})_{\text{ring}}$  band at  $548\text{ cm}^{-1}$ . These Raman spectral signatures can be attributed to the differences in intermolecular interactions and different modes of packing of the two crystalline polymorphs.

Other features which exhibit the differences in the Raman spectra of the two polymorphic forms are bands shifts and splitting. The  $\nu_{as}(\text{SO}_2)$ , aromatic ring vibration and out-of-plane  $\delta(\text{CH})_{\text{ring}}$  bands are shifted from 1326, 1092 and 829  $\text{cm}^{-1}$  in the spectrum of polymorph III to 1336, 1083 and 837  $\text{cm}^{-1}$  in the spectrum of polymorph I, respectively. On the other hand, the band at 566  $\text{cm}^{-1}$  in the spectrum of polymorph III is split into a doublet whose component bands are  $\sim 19 \text{ cm}^{-1}$  apart in the spectrum of polymorph I; this feature can be attributed to the lowering of symmetry and the decoupling of a degenerate vibrational mode.

The low-frequency modes, arising largely from lattice vibrations, are very sensitive to structural changes in the solid-state. For example, the bands at 301 and 266  $\text{cm}^{-1}$  in the spectrum of polymorph III are not observed in the spectrum of polymorph I, while the bands at 338, 314 and 288  $\text{cm}^{-1}$  in the spectrum of polymorph I are not observed in the spectrum of polymorph III. In addition, the intensity of the skeletal mode band at 213  $\text{cm}^{-1}$  in the spectrum of polymorph III is substantially reduced and shifted to 207  $\text{cm}^{-1}$  in the spectrum of polymorph I. The spectral differences in this region between two polymorphs can be explained by the differences in the intermolecular interactions and differences in crystal symmetry in the two forms.

The present study has allowed the assignment of specific Raman features that are characteristic of each of the polymorphs III and I of SZ investigated.

**Table 7.2. Raman spectral wavenumbers and proposed assignments for SZ polymorphs III&I.**

Polymorph III	Polymorph I	Proposed Assignment
	1630 w	$\delta(\text{NH}_2)$
1596 ms	1595 s	$\delta(\text{NH}_2)$
1569 vw	1570 sh,w	Ring stretch
1531 m	1530 mw	
	1499 w	$\nu(\text{C}=\text{N})$
1326 mw	1336 w	$\nu_{\text{as}}(\text{SO}_2)$
	1317 w	$\nu_{\text{as}}(\text{SO}_2)$
1290 w		In-plane $\delta(\text{CH})_{\text{ring}}$
1254 m	1250 mw	In-plane $\delta(\text{CH})$
1175 vw		$\delta(\text{CH})$
1132 s	1128 s	$\nu(\text{SO}_2)$
1092 mw	1083 mw	Aromatic ring vibration having some $\nu(\text{C}-\text{S})$ character
1070 mw	1072 sh,w	In-plane $\delta(\text{CC})$
	1007 vw	In-plane $\delta(\text{CC})_{\text{ring}}$
	976 vw	In-plane $\delta(\text{CH})_{\text{chain}}$
953 sh,m	959 vw	
934 m		Out-of-plane $\delta(\text{CH})_{\text{chain}}$
	921 w	Out-of-plane $\delta(\text{CH})_{\text{chain}}$
879 vw		In-plane $\delta(\text{CC})_{\text{ring}}$
855 w	861 w	
829 mw	837 m	Out-of-plane $\delta(\text{CH})_{\text{ring}}$
805 mw		In-plane $\delta(\text{CC})_{\text{ring}}$
	780 vw	Out-of-plane $\delta(\text{CC})_{\text{ring}}$
731 m	734 mw	NH wagging
678 mw	682 m	Out-of-plane $\delta(\text{CCC})_{\text{ring}}$
645 sh,ms	644 sh,w	
628 s	629 s	Ring deformation
566 mw	567 mw	
	548 mw	In-plane $\delta(\text{CCC})_{\text{ring}}$
504 mw	503 w	
445 m	448 mw	In-plane $(\text{CCC})_{\text{chain}}$ skeletal deformation
416 w	408 mw	
376 m		Out-of-plane $(\text{CCC})$ skeletal deformation
349 m	353 w	Out-of-plane $(\text{CCC})$ skeletal deformation
	338 w	
	314 w	
301 ms		
	288 m	
266 w		
213 ms	207 w	Skeletal mode
179 m	179 w	

#### 7.3.2.4. Near infrared Spectroscopy

The NIR spectra of both polymorphs over the wavelength range of 1100 to 2500 nm are shown in Figure 7.13. Both spectra appear complex, with more than 40 well-resolved peaks being identified. The wavelengths and proposed assignments of the NIR bands are given in Table 7.3. NIR spectral bands at 2452, 2290, 2225, 2106, 1950, 1928, 1911, 1865, 1644, 1562 and 1324 nm are characteristic of polymorph III, whereas bands at 2394, 2178, 1970, 1767, 1489, 1455, 1304, 1284, 1207 and 1184 nm are characteristic of polymorph I. There are several observed peak shifts from 2460, 2311, 2197, 2141, 2092, 2035, 2013, 1818, 1743 and 1518 nm of polymorph III to 2466, 2332, 2204, 2133, 2084, 2041, 2001, 1824, 1733 and 1524 nm of polymorph I, respectively. From the NIR spectroscopic analysis carried out in the present work, there are several spectral bands present which can be used for the differentiation between polymorphic forms III and I of SZ.

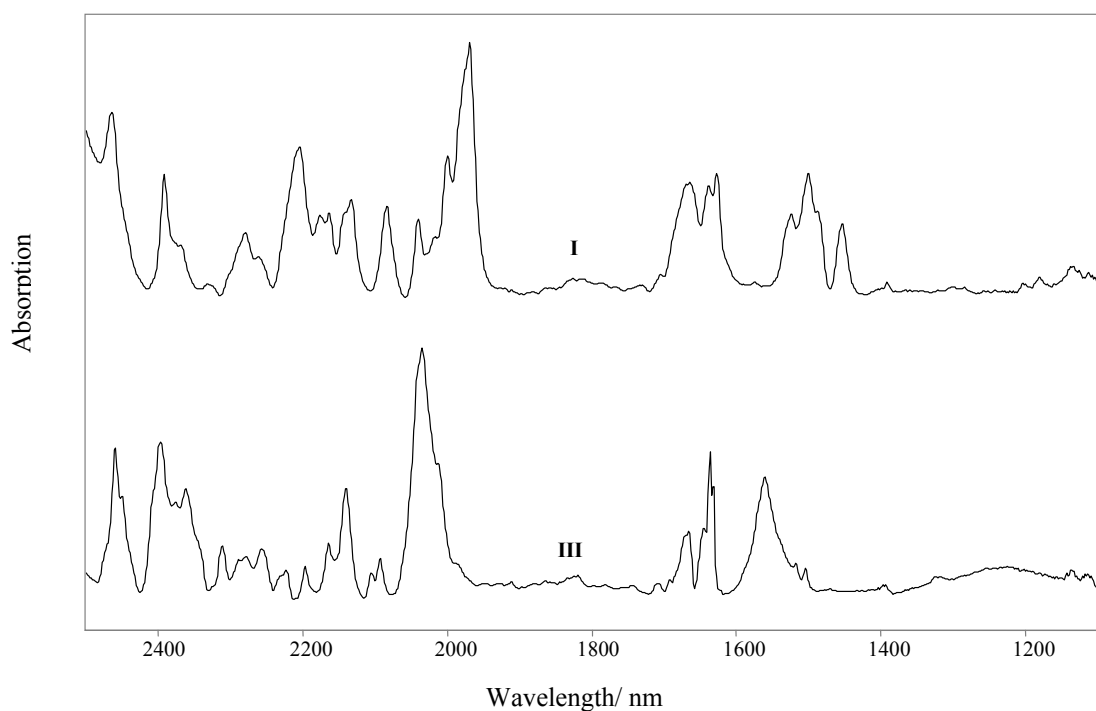


**Figure 7.13. NIR spectra of SZ polymorphs III and I.**

**Table 7.3. NIR spectral wavelengths/nm and proposed assignments for SZ polymorphs III&I.**

Polymorph III	Polymorph I	Proposed Assignment
2460 s	2466 s	Combination C-H stretching
2452 sh,s		Combination C-H stretching
2397 s	2397 s	Combination C-H stretching
	2394 sh,m	
2378 ms		Combination C-H stretching
2364 s		Combination C-H stretching
2311 m	2332 w	Combination C-H stretching
2290 m		Combination C-H stretching
2278 m	2281 ms	Combination C-H stretching
2258 m	2261 m	Combination C-H stretching
2225 mw		Combination C-H stretching
2197 mw	2204 s	Combination N-H stretching, combination O-H stretching
	2178 m	Combination N-H stretching, combination O-H stretching
2165 m	2165 m	Combination N-H stretching, combination O-H stretching
2141 s	2133 ms	Combination N-H stretching, combination O-H stretching
2106 mw		Combination N-H stretching, combination O-H stretching
2092 m	2084 ms	Combination N-H stretching, combination O-H stretching
2035 vs	2041 m	Combination N-H stretching, combination O-H stretching
2013 sh,s	2001 s	Combination N-H stretching, combination O-H stretching
	1970 vs	
1950 vw		
1928 vw		
1911 vw		
1882 vw	1885 vw	
1865 vw		
1818 w	1824 w	
1783 vw	1786 w	First overtone C-H stretching
	1767 vw	First overtone C-H stretching
1743 vw	1733 vw	First overtone C-H stretching
1709 w	1706 w	First overtone C-H stretching
1666 ms	1664 s	First overtone C-H stretching
1644 ms		
1637 s	1641 s	
	1629 s	
1562 s		
1518 mw	1524 s	
1503 mw	1502 s	First overtone N-H stretching, first overtone O-H stretching
	1489 sh,s	First overtone N-H stretching, first overtone O-H stretching
	1455 s	First overtone N-H stretching, first overtone O-H stretching
1395 w	1394 w	Combination C-H stretching
1324 w		Combination C-H stretching
	1304 w	Combination C-H stretching
	1284 w	
	1207 w	Second overtone C-H stretching

**Table 7.3. (Continued)**

Polymorph III	Polymorph I	Proposed Assignment
	1184 w	Second overtone C-H stretching
1135 w	1138 w	Second overtone C-H stretching
1115 w	1113 w	Second overtone C-H stretching

#### 7.3.2.5. The simultaneous *in situ* Raman –DSC method

The polymorphic transformation from form III to form I was monitored *in situ* at the following temperatures 20, 50, 100, 150, 155°C, 160-178°C at 1 degree interval, 180, 185, 190, and 195-205 °C also at 1 degree interval. Typical spectral results are shown in Figures 7.14 and 7.15. Several changes in the collected spectra were observed during the thermal transformation of polymorph III to polymorph I, with observed changes to the relative intensities and positions of a number of peaks. The Raman spectra of polymorph III change systematically with increasing temperature until the steady state is reached; at this stage the crystals are identified as polymorph I. This was verified by X-ray powder diffraction patterns collected from the sample. The detection of the difference depends upon the inherent differences in polymorphs III and I noted in the Raman spectral regions defined in Table 7.2.

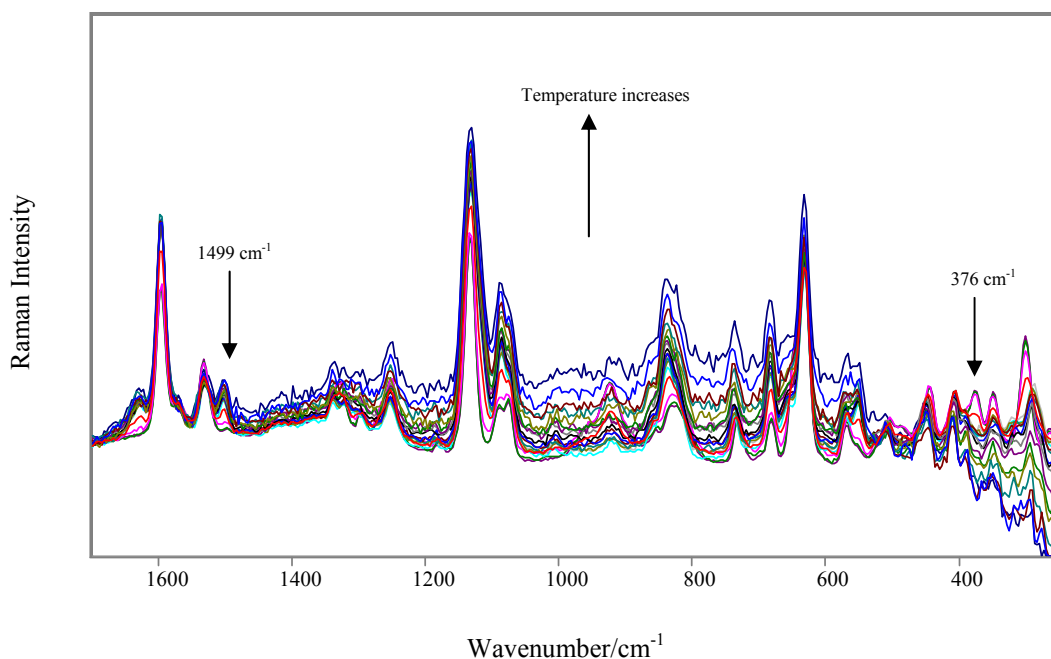


**Figure 7.14.** Typical Raman spectra collected during conversion of SZ polymorph III into polymorph I on heating at 150, 155°C then from 160 to 176 °C at 1 degree interval, (250cm<sup>-1</sup> – 1700 cm<sup>-1</sup>).

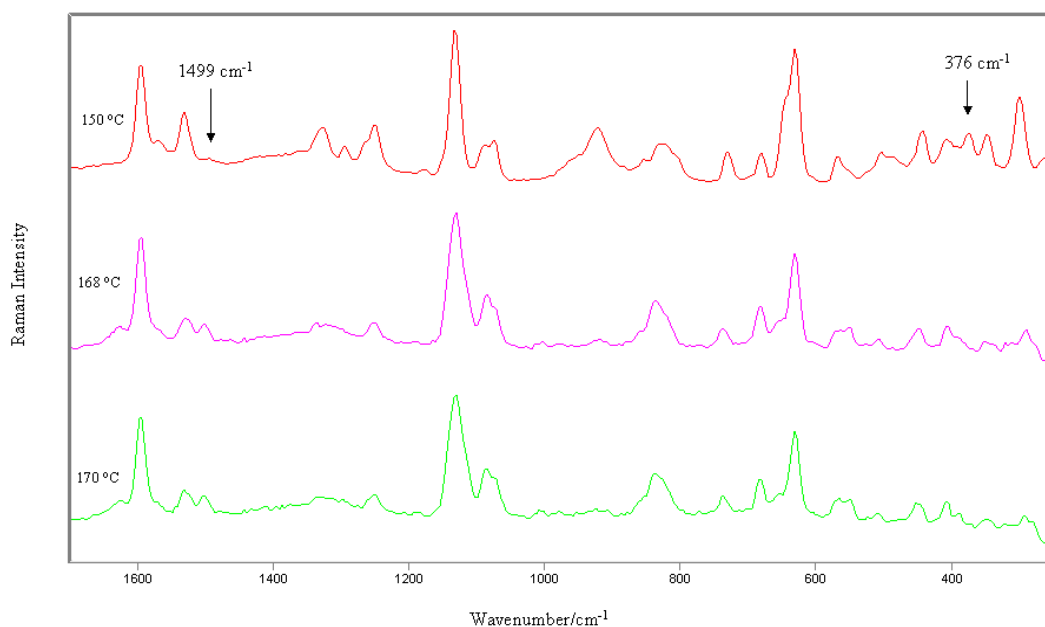


**Figure 7.15.** Typical Raman spectra collected during conversion of SZ polymorph III into polymorph I on heating at 150, 168 and 170°C.

The main differences between the polymorphs of SZ lie in the hydrogen bonding and its effects on the arrangement of the molecules in the crystals (Kruger and Gafner,

1972). Single crystal structures (Kruger and Gafner, 1972) show the hydrogen bonding schemes for SZ polymorphs III and I, imine nitrogen (C7=N) is not involved in the hydrogen bonding of polymorph III but it is in that of polymorph I. The appearance of the band at  $1499\text{ cm}^{-1}$  in polymorph I is attributed to a shift to lower wavenumber (from  $1531\text{ cm}^{-1}$  in polymorph III) of the  $\nu$  (C7=N) bond (Lin-Vien et al., 1991) corresponding with this change in the hydrogen bonding for polymorph I (Figure 7.12).

The peak areas of the out-of-plane (CCC) skeletal deformation band at  $376\text{ cm}^{-1}$ , characteristic of polymorph III and the  $\nu$ (C7=N) band at  $1499\text{ cm}^{-1}$ , characteristic of polymorph I, (indicated by arrows in Figures 7.14 and 7.15), have been plotted against the temperature degrees (Figure 7.16). Clearly, Raman spectroscopy reveals that polymorph III is the only form that presents from 20 to  $150^{\circ}\text{C}$ , when it starts to melt and its characteristic peak at  $376\text{ cm}^{-1}$  starts to disappear; at the same time, the  $\nu$  (C7=N) band characteristic of polymorph I then starts to appear and reaches its maximum at  $170^{\circ}\text{C}$  after the complete melting of polymorph III, then starts to decrease gradually until the complete melting of polymorph I is observed at  $202^{\circ}\text{C}$ . Therefore, we can deduce that the transition temperature of the polymorphic conversion from form III to form I is  $\sim 160^{\circ}\text{C}$ .

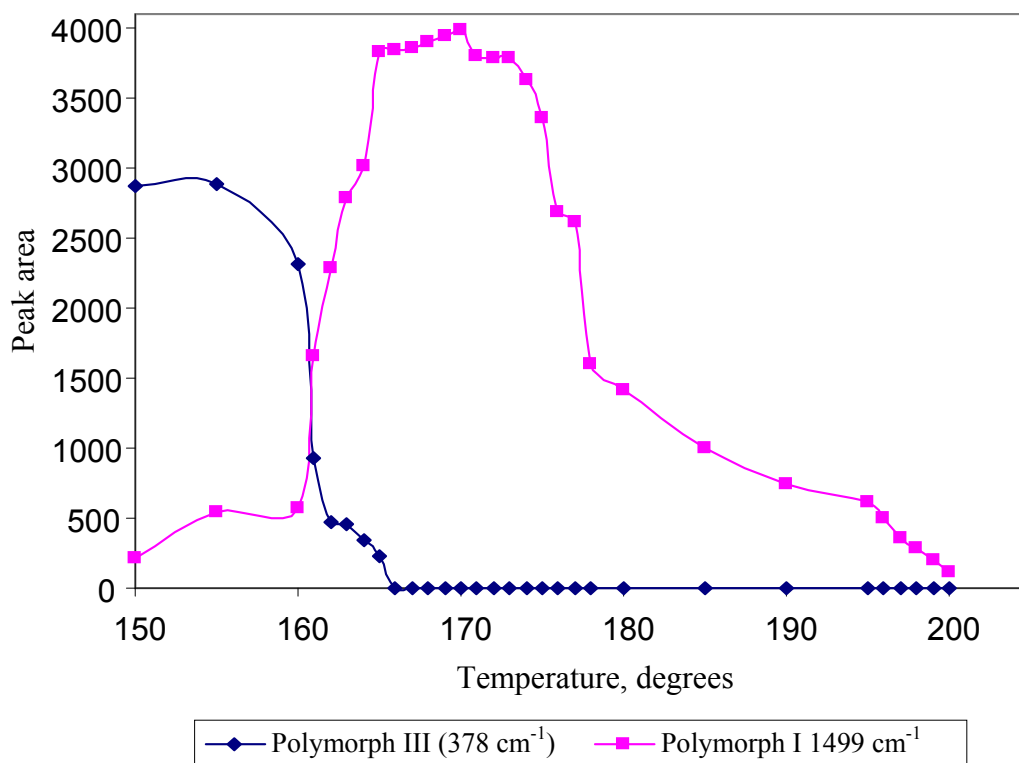


**Figure 7.16. Temperature dependence of the peak areas of SZ polymorphs III and I.**

The two polymorphs are related enantiotropically (Lagas and Lerk, 1981). The transition temperature of polymorph III to I was previously reported using dissolution studies as ( $\sim 103^{\circ}\text{C}$ ) (Lagas and Lerk, 1981) and estimated from the DSC curve as between ( $105\text{-}170^{\circ}\text{C}$ ) (Lagas and Lerk, 1981). Again, this discrepancy in the estimation of the transition temperature from ( $\sim 103^{\circ}\text{C}$ ) to ( $\sim 170^{\circ}\text{C}$ ) is perhaps not surprising as mentioned earlier. However, the combined approach of the current study using both DSC and Raman methods is the ideal complement to thermal analysis alone, so it is possible to obtain a complete picture of the chemical and physical changes occurring in the thermal process of conversion from polymorph III to polymorph I, as shown in Figures 7.14 and 7.15.

#### 7.4. Conclusions

From the Raman and NIR spectroscopic analysis carried out in the present work it is possible to identify the characteristic spectral bands of SX polymorphs (I and II) and SZ polymorphs (III and I). The combination of the two techniques removes ambiguity from the data collected from the two separate techniques. This is due to the complementary nature of the two spectroscopies, which allows for the production of a complete characterisation of the chemical composition of pharmaceutical materials.

At the same time, the methodology described here provides a simple easy-to-use technique for on-line monitoring and determination of the transition temperature when a polymorphic conversion in the solid state is complete. An unambiguous assignment of the SX and SZ spectra to the appropriate form is thus facilitated. This system will also be of utility when there are several phase changes within a wide temperature interval. Use of the fibre-optic probe improves the versatility of the system by allowing conventional DSC analysis. Further use for the method could be demonstrated in other pharmaceutical and polymer research, where samples in some cases are unique, and parallel measurements do not give reliable results. The minimum need for sample preparation in Raman spectroscopy also makes it suitable for measurements where the high purity of the samples is essential.

The advantage of Raman spectroscopy over other analytical techniques lies in its ability to monitor *in situ* the progress of the phase transformation between polymorphs which can allow a better understanding of such transformations and so enabled improved control of processes such as the isolation and drying of crystalline pharmaceutical materials. *In situ* measurements avoid running the reaction separately

from an off-line analytical evaluation and having to transport the reacting samples for analysis, during which samples may undergo further phase transformation. On the basis of the insight provided by Raman spectroscopy coupled with an *in situ* immersion probe and DSC, we are able to efficiently monitor the polymorphic transformation of SX and SZ over a relatively wide range of temperature degrees in the solid state.

Further studies should address the methodology of the quantitative investigation of the polymorphic transformation of SX polymorphs and qualitative and quantitative investigation of the all other known polymorphic forms of SZ using simultaneous *in situ* Raman spectroscopy and DSC. This aspect could be examined using the Raman data of this study.

## 8.1. Conclusions

The main goal of this research project was the evaluation of the potential and suitability of vibrational spectroscopic techniques (Raman, FT-IR and FT-NIR spectroscopy) as tools for the solid-state characterisation of several drugs used in the management of certain respiratory disorders. The Raman spectra of budesonide, terbutaline hemisulphate, ipratropium bromide and salmeterol xinafoate polymorph II were reported for the first time. The results have highlighted the power of these techniques to generate reproducible low noise spectra. However, the spectra produced are complicated for certain drugs owing to their chemical composition. Spectral and structural characteristics are not readily apparent upon simple visual examination. Quantum chemical calculations have been shown to offer the potential to improve understanding of the structural properties of solid-state pharmaceuticals and be a vital aspect of a fundamental spectral assignment approach. In this way it should be possible for quantum chemistry to assist quality control development in the same way that it has facilitated drug discovery for many years. The dependence of the Raman spectra of salmeterol xinafoate polymorphs upon the laser excitation wavelength was highlighted. It has been shown that NIR spectra can be obtained noninvasively and rapidly through USP vials. Pharmaceutical excipients can be readily identified *in situ* by NIR spectroscopy, although several samples from different manufacturers and materials with different physical properties were used. NIR spectroscopy has been shown to be an effective tool for the characterisation and differentiation of salmeterol xinafoate polymorphs and two polymorphic forms of sulfathiazole. The use of simultaneous *in situ* Raman spectroscopy and differential scanning calorimetry for the preliminary investigation of the solid-state polymorphic transformation of certain pharmaceutical systems has been presented, thus providing a new method for the solid-state estimation

of the transition temperature of the enantiotropically related pharmaceutical polymorphs. This methodology represents the first analytical record reported for the simultaneous *in situ* use of portable Raman spectroscopy and differential scanning calorimetry for the investigation of pharmaceutical polymorphic systems.

## **8.2. Further work**

The use of vibrational spectroscopy in conjunction with quantum chemical calculations for the solid-state characterisation of pharmaceuticals has considered a limited number of drugs used in the management of certain respiratory disorders but from different chemical entities, therefore, further work should be carried out to include a larger volume of pharmaceutical compounds from different chemical and pharmacological groups to allow a better understanding of relevant pharmaceutical systems.

The combined approach of the current study using both DSC and Raman methods is the ideal complement to thermal analysis alone for the correct interpretation of the DSC thermal events and provides a simple easy-to-use technique for on-line monitoring and determination of the completion of polymorphic conversion in the solid state. Changes of structure during the heating of the sample, for which no apparent DSC thermal event is detectable, have been demonstrated in this combined DSC and Raman study so it is possible to obtain a complete picture of the chemical and physical changes occurring in the thermal process of conversion of the polymorphic forms of specified drugs. An unambiguous assignment of the drug spectra to the appropriate form is thus facilitated. This system will also be of use for structural studies when there are several phase changes occurring within a wide temperature interval. Further use for the method could be demonstrated in pharmaceutical and polymer research, where samples in some cases

are unique, and parallel measurements do not give reliable results. Current work has only concentrated upon a qualitative polymorphic conversion and in the future, quantitative investigation of the polymorphic conversion should be considered. This approach is recommended for further work regarding pharmaceutical polymorphic systems since it is non-destructive and for which minimal or no sample preparation is required, particularly where maintenance of high sample purity is essential.

- Aaltonen, J., Heinanen, P., Peltonen, L., Kortejarvi, H., Tanninen, V. P., Christiansen, L., Hirvonen, J., Yliruusi, J. & Rantanen, J. (2006) *In situ* measurement of solvent-mediated phase transformations during dissolution testing. *Journal of Pharmaceutical Sciences*, 95, 2730 - 2737.
- Aaltonen, J., Kogermann, K., Strachan, C. J. & Rantanen, J. (2007a) In-line monitoring of solid-state transitions during fluidisation. *Chemical Engineering Science*, 62, 408-415.
- Aaltonen, J., Rantanen, J., Siiriä, S., Karjalainen, M., Jørgensen, A., Laitinen, N., Savolainen, M., Seitavuopio, T. P., Louhi-Kultanen, M. & Yliruusi, J. (2003) Polymorph screening using near-infrared spectroscopy. *Analytical Chemistry*, 75, 5267-5273.
- Aaltonen, J., Strachan, C. J., Pöllänen, K., Yliruusi, J. & Rantanen, J. (2007b) Hyphenated spectroscopy as a polymorph screening tool. *Journal of Pharmaceutical and Biomedical Analysis*, 44, 477-483.
- Agatonovic-Kustrin, S. & Alany, R. (2001) Application of diffuse reflectance infrared Fourier transform spectroscopy combined with artificial neural networks in analysing enantiomeric purity of terbutaline sulphate bulk drug. *Analytica Chimica Acta*, 449, 157-165.
- Aguirre-Mendez, C. R., Rodolfo J. (2007) A Raman spectroscopic method to monitor magnesium stearate in blends and tablets. *Pharmaceutical Technology Europe*, 19, 53 - 61.
- Airaksinen, S., Luukkonen, P., Joergensen, A., Karjalainen, M., Rantanen, J. & Yliruusi, J. (2003) Effects of excipients on hydrate formation in wet masses containing theophylline. *Journal of Pharmaceutical Sciences*, 92, 516-528.
- Akalin, E. & Akyuz, S. (2007) Vibrational structure of free and hydrogen bonded complexes of isoniazid: FT-IR, FT-Raman and DFT study. *Journal of Molecular Structure*, 834, 492-497.
- Al-Zoubi, N., Koundourellis, J. E. & Malamataris, S. (2002) FT-IR and Raman spectroscopic methods for identification and quantitation of orthorhombic and monoclinic paracetamol in powder mixtures. *Journal of Pharmaceutical and Biomedical Analysis*, 29, 459-467.
- Albertsson, J., Oskarsson, A. & Svensson, C. (1978) X-ray study of budesonide: Molecular structures and solid solutions of the (22S) and (22R) epimers of 11 $\beta$ , 21-dihydroxy-16 $\alpha$ , 17 $\alpha$ -propylmethylenedioxy-1, 4-pregnadiene-3, 20-dione. *Acta Crystallographica B* 34, 3027-3036.
- Ali, H. R., Edwards, H. G., Kendrick, J., Munshi, T. & Scowen, I. J. (2007) Vibrational spectroscopic study of budesonide. *Journal of Raman Spectroscopy*, 38, 903 - 908.

- Ali, H. R. H., Edwards, H. G., Kendrick, J. & Scowen, I. J. (2009a) Vibrational spectroscopic study of fluticasone propionate. *Spectrochimica Acta Part A*, 72, 244-277.
- Ali, H. R. H., Edwards, H. G. M., Hargreaves, M. D., Munshi, T., Scowen, I. J. & Telford, R. J. (2008) Vibrational spectroscopic characterisation of salmeterol xinafoate polymorphs and a preliminary investigation of their transformation using simultaneous *in situ* portable Raman spectroscopy and differential scanning calorimetry. *Analytica Chimica Acta*, 620, 103-112.
- Ali, H. R. H., Edwards, H. G. M., Kendrick, J. & Scowen, I. J. (2009b) Vibrational spectroscopic study of salbutamol hemisulfate. *Drug Testing and Analysis*, 1, 51-56.
- Amado, A. M., Fiuza, S. M., Marques, M. P. M. & De Carvalho, L. (2007a) Conformational and vibrational study of platinum (II) anticancer drugs: cis-diamminedichloroplatinum (II) as a case study. *Journal of Chemical Physics*, 127, 185104 - 185113.
- Amado, A. M., Nolasco, M. M. & Ribeiro-Claro, P. J. (2007b) Probing pseudopolymorphic transitions in pharmaceutical solids using Raman spectroscopy: hydration and dehydration of theophylline. *Journal of Pharmaceutical Sciences*, 96, 1366 - 1379.
- Andrew, J. J., Browne, M. A., Clark, I. E., Hancewicz, T. M. & Millichope, A. J. (1998) Raman imaging of emulsion systems. *Applied Spectroscopy*, 52, 790 - 796.
- Angel, S. M., Carter, J. C., Stratis, D. N., Marquardt, B. J. & Brewer, W. E. (1999) Some new uses for filtered fiber-optic Raman probes: *in situ* drug identification and *in situ* and remote Raman imaging. *Journal of Raman Spectroscopy*, 30, 795-805.
- Anquetil, P. A., Brenan, C. J. H., Marcolli, C. & Hunter, I. W. (2003) Laser Raman spectroscopic analysis of polymorphic forms in microliter fluid volumes. *Journal of Pharmaceutical Sciences*, 92, 149-160.
- Anwar, J., Tarling, S. E. & Barnes, P. (1989) Polymorphism of sulfathiazole. *Journal of Pharmaceutical Sciences*, 78, 337-342.
- Apperley, D. C., Fletton, R. A., Harris, R. K., Lancaster, R. W., Tavener, S. & Threlfall, T. L. (1999) Sulfathiazole polymorphism studied by magic-angle spinning NMR. *Journal of Pharmaceutical Sciences*, 88, 1275-1280.
- Asher, S. A. & Johnson, C. R. (1984) Raman spectroscopy of a coal liquid shows that fluorescence interference is minimized with ultraviolet excitation. *Science*, 225, 311-313.
- Atha, D. H., Coxon, B., Reipa, V. & Gaigalas, A. K. (1995) Physicochemical characterization of low molecular weight heparin. *Journal of Pharmaceutical Sciences*, 84, 360-364.

- Atha, D. H., Gaigalas, A. K. & Reipa, V. (1996) Structural analysis of heparin by Raman spectroscopy. *Journal of Pharmaceutical Sciences*, 85, 52-56.
- Auer, M. E., Griesser, U. J. & Sawatzki, J. (2003) Qualitative and quantitative study of polymorphic forms in drug formulations by near infrared FT-Raman spectroscopy. *Journal of Molecular Structure*, 661, 307-317.
- Ayala, A. P. (2007) Polymorphism in drugs investigated by low wavenumber Raman scattering. *Vibrational Spectroscopy*, 45, 112-116.
- Ayala, A. P., Siesler, H. W., Wardell, S., Boechat, N., Dabbene, V. & Cuffini, S. L. (2007) Vibrational spectra and quantum mechanical calculations of antiretroviral drugs: nevirapine. *Journal of Molecular Structure*, 828, 201-210.
- Baias, M. P., A.; Chis, V.; Cozar, O.; Vasilescu, M. (2006) Experimental and theoretical investigation of 5-para-fluoro-benzilidene-thiazolidine-2-thione-4-one. *Journal of Optoelectronics and Advanced Materials*, 8, 205-207.
- Bailey, L., Navarro, R. & Hernanz, A. (1999) Vibrational study of 5-iodo-2'-deoxyuridine, IDU. *Journal of Molecular Structure*, 480, 465-469.
- Bain, B. M., Harrison, G., Jenkins, K. D., Pateman, A. J. & Shenoy, E. V. (1993) A sensitive radioimmunoassay, incorporating solid-phase extraction, for fluticasone 17-propionate in plasma. *Journal of Pharmaceutical and Biomedical Analysis*, 11, 557- 561.
- Bandi, N., Wei, W., Roberts, C. B., Kotra, L. P. & Kompella, U. B. (2004) Preparation of budesonide–and indomethacin–hydroxypropyl-β-cyclodextrin (HPBCD) complexes using a single-step, organic-solvent-free supercritical fluid process. *European Journal of Pharmaceutical Sciences*, 23, 159-168.
- Banwell, C. N. (1972) *Fundamentals of Molecular Spectroscopy*, London, McGraw-Hill Book Company.
- Baran, E. J. D. M., Domenico (1993) Vibrational spectrum and thermal behaviour of (NH<sub>4</sub>)<sub>17</sub>Na[NaW<sub>21</sub>Sb<sub>9</sub>O<sub>86</sub>].28H<sub>2</sub>O (HP-23); a promising drug drug in AIDS therapy. *Acta Farmaceutica Bonaerense*, 12, 29 - 34.
- Baranska, M. & Proniewicz, L. M. (1999) FT-IR and FT-Raman spectra of cimetidine and its metal complexes. *Journal of Molecular Structure*, 511, 153-162.
- Barbas, R., Martí, F., Prohens, R. & Puigjaner, C. (2006) Polymorphism of norfloxacin: evidence of the enantiotropic relationship between polymorphs A and B. *Crystal Growth & Design*, 6, 1463-1467.
- Basavoju, S., Boström, D. & Velaga, S. P. (2006) Pharmaceutical cocrystal and salts of norfloxacin. *Crystal Growth & Design*, 6, 2699-2708.

- Basavoju, S., Boström, D. & Velaga, S. P. (2008) Indomethacin–saccharin cocrystal: design, synthesis and preliminary pharmaceutical characterization. *Pharmaceutical Research*, 25, 530-541.
- Bass, V. C. (1978a) Identification of benzodiazepens by Raman spectroscopy. *Journal of Forensic Sciences*, 23, 311 - 318.
- Bass, V. C. (1978b) The identification of sympathomimetic amines by Raman spectroscopy. *Forensic Science*, 11, 57 - 65.
- Beach, S., Latham, D., Sidgwick, C., Hanna, M. & York, P. (1999) Control of the physical form of salmeterol xinafoate. *Organic Process Research and Development*, 3, 370-376.
- Becke, A. D. (1988) Density-functional exchange-energy approximation with correct asymptotic behavior. *Physical Review A*, 38, 3098-3100.
- Beckenkamp, K., Ohm, M., Molt, K. & Mandal, O. (2001) The challenge of identity testing; the reliable control of production processes through the combined use of NIR/Raman-and x-ray fluorescence spectrometry. *European Pharmaceutical Review*, 4, 28-33.
- Beckstead, H. D., Neville, G. A. & Shurvell, H. F. (1993) Differentiation of solvated spironolactone samples by FT-Raman and FT-IR diffuse reflectance spectroscopy. *Analytical and Bioanalytical Chemistry*, 345, 727-732.
- Behme, R. J. & Brooke, D. (1991) Heat of fusion measurement of a low melting polymorph of carbamazepine that undergoes multiple-phase changes during differential scanning calorimetry analysis. *Journal of Pharmaceutical Sciences*, 80, 986-990.
- Bell, S. E. J., Gowen, A. A., O'donnell, C. P. & Cullen, P. J. (2008) Recent applications of chemical imaging to pharmaceutical process monitoring and quality control. *European Journal of Pharmaceutics and Biopharmaceutics*, 69, 10-22.
- Bell, S. E. J., Walker, G., Vann, M., Jones, D. S. & Andrews, G. (2007) Fluidised bed characterisation using Raman spectroscopy: Applications to pharmaceutical processing. *Chemical Engineering Science*, 62, 3832-3838.
- Bellows, J. C., Chen, F. P. & Prasad, P. N. (1977) Determination of drug polymorphs by laser Raman spectroscopy. I. ampicillin and griseofulvin. *Drug Development and Industrial Pharmacy*, 3, 451-458.
- Belu, A., Mahoney, C. & Wormuth, K. (2008) Chemical imaging of drug eluting coatings: combining surface analysis and confocal Raman microscopy. *Journal of Controlled Release*, 126, 111-121.
- Berlman, I. B. (1971) Handbook of fluorescence spectra of aromatic molecules. Academic Press, New York.

- Bertoluzza, A., Fagnano, C., Monti, P., Caramazza, R. & Cellini, M. (1986) Raman spectra of the human lens in relation to pathology and the anticataract effect of drugs. *Journal of Raman Spectroscopy*, 17, 133-137.
- Binoy, J., Abraham, J. P., Joe, I. H., Jayakumar, V. S., Pettit, G. R. & Nielsen, O. F. (2004) NIR-FT Raman and FT-IR spectral studies and ab initio calculations of the anti-cancer drug combretastatin-A4. *Journal of Raman Spectroscopy*, 35, 939-946.
- Blanco, M., Coello, J., Eustaquio, A., Iturriaga, H. & MasPOCH, S. (1999) Development and validation of a method for the analysis of a pharmaceutical preparation by near-infrared diffuse reflectance spectroscopy. *Journal of Pharmaceutical Sciences*, 88, 551-556.
- Boddapati, S., Butler, L. D., Im, S. & Deluca, P. P. (1980) Identification of subvisible crystals of barium sulfate in parenteral solutions. *Journal of Pharmaceutical Sciences*, 69, 608-611.
- Bolton, B. A. & Prasad, P. N. (1981) Laser Raman investigation of pharmaceutical solids: griseofulvin and its solvates. *Journal of Pharmaceutical Sciences*, 70, 789-93.
- Bolton, B. A. & Prasad, P. N. (1984) Laser Raman investigation of drug polymer conjugates-sulfathiazole povidone coprecipitates. *Journal of Pharmaceutical Sciences*, 73, 1849-1851.
- Bondesson, L., Mikkelsen, K. V., Luo, Y., Garberg, P. & Lgren, H. (2007) Hydrogen bonding effects on infrared and Raman spectra of drug molecules. *Spectrochimica Acta Part A*, 66, 213-224.
- Bouchaour, T. (1986) Laser Raman studies of interactions between antimicrotubular agents and cysteine. *Journal of Molecular Structure*, 143, 419-422.
- Brattsand, R., Thalen, A., Roempke, K., Kallstrom, L. & Gruvstad, E. (1982) Influence of 16a, 17a-acetal substitution and steroid nucleus fluorination on the topical to systemic activity ratio of glucocorticoids. *Journal of Steroid Biochemistry*, 16, 779-786.
- Breitenbach, J., Schrof, W. & Neumann, J. (1999) Confocal Raman-spectroscopy: analytical approach to solid dispersions and mapping of drugs. *Pharmaceutical Research*, 16, 1109-1113.
- Brody, R. H. (2000) Applications of FT-Raman Spectroscopy to Biomaterials. . *Chemical and Forensic Sciences*. Bradford, Bradford.
- Broman, E., Khoo, C. & Taylor, L. S. (2001) A comparison of alternative polymer excipients and processing methods for making solid dispersions of a poorly water soluble drug. *International Journal of Pharmaceutics*, 222, 139-151.

- Bugay, D. E., Henck, J.-O., Longmire, M. L. & Thorley, F. C. (2007) Raman Analysis of Pharmaceuticals. IN Pivonka, D. E., Chalmers, J. M. & Griffiths, P. R. (Eds.) *Applications of Vibrational Spectroscopy in Pharmaceutical Research and Development*. West Lafayette, USA.
- Bugay, D. E. & Smith, P. A. M. (2004) Raman Spectroscopy IN A. C. Moffat, Osselton, M. D. & Widdop, B. (Eds.) *Clarke's Analysis of Drugs and Poisons*. London, Pharmaceutical Press.
- Burger, A. & Dialer, R. D. (1983) New investigational results of sulfathiazole polymorphism. *Acta Helvetica*, 58, 72-78.
- Burger, A., Henck, J., Hetz, S., Rollinger, J. M., Weissnicht, A. A. & Stottner, H. (2000) Energy/temperature diagram and compression behavior of the polymorphs of D-mannitol. *Journal of Pharmaceutical Sciences*, 89, 457-468.
- Burneau, A. & Carteret, C. (2000) Near infrared and ab initio study of the vibrational modes of isolated silanol on silica. *Physical Chemistry Chemical Physics*, 2, 3217-3226.
- Butler, C. A. & Cooney, R. P. (1993) Normal coordinate analysis and MNDO calculations: assignment of the vibrational spectrum of acridine. *Journal of Raman Spectroscopy*, 24, 199-205.
- Campbell Roberts, S. N., Williams, A. C., Grimsey, I. M. & Booth, S. W. (2002) Quantitative analysis of mannitol polymorphs. FT-Raman spectroscopy. *Journal of Pharmaceutical and Biomedical Analysis*, 28, 1135-1147.
- Carlton, R. A., Difeo, T. J., Powner, T. H., Santos, I. & Thompson, M. D. (1996) Preparation and characterization of polymorphs for an LTD 4 antagonist, RG 12525. *Journal of Pharmaceutical Sciences*, 85, 461-467.
- Caspers, P. J., Lucassen, G. W., Wolthuis, R., Bruining, H. A. & Puppels, G. J. (1998) In vitro and in vivo Raman spectroscopy of human skin. *Biospectroscopy*, 4, 31-40.
- Chalmers, J. M. & Dent, G. (2006) Vibrational spectroscopic methods in pharmaceutical solid-state characterization. *Polymorphism*, 95-138.
- Chalus, P., Roggo, Y., Walter, S. & Ulmschneider, M. (2005) Near-infrared determination of active substance content in intact low-dosage tablets. *Talanta*, 66, 1294-1302.
- Chan, F. C., Anwar, J., Cernik, R., Barnes, P. & Wilson, R. M. H. (1999) Ab initio structure determination of sulfathiazole polymorph V from synchrotron X-ray powder diffraction data. *Journal of Applied Crystallography* 32, 436-441.
- Chan, K. L. A., Fleming, O. S., Kazarian, S. G., Vassou, D., Chryssikos, G. D. & Gionis, V. (2004) Polymorphism and devitrification of nifedipine under

- controlled humidity: a combined FT-Raman, IR and Raman microscopic investigation. *Journal of Raman Spectroscopy*, 35, 353-359.
- Chase, D. B. & Rabolt, J. F. (1994) *Fourier Transform Raman Spectroscopy: From Concept to Experiment*, Boston, Academic Press.
- Cheung, E. Y., Harris, K. D. M., Johnston, R. L., Hadden, K. L. & Zakrzewski, M. (2003) Polymorphism of a novel sodium ion channel blocker. *Journal of Pharmaceutical Sciences*, 92, 2017-2026.
- Choi, S. H., Kim, S. Y., Ryoo, J. J. & Lee, K. P. (2001) Complexation of the non-steroidal anti-inflammatory drug loxoprofen with modified and unmodified  $\beta$ -cyclodextrins. *Journal of Inclusion Phenomena and Macrocyclic Chemistry*, 40, 139-146.
- Choi, Y. & Lubman, D. M. (1992) Analytical spectroscopy and structure of biomolecules using an ab initio computational method. *Analytical Chemistry*, 64, 2726-2734.
- Chrit, L., Bastien, P., Sockalingum, G. D., Batisse, D., Leroy, F., Manfait, M. & Hadjur, C. (2006) An in vivo randomized study of human skin moisturization by a new confocal Raman fiber-optic microprobe: assessment of a glycerol-based hydration cream. *Skin Pharmacology and Applied Skin Physiology*, 19, 207-215.
- Cimpoi, C., Casoni, D., Hosu, A., Miclaus, V., Hodisan, T. & Damian, G. (2005) Separation and identification of eight hydrophilic vitamins using a new TLC method and Raman spectroscopy. *Journal of Liquid Chromatography & Related Technologies*, 28, 2551-2559.
- Cinta-Pinzaru, S., Peica, N., Kustner, B., Schlucker, S., Schmitt, M., Frosch, T., Faber, J. H., Bringmann, G. & Popp, J. (2006) FT-Raman and NIR-SERS characterization of the antimalarial drugs chloroquine and mefloquine and their interaction with hematin. *Journal of Raman Spectroscopy*, 37, 326-334.
- Cipriani, P. & Smith, C. Y. (2008) Characterization of thalidomide using Raman spectroscopy. *Spectrochimica Acta Part A*, 69, 333-337.
- Clarke, F. C., Jamieson, M. J., Clark, D. A., Hammond, S. V., Jee, R. D. & Moffat, A. C. (2001a) Chemical image fusion. The synergy of FT-NIR and Raman mapping microscopy to enable a more complete visualization of pharmaceutical formulations. *Analytical Chemistry*, 73, 2213-2220.
- Clarke, F. C., Jamieson, M. J., Clark, D. A., Hammond, S. V., Jee, R. D. & Moffat, A. C. (2001b) Correction-Chemical image fusion. The synergy of FT-NIR and Raman mapping microscopy to enable a more complete visualization of pharmaceutical formulations. *Analytical Chemistry*, 73, 2369.
- Clarkson, P. M. & Thompson, H. S. (1997) Drugs and sport. Research findings and limitations. *Sports Medicine*, 24, 366-384.

- Colline, A., Bolard, J., Chinsky, L., Fang, J. & Rinehart, K. L. J. (1985) Raman spectra of nystatin influence of impurities. *The Journal of Antibiotics*, 38, 181-185.
- Colthup, N. B., Daly, L. H. & Wiberley, S. E. (1975) *Introduction to Infrared and Raman Spectroscopy*, Academic Press New York.
- Compton, D. A. C. & Compton, S. V. (1991) Examination of packaged consumer goods by using FT-Raman spectrometry. *Applied Spectroscopy*, 45, 1587-1589.
- Corrigan, D. O., Corrigan, O. I. & Healy, A. M. (2006) Physicochemical and in vitro deposition properties of salbutamol sulphate/ipratropium bromide and salbutamol sulphate/excipient spray dried mixtures for use in dry powder inhalers. *International Journal of Pharmaceutics*, 322, 22-30.
- Cozar, O., Chis, V., David, L. & Baias, M. (2006) Experimental and density functional theory investigation of some biomedical compounds. *Journal of Optoelectronics and Advanced Materials*, 8, 164 - 171.
- Cuffini, S. L., Ellena, J. F., Mascarenhas, Y. P., Ayala, A. P., Sielser, H. W., Filho, J. M., Monti, G. A., Aiassa, V. & Sperandeo, N. R. (2007) Physicochemical characterization of deflazacort: thermal analysis, crystallographic and spectroscopic study. *Steroids*, 72, 261-269.
- Curin, A. (1997) Study of crystal modifications of lansoprazole using FT-IR spectroscopy, solid-state NMR Spectroscopy and FT-Raman spectroscopy. *Farmaceutski Vestnik*, 48, 290-291.
- Cutmore, E. & Skett, P. W. (1993) Application of Fourier transform Raman spectroscopy to a range of compounds of pharmaceutical interest. *Spectrochimica Acta. Part A*, 49, 809-818.
- D'cunha, R. (1983) Raman and IR studies of the antileprotic drug dapsone. *Spectrochimica Acta Part A*, 39, 331-336.
- Dalton, C. R., Clas, S., Singh, J., Khougaz, K. & Bilbeisi, R. (2006) Investigating the hydrate conversion propensity of different etoricoxib lots. *Journal of Pharmaceutical Sciences*, 95, 56 - 69.
- Davies, M. C., Binns, J. S., Melia, C. D., Hendra, P. J., Bourgeois, D., Church, S. P. & Stephenson, P. J. (1990) FT Raman spectroscopy of drugs in polymers. *International Journal of Pharmaceutics*, 66, 223-232.
- Day, J. S. (2002) Studies of Controlled Substances and the Enhancement of Fingerprint. *Department of Chemical and Forensic Sciences*. Bradford, Bradford.
- De Beer, T. R. M., Baeyens, W. R. G., Heyden, Y. V., Remon, J. P., Vervaet, C. & Verpoort, F. (2007a) Influence of particle size on the quantitative determination of salicylic acid in a pharmaceutical ointment using FT-Raman spectroscopy. *European Journal of Pharmaceutical Sciences*, 30, 229-235.

- De Beer, T. R. M., Baeyens, W. R. G., Ouyang, J., Vervaet, C. & Remon, J. P. (2006) Raman spectroscopy as a process analytical technology tool for the understanding and the quantitative in-line monitoring of the homogenization process of a pharmaceutical suspension. *Analyst*, 131, 1137-1144.
- De Beer, T. R. M., Baeyens, W. R. G., Vermeire, A., Broes, D., Remon, J. P. & Vervaet, C. (2007b) Raman spectroscopic method for the determination of medroxyprogesterone acetate in a pharmaceutical suspension: validation of quantifying abilities, uncertainty assessment and comparison with the high performance liquid chromatography reference method. *Analytica Chimica Acta*, 589, 192-199.
- De Beer, T. R. M., Vergote, G. J., Baeyens, W. R. G., Remon, J. P., Vervaet, C. & Verpoort, F. (2004) Development and validation of a direct, non-destructive quantitative method for medroxyprogesterone acetate in a pharmaceutical suspension using FT-Raman spectroscopy. *European Journal of Pharmaceutical Sciences*, 23, 355-362.
- De Carvalho, L. A., Marques, M. P. & Tomkinson, J. (2006) Drug-excipient interactions in ketoprofen: A vibrational spectroscopy study. *Biopolymers*, 82, 420 - 424.
- De Faria, D. & Santos, P. S. (1991) Primaquine diphosphate and its cation radical: a spectrochemical investigation. *Spectrochimica Acta Part A*, 47, 1653-1660.
- De Spiegeleer, B., Baert, B., Diericx, N., Seghers, D., Verpoort, F., Van Vooren, L., Burvenich, C. & Slegers, G. (2007) Assessment of the solid-state composition of an active salicylanilide compound by FT-Raman spectroscopy. *Journal of Pharmaceutical and Biomedical Analysis*, 44, 254-257.
- De Spiegeleer, B., Seghers, D., Wieme, R., Schaubroeck, J., Verpoort, F., Slegers, G. & Van Vooren, L. (2005) Determination of the relative amounts of three crystal forms of a benzimidazole drug in complex finished formulations by FT-Raman spectroscopy. *Journal of Pharmaceutical and Biomedical Analysis*, 39, 275-280.
- De Veij, M., Deneckere, A., Vandenabeele, P., De Kaste, D. & Moens, L. (2008) Detection of counterfeit Viagra® with Raman spectroscopy. *Journal of Pharmaceutical and Biomedical Analysis*, 46, 303-309.
- De Veij, M., Vandenabeele, P., Hall, K. A., Fernandez, F. M., Green, M. D., White, N. J., Dondorp, A. M., Newton, P. N. & Moens, L. (2007) Fast detection and identification of counterfeit antimalarial tablets by Raman spectroscopy. *Journal of Raman Spectroscopy*, 38, 181-187.
- Deeley, C. M. S., R. A.; Threlfall, T. L. (1991) A comparison of Fourier transform infrared and near-infrared Fourier transform Raman spectroscopy for quantitative measurements: an application in polymorphism. *Spectrochimica Acta Part A*, 47 1217 - 1223.

- Deisingh, A. K. (2005) Pharmaceutical counterfeiting. *Analyst*, 130, 271-279.
- Delhaye, M., Barbillat, J., Aubard, J., Bridoux, M. & Da Silva, E. (1996) Raman Microscopy: Developments and Applications IN Corset, T. G. (Ed.) London, Academic Press.
- Dennis, A. C., Mcgarvey, J. J., Woolfson, A. D., Mccafferty, D. F. & Moss, G. P. (2004) A Raman spectroscopic investigation of bioadhesive tetracaine local anaesthetic formulations. *International Journal of Pharmaceutics*, 279, 43-50.
- Docoslis, A., Huszarik, K. L., Papageorgiou, G. Z., Bikiaris, D., Stergiou, A. & Georgarakis, E. (2007) Characterization of the distribution, polymorphism, and stability of nimodipine in its solid dispersions in polyethylene glycol by micro-Raman spectroscopy and powder X-ray diffraction. *The AAPS Journal*, 9, E361-70.
- Drake, A. (2004) Infra-red Spectroscopy. IN A. C. Moffat, M. D. O. & Widdop, B. (Eds.) *Clarke's Analysis of Drugs and Poisons*. London, Pharmaceutical Press.
- Durig, J. R., Zheng, C., Williams, M. J., Stidham, H. D. & Guirgis, G. A. (2004) Conformational stability from variable temperature infrared spectra of krypton solutions, ab initio calculations, vibrational assignment, and structural parameters of 1, 3-difluoropropane. *Spectrochimica Acta Part A*, 60, 1659-1676.
- Dyrby, M., Engelsen, S. B., Nørgaard, L., Bruhn, M. & Lundsberg-Nielsen, L. (2002) Chemometric quantitation of the active substance (containing CN) in a pharmaceutical tablet using near-infrared (NIR) transmittance and NIR FT-Raman spectra. *Applied Spectroscopy*, 56, 579 - 585.
- Edwards, H. G., Lawson, E. E., Barry, B. W. & Williams, A. C. (1998) Interaction of salicylic acid with verrucae assessed by FT-Raman spectroscopy. *Journal of Drug Targeting*, 5, 343-351.
- Edwards, H. G. M., Anigbogu, A. N. C., Williams, A. C. & Barry, B. W. (1995a) Fourier transform Raman spectroscopy of interactions between the penetration enhancer dimethyl sulfoxide and human stratum corneum. *International Journal of Pharmaceutics*, 125, 265-282.
- Edwards, H. G. M., Armstrong, C. L., Farwell, D. W. & Williams, A. C. (1996a) Fourier transform Raman microscopic study of drug distribution in a transdermal drug delivery device. *Vibrational Spectroscopy*, 11, 105-113.
- Edwards, H. G. M., Barry, B. W. & Williams, A. C. (1992) Fourier transform Raman and infrared vibrational study of human skin: Assignment of spectral bands. *Journal of Raman Spectroscopy*, 23, 641-645.
- Edwards, H. G. M., Brown, A. B., York, P., Williams, A. C. & Worthington, H. (1993a) Solid state characterization of salbutamol salts using FT-Raman and SSNMR spectroscopy. *Journal of Pharmacy and Pharmacology*, 45, 1135-1135.

- Edwards, H. G. M., Caspers, P. J., Williams, A. C., Carter, E. A., Barry, B. W., Bruining, H. A. & Puppels, G. J. (2002) Monitoring the penetration enhancer dimethyl sulfoxide in human stratum corneum in vivo by confocal Raman spectroscopy. *Pharmaceutical Research*, 19, 1577-1580.
- Edwards, H. G. M., Lawson, E. E. & Johnson, A. F. (1995b) FT Raman spectroscopic study of the wavenumber region 2800-2630  $\text{cm}^{-1}$  of selected organic compounds. *Spectrochimica Acta Part A*, 51, 2057-2066.
- Edwards, H. G. M., Munshi, T. & Anstis, M. (2005) Raman spectroscopic characterisations and analytical discrimination between caffeine and demethylated analogues of pharmaceutical relevance. *Spectrochimica Acta Part A*, 61, 1453-1459.
- Edwards, H. G. M., Munshi, T. & Page, K. (2007) Analytical discrimination between sources of ginseng using Raman spectroscopy. *Analytical and Bioanalytical Chemistry*, 389, 2203-2215.
- Edwards, H. G. M., Schallreuter, K. U., Wood, J. M., Farwell, D. W. & Moore, J. (1996b) Oxybenzone oxidation following solar irradiation of skin: Photoprotection versus antioxidant inactivation. *The Journal of Investigative Dermatology*, 106, 583-586.
- Edwards, H. G. M., Williams, A. C. & Barry, B. W. (1994) Comparison of Fourier transform Raman spectra of mammalian and reptilian skin. *Analyst*, 119, 563-566.
- Edwards, H. G. M., Williams, A. C., Barry, B. W. & Farwell, D. W. (1993b) A critical comparison of some Raman spectroscopic techniques for studies of human stratum corneum. *Pharmaceutical Research*, 10, 1642-1647.
- El-Hagrasy, A. (2006) Application of Raman spectroscopy for quantitative in-line monitoring of tablet coating. *American Pharmaceutical Review*, 9, 40-45.
- Eliasson, C. & Matousek, P. (2007) Noninvasive authentication of pharmaceutical products through packaging using spatially offset Raman spectroscopy. *Analytical Chemistry*, 79, 1696-1701.
- Erckens, R. J., Jongsma, F. H. M., Wicksted, J. P., Hendrikse, F., March, W. F. & Motamedi, M. (2001) Drug-induced corneal hydration changes monitored in vivo by non-invasive confocal Raman spectroscopy. *Journal of Raman Spectroscopy*, 32, 733-738.
- Failloux, N., Bonnet, I., Baron, M. H. & Perrier, E. (2003) Quantitative analysis of vitamin A degradation by Raman spectroscopy. *Applied Spectroscopy*, 57, 1117-1122.
- Fdm *Electronic Handbook of FTIR Spectra*, [http://www.fdmspectra.com/fdm\\_ehb.htm](http://www.fdmspectra.com/fdm_ehb.htm).

- Fechner, P. M., Wartewig, S., Fütting, M., Heilmann, A., Neubert, R. H. H. & Kleinebudde, P. (2003) Properties of microcrystalline cellulose and powder cellulose after extrusion/spheronization as studied by fourier transform Raman spectroscopy and environmental scanning electron microscopy. *The AAPS Journal*, 5, 77-89.
- Févoite, G. (2007) *In situ* Raman spectroscopy for in-line control of pharmaceutical crystallization and solids elaboration processes: A Review. *Chemical Engineering Research and Design*, 85, 906-920.
- Fini, G. (2004) Applications of Raman spectroscopy to pharmacy. *Journal of Raman Spectroscopy*, 35, 335-337.
- Flemming, A. & Picker-Freyer, K. M. (2008) Compaction of lactose drug mixtures: quantification of the extent of incompatibility by FT-Raman spectroscopy. *European Journal of Pharmaceutics and Biopharmaceutics*, 68, 802-810.
- Foresman, J. B. & Frisch, A. (1996) *Exploring Chemistry with Electronic Structure Methods*, Gaussian, Inc., Pittsburgh, PA.
- Freeman, T. L., Cope, S. E., Stringer, M. R., Cruse-Sawyer, J. E., Brown, S. B., Batchelder, D. N. & Birbeck, K. (1998) The use of Raman mapping to determine the subcellular distribution of zinc phthalocyanines. *Internet Journal of Vibrational Spectroscopy*, 3.
- Fuller, R., Johnson, M. & Bye, A. (1995) Fluticasone propionate—an update on preclinical and clinical experience. *Respiratory Medicine*, 89, 3-18.
- Gamberini, M. C., Baraldi, C., Tinti, A., Palazzoli, F. & Ferioli, V. (2007) Vibrational study of tamoxifen citrate polymorphism. *Journal of Molecular Structure*, 840, 29-37.
- Gamberini, M. C., Baraldi, C., Tinti, A., Rustichelli, C., Ferioli, V. & Gamberini, G. (2006) Solid state characterization of chloramphenicol palmitate. Raman spectroscopy applied to pharmaceutical polymorphs. *Journal of Molecular Structure*, 785, 216-224.
- Gambino, D., Otero, L., Vieites, M., Boiani, M., González, M., Baran, E. J. & Cerecetto, H. (2007) Vibrational spectra of palladium 5-nitrofuryl thiosemicarbazone complexes: experimental and theoretical study. *Spectrochimica Acta Part A*, 68, 341-348.
- Gandhi, R. B., Bogardus, J. B., Bugay, D. E., Perrone, R. K. & Kaplan, M. A. (2000) Pharmaceutical relationships of three solid state forms of stavudine. *International Journal of Pharmaceutics*, 201, 221-237.
- Ganjali, M. R., Norouzi, P., Ghorbani, M. & Sepehri, A. (2005) Fourier transform cyclic voltammetric technique for monitoring ultratrace amounts of salbutamol at gold ultra microelectrode in flowing solutions. *Talanta*, 66, 1225-1233.

- Geze, A., Boury, F., Benoit, J. P., Chourpa, I. & Dubois, P. (1999) Direct qualitative and quantitative characterization of a radiosensitizer, 5-iodo-2'-deoxyuridine within biodegradable polymeric microspheres by FT-Raman spectroscopy. *Analyst*, 124, 37-42.
- Gift, A. D. & Taylor, L. S. (2007) Hyphenation of Raman spectroscopy with gravimetric analysis to interrogate water–solid interactions in pharmaceutical systems. *Journal of Pharmaceutical and Biomedical Analysis*, 43, 14-23.
- Giron, D. (1995) Thermal analysis and calorimetric methods in the characterisation of polymorphs and solvates. *Thermochimica Acta*, 248, 1-59.
- Glice, M. M., Les, A. & Bajdor, K. (1998) IR, Raman and theoretical ab initio RHF study of aminoglutethimide—an anticancer drug. *Journal of Molecular Structure*, 450, 141-153.
- Grasselli, J. G., Snavely, M. K. & Bulkin, B. J. (1981) *Chemical Applications of Raman Spectroscopy*, New York, Wiley.
- Griesser, U. J. A., M. E.; Burger, A. (1999) The polymorphic drug substances of the European Pharmacopoeia. Part 10. Diprophylline. *Scientia Pharmaceutica*, 67, 319 - 330.
- Griessers, U. J. B., Artur; Mereiter, Kurt (1997) The polymorphic drug substances of the European Pharmacopoeia. Part 9. physicochemical properties and crystal structure of acetazolamide crystal forms. *Journal of Pharmaceutical Sciences*, 86, 352 - 358.
- Grunenberg, A., Keil, B. & Henck, J. O. (1995) Polymorphism in binary mixtures, as exemplified by nimodipine. *International Journal of Pharmaceutics*, 118, 11-21.
- Gu, C. H. & Grant, D. J. W. (2001) Estimating the relative stability of polymorphs and hydrates from heats of solution and solubility data. *Journal of Pharmaceutical Sciences*, 90, 1277-1287.
- Guest, M. F., Bush, I. J., Van Dam, H. J. J., Sherwood, P., Thomas, J. M. H., Van Lenthe, J. H., Havenith, R. W. A. & Kendrick, J. (2005) The GAMESS-UK electronic structure package: algorithms, developments and applications.
- Gunasekaran, S., Devi, T. S. R. & Sakthivel, P. S. (2007a) FTIR, FT Raman and UV-visible spectral measurements and analysis on atorvastatin calcium. *Asian Journal of Chemistry*, 19, 335 - 346.
- Gunasekaran, S., Natarajan, R. K. & Renganayaki, V. (2007b) Qualitative analysis of some antidiabetic drugs by spectroscopic measurements. *Asian Journal of Chemistry*, 19, 315 - 327.
- Gunasekaran, S., Natarajan, R. K., Renganayaki, V. & Natarajan, S. (2006a) Vibrational spectra and thermodynamic analysis of metformin. *Indian Journal of Pure & Applied Physics*, 44, 495-500.

- Gunasekaran, S., Thilak Kumar, R. & Ponnusamy, S. (2006b) Vibrational spectra and normal coordinate analysis of diazepam, phenytoin and phenobarbitone. *Spectrochimica Acta Part A*, 65, 1041-1052.
- Gunasekaran, S. K., R. Thilak; Ponnusamy, S.; Pushparaj, S. Edward (2005a) Vibrational spectra and normal coordinate analysis of isoniazid. *Indian Journal of Physics*, 79, 171-175.
- Gunasekaran, S. N., R. K., Rathikha, R.; Syamala D. (2005b) Fourier transform infrared and Fourier transform Raman spectra and normal co-ordinate analysis of benzocaine. *Indian Journal of Physics*, 79, 509-513.
- Gunsekarana, S. & Sankari, G. (2005) Analysis of cyanocobalamin by spectroscopic measurements. *Acta Ciencia Indica Physics*, 31, 61 - 70.
- Guo-Feng, Y., Xiao-Chong, G., Rui-Chang, G., Zhao-Xun, Y. & Zhi-Qiang, A. (2007) Synthesis of fluticasone propionate. *Hecheng Huaxue*, 15, 510 - 512.
- Gustafsson, C., Nystroem, C., Lennholm, H., Bonferoni, M. C. & Caramella, C. M. (2003) Characteristics of hydroxypropyl methylcellulose influencing compactibility and prediction of particle and tablet properties by infrared spectroscopy. *Journal of Pharmaceutical Sciences*, 92, 494-504.
- Hall, K. A., Newton, P. N., Green, M. D., De, V., Vandenabeele, P., Pizzanelli, D., Mayxay, M., Dondorp, A. & Fernandez, F. M. (2006) Characterization of counterfeit artesunate antimalarial tablets from southeast asia. *The American Journal of Tropical Medicine and Hygiene*, 75, 804 - 811.
- Hamedani, R., Feldman, R. D. & Feagan, B. G. (1997) Drug development in inflammatory bowel disease: Budesonide-a model of targeted therapy. *Alimentary Pharmacology and Therapeutics*, 11, 98-108.
- Harju, M. E. E. (1993) Solid-state transition mechanisms of ammonium nitrate phases IV, III, and II investigated by simultaneous Raman spectrometry and differential scanning calorimetry. *Applied Spectroscopy*, 47, 1926-1930.
- Harju, M. E. E., Valkonen, J. & Jayasooriya, U. A. (1991) Simultaneous application of Fourier transform Raman spectroscopy and differential scanning calorimetry for the *in situ* investigation of phase transitions in condensed matter. *Spectrochimica acta Part A*, 47, 1395-1398.
- Harris, R. K., Hodgkinson, P., Larsson, T., Muruganantham, A., Ymén, I., Yufit, D. S. & Zorin, V. (2008) Characterization of polymorphs and solvates of terbutaline sulfate. *Crystal Growth & Design*, 8, 80-90.
- Hausman, D. S., Cambron, R. T. & Sakr, A. (2005a) Application of on-line Raman spectroscopy for characterizing relationships between drug hydration state and tablet physical stability. *International Journal of Pharmaceutics*, 299, 19-33.

- Hausman, D. S., Cambron, R. T. & Sakr, A. (2005b) Application of Raman spectroscopy for on-line monitoring of low dose blend uniformity. *International Journal of Pharmaceutics*, 298, 80-90.
- Heinz, A., Savolainen, M., Rades, T. & Strachan, C. J. (2007) Quantifying ternary mixtures of different solid-state forms of indomethacin by Raman and near-infrared spectroscopy. *European Journal of Pharmaceutical Sciences*, 32, 182-192.
- Hendra, P. J., Jones, C. & Warnes, G. (1991) *Fourier Transform Raman spectroscopy : Instrumentation and Chemical Applications*, London, Ellis Horwood.
- Hendra, P. J., Tudor, A. M., Melia, C. D., Binns, J. S., Church, S. & Davies, M. C. (1990) The application of Fourier-transform Raman spectroscopy to the analysis of pharmaceuticals and biomaterials. *Journal of Pharmaceutical and Biomedical Analysis*, 8, 717-720.
- Henson, M. J. & Zhang, L. (2006) Drug characterization in low dosage pharmaceutical tablets using Raman microscopic mapping. *Applied Spectroscopy*, 60, 1247-1255.
- Hernandez, B., Ellass, A., Navarro, R., Vergoten, G. & Hernanz, A. (1998) Vibrational force field calculations of Ara-A. Application to the analysis of Its infrared and Raman spectra. *Journal of Physical Chemistry B*, 102, 4233-4239.
- Hernandez, B., Navarro, R., Hernanz, A. & Vergoten, G. (2002) Ab initio Hartree-Fock/6-31G\*\* calculation on 9--D-arabinofuranosyladenine-5-monophosphate molecule: Application to the analysis of its IR and Raman spectra. *Biopolymers* 67, 440-455.
- Hickel, D., Carpy, A., Laguerre, M. & Leger, J. M. (1982) Sulfate de tert-butyl [(dihydroxy-3, 5 phenyl)-2 hydroxy-2 ethyl] ammonium (sulfate de terbutaline) hydrate. *Acta Crystallographica B*, 38, 632-635.
- Hosomi, K., Okuno, A., Umetani, Y., Araya, T., Matsuyama, K., Haginaka, J., Mifune, M. & Saito, Y. (2004) Coloration of phenothiazines with metal-containing drugs. *Journal of the Pharmaceutical Society of Japan*, 124, 587-598.
- Hu, Y., Wikström, H., Byrn, S. R. & Taylor, L. S. (2007) Estimation of the transition temperature for an enantiotropic polymorphic system from the transformation kinetics monitored using Raman spectroscopy. *Journal of Pharmaceutical and Biomedical Analysis*, 45, 546-551.
- Hughes, D., Hursthouse, M. B., Lancaster, R. W., Taverner, S., Threlfall, T. L. & Turner, P. (1997) How many polymorphs has sulfathiazole. *Journal of Pharmacy and Pharmacology*, 49, S4-20.
- Hughes, D. S., Hursthouse, M. B., Threlfall, T. & Taverner, S. (1999) A new polymorph of sulfathiazole. *Crystal Structure Communications*, 55, 1831-1833.

- Hvizdos, K. M. & Jarvis, B. (2000) Budesonide inhalation suspension: A review of its use in infants, children and adults with Inflammatory respiratory disorders. *Drugs*, 60, 1141 - 1178.
- Hwang, M. S., Cho, S., Chung, H. & Woo, Y. A. (2005) Nondestructive determination of the ambroxol content in tablets by Raman spectroscopy. *Journal of Pharmaceutical and Biomedical Analysis*, 38, 210-215.
- Iliescu, T., Baia, M. & Miclaus, V. (2004) A Raman spectroscopic study of the diclofenac sodium- $\beta$ -cyclodextrin interaction. *European Journal of Pharmaceutical Sciences*, 22, 487-495.
- Info, S., Basavoju, S., Boström, D. & Velaga, S. P. (2006) Pharmaceutical cocrystal and salts of norfloxacin. *Crystal Growth & Design*, 6, 2699-2708.
- Info, S., Griesser, U. J., Jetti, R. K. R., Haddow, M. F., Brehmer, T., Apperley, D. C., King, A. & Harris, R. K. (2008) Conformational polymorphism in oxybuprocaine hydrochloride. *Crystal Growth & Design*, 8, 44-56.
- Ishizaki, H., McKay, R. H., Norton, T. R., Yasunobu, K. T., Lee, J. & Tu, A. T. (1979) Conformational studies of peptide heart stimulant anophleulin A. Laser Raman, circular dichroism, fluorescence spectral studies, and Chou-Fasman calculations. *Journal of Biological Chemistry*, 254, 9651-9656.
- Islam, M. T., Rodr, E. D., Guez-Hornedo, N. E. D., Ciotti, S. & Ackermann, C. (2004) The potential of Raman spectroscopy as a process analytical technique during formulations of topical gels and emulsions. *Pharmaceutical Research*, 21, 1844-1851.
- Izolani, A. O., De Moraes, M. T. & Claudio, A. T. S. (2003) Fourier transform Raman spectroscopy of drugs: quantitative analysis of 1-phenyl-2, 3-dimethyl-5-pyrazolone-4-methylaminomethane sodium sulfonate:(dipyron). *Journal of Raman Spectroscopy*, 34, 837-843.
- James, R. W. (1982) *The Optical Principles of the Diffraction of X-Rays*, Ox Bow Press.
- Jedvert, I., Josefson, M. & Langkilde, F. (1998) Quantification of an active substance in a tablet by NIR and Raman spectroscopy. *Journal of Near Infrared Spectroscopy*, 6, 279-290.
- Jee, R. D. (2004) Near-infrared spectroscopy. IN A. C. Moffat, M. D. O. A. B. W. (Ed.) *Clarke's analysis of drugs and poisons*. London, Pharmaceutical Press.
- Jensen, F. (2007) *Introduction to Computational Chemistry*, Chichester.
- Johansson, J., Sparén, A., Svensson, O., Folestad, S. & Claybourn, M. (2007) Quantitative transmission Raman spectroscopy of pharmaceutical tablets and capsules. *Applied Spectroscopy*, 61, 1211-1218.

- Jørgensen, A., Rantanen, J., Karjalainen, M., Khriachtchev, L., Räsänen, E. & Yliruusi, J. (2002) Hydrate formation during wet granulation studied by spectroscopic methods and multivariate analysis. *Pharmaceutical Research*, 19, 1285-1291.
- Jubert, A., Legarto, M. L., Massa, N. E., Lopez Tevez, L. & Beatriz Okulik, N. (2006) Vibrational and theoretical studies of non-steroidal anti-inflammatory drugs ibuprofen[2-(4-isobutylphenyl) propionic acid]; naproxen[6-methoxy- $\alpha$ -methyl-2-naphthalene acetic acid] and tolmetin acids[1-methyl-5-(4-methylbenzoyl)-1H-pyrrole-2-acetic acid]. *Journal of Molecular Structure*, 783, 34-51.
- Kanke, M. & Sekiguch, K. (1973) Dissolution behaviour of solid drugs. I. Improvement and simplification of dissolution rate measurement, and its application to solubility determinations. *Chemical & Pharmaceutical Bulletin*, 21, 871 - 877.
- Karabas, I., Orkoula, M. G. & Kontoyannis, C. G. (2007) Analysis and stability of polymorphs in tablets: The case of risperidone. *Talanta*, 71, 1382-1386.
- Katainen, E., Niemelä, P., Harjunen, P., Suhonen, J. & Järvinen, K. (2005) Evaluation of the amorphous content of lactose by solution calorimetry and Raman spectroscopy. *Talanta*, 68, 1-5.
- Kauffman, J. F., Dellibovi, M. & Cunningham, C. R. (2007) Raman spectroscopy of coated pharmaceutical tablets and physical models for multivariate calibration to tablet coating thickness. *Journal of Pharmaceutical and Biomedical Analysis*, 43, 39-48.
- Kauppinen, J. K., Moffat, D. J., Mantsch, H. H. & Cameron, D. G. (1981) Fourier self-deconvolution: A method for resolving intrinsically overlapped bands. *Applied Spectroscopy*, 35, 271 - 276.
- Kazarian, S. G. & Martirosyan, G. G. (2002) Spectroscopy of polymer/drug formulations processed with supercritical fluids: *in situ* ATR-IR and Raman study of impregnation of ibuprofen into PVP. *International Journal of Pharmaceutics*, 232, 81-90.
- Kern, A. S. B., Collins, W. J., Cambron, R. T. & Redman-Furey, N. L. (2005) Use of a TG/DTA/Raman system to monitor dehydration and phase conversions. *Journal of ASTM International*, 2.
- Khankari, R. K. & Grant, D. J. W. (1995) Pharmaceutical hydrates. *Thermochimica Acta*, 248, 61-79.
- Kim, J., Noh, J., Chung, H., Woo, Y. A., Kemper, M. S. & Lee, Y. (2007a) Direct, non-destructive quantitative measurement of an active pharmaceutical ingredient in an intact capsule formulation using Raman spectroscopy. *Analytica Chimica Acta*, 598, 280-285.
- Kim, M., Chung, H., Woo, Y. & Kemper, M. S. (2007b) A new non-invasive, quantitative Raman technique for the determination of an active ingredient in

- pharmaceutical liquids by direct measurement through a plastic bottle. *Analytica Chimica Acta*, 587, 200-207.
- King, T. H., Mann, C. K. & Vickers, T. J. (1985) Determination of phenylpropanolamine hydrochloride and acetaminophen in pharmaceutical preparations by Raman spectroscopy. *Journal of Pharmaceutical Sciences*, 74, 443-447.
- Kirk, J. H., Dann, S. E. & Blatchford, C. G. (2007) Lactose: A definitive guide to polymorph determination. *International Journal of Pharmaceutics*, 334, 103-114.
- Kobayashi, R., Fujimaki, Y., Ukita, T. & Hiyama, Y. (2006) Monitoring of solvent-mediated polymorphic transitions using *in situ* analysis tools. *Organic Process Research & Development*, 10, 1219-1226.
- Kogermann, K., Aaltonen, J., Strachan, C. J., Pöllänen, K., Veski, P., Heinämäki, J., Yliruusi, J. & Rantanen, J. (2007) Qualitative *in situ* analysis of multiple solid-state forms using spectroscopy and partial least squares discriminant modeling. *Journal of Pharmaceutical Sciences*, 96, 1802-1820.
- Koleva, B. B., Kolev, T. M., Tsalev, D. L. & Spitteller, M. (2008) Determination of phenacetin and salophen analgetics in solid binary mixtures with caffeine by infrared linear dichroic and Raman spectroscopy. *Journal of Pharmaceutical and Biomedical Analysis*, 46, 267 - 273.
- Kontoyannis, C. G. (1995) Quantitative determination of CaCO<sub>3</sub> and glycine in antacid tablets by laser Raman spectroscopy. *Journal of Pharmaceutical and Biomedical Analysis*, 13, 73-76.
- Krämer, K. & Ebel, S. (2000) Application of NIR reflectance spectroscopy for the identification of pharmaceutical excipients. *Analytica Chimica Acta*, 420, 155-161.
- Kruger, G. J. & Gafner, G. (1972) The crystal structures of polymorphs I and III of sulphathiazole. *Acta Crystallographica B* 28, 272-283.
- Kuiper, H. A., Noordam, M. Y., Van Dooren-Flipsen, M. M., Schilt, R. & Roos, A. H. (1998) Illegal use of beta-adrenergic agonists: European community. *Journal of Animal Science*, 76, 195 - 207.
- Kure, B. & Morris, M. D. (1976) Raman spectra of phenothiazine and some pharmaceutical derivatives. *Talanta*, 23, 398-400.
- Lagas, M. & Lerk, C. F. (1981) The polymorphism of sulphathiazole. *International Journal of Pharmaceutics*, 8, 11-24.
- Lang, K. R. (1995) *Sun, Earth and Sky*, New York, Springer-Verlag.

- Langkilde, F. W., Sjöblom, J., Tekenbergs-Hjelte, L. & Mrak, J. (1997) Quantitative FT-Raman analysis of two crystal forms of a pharmaceutical compound. *Journal of Pharmaceutical and Biomedical Analysis*, 15, 687-696.
- Leach, A. R. (2001) *Molecular Modelling: Principles and Applications*, Prentice Hall.
- Lee, C., Yang, W. & Parr, R. G. (1988) Development of the Colle-Salvetti correlation-energy formula into a functional of the electron density. *Physical Review B*, 37, 785-789.
- Lehto, V. P., Tenho, M., Vähä-Heikkilä, K., Harjunen, P., Päällysaho, M., Väliisaari, J., Niemelä, P. & Järvinen, K. (2006) The comparison of seven different methods to quantify the amorphous content of spray dried lactose. *Powder Technology*, 167, 85-93.
- Lester, C., Lubey, G., Dicks, M., Andol, G., Vaughn, D., Cambron, R. T., Poiesz, K. & Redman-Furey, N. (2006) Dehydration of risedronate hemi-pentahydrate: Analytical and physical characterization. *Journal of Pharmaceutical Sciences*, 95, 2631-2644.
- Liang, J. K., Byrn, Stephen (2007) On-line Raman spectroscopy in pharmaceutical process development: application and future prospects. *American Pharmaceutical Review*, 10, 45 - 51.
- Lin-Vien, D., Colthup, N. B., Fateley, W. G. & Grasselli, J. G. (1991) *The Handbook of Infrared and Raman Characteristic Frequencies of Organic Molecules*, Academic Press San Diego.
- Lin, W. Q., Jiang, J. H., Yang, H. F., Ozaki, Y., Shen, G. L. & Yu, R. Q. (2006) Characterization of chloramphenicol palmitate drug polymorphs by Raman mapping with multivariate image segmentation using a spatial directed agglomeration clustering method. *Analytical Chemistry*, 78, 6003-6011.
- Ling, J., Weitman, S. D., Miller, M. A., Moore, R. V. & Bovik, A. C. (2002) Direct Raman imaging techniques for study of the subcellular distribution of a drug. *Applied Optics*, 41, 6006-6017.
- López-Sánchez, M., Ruedas-Rama, M. J., Ruiz-Medina, A., Molina-Díaz, A. & Ayora-Canada, M. J. (2008) Pharmaceutical powders analysis using FT-Raman spectrometry: Simultaneous determination of sulfathiazole and sulfanilamide. *Talanta*, 74, 1603-1607.
- Lu, G. W., Hawley, M., Smith, M., Geiger, B. M. & Pfund, W. (2006) Characterization of a novel polymorphic form of celecoxib. *Journal of Pharmaceutical Sciences*, 95, 305 - 317.
- Manfait, M., Alix, A. J. P., Labarre, J. F. & Sournies, F. (1982a) Raman and infrared studies on new anticancer inorganic ring systems. 1. hexaziridinocyclotriphosphazene. *Journal of Raman Spectroscopy*, 12, 212 -216.

- Manfait, M., Alix, A. J. P., Lahana, R. & Labarre, J. F. (1982b) Raman and infrared studies on new anticancer inorganic ring systems. 2. pentaziridinocyclodiphosphathiazene. *Journal of Raman Spectroscopy*, 13, 44 - 52.
- Mao, J. & Xu, J. (2006) Discrimination of herbal medicines by molecular spectroscopy and chemical pattern recognition. *Spectrochimica Acta Part A*, 65, 497-500.
- Markopoulou, C. K., Koundourellis, J. E., Orkoula, M. G. & Kontoyannis, C. G. (2008) Quantitative nondestructive methods for the determination of ticlopidine in tablets using reflectance near-infrared and Fourier transform Raman spectroscopy. *Applied Spectroscopy*, 62, 251-257.
- Marques, M. P. M., Oliveria, P. J., Moreno, A. J. M. & De Carvalho, L. (2002) Study of carvedilol by combined Raman spectroscopy and ab initio MO calculations. *Journal of Raman Spectroscopy*, 33, 778-783.
- Martindale (2005) The Extra Pharmacopoeia. IN Sweetman, S. C. (Ed.) 34<sup>th</sup> ed. London, The Pharmaceutical Press.
- Matousek, P. (2006) Inverse spatially offset Raman spectroscopy for deep noninvasive probing of turbid media. *Applied Spectroscopy*, 60, 1341-1347.
- Matousek, P. & Parker, A. W. (2006) Bulk Raman analysis of pharmaceutical tablets. *Applied Spectroscopy*, 60, 1353-1357.
- Matousek, P. & Parker, A. W. (2007) Non-invasive probing of pharmaceutical capsules using transmission Raman spectroscopy. *Journal of Raman Spectroscopy*, 38, 563 - 567.
- Maurin, M. B., Vickery, R. D., Rabel, S. R., Rowe, S. M., Everlof, J. G., Nemeth, G. A., Campbell, G. C. & Foris, C. M. (2002) Polymorphism of roxifiban. *Journal of Pharmaceutical Sciences*, 91, 2599-2604.
- Mazurek, S. & Szostak, R. (2006a) Quantitative determination of captopril and prednisolone in tablets by FT-Raman spectroscopy. *Journal of Pharmaceutical and Biomedical Analysis*, 40, 1225-1230.
- Mazurek, S. & Szostak, R. (2006b) Quantitative determination of diclofenac sodium and aminophylline in injection solutions by FT-Raman spectroscopy. *Journal of Pharmaceutical and Biomedical Analysis*, 40, 1235-1242.
- McCreery, R. L. (2000) *Raman Spectroscopy for Chemical Analysis*, New York, John Wiley & Sons, Inc.
- McCreery, R. L., Horn, A. J., Spencer, J. & Jefferson, E. (1998) Noninvasive identification of materials inside USP vials with Raman spectroscopy and a Raman spectral library. *Journal of Pharmaceutical Sciences*, 87, 1-8.

- Mehrens, S. M., Kale, U. J. & Qu, X. (2005) Statistical analysis of differences in the Raman spectra of polymorphs. *Journal of Pharmaceutical Sciences*, 94, 1354-1367.
- Miani, A., Raugeri, S., Carloni, P. & Helfand, M. S. (2007) Structure and Raman spectrum of clavulanic acid in aqueous solution. *Journal of Physical Chemistry B*, 111, 2621 - 2630.
- Michalska, D. (1993) The Raman and IR spectra and normal coordinate analysis of 3-(N-phenylacetyl-amino)-2, 6-piperidinedione, antineoplaston A10, the new antitumour drug. *Spectrochimica Acta Part A*, 49, 303–314.
- Michalska, D. & Wysokinski, R. (2005) The prediction of Raman spectra of platinum (II) anticancer drugs by density functional theory. *Chemical Physics Letters*, 403, 211-217.
- Miroshnyk, I., Khriachtchev, L., Mirza, S., Rantanen, J., Heinämäki, J. & Yliruusi, J. (2006) Insight into thermally induced phase transformations of erythromycin A dihydrate. *Crystal Growth & Design*, 6, 369-374.
- Mirza, S., Miroshnyk, I., Rantanen, J., Aaltonen, J., Harjula, P., Kiljunen, E., Heinämäki, J. & Yliruusi, J. (2007) Solid-state properties and relationship between anhydrate and monohydrate of baclofen. *Journal of Pharmaceutical Sciences*, 96, 2399-2408.
- Moloney, E., O'keane, C., Wood, F. & Burke, C. (2003) A rare cause of wheeze in a young adult. *Postgraduate Medical Journal*, 79, 543.
- Moroni, L., Gellini, C., Miranda, M. M., Salvi, P. R., Foresti, M. L., Innocenti, M., Loglio, F. & Salvietti, E. (2008) Raman and infrared characterization of the vibrational properties of the antimalarial drug artemisinin. *Journal of Raman Spectroscopy*, 39, 276-283.
- Moynihan, H. A. & O'hare, I. P. (2002) Spectroscopic characterisation of orthorhombic and monoclinic paracetamol. *International Journal of Pharmaceutics*, 247, 179-185.
- Muglia, C. I. & Baran, E. J. (2000) Vibrational spectrum of bis (pyrrolidine-N-carbodithioato)-oxovanadium (IV): A new insulin-mimetic vanadyl complex. *Acta Farmaceutica Bonaerense*, 19, 21-24.
- Neese, F. (2004) ORCA—An ab initio, Density Functional and Semiempirical Program Package, Version 2.4. *Max-Planck-Institut fuer Bioanorganische Chemie, Muelheim and der Ruhr*.
- Neugebauer, U., Szeghalmi, A., Schmitt, M., Kiefer, W., Popp, J. & Holzgrabe, U. (2005) Vibrational spectroscopic characterization of fluoroquinolones. *Spectrochimica Acta Part A*, 61, 1505-1517.

- Neville, G. A., Beckstead, H. D., Black, D. B., Dawson, B. A. & Shurvell, H. F. (1994) Vibrational and NMR spectroscopic study of aged flurazepam mono- and dihydrochloride salts for content identity. *Journal of Pharmaceutical Sciences*, 83, 1274-1279.
- Neville, G. A., Beckstead, H. D. & Shurvell, H. F. (1992) Utility of Fourier transform-Raman and Fourier transform-infrared diffuse reflectance spectroscopy for differentiation of polymorphic spironolactone samples. *Journal of Pharmaceutical Sciences*, 81, 1141-1146.
- Niemczyk, T. M., Delgado-Lopez, M., Allen, F. S., Clay, J. T. & Arneberg, D. L. (1998a) Quantitative assay of bucindolol in gel capsules using infrared and Raman spectroscopy. *Applied Spectroscopy*, 52, 513 - 518.
- Niemczyk, T. M., Delgado-Lopez, M. M. & Allen, F. S. (1998b) Quantitative determination of bucindolol concentration in intact gel capsules using Raman spectroscopy. *Analytical Chemistry*, 70, 2762-2765.
- Noonan, K. Y., Beshire, M., Darnell, J. & Frederick, K. A. (2005) Qualitative and quantitative analysis of illicit drug mixtures on paper currency using Raman microspectroscopy. *Applied Spectroscopy*, 59, 1493-1497.
- O'Brien, L. E., Timmins, P., Williams, A. C. & York, P. (2004) Use of *in situ* FT-Raman spectroscopy to study the kinetics of the transformation of carbamazepine polymorphs. *Journal of Pharmaceutical and Biomedical Analysis*, 36, 335-340.
- Okumura, T. & Otsuka, M. (2005) Evaluation of the microcrystallinity of a drug substance, indomethacin, in a pharmaceutical model tablet by chemometric FT-Raman spectroscopy. *Pharmaceutical research*, 22, 1350-1357.
- Oliva, M. A., Olsina, R. A. & Masi, A. N. (2005) Sensitive detection of salbutamol using europium-enhanced fluorescence with trioctylphosphine oxide (TOPO) as coligand. *Analyst*, 130, 1312-1317.
- Olsen, B. A. & Kiehl, D. E. (2006) Authentication and fingerprinting of suspect counterfeit drugs. *American Pharmaceutical Review*, 9, 115 - 118.
- Orkoula, M. G., Kontoyannis, C. G., Markopoulou, C. K. & Koundourellis, J. E. (2004) Development of methodologies based on HPLC and Raman spectroscopy for monitoring the stability of lovastatin in solid state in the presence of gallic acid. *Journal of Pharmaceutical and Biomedical Analysis*, 35, 1011-1016.
- Orkoula, M. G., Kontoyannis, C. G., Markopoulou, C. K. & Koundourellis, J. E. (2006) Quantitative analysis of liquid formulations using FT-Raman spectroscopy and HPLC The case of diphenhydramine hydrochloride in Benadryl®. *Journal of Pharmaceutical and Biomedical Analysis*, 41, 1406-1411.
- Orkoula, M. G., Kontoyannis, C. G., Markopoulou, C. K. & Koundourellis, J. E. (2007) Validation of a direct non-destructive quantitative analysis of amiodarone

- hydrochloride in Angoron® formulations using FT-Raman spectroscopy. *Talanta*, 73, 258-261.
- Park, S. C., Kim, M., Noh, J., Chung, H., Woo, Y., Lee, J. & Kemper, M. S. (2007) Reliable and fast quantitative analysis of active ingredient in pharmaceutical suspension using Raman spectroscopy. *Analytica Chimica Acta*, 593, 46-53.
- Pavel, I., Cota, S., Cinta-Pinzaru, S. & Kiefer, W. (2005) Raman, surface enhanced Raman spectroscopy, and DFT calculations: A powerful approach for the identification and characterization of 5-fluorouracil anticarcinogenic drug species. *Journal of Physical Chemistry A*, 109, 9945-9952.
- Pekka, H., Kirsi, J., Jukka, R., Staffan, S. & Anne, J. (2007) Characterisation of blends of paracetamol and citric acid. *Journal of Pharmacy and Pharmacology*, 59, 373-381.
- Pelletier, M. J. (1999) *Analytical Applications of Raman Spectroscopy*, Oxford, Blackwell Science Ltd.
- Pereira, B. G., Vianna-Soares, C. D., Righi, A., Pinheiro, M. V. B., Flores, M. Z. S., Bezerra, E. M., Freire, V. N., Lemos, V., Caetano, E. W. S. & Cavada, B. S. (2007) Identification of lamivudine conformers by Raman scattering measurements and quantum chemical calculations. *Journal of Pharmaceutical and Biomedical Analysis*, 43, 1885-1889.
- Pestaner, J. P., Mullick, F. G. & Centeno, J. A. (1996) Characterization of acetaminophen: molecular microanalysis with Raman microprobe spectroscopy. *Journal of Forensic Sciences*, 41, 1060-1063.
- Petty, C. & Cahoon, N. (1993) The analysis of thin layer chromatography plates by near-infrared FT-Raman. *Spectrochimica acta Part A*, 49, 645-655.
- Pfeffer-Hennig, S. & Bellus, M. (2004) Application of FT-Raman and FT-IR spectroscopy in pharmaceutical development. *American Pharmaceutical Review*, 7, 48-53.
- Pharmacopoeia, B. (2001) London.
- Pharmacopoeia, E. (1997) IN Europe, C. O. (Ed.) 3<sup>rd</sup> ed. Strasbourg.
- Phillipps, G. H., Bailey, E. J., Bain, B. M., Borella, R. A., Buckton, J. B., Clark, J. C., Doherty, A. E., English, A. F. & Fazakerley, H. (1994) Synthesis and structure-activity relationships in a series of antiinflammatory corticosteroid analogs, halomethyl androstane-17. beta.-carbothioates and-17. beta.-carbosenoates. *Journal of Medicinal Chemistry*, 37, 3717-3729.
- Pinzaru, S. C., Pavel, I., Leopold, N. & Kiefer, W. (2004) Identification and characterization of pharmaceuticals using Raman and surface-enhanced Raman scattering. *Journal of Raman Spectroscopy*, 35, 338-346.

- Polla, G. I., Vega, D. R., Lanza, H., Tombari, D. G., Baggio, R., Ayala, A. P., Filho, J. M., Fernández, D., Leyva, G. & Dartayet, G. (2005) Thermal behaviour and stability in Olanzapine. *International Journal of Pharmaceutics*, 301, 33-40.
- Porter, W. W. (2008) Polymorphism in carbamazepine cocrystals. *Crystal Growth & Design*, 8, 14-16.
- Prabakaran, A. R. & Mohan, S. (1990) Laser Raman studies of sulfa drug molecules. *National Academy Science Letters (India)*, 13, 423 - 425.
- Pratiwi, D., Fawcett, J. P., Gordon, K. C. & Rades, T. (2002) Quantitative analysis of polymorphic mixtures of ranitidine hydrochloride by Raman spectroscopy and principal components analysis. *European Journal of Pharmaceutics and Biopharmaceutics*, 54, 337-341.
- Price, C. P., Grzesiak, A. L. & Matzger, A. J. (2005) Crystalline polymorph selection and discovery with polymer heteronuclei. *Journal of American Chemical Society*, 127, 5512-5517.
- Priebe, H., Dugstad, H., Gacek, M., Hagen, E., Homestad, O. M., Larsen, A., Sjogren, C. E. & Thomassen, T. (1995) Synthesis and characterization of iodixanol. *Acta Radiologica Supplement*, 399, 21-31.
- Qu, H., Louhi-Kultanen, M. & Kallas, J. (2006a) Solubility and stability of anhydrate/hydrate in solvent mixtures. *International Journal of Pharmaceutics*, 321, 101-107.
- Qu, H., Louhi-Kultanen, M., Rantanen, J. & Kallas, J. (2006b) Solvent-mediated phase transformation kinetics of an anhydrate/hydrate system. *Crystal Growth & Design*, 6, 2053-2060.
- Raghavan, K., Dwivedi, A., Campbell, G. C. & Hussain, M. A. (1994) A spectroscopic investigation of DuP 747 polymorphs. *Journal of Pharmaceutical and Biomedical Analysis*, 12, 777-785.
- Rama, M. J. R., López-Sánchez, M., Ruiz-Medina, A., Molina-Díaz, A. & Ayora-Cañada, M. J. (2005) Flow-through sensor with Fourier transform Raman detection for determination of sulfonamides. *Analyst*, 130, 1617-1623.
- Raman, C. V. & Krishnan, K. S. (1928) A new type of secondary radiation. *Nature*, 121, 501 - 502.
- Ramos, F., Cristino, A., Carrola, P., Eloy, T., Silva, J. M., Castilho, M. C. & Noronha Da Silveira, M. I. (2003) Clenbuterol food poisoning diagnosis by gas chromatography-mass spectrometric serum analysis. *Analytica Chimica Acta*, 483, 207-213.
- Rantanen, J. (2007) Process analytical applications of Raman spectroscopy. *Journal of Pharmacy and Pharmacology*, 59, 171-177.

- Rantanen, J., Wikström, H., Rhea, F. E. & Taylor, L. S. (2005) Improved understanding of factors contributing to quantification of anhydrate/hydrate powder mixtures. *Applied Spectroscopy*, 59, 942-951.
- Rastogi, V. K., Jain, V., Yadav, R. A., Singh, C. & Palafox, M. A. (2000) Fourier transform Raman spectrum and ab initio and density functional computations of the vibrational spectrum, molecular geometry, atomic charges and some molecular properties of the anticarcinogenic drug 5-fluorouracil. *Journal of Raman Spectroscopy*, 31, 595-604.
- Reich, G. (2005) Near-infrared spectroscopy and imaging: Basic principles and pharmaceutical applications. *Advanced Drug Delivery Reviews*, 57, 1109-1143.
- Ricci, C., Eliasson, C., Macleod, N. A., Newton, P. N., Matousek, P. & Kazarian, S. G. (2007) Characterization of genuine and fake artesunate anti-malarial tablets using Fourier transform infrared imaging and spatially offset Raman spectroscopy through blister packs. *Analytical and Bioanalytical Chemistry*, 389, 1525-1532.
- Ringqvist, A., Taylor, L. S., Ekelund, K., Ragnarsson, G., Engström, S. & Axelsson, A. (2003) Atomic force microscopy analysis and confocal Raman microimaging of coated pellets. *International Journal of Pharmaceutics*, 267, 35-47.
- Rivas, L., Sánchez-Cortés, S., Stanicova, J., Garcí'a-Ramos, J. V. & Miskovsky, P. (1999) FT-Raman, FTIR and surface-enhanced Raman spectroscopy of the antiviral and antiparkinsonian drug amantadine. *Vibrational Spectroscopy*, 20, 179-188.
- Rodriguez-Hornedo, N., Nehm, S. J., Seefeldt, K. F., Pagan-Torres, Y. & Falkiewicz, C. J. (2006) Reaction crystallization of pharmaceutical molecular complexes. *Molecular Pharmaceutics*, 3, 362-367.
- Rodriguez-Perez, A. I., Rodriguez-Tenreiro, C., Alvarez-Lorenzo, C., Taboada, P., Concheiro, A. & Torres-Labandeira, J. J. (2006) Sertaconazole/hydroxypropyl-beta-cyclodextrin complexation: Isothermal titration calorimetry and solubility approaches. *Journal of Pharmaceutical Sciences*, 95, 1751-1762.
- Roggo, Y., Roeseler, C. & Ulmschneider, M. (2004) Near infrared spectroscopy for qualitative comparison of pharmaceutical batches. *Journal of Pharmaceutical and Biomedical Analysis*, 36, 777-786.
- Rollinger, J. M. & Burger, A. (2002) Physico-chemical characterization of hydrated and anhydrous crystal forms of amlodipine besylate. *Journal of Thermal Analysis and Calorimetry*, 68, 361-372.
- Rollinger, J. M., Gstrein, E. M. & Burger, A. (2002) Crystal forms of torasemide: new insights. *European Journal of Pharmaceutics and Biopharmaceutics*, 53, 75-86.
- Romero-Torres, S., Perez-Ramos, J. D., Morris, K. R. & Grant, E. R. (2006) Raman spectroscopy for tablet coating thickness quantification and coating

- characterization in the presence of strong fluorescent interference. *Journal of Pharmaceutical and Biomedical Analysis*, 41, 811-819.
- Romero-Torres, S., Pérez-Ramos, J. D., Morris, K. R. & Grant, E. R. (2005) Raman spectroscopic measurement of tablet-to-tablet coating variability. *Journal of Pharmaceutical and Biomedical Analysis*, 38, 270-274.
- Romero-Torres, S., Wikstrom, H., Grant, E. R. & Taylor, L. S. (2007) Monitoring of mannitol phase behavior during freeze-drying using non-invasive Raman spectroscopy. *PDA Journal of Pharmaceutical Science and Technology / PDA*, 61, 131-45.
- Rossi, B., Verrocchio, P., Viliani, G., Scarduelli, G., Guella, G. & Mancini, I. (2006) Vibrational properties of inclusion complexes: The case of indomethacin-cyclodextrin. *The Journal of Chemical Physics*, 125, 044511-1-044511-7.
- Sajan, D., Laladhas, K. P., Joe, I. H. & Jayakumar, V. S. (2005) Vibrational spectra and density functional theoretical calculations on the antitumor drug, plumbagin. *Journal of Raman Spectroscopy*, 36, 1001 - 1011.
- Sandler, N., Savolainen, M., Saupe, A., Strachan, C. & Rades, T. (2007) Applications of Raman spectroscopy in aqueous environments using Raman spectroscopy to characterize pharmaceutical materials and processes. *Pharmaceutical Technology Europe*, 19, 24.
- Santi, E., Torre, M. H., Kremer, E., Etcheverry, S. B. & Baran, E. J. (1993) Vibrational spectra of the copper (II) and nickel (II) complexes of piroxicam. *Vibrational Spectroscopy*, 5, 285-293.
- Šašić, S. (2007a) An in-depth analysis of Raman and near-infrared chemical images of common pharmaceutical tablets. *Applied Spectroscopy*, 61, 239 - 250.
- Šašić, S. (2007b) Raman mapping of low-content API pharmaceutical formulations. I. Mapping of alprazolam in alprazolam/xanax tablets. *Pharmaceutical Research*, 24, 58-65.
- Šašić, S. (2008) Chemical imaging of pharmaceutical granules by Raman global illumination and near-infrared mapping platforms. *Analytica Chimica Acta*, 611, 73-79.
- Šašić, S. & Clark, D. A. (2006) Defining a strategy for chemical imaging of industrial pharmaceutical samples on Raman line-mapping and global illumination instruments. *Applied Spectroscopy*, 60, 494-502.
- Šašić, S., Clark, D. A., Mitchell, J. C. & Snowden, M. J. (2004) A comparison of Raman chemical images produced by univariate and multivariate data processing: a simulation with an example from pharmaceutical practice. *Analyst*, 129, 1001-1007.

- Šašić, S., Clark, D. A., Mitchell, J. C. & Snowden, M. J. (2005a) Analyzing Raman maps of pharmaceutical products by sample-sample two-dimensional correlation. *Applied Spectroscopy*, 59, 630-638.
- Šašić, S., Clark, D. A., Mitchell, J. C. & Snowden, M. J. (2005b) Raman line mapping as a fast method for analyzing pharmaceutical bead formulations. *Analyst*, 130, 1530-1536.
- Savolainen, M., Heinz, A., Strachan, C., Gordon, K. C., Yliruusi, J., Rades, T. & Sandler, N. (2007a) Screening for differences in the amorphous state of indomethacin using multivariate visualization. *European Journal of Pharmaceutical Sciences*, 30, 113-123.
- Savolainen, M., Jouppila, K., Pajamo, O., Christiansen, L., Strachan, C., Karjalainen, M. & Rantanen, J. (2007b) Determination of amorphous content in the pharmaceutical process environment. *Journal of Pharmacy and Pharmacology*, 59, 161-170.
- Scadding, G. K., Lund, V. J., Jacques, L. A. & Richards, D. H. (1995) A placebo-controlled study of fluticasone propionate aqueous nasal spray and beclomethasone dipropionate in perennial rhinitis: efficacy in allergic and non-allergic perennial rhinitis. *Clinical & Experimental Allergy*, 25, 737-743.
- Schmidt, A., Lindner, A. S., Casado, J. & Ramirez, F. J. (2007) Vibrational spectra and quantum chemical calculations of uracilyl-pyridinium mesomeric betaine. *Journal of Raman Spectroscopy*, 38, 1500 - 1509.
- Schmidt, A. C. (2005a) The role of molecular structure in the crystal polymorphism of local anesthetic drugs: Crystal polymorphism of local anesthetic drugs, part X. *Pharmaceutical Research*, 22, 2121-2133.
- Schmidt, A. C. (2005b) Solid-state characterization of chlorprocaine hydrochloride: Part VI. Crystal polymorphism of local anaesthetic drugs. *Journal of Thermal Analysis and Calorimetry*, 81, 291-297.
- Schmidt, A. C. (2005c) Solid-state characterization of falcaine hydrochloride and isomorphous dyclonine hydrochloride Part IV. Crystal polymorphism of local anaesthetic drugs. *European Journal of Pharmaceutical Sciences*, 25, 407-416.
- Schmidt, A. C. (2005d) Structural characteristics and crystal polymorphism of three local anaesthetic bases Crystal polymorphism of local anaesthetic drugs: Part VII. *International Journal of Pharmaceutics*, 298, 186-197.
- Schmidt, A. C., Niederwanger, V. & Griesser, U. J. (2004) Solid-state forms of prilocaine hydrochloride: Crystal polymorphism of local anaesthetic drugs, Part II. *Journal of Thermal Analysis and Calorimetry*, 77, 639-652.
- Schmidt, A. C. & Schwarz, I. (2005) Solid state characterization of hydroxyprocaine hydrochloride. Crystal polymorphism of local anaesthetic drugs, part VIII. *Journal of Molecular Structure*, 748, 153-160.

- Schmidt, A. C. & Schwarz, I. (2006) Solid-state characterization of non-stoichiometric hydrates of ester-type local anaesthetics Part XI. Crystal polymorphism of local anaesthetic drugs. *International Journal of Pharmaceutics*, 320, 4-13.
- Schmidt, A. C., Schwarz, I. & Mereiter, K. (2006) Polymorphism and pseudopolymorphism of salicaine and salicaine hydrochloride crystal polymorphism of local anaesthetic drugs, part V. *Journal of Pharmaceutical Sciences*, 95, 1097 - 1113.
- Schmidt, A. C., Senfter, N. & Griesser, U. J. (2003a) Crystal polymorphism of local anaesthetic drugs. Part I: Pramocaine base in comparison with pramocaine hydrochloride. *Journal of Thermal Analysis and Calorimetry*, 73, 397-408.
- Schmidt, A. G., Wartewig, S. & Picker, K. M. (2003b) Potential of carrageenans to protect drugs from polymorphic transformation. *European Journal of Pharmaceutics and Biopharmaceutics*, 56, 101-110.
- Schrader, B. (1995) General Survey of Vibrational spectroscopy IN Schrader, B. (Ed.) *Infrared and Raman Spectroscopy*. Weinheim.
- Schulz, H. (2005) Rapid analysis of medicinal and aromatic plants by non-destructive vibrational spectroscopy methods. *Acta Horticulturae*.
- Schulz, H., Baranska, M., Quilitzsch, R. & Schütze, W. (2004) Determination of alkaloids in capsules, milk and ethanolic extracts of poppy (*Papaver somniferum* L.) by ATR-FT-IR and FT-Raman spectroscopy. *Analyst*, 129, 917-920.
- Seefeldt, K., Miller, J., Alvarez-Nunez, F. & Rodriguez-Hornedo, N. (2007) Crystallization pathways and kinetics of carbamazepine-nicotinamide cocrystals from the amorphous state by *in situ* thermomicroscopy, spectroscopy, and calorimetry studies. *Journal of Pharmaceutical Sciences*, 96, 1147 - 1158.
- Sengupta, R. & Dattagupta, J. K. (1996) A  $\beta$ -adrenergic agonist: protonated terbutaline hemisulfate. *Acta Crystallographica C*, 52, 162-164.
- Severdia, A. G. & Siek, K. (2002) Fourier transform Raman spectroscopy for identification and differentiation between dosage strengths of an active drug in white opaque hard gelatin capsules. *Applied Spectroscopy*, 56, 545 - 548.
- Shackman, J. G., Giles, J. H. & Denton, M. B. (2000) Pharmaceutical Reaction Monitoring by Raman Spectroscopy. IN Denton, M. B. (Ed.) *Further Developments in Scientific Optical Imaging*. London, Royal Society of Chemistry.
- Shaver, J. M. (2001) Chemometrics for Raman Spectroscopy. Handbook of Raman Spectroscopy: Practical Spectroscopy Series Vol. 28. Marcel Dekker Inc, New York.

- Sheikhzadeh, M., Rohani, S., Jutan, A., Manifar, T., Murthy, K. & Horne, S. (2006) Solid-state characterization of bupirone hydrochloride polymorphs. *Pharmaceutical Research*, 23, 1043-1050.
- Sherman Hsu, C. P. (1997) Infrared Spectroscopy. *Handbook of Instrumental Techniques for Analytical Chemistry*. Upper Saddle River, NJ: Prentice-Hall.
- Silva, C., Leopoldino, A. M., Silva, E. H. T., Espinoza, V. A. A. & Taft, C. A. (2005) Computer-aided design of a novel ligand for retinoic acid receptor in cancer chemotherapy. *International Journal of Quantum Chemistry*, 102, 1131-1135.
- Sipos, P., Szucs, M., Szabó, A., Eros, I. & Szabó-Révész, P. (2008) An assessment of the interactions between diclofenac sodium and ammonio methacrylate copolymer using thermal analysis and Raman spectroscopy. *Journal of Pharmaceutical and Biomedical Analysis*, 46, 288-294.
- Skorda, D. & Kontoyannis, C. G. (2008) Identification and quantitative determination of atorvastatin calcium polymorph in tablets using FT-Raman spectroscopy. *Talanta*, 74, 1066-1070.
- Skoulika, S. G. & Georgiou, C. A. (2001) Spectroscopic techniques-rapid quantitative determination of ciprofloxacin in pharmaceuticals by use of solid-state FT-Raman spectroscopy. *Applied Spectroscopy*, 55, 1259-1265.
- Skoulika, S. G. & Georgiou, C. A. (2003) Rapid, noninvasive quantitative determination of acyclovir in pharmaceutical solid dosage forms through their poly (vinyl chloride) blister package by solid-state Fourier transform Raman spectroscopy. *Applied Spectroscopy*, 57, 407-412.
- Spencer, C. M. & Mctavish, D. (1995) Budesonide: A review of its pharmacological properties and therapeutic efficacy in inflammatory bowel disease. *Drugs*, 50, 854-872.
- Sprunt, J. C. & Jayasooriya, U. A. (1997) Simultaneous FT-Raman differential scanning calorimetry measurements using a low-cost fiber-optic probe. *Applied spectroscopy*, 51, 1410 - 1414.
- Sprunt, J. C., Jayasooriya, U. A. & Wilson, R. H. (2000) A simultaneous FT-Raman-DSC (SRD) study of polymorphism in sn-1, 3-distearoyl-2-oleoylglycerol (SOS). *Physical Chemistry Chemical Physics*, 2, 4299-4305.
- Starbuck, C., Spartalis, A., Wai, L., Wang, J., Fernandez, P., Lindemann, C. M., Zhou, G. X. & Ge, Z. (2002) Process optimization of a complex pharmaceutical polymorphic system via *in situ* Raman spectroscopy. *Crystal Growth & Design*, 2, 515-522.
- Steele, D. F., Young, P. M., Price, R., Smith, T., Edge, S. & Lewis, D. (2004) The potential use of Raman mapping to investigate *in vitro* deposition of combination pressurized metered-dose inhalers. *The AAPS Journal*, 6, 41-44.

- Stowell, G. W., Behme, R. J., Denton, S. M., Pfeiffer, I., Sancilio, F. D., Whittall, L. B. & Whittle, R. R. (2002) Thermally-prepared polymorphic forms of cilostazol. *Journal of Pharmaceutical Sciences*, 91, 2481-2488.
- Strachan, C. J., Howell, S. L., Rades, T. & Gordon, K. C. (2004a) A theoretical and spectroscopic study of carbamazepine polymorphs. *Journal of Raman Spectroscopy*, 35, 401-408.
- Strachan, C. J., Pratiwi, D., Gordon, K. C. & Rades, T. (2004b) Quantitative analysis of polymorphic mixtures of carbamazepine by Raman spectroscopy and principal components analysis. *Journal of Raman Spectroscopy*, 35, 347-352.
- Strachan, C. J., Rades, T. & Gordon, K. C. (2007a) A theoretical and spectroscopic study of-crystalline and amorphous indometacin. *Journal of Pharmacy and Pharmacology*, 59, 261-269.
- Strachan, C. J., Rades, T., Gordon, K. C. & Rantanen, J. (2007b) Raman spectroscopy for quantitative analysis of pharmaceutical solids. *Journal of Pharmacy and Pharmacology*, 59, 179-192.
- Sulub, Y., Lobrutto, R., Vivilecchia, R. & Wabuyele, B. W. (2008) Content uniformity determination of pharmaceutical tablets using five near-infrared reflectance spectrometers: A process analytical technology (PAT) approach using robust multivariate calibration transfer algorithms. *Analytica Chimica Acta*, 611, 143 - 150.
- Svensson, O., Josefson, M. & Langkilde, F. W. (2000) The synthesis of metoprolol monitored using Raman spectroscopy and chemometrics. *European Journal of Pharmaceutical Sciences*, 11, 141-155.
- Szelagiewicz, M., Marcolli, C., Cianferani, S., Hard, A. P., Vit, A., Burkhard, A., Von Raumer, M., Hofmeier, U. C., Zilian, A. & Francotte, E. (1999) *In situ* characterization of polymorphic forms: The potential of Raman techniques. *Journal of Thermal Analysis and Calorimetry*, 57, 23-43.
- Szostak, R. & Mazurek, S. (2002) Quantitative determination of acetylsalicylic acid and acetaminophen in tablets by FT-Raman spectroscopy. *Analyst*, 127, 144-148.
- Szostak, R. & Mazurek, S. (2004) FT-Raman quantitative determination of ambroxol in tablets. *Journal of Molecular Structure*, 704, 229-233.
- Taddei, P., Torreggiani, A. & Simoni, R. (2001) Influence of environment on piroxicam polymorphism: Vibrational spectroscopic study. *Biopolymers* 62, 68-78.
- Tantipolphan, R., Rades, T., Strachan, C. J., Gordon, K. C. & Medicott, N. J. (2006) Analysis of lecithin-cholesterol mixtures using Raman spectroscopy. *Journal of Pharmaceutical and Biomedical Analysis*, 41, 476-484.
- Taskinen, J. & Yliruusi, J. (2003) Prediction of physicochemical properties based on neural network modelling. *Advanced Drug Delivery Reviews*, 55, 1163-1183.

- Taylor, L. S. & Langkilde, F. W. (2000) Evaluation of solid-state forms present in tablets by Raman spectroscopy. *Journal of Pharmaceutical Sciences*, 89, 1342-1353.
- Taylor, L. S., York, P., Williams, A. C. & Mehta, V. (1997) Characterization of frozen glucose solutions. *Pharmaceutical Development and Technology*, 2, 395-402.
- Taylor, L. S. & Zograf, G. (1997) Spectroscopic characterization of interactions between PVP and indomethacin in amorphous molecular dispersions. *Pharmaceutical Research*, 14, 1691-1698.
- Telang, C., Suryanarayanan, R. & Yu, L. (2003) Crystallization of D-mannitol in binary mixtures with NaCl: Phase diagram and polymorphism. *Pharmaceutical Research*, 20, 1939-1945.
- Theophilus, A., Moore, A., Prime, D., Rossomanno, S., Whitcher, B. & Chrystyn, H. (2006) Co-deposition of salmeterol and fluticasone propionate by a combination inhaler. *International Journal of Pharmaceutics*, 313, 14-22.
- Thorley, F. C., Baldwin, K. J., Lee, D. C. & Batchelder, D. N. (2006) Dependence of the Raman spectra of drug substances upon laser excitation wavelength. *Journal of Raman Spectroscopy*, 37, 335-341.
- Thosar, S. S., Forbess, R. A., Kemper, M. & Shukla, A. J. (1999) Determination of copolymer ratios of poly (lactide-co-glycolide) using near-infrared spectroscopy. *Journal of Pharmaceutical and Biomedical Analysis*, 20, 107-114.
- Tian, F., Saville, D. J., Gordon, K. C., Strachan, C. J., Zeitler, J. A., Sandler, N. & Rades, T. (2007) The influence of various excipients on the conversion kinetics of carbamazepine polymorphs in aqueous suspension. *Journal of Pharmacy and Pharmacology*, 59, 193-201.
- Ticehurst, M. D., Rowe, R. C. & York, P. (1994) Determination of the surface properties of two batches of salbutamol sulphate by inverse gas chromatography. *International Journal of Pharmaceutics*, 111, 241-249.
- Tobón-Zapata, G. E., Etcheverry, S. B. & Baran, E. J. (1997) Vibrational spectrum of sanocrysin. *Spectrochimica Acta Part A*, 53, 183-188.
- Todica, M., Pop, C. V., Dinte, E., Farcau, C. & Astilean, S. (2007) Preliminary investigation by Raman spectroscopy of some polymeric matrix with pharmaceutical applications. *Modern Physics Letters B*, 21, 987-995.
- Tong, H. H. Y., Shekunov, B. Y., York, P. & Chow, A. H. L. (2003) Thermal analysis of trace levels of polymorphic impurity in salmeterol xinafoate samples. *Pharmaceutical Research*, 20, 1423-1429.

- Tong, H. H. Y., Yu Shekunov, B., York, P. & Chow, A. H. L. (2001) Characterization of two polymorphs of salmeterol xinafoate crystallized from supercritical fluids. *Pharmaceutical Research*, 18, 852-858.
- Torreggiani, A., Tamba, M., Trincherò, A. & Fini, G. (2003) A spectroscopic and pulse radiolysis study of allopurinol and its copper complex. *Journal of Molecular Structure*, 651, 91-99.
- Trincherò, A., Bonora, S., Tinti, A. & Fini, G. (2004) Spectroscopic behavior of copper complexes of nonsteroidal anti-inflammatory drugs. *Biopolymers*, 74, 120-124.
- Tu, A. T. (1982) *Raman Spectroscopy in Biology: Principles and Application*, New York, Wiley.
- Turrell, G. (1996) The Raman Effect. IN G. Turrell & Corset, J. (Eds.) *Raman Microscopy: Developments and Applications*. London, Academic Press.
- Ueda, H. & Nagai, T. (1981) Solid-state nuclear magnetic resonance spectroscopy and Raman spectroscopy of the inclusion compound of tolbutamide with  $\beta$ -cyclodextrin. *Chemical & Pharmaceutical Bulletin*, 29, 2710-2714.
- Urakami, K., Shono, Y., Higashi, A., Umemoto, K. & Godo, M. (2002) A novel method for estimation of transition temperature for polymorphic pairs in pharmaceuticals using heat of solution and solubility data. *Chemical & Pharmaceutical Bulletin*, 50, 263-267.
- Urlaub, E. P., J.; Roman, V. E., Kiefer, W.; Lankers, M.; Rossling, G. (1998) Raman spectroscopic monitoring of the polymerization of cyanoacrylate. *Chemical Physics Letters*, 298 177 - 182.
- Vale, A. (2003)  $\beta$ 2-agonists. *Medicine*, 31, 36-36.
- Van Grieken, R. E. & Markowicz, A. A. (1993) *Handbook of X-Ray Spectrometry: Methods and Techniques*, Marcel Dekker.
- Van Hoof, P., Lammers, R., V. Puijenbroek, R., V/D Schans, M., Carlier, P. & Kellenbach, E. (2002) Polymorphism of the CNS active drug Org 13011: The application of high temperature analysis to detect new polymorphs. *International Journal of Pharmaceutics*, 238, 215-228.
- Vankeirsbilck, T., Vercauteren, A., Baeyens, W., Van Der Weken, G., Verpoort, F., Vergote, G. & Remon, J. P. (2002) Applications of Raman spectroscopy in pharmaceutical analysis. *Trends in Analytical Chemistry*, 21, 869-877.
- Variankaval, N. E., Jacob, K. I. & Dinh, S. M. (1999) Crystallization of beta-estradiol in an acrylic transdermal drug delivery system. *Journal of Biomedical Materials Research*, 44, 397 - 406.

- Variankaval, N. E., Jacob, K. I. & Dinh, S. M. (2000) Characterization of crystal forms of  $\beta$ -estradiol- thermal analysis, Raman microscopy, X-ray analysis and solid-state NMR. *Journal of crystal growth*, 217, 320-331.
- Variankaval, N. E. J., K. I., Dinh, S. M. (2002) Polymorphism of 17 $\beta$ -estradiol in a transdermal drug delivery system. *Journal of Materials Science: Materials in Medicine* 13, 271 - 280.
- Vassou, D., Gionis, V. & Chryssikos, G. D. (2005) Glassy drugs: A Raman investigation of binary dihydropyridine systems. *Physics and Chemistry of Glasses*, 46, 144 - 147.
- Vega, D. R., Polla, G., Martinez, A., Mendioroz, E. & Reinoso, M. (2007) Conformational polymorphism in bicalutamide. *International Journal of Pharmaceutics*, 328, 112-118.
- Veiga, F., Fernandes, C. & Maincent, P. (2001) Influence of the preparation method on the physicochemical properties of tolbutamide/cyclodextrin binary systems. *Drug Development and Industrial Pharmacy*, 27, 523-532.
- Veiga, F., Teixeira-Dias, J. J. C., Kedzierewicz, F., Sousa, A. & Maincent, P. (1996) Inclusion complexation of tolbutamide with  $\beta$ -cyclodextrin and hydroxypropyl- $\beta$ -cyclodextrin. *International Journal of Pharmaceutics*, 129, 63-71.
- Vergote, G. J., De Beer, T. R. M., Vervaet, C., Remon, J. P., Baeyens, W. R. G., Diericx, N. & Verpoort, F. (2004) In-line monitoring of a pharmaceutical blending process using FT-Raman spectroscopy. *European Journal of Pharmaceutical Sciences*, 21, 479-485.
- Vergote, G. J., Vervaet, C., Remon, J. P., Haemers, T. & Verpoort, F. (2002) Near-infrared FT-Raman spectroscopy as a rapid analytical tool for the determination of diltiazem hydrochloride in tablets. *European Journal of Pharmaceutical Sciences*, 16, 63-67.
- Virágh, M. (2003) Quantitative analysis of mixtures of drug delivery system components by Raman microscopy. *Polymers for Advanced Technologies*, 14, 784-789.
- Vogt, F. G., Cohen, D. E., Bowman, J. D., Spoor, G. P., Zuber, G. E., Trescher, G. A., Dell'orco, P. C., Katrincic, L. M., Debrosse, C. W. & Curtis Haltiwanger, R. (2005) Structural analysis of polymorphism and solvation in tranilast. *Journal of Pharmaceutical Sciences*, 94, 651-665.
- Votion, D., Ghafir, Y., Munsters, K., Duvivier, D. H., Art, T. & Lekeux, P. (1997) Aerosol deposition in equine lungs following ultrasonic nebulisation versus jet aerosol delivery system. *Equine Veterinary Journal*, 29, 388-393.
- Vueba, M. L., Pina, M. E. & Batista, C. L. A. (2008) Conformational stability of ibuprofen: Assessed by DFT calculations and optical vibrational spectroscopy. *Journal of Pharmaceutical Sciences*, 97, 834-48.

- Wagner, C. C. & Baran, E. J. (1999) Vibrational spectrum of a platinum complex of piroxicam. *Spectroscopy Letters*, 32, 953-961.
- Wagner, C. C., Baran, E. J. & Piro, O. E. (1999) Characterization of bis (isoorotato) diaquamagnesium (II) dihydrate: A potentially useful complex for magnesium supplementation. *Journal of Inorganic Biochemistry*, 73, 259-263.
- Wang, C., Vickers, T. J. & Mann, C. K. (1997) Direct assay and shelf-life monitoring of aspirin tablets using Raman spectroscopy. *Journal of Pharmaceutical and Biomedical Analysis*, 16, 87-94.
- Ward, S., Perkins, M., Zhang, J., Roberts, C. J., Madden, C. E., Luk, S. Y., Patel, N. & Ebbens, S. J. (2005) Identifying and mapping surface amorphous domains. *Pharmaceutical research*, 22, 1195-1202.
- Wartewig, S. & Neubert, R. H. H. (2005) Pharmaceutical applications of mid-IR and Raman spectroscopy. *Advanced Drug Delivery Reviews*, 57, 1144-1170.
- Watts, P. J., Tudor, A., Church, S. J., Hendra, P. J., Turner, P., Melia, C. D. & Davies, M. C. (1991) Fourier transform-Raman spectroscopy for the qualitative and quantitative characterization of sulfasalazine-containing polymeric microspheres. *Pharmaceutical Research*, 8, 1323-1328.
- Wenslow, R. M., Baum, M. W., Ball, R. G., Mccauley, J. A. & Varsolona, R. J. (2000) A spectroscopic and crystallographic study of polymorphism in an aza-steroid. *Journal of Pharmaceutical Sciences*, 89, 1271-1285.
- Weyer, L. G. & Lo, S. C. (2002) Spectra–Structure Correlations in the Near-infrared. IN Chalmers, J. M. (Ed.) *Handbook of Vibrational Spectroscopy*. New York, John Wiley & Sons.
- Wikstroem, H., Marsac, P. J. & Taylor, L. S. (2005) In-line monitoring of hydrate formation during wet granulation using Raman spectroscopy. *Journal of Pharmaceutical Sciences*, 94, 209-219.
- Wikström, H., Lewis, I. R. & Taylor, L. S. (2005) Comparison of sampling techniques for in-line monitoring using Raman spectroscopy. *Applied Spectroscopy*, 59, 934-941.
- Wikström, H., Romero-Torres, S., Wongweragiat, S., Stuart Williams, J. A., Grant, E. R. & Taylor, L. S. (2006) On-line content uniformity determination of tablets using low-resolution Raman spectroscopy. *Applied Spectroscopy*, 60, 672-681.
- Williams, A. C. (2001) Some Pharmaceutical Applications of Raman Spectroscopy. IN Lewis, I. R. & Edwards, H. G. M. (Eds.) *Handbook of Raman spectroscopy : from the Research Laboratory to the Process Line*. Marcel Dekker New York.

- Williams, A. C., Cooper, V. B., Thomas, L., Griffith, L. J., Petts, C. R. & Booth, S. W. (2004) Evaluation of drug physical form during granulation, tableting and storage. *International Journal of Pharmaceutics*, 275, 29-39.
- Williams, P. A. M. B., E. J., Mercader, R. C. (2000) Preparation and characterization of new suprofen complexes of Fe(III), Co(II) and Ni (II). *Coordination Chemistry*, 50, 29-37.
- Wysokinski, R., Kuduk-Jaworska, J. & Michalska, D. (2006a) Electronic structure, Raman and infrared spectra, and vibrational assignment of carboplatin. Density functional theory studies. *Journal of Molecular Structure*, 758, 169-179.
- Wysokinski, R., Michalska, D., Bienko, D. C., Ilakiamani, S., Sundaraganesan, N. & Ramalingam, K. (2006b) Density functional study on the molecular structure, infrared and Raman spectra, and vibrational assignment for 4-thiocarbamoylpyridine. *Journal of Molecular Structure*, 791, 70-76.
- Yamini, Y., Reimann, C. T., Vatanara, A. & Jönsson, J. L. (2006) Extraction and preconcentration of salbutamol and terbutaline from aqueous samples using hollow fiber supported liquid membrane containing anionic carrier. *Journal of Chromatography A*, 1124, 57-67.
- Yang, H. & Irudayaraj, J. (2002) Rapid determination of vitamin C by NIR, MIR and FT-Raman techniques. *Journal of Pharmacy and Pharmacology*, 54, 1247-1255.
- Yokoi, Y., Yonemochi, E. & Terada, K. (2005) Effects of sugar ester and hydroxypropyl methylcellulose on the physicochemical stability of amorphous cefditoren pivoxil in aqueous suspension. *International Journal of Pharmaceutics*, 290, 91-99.
- Young, D. C. (2001) *Computational chemistry*, New York, Wiley-Interscience.
- Yu, L. (1995) Inferring thermodynamic stability relationship of polymorphs from melting data. *Journal of Pharmaceutical Sciences*, 84, 966-974.
- Yu, L., Reutzel, S. M. & Stephenson, G. A. (1998) Physical characterization of polymorphic drugs: an integrated characterization strategy. *Pharmaceutical Science & Technology Today*, 1, 118-127.
- Zeitler, J. A., Newnham, D. A., Taday, P. F., Threlfall, T. L., Lancaster, R. W., Berg, R. W., Strachan, C. J., Pepper, M., Gordon, K. C. & Rades, T. (2006) Characterization of temperature-induced phase transitions in five polymorphic forms of sulfathiazole by terahertz pulsed spectroscopy and differential scanning calorimetry. *Journal of Pharmaceutical Sciences*, 95, 2486 - 2498.
- Zhang, G., Flach, C. R. & Mendelsohn, R. (2007a) Tracking the dephosphorylation of resveratrol triphosphate in skin by confocal Raman microscopy. *Journal of Controlled Release*, 123, 141-147.

- Zhang, G., Moore, D. J., Sloan, K. B., Flach, C. R. & Mendelsohn, R. (2007b) Imaging the prodrug-to-drug transformation of a 5-fluorouracil derivative in skin by confocal Raman microscopy. *Journal of Investigative Dermatology*, 127, 1205 - 1209.
- Zhang, G. G. Z., Gu, C., Zell, M. T., Burkhardt, R. T., Munson, E. J. & Grant, D. J. W. (2002) Crystallization and transitions of sulfamerazine polymorphs. *Journal of Pharmaceutical Sciences*, 91, 1089-1100.
- Zhang, L., Henson, M. J. & Sekulic, S. S. (2005) Multivariate data analysis for Raman imaging of a model pharmaceutical tablet. *Analytica Chimica Acta*, 545, 262-278.
- Zhou, G., Wang, J., Ge, Z. & Sun, Y. (2002) Ensuring robust polymorph isolation using *in-situ* Raman spectroscopy. *American Pharmaceutical Review*, 5, 74-80.
- Zoppetti, G., Puppini, N., Ospitali, F. & Fini, A. (2007) Solid state characterization of progesterone in a freeze dried 1: 2 progesterone/HPBCD mixture. *Journal of Pharmaceutical Sciences*, 96, 1729-1736.
- Zupancic, V., Ograjšek, N., Kotar-Jordan, B. & Vrečer, F. (2005) Physical characterization of pantoprazole sodium hydrates. *International Journal of Pharmaceutics*, 291, 59-68.

**PHARMACEUTICAL APPLICATIONS OF LASER  
RAMAN SPECTROSCOPY**

**HASSAN REFAT HASSAN ALI  
Ph.D.**

**2009**

**PHARMACEUTICAL APPLICATIONS OF LASER  
RAMAN SPECTROSCOPY**

**Vibrational spectroscopic studies and solid state analysis of drugs used  
in the management of respiratory disorders**

Hassan Refat Hassan Ali  
BSc, MSc, AMRSC

Submitted to the University of Bradford for the Degree of Doctor of Philosophy

Chemical and Forensic Sciences  
University of Bradford  
Bradford  
UK

April 2009

## **Chapter 1**

### **Introduction**

## **Chapter 2**

# **Vibrational spectroscopy, spectral pre-processing and computational chemistry**

## **Chapter 3**

### **Raman spectroscopy as a primary tool in drug analysis**

**Part I**

**Chapter 4**

**Vibrational spectroscopic studies of drugs used in the management of  
respiratory disorders**

## **Chapter 5**

**Dependence of the Raman spectra of salmeterol xinafoate polymorphs upon laser excitation wavelength**

## **Chapter 6**

**Noninvasive *in situ* identification and band assignments of some pharmaceutical excipients inside USP vials with FT- near-infrared spectroscopy**

## **Part II**

### **Chapter 7**

**A preliminary investigation of the polymorphic transformation of salmeterol xinafoate and sulfathiazole using simultaneous *in situ* Raman spectroscopy and differential scanning calorimetry**

## **Chapter 8**

### **Conclusions and Further Work**

## References